STRUCTURAL ANALYSIS OF GINSENOSIDES AND SUGARS:

An electrospray and tandem mass spectrometry study

By

SUZANNE ACKLOO, B.Sc.

A Thesis Submitted to the School of Graduate Studies
In Partial Fulfilment of the Requirements for the Degree of
Doctor of Philosophy

McMaster University

Structural analysis of ginsenosides and sugars:

An electrospray and tandem mass spectrometry study

For my parents Helen and Raymond,
my siblings Dave, Lizzie, MH, Alex and Ray,
and me.

Doctor of Philosophy (2001)
Chemistry

McMaster University
Hamilton, Ontario
Canada

Title: **Structural Analysis of Ginsenosides and Sugars:**
An Electrospray and Tandem Mass Spectrometry Study

Author: Suzanne Ackloo, B.Sc. (York University)

Supervisors: Professor Brian E. McCarry and Professor Johan K. Terlouw

Number of pages: xviii, 298

Abstract

Carbohydrates are an abundant class of biological molecules. This thesis presents methodologies for structure characterization of a class of triterpene glycosides, the ginsenosides, sugars and polyols. The sugars included simple monosaccharides, as well as complex saccharides such as the carrageenans, a family of sulfated polysaccharides. The methodologies employed positive and negative ion electrospray ionization (ESI) mass spectrometry and tandem mass spectrometry (MS/MS).

Positive ion electrospray mass spectrometry (ESMS) of solutions containing a ginsenoside and any alkali metal ion produced the $[M+metal]^+$ ion. By contrast, when the transition metal ions, Ni^{++}, Co^{++} and Zn^{++}, are used, the $[M+metal-H]^+$ ion was observed. Collision-induced dissociation (CID) of the metal attachment ions accommodated their structure characterization. The relative intensity ratio of the product ions provided information on the point of attachment of the sugars to the core, as well as whether they are monosaccharides or disaccharides.

Negative ion ESMS of basic solutions of ginsenosides showed a peak corresponding to the $[M-H]^-$ ion whose CID spectrum provided the identity of the core, the sugars comprised in the ginsenoside and their order of attachment to the ginsenoside. Both positive and negative ion CID experiments provided information that can be used to propose a structure for ginsenosides. In line with this, these methodologies were used to develop a liquid chromatography mass spectrometry (LC/MS) and LC/MS/MS method for separation and structural characterization of new ginsenosides from root extracts. The structure proposals for ten new ginsenosides are provided.

The carrageenans are a family of partially sulfated polysaccharides of which there are three major types, *kappa* (k), *iota* (i) and *lamda* (l). These types are different because each has a disaccharide subunit containing a specific number of sulfate groups with Na^+ counterions. Both matrix-assisted laser/desorption ionization time-of-flight mass spectrometry and negative ion ESMS proved to be useful structure probes for these compounds. Dilute solutions of carrageenans undergo H^+ exchange and subsequent expulsion of SO_3 thus generating a carrageenan with lower sulfate content.

Ginsenosides differing *only* in the presence of geometric isomeric sugars are not differentiated by CID experiments. This observation raised the question of differentiating geometric and (stereo) isomeric polyols using ESMS and MS/MS experiments. Two approaches were investigated to address this question; the first employing negative ion, and the other positive ion mode.

The structures of polyols and sugars were analyzed as their boric acid complexes by negative ion infusion ESMS and MS/MS experiments. The positive ion approach employed complexation to oxovanadium(IV), VO^{++}. In both systems, ethylene glycol the simplest polyol was employed as the internal standard. Full scan ESMS experiments provided information on the ease of complexation of the analyte relative to ethylene glycol by comparing the intensity ratio of ions corresponding to their complexes with boric acid and VO^{++}. CID experiments probed the structures of these complexes. Both methodologies were valuable for differentiating geometric and stereoisomeric diols, and isomeric methyl glycosides.

Both ESI and MALDI involve solution- and gas-phase processes. A small chemical ionization mass spectrometry project involving alkylation reactions of N-

ethyl- and N-methylaniline, and *o*-, *m*- and *p*-ethyl- and *o*-, *m*- and *p*-methylaniline with iodomethane and iodoethane was undertaken. It was observed that the N-site is the primary site for alkylation.

Preface

This thesis describes the results obtained by the author during four years of research in electrospray mass spectrometry. Analyses of ginsenosides, sugars and polyols employed complexation to metal ions and boric acid. It is a well-known fact that electrospray mass spectra reflect solution-phase as well as gas-phase processes. Thus, electrospray ionization is well suited to the analysis of complexes formed in solution, such as the borates, and adducts that may arise from gas-phase chemistry, such as metal ion complexation. Ion-molecule reactions of N-(m)ethylaniline and the ring-alkyl anilines with iodoethane and iodomethane are also studied. Collaborative contributions from Dr Peter C. Burgers (Chapters 4 and 5), and Dr Alex G. Harrison (Chapter 7) are greatly appreciated.

The permission of The Royal Society of Chemistry and John Wiley & Sons, Ltd. to reproduce data and text which have been previously published is appreciated.

List of Publications

[7] **S.Z. Ackloo**, J.K. Terlouw and A.G. Harrison, The site of alkylation of N-methyl- and N-ethylaniline in the gas phase: A tandem mass spectrometry study – in preparation

[6] **S.Z. Ackloo**, B.E. McCarry and J.K. Terlouw, Structural Analysis of Oxovanadium (VO^{++}) Complexes of Sugars and Diols using Electrospray Mass Spectrometry – in preparation

[5] **S.Z. Ackloo**, J.K. Terlouw and B.E. McCarry, LC/MS and LC/MS/MS of *Panax quinquefolium* L. (American Ginseng) root extracts: Separation and structural characterization of new ginsenosides – in preparation

[4] **S. Ackloo**, J.K. Terlouw, P.J.A. Ruttink and P.C Burgers, Carrageenan Analysis by Matrix-assisted Laser Desorption/Ionization and Electrospray Ionization Mass Spectrometry I.*kappa*-Carrageenans, *Rapid Commun. Mass Spectrom.*, **2001**, *15*, 1152.

[3] **S.Z. Ackloo**, R.W. Smith, J.K. Terlouw and B.E. McCarry, Characterization of ginseng saponins using electrospray mass spectrometry and collision-induced dissociation experiments of metal-attachment ions, *The Analyst*, **2000**, *125*, 591.

[2] **S.Z. Ackloo**, P.C. Burgers, B.E. McCarry and J.K. Terlouw, Structural Analysis of Diols by Electrospray Mass Spectrometry on Boric Acid Complexes, *Rapid Commun. Mass Spectrom.*, **1999**, *13*, 2406.

[1] J.E. Nam Shin, **S.Z. Ackloo**, A.S. Mainkar, M.A. Monteiro, H. Pang, J.L. Penner and G.O. Aspinall, Lipo-oligosaccharides of Campylobacter jejuni serotype O:10. Structures of core oligosaccharide regions from a bacterial isolate from a patient with the Miller-Fisher syndrome and from the serotype reference strain, *Carbohydr. Res.*, **1998**, *305*, 223.

Acknowledgements

Although one of the goals of completing a Ph.D. degree is to carry out independent research, it is rarely possible to do so without supervision. I would like to thank my Ph.D. supervisors, Dr Brian E. McCarry and Dr Johan K. Terlouw, for their mentorship, patience and friendship. I have been quite fortunate to have had you both as my supervisors. I would like to thank Dr John D. Brennan for his valuable input on my projects.

I am also indebted to Dr Peter C. Burgers for his contributions to the boric acid project and for giving me the opportunity to contribute to the carrageenan work. Appreciation is also extended to Dr Alex G. Harrison for giving me the opportunity to collaborate with him on the anilines project.

The motivating professional and personal interactions with past and present members of both Dr McCarry's and Dr Terlouw's research groups, as well as the McMaster Regional Centre for Mass Spectrometry have been of great value: Dr M. Kirk Green, Dr Richard W. Smith, Leah Allan, Tadek Olech, Dr Laurie Allan, Lena Andrew, Dr Adrienne Boden, Rachel Chen, Brian Edwards, Kevin Guo, Lisa Heydorn, Marie Rosati, M. Anna Trikoupis and Wendy Zhang.

Thanks go to my (other) close friends Stacey Brydges, Akiko Lin, Dr Elena Manolopoulos, Dr Mustafa Mohamed, Tracy Morkin, Suresh Pawaroo, and Dr Darren Reid. You as well as Adrienne, Laurie, Lena and Lisa are an important part of my life.

Finally, and most importantly, my love and gratitude go to my parents, Helen and Raymond, and my siblings, Dave, Lizzie, MH, Alex and Ray. Without my parents' sacrifices, I would not have been able to *start* this work. Thank you.

Table of Contents

List of Figures

Page

List of Abbreviations

B	=	magnetic sector
BH	=	boric acid
BSE	=	bidentate stabilization energy
CCSD(T)	=	coupled cluster singles doubles and triples
CI	=	chemical ionization
CID	=	collision-induced dissociation
deoxyhex	=	deoxyhexose sugar
DHBA	=	dihydroxy benzoic acid
DP	=	degree of polymerization
EG	=	ethylene glycol
EI	=	electron ionization
ESA	=	electrostatic analyzer
ESI	=	electrospray ionization
ESMS	=	electrospray mass spectrometry
eV	=	electron volt (1 eV = 23.061 kcal/mol or 96.487kJ/mol)
hex	=	hexose sugar
ΔH_f	=	enthalpy of formation
HPLC	=	high performance liquid chromatography
IE	=	ionization energy
LC/MS	=	liquid chromatography / mass spectrometry
LC/MS/MS	=	liquid chromatography / mass spectrometry / mass spectrometry
MALDI	=	matrix-assisted laser/desorption ionization
MI	=	metastable ion
MS/MS	=	tandem mass spectrometry
m/z	=	mass-to-charge ratio
PA	=	proton affinity
pent	=	pentose sugar
r, R	=	radius
RP	=	reversed-phase
ZAB-R	=	BEE three-sector mass spectrometer

Chapter 1

Introduction

Carbohydrates play a key role in cell-cell adhesion, cell-substrate adhesion and cell mobility [1]. Most often, this role is realized via a class of biomolecules named glycoconjugates, which include triterpene glycosides, glycoproteins (and glycopeptides), glycolipids, and lipopolysaccharides. The cell-cell adhesive properties, which carbohydrates bestow onto invasive organisms such as parasites, accommodate the parasite's 'silent' entrance into the host [2]. This is one (important) reason to develop methods for structural characterization of sugars (and their conjugates) and thus derive structure/function relationships.

One important (biological) source of sugars and glycoconjugates are root extracts. The analysis of sugars from this source presents quite a challenge. Root extracts contain different types of sugars and glycoconjugates, each at different concentrations. However, they also contain a myriad of other components in addition to the compounds of interest, which may be potential interferences. Therefore, the method chosen for their characterization requires that it be sensitive as well as selective.

Sugars present a complex structural problem [3] because they form linear structures, as well as branching structures from any of the free hydroxyl groups on the ring. A complex problem is usually made more manageable by breaking it down into smaller parts. Mass spectrometry is an analytical tool that

accomplishes this task. Mass spectrometric analysis provides molecular mass, expressed as the mass-to-charge (m/z) ratio, and structural information. In addition, the sensitivity and selectivity accessible with mass spectrometry, relative to conventional techniques for analyzing sugars, has fostered increased interest in its use to probe the structure of sugars.

It is well-known that metal ions form complexes with carbohydrates. The formation of adducts between sugars (or glycoconjugates) and specific complexing agents, e.g., metal ions, are one way by which these compounds are analyzed by mass spectrometry. The principles upon which metal ions complex to sugars reside in the field of coordination chemistry. Descriptions of these principles are given in section 1. In general, metal ion complexation has been used advantageously in mass spectrometric analysis of a number of compounds including sugars [4]. Structural information obtained from mass spectrometric analyses of metal ion adducts of sugars includes molecular mass, linkage and sequence information. This information is obtained from cross-ring and glycosidic bond cleavage; see section 5.iii.

Traditional mass spectrometric analysis of sugars involved derivatization prior to analysis. These analyses employed electron ionization (EI) and chemical ionization (CI) mass spectrometry. In *general*, EI [5] and CI [6] mass spectrometry provide complementary information; EI mass spectrometry provides structural information, whereas CI mass spectrometry provides molecular mass. There are two reasons for this. EI ionization produces odd electron ions, $M^{\bullet+}$, whereas CI produces even-electron ions, M^+. Since $M^{\bullet+}$ has an unpaired electron, it is less stable than M^+, which has all its electrons paired.

Additionally, the internal energy of ions generated by (the most commonly used) 70 eV electrons in EI ionization is larger than that of ions generated by CI. Therefore, $M^{\bullet+}$ ions have more energy available for fragmentation relative to M^{+} ions generated by CI. Nevertheless, molecular mass information may be obtained from EI experiments employing low-energy electrons. These experiments generate $M^{\bullet+}$ ions containing less internal energy, and which have access to fewer fragmentation pathways relative to $M^{\bullet+}$ ions formed from 70 eV electrons.

Ionization techniques based on field-induced and energy-sudden mechanisms [7], have revolutionized mass spectrometric analysis of sugars. These ionization methods seldom require that the sugar be derivatized prior to analysis. Electrospray ionization (ESI) [8] and matrix-assisted laser desorption ionization (MALDI) [9] are two techniques which do not require derivatization of the sugar or glycoconjugate prior to analysis.

Structural analysis of sugars and triterpene glycosides using ESMS and tandem mass spectrometry techniques, comprise a major part of the work described in this thesis. One project using MALDI mass spectrometry of a class of polymeric sugars, the carrageenans, is presented. Additionally, in light of the fact that gas-phase chemistry contributes to the ions generated by ES ionization [8] and MALDI [9], a small project on the alkylation reactions of N-ethyl- and N-methylaniline by iodomethane and iodoethane, respectively, is described.

Since CI, ES and MALDI generate even electron ions of biomolecules, e.g., sugars, the molecular mass of the analyte of interest is obtained, with minimal fragmentation. A brief overview of the ionization methods relevant to the

focus of the thesis is given in section 2. A fundamental description of these methods, and a report of their use in the analysis of sugars and glycoconjugates are provided in section 3.

When structural information is not readily obtained from the mass spectrum, tandem mass spectrometric (MS/MS) [10] techniques are employed. MS/MS techniques when done in conjunction with field-desorption and 'energy-sudden' ionization methods have provided a wealth of structural information on sugars and glycoconjugates. The instrumentation employed in the work presented in this thesis is described in section 4. MS/MS techniques are described in section 5, along with a discussion of its use to probe the structure of sugars.

As mentioned, analysis of carbohydrates and glycoconjugates from biological sources entails separation from complex matrices such as root extracts. In the field of separation science, high pressure liquid chromatography (HPLC) [11] is a powerful method for separating polar, non-volatile compounds such as sugars. The principles of liquid chromatographic separation, as well as its combination with mass spectrometry are described in section 6. This hybrid technique [12] has proved to be a powerful tool for the separation and structural analysis of polar, non-volatile, neutral compounds.

1. Coordination of metal ions to compounds containing multiple *O*-atoms

Of particular importance to the research presented in Chapter 2 to Chapter 6, inclusive, is complexation to molecules containing multiple *O*-atoms.

The complexing agents employed in these projects are metal ions, including oxovanadium (VO^{++}), and boric acid.

Chapter 2 discusses a method for the structural characterization of triterpene glycosides called ginsenosides. This method is based on metal ion complexation. Chapters 5 and 6 present two approaches to evaluate the structural relationship between hydroxyl groups in a compound. The theory of complexation of boric acid, and oxovanadium(IV) with sugars is discussed in Chapters 5 and 6, respectively. A brief overview of metal ion complexation is given here.

Oxygen plays a specific role in its chemical compounds, especially in its complexes [13]. The donor capacity of oxygen is of importance when it is complexed with a metal ion having accessible *d* or *f* orbitals, e.g., transition metal ions. The π-electrons in oxygen are 'donated' to the *d* or *f* orbitals forming π-donor bonds.

Another concept which is related to the binding strength of the *O*-atom with metal ions is the 'hard and soft acids and bases' principle [13b]. The principle states that "hard acids bind strongly to hard bases and soft acids bind strongly to soft bases" [13b]. Therefore, metal ions that are 'hard acids', e.g., the alkali metal ions and VO^{++} bind effectively with 'hard bases' such as R–OH, where R is an alkyl group. The borderline acids Ni^{++}, Co^{++}, Zn^{++} have also been employed in the work presented in Chapter 2.

Sugars are one class of compounds having multiple *O*-atoms [14a]. Only those isomers having suitably positioned hydroxyl groups can interact with metal ions. The stability of the complexes between carbohydrates and metal ions is

dependent on the orientation and number of the hydroxyl groups involved in forming the complex [14b,c]. In the case of cyclic monosaccharides, the *cis-cis* configuration is most favourable. This is accomplished by *pyranose* sugars having an axial-equatorial-axial orientation of the hydroxyl groups; see Scheme 1.i.a. With sugars in the *furanose* conformation, complexation occurs with two *cis* hydroxyl groups and the ring oxygen [14d], see Scheme 1.i.b.

It is likely that complexation of metal ions with carbohydrates takes place via a mechanism similar to that which occurs between crown ethers and metal ions [15].

a) M^+ binding in a hexopyranose b) M^+ binding in a hexofuranose

Scheme 1-1.i. Proposed interaction between a sugar and a metal ion

The fixed radius of the cavity of crown ethers makes them more suitable for selectively forming complexes with specific metal ions [15]. It is a well-known fact that 15-crown-5 binds Na^+ more efficiently than it does K^+ and that the converse is true for 18-crown-6. Thus, it is likely that the strength of the adduct formed between a metal ion and carbohydrates is influenced by the ionic radius of the metal. It has been reported that an ionic radius of ca. 1 Å [14c] is most suitable for forming a complex with sugars. Intrinsic Na^+ (ionic radius ~ 0.95 Å) is present in all common solvents and is difficult to replace or remove. Therefore, a Na^+ salt

is frequently used as an additive in mass spectrometry experiments based on metal ion complexation to *O*-atom containing compounds.

Traditional methods for investigating sugar-metal ion complexes in solution include potentiometry [16a] and nuclear magnetic resonance (NMR) spectroscopy [16b]. However, mass spectrometry has become increasingly important in this field. In general, analysis of sugar-metal ion complexes by mass spectrometry provides molecular mass. However, information about bond connectivity is also required.

It has been argued that complexation reactions are structure-specific [14b,c]. Therefore, the structure of the complex – between metal ions or boric acid and sugars – should provide information about the structure of the sugar. Since insufficient structural information is obtained from ionization techniques generating even-electron ions, tandem mass spectrometry (MS/MS) experiments (see section 5.ii.) on the metal-attachment ions and borate complexes are performed; see Chapters 2 to 6.

2. Brief overview of ionization methods in mass spectrometry

In an insightful statement, J.J. Thomson, one of the early pioneers in mass spectrometry described both its power and potential,

> "I feel sure that there are many problems in Chemistry which could be solved with far greater ease by this than by any other method. The method is surprisingly sensitive ... requires an infinitesimal amount of material and does not require this to be specifically purified..." [17].

Thomson's' work was followed by Dempster's [18] and Aston's [19]. In less than 100 years since these original experiments, there has been a multitude of

advances in mass spectrometry – including both instrumentation and ionization methods – enabling analysis of a range of structurally different compounds.

A large part of the research in mass spectrometry is governed by electron impact ionization (EI) [5] and chemical ionization (CI) [6]. Although both EI and CI accomplished analysis of some involatile and thermally labile compounds, the majority of mass spectrometric analyses, using EI and CI, are limited to volatile compounds. Moreover, there was increasing interest in mass spectrometric analysis of molecules with molecular mass larger than was routinely accessible with EI and CI. This demand was met with the implementation of ionization methods, which accomplish transfer of molecules directly from the condensed phase – liquid and solid – to the gas-phase.

These ionization methods are categorized as: 1) energy-sudden and 2) field-induced desorption/ionization methods [7]. These energy-sudden techniques may be considered as an extrapolation from Beuhler et al. [20]. These researchers have observed that *fast* desorption of peptides from the condensed phase resulted in minimal (thermal) decomposition. The rationale was that at high temperatures, the rate of vaporization surpasses the rate of thermal decomposition. Therefore, by rapidly achieving a high temperature in the vicinity of the (thermally labile) sample, vaporization would be favoured relative to decomposition. Ionization methods which are based on energy-sudden mechanisms are: desorption chemical ionization (DCI) [21] / electron impact (DEI) [22], plasma desorption (PD) [23], laser desorption (LD) [24], fast-atom bombardment (FAB) [25], and matrix-assisted laser/desorption ionization (MALDI) [9].

Field-induced desorption/ionization methods employ strong electrostatic fields to desorb and ionize analyte molecules. These methods are: field desorption (FD) [26], thermospray (TS) [27], and electrospray (ES) [8]. Mass spectrometric analysis of compounds with low volatility was improved by implementing energy-sudden or field-induced ionization methods. Descriptions of CI, FAB-MS, ES and MALDI are provided along with their use in the analysis of sugars. FAB-MS is not used in the work described in the thesis, but it has seen considerable use in the analysis of sugars and glycoconjugates.

3. Mass spectrometry of sugars and their conjugates

3.i. Structure characterization of sugars

Structural analysis of sugars requires determination of: a) molecular mass, b) ring conformation, i.e., *pyranose* versus *furanose*, c) the anomeric configuration, i.e., α versus β, d) linkage type, and e) the sequence of the sugar residues [28]. Methods of analyzing sugars, both glycones and aglycones include: size-exclusion chromatography; gas chromatography mass spectrometry; direct chemical ionization mass spectrometry; field desorption mass spectrometry; plasma desorption mass spectrometry; laser desorption mass spectrometry; fast-atom bombardment mass spectrometry (FAB-MS); and nuclear magnetic resonance spectroscopy. Brief overviews of the structural information obtained with CI, FAB-MS, ESI and MALDI are provided.

3.ii. Electron impact (EI) and chemical ionization (CI)

An electron ionization (EI) mass spectrum is a reflection of the process where a beam of ~70 eV electrons interacts with the analyte (M) [5]. The radical cations, $M^{\bullet+}$, thus generated have a range of internal energies. Therefore, the 70 eV EI mass spectra of quite a few compounds do not contain abundant, or in some cases even detectable molecular ions [5]. If this is the case, ionization techniques which produce even-electron ions may be used advantageously.

Protonation of the sample molecules, yielding $[M+H]^+$ions, was observed in EI mass spectra when high analyte pressures were employed [6]. The realization that these even-electron ions do not readily dissociate attracted the interest of researchers. In 1966, Munson and Field [6a] described the technique of chemical ionization mass spectrometry (CIMS). In CIMS, a reagent gas is introduced into the source at a pressure of ca. 1 Torr. The analyte is also introduced into the source, but at a pressure that is 10^3-fold less than the reagent gas. Since the reagent gas molecules are present in large excess relative to the analyte molecules, there is a much higher probability that the electrons ionize reagent gas molecules to form reagent gas ions.

The mechanism by which the analyte becomes ionized is dependent upon the analyte molecule, M, and the reagent gas, B [6b]. In general, the analyte molecule, M, becomes ionized via ion-molecule reactions with the reagent gas ion, BH^+ [6c]. One such ion-molecule reaction is proton transfer.

$$BH^+ + M \longrightarrow MH^+ + B$$

A common reagent gas, B, is CH_4, and the most abundant reagent gas ion in the CH_4 plasma is CH_5^+. For the purposes of this discussion, the analyte molecule

will be N-ethyl-N-methylaniline. In the proton transfer reaction between CH_5^+ and N-ethyl-N-methylaniline, the latter will abstract a proton from the reagent ion because its proton affinity (PA) is larger than that of CH_4, by about 90 kcal/mol [29].

The extent of fragmentation of protonated N-ethyl-N-methylaniline is dependent on its internal energy, which is (in turn) governed by the exothermicity of the proton transfer reaction. Thus, the gas-phase properties of the reagent gas are important for predicting or even directing the outcome of the CI experiment. If the PA values of the reagent ion and the analyte molecule are comparable, or if the PA of the reagent ion is larger than the PA of the molecule, an adduct ion between the sample and the reagent ion may form. These adducts also provide information about the molecular mass of the analyte.

A 'variation' of conventional EI and CI is based on (thermal) desorption of the sample. These techniques are named direct electron impact (DEI) [22] and direct chemical ionization (DCI) [21]. These procedures originated when it was observed that evaporation of the compound of interest close to the region of ionization reduced thermal degradation [30]. The compound to be analyzed is dissolved in a suitable solvent and placed on a direct insertion probe. The sample is desorbed by increasing the temperature of the probe tip at a prescribed rate. Involatile compounds are best analyzed by employing a high rate of increase of the temperature.

CI mass spectrometry of sugars with and without GC separation has been reviewed [31]. Although some underivatized sugars have been analyzed using CI, derivatization *improved* amenability of sugars to CI mass spectrometry.

The most widely used derivatives in CI mass spectral analyses of sugars are acetates and methyl- or trimethylsilyl-ethers [31]. Gas chromatography accommodated differentiation of isomeric sugars based on relative retention times, but even when the sugar was derivatized, CI did not always provide a molecular mass. This is, in part, a result of the instability of the derivative employed.

Analysis of sugars by DCI [32] has been more successful than CI. DCI analysis of sugars, both with [32f,g] and without [32a-d,e] derivatization, has been reported. Commonly used reagent gases for DCI experiments are methane, isobutane and ammonia. It was observed that ammonia DCI [32f] offers lower detection limits than methane or isobutane DCI. The fragmentation observed in DCI experiments provided molecular mass, sequence information, and to some extent, linkage information.

3.iii. Fast-atom bombardment (FAB)

Fast-atom bombardment mass spectrometry (FAB-MS) [25] is related to the techniques secondary ion mass spectrometry (SIMS) [33] and liquid SIMS (LSIMS) [33]. Chronologically, SIMS – referred to as 'static' SIMS – preceded FAB-MS, which in turn preceded LSIMS. In fact, the acronyms FAB-MS and LSIMS are used interchangeably. These two techniques differ because the former entails bombardment of the sample with atoms, while the latter technique employs ions.

FAB-MS involves bombardment of a film of analyte dissolved in a matrix, e.g., glycerol, by a beam of either Argon (Ar) or Xenon (Xe). The atoms have

translational energy in the keV regime. Collision between the sputtering agent, Ar or Xe, and the sample – the analyte plus matrix – results in transfer of sufficient energy to cause desorption of the sample.

There is no single ionization mechanism which can describe the formation of all the ions observed in a FAB mass spectrum. It was proposed that both gas-phase [35a,b] and solution-phase chemistry [35c] contribute to the ions observed in a FAB mass spectrum. Since FAB-MS analysis is performed on samples in the liquid phase, it is not surprising that correlations have been drawn between solution-phase chemistry and the ions observed in the FAB mass spectrum. The gas-phase reactions are presumed to occur in the region just above the sample surface; this region is referred to the 'selvedge' region. A gas-phase mechanism is proposed to be responsible for formation of adducts between the analyte molecules and metal ions [35d].

FAB-MS has been used for structure characterization of sugars [36]. Some underivatized sugars are amenable to analysis by FAB-MS. These sugars are observed as either the $[M+H]^+$ or $[M+metal]^+$ adducts [37]. Derivatization, including the methyl ether, acetate and permethylated alditol acetate [38], improved analysis of sugars by FAB-MS.

As described in the preceding sections, mass spectrometric analysis of sugars and glycoconjugates has been enhanced by the use of 'energy-sudden' and field-induced desorption techniques [7]. These techniques accommodate desorption and ionization of the analyte. Although FAB-MS is still being used for structural analysis of sugars and their conjugates, there are two major drawbacks to the method. Achievement of optimum sensitivity requires

derivatization prior to analysis, and a larger quantity of sample is required to obtain a mass spectrum with sensitivity comparable to ESMS or MALDI-MS.

At present, ESI [8], a field-induced desorption/ionization technique and MALDI [9], an energy-sudden desorption/ionization technique, are most frequently used to analyze sugars.

3.iv. Electrospray ionization (ESI)

Electrospray (ES) [8] is a method by which ions in the solution-phase are transferred to the gas-phase. ES is one ionization technique based on the principle of droplet charging; the others are TS [27] and ionspray (IS) [39]. Both ES and IS are techniques which employ an induced electric field to initiate droplet formation from the sample solution into an atmospheric pressure ionization source. TS ionization is the process where the sample solution is vapourized, without application of an externally applied electric field, before entry into a low-pressure ion source. This process requires addition of an electrolyte in order to enhance ionization efficiency.

The differences between IS and ES are: a) IS employs a sheath of nitrogen gas around the capillary through which the sample solution is delivered; and 2) the solvent flow rate in IS can be as high as 200 μL/min, whereas in ES it is not usually higher than about 20 μL/min. The Micromass Quattro LC ES mass spectrometer, used for the larger part of the Ph.D. work, is equipped with a capillary having a coaxial flow of N_2. However, the flow rate range employed was much lower (10 - 50 μL/min), than is employed in IS. The nebulizing gas provides some of the energy required to induce droplet formation, thus improving droplet

formation, and ionization efficiency of analyte molecules delivered at high solvent flow rates.

The progress of ES ionization may be divided into the period when it was being used for applications other than mass spectrometry, e.g., spray painting [40], and the period when it was being modified for the purposes of mass spectrometry. In ES, an aerosol of highly charged droplets is formed in the presence of an electric field. In an interesting coincidence, Zeleny et al. [41] reported this process about the same time as the pioneering work reported by Thomson [17], Aston [18], and Dempster [19].

Lenard [42a] explained that ES involves formation of an electric double layer of a liquid surface at an air boundary. This theory was supported by observations made by Coehn and Mozer [42b] and Chapman [43]. The latter researchers showed that charged droplets having diameters less than 10^{-6} cm are formed when a liquid surface is ruptured via bubbling and/or spraying. Investigations into improving the process of electrostatic painting showed that the rate of droplet formation increased as the electric field at the surface of the droplet [44]. In addition, Hines inferred that there is an interdependence of applied voltage, flow rate, electrical conductivity, viscosity, density and surface tension. These inferences were a prelude to fundamental investigations that were undertaken by researchers in the field of ESMS. These investigations, and the current state of ES, have been recently reviewed [8].

The pioneers of ESMS are Dole et al. [45a], Yamashita and Fenn [45b,c] and Aleksandrov et al. [45d]. At very similar times, these researchers independently reported the ESMS technique. The mechanism of ES may be

divided into three stages: 1) droplet formation, 2) droplet shrinkage, and 3) ion formation and transfer from atmospheric pressure to a vacuum. The value of the field at the capillary tip is given by E_C [46].

$$E_C = 2V_C/[r_C \ln(4d/r_C)]$$

where: V_C = applied potential, r_C = capillary outer radius, and d = distance from the capillary tip to the counter-electrode

The electric field at the tip of the capillary penetrates the surface of the solution. The field accommodates charge separation between unlike charges, as well as accumulation of ions with the same polarity – as the bias on the metal capillary – at the surface of the droplet. Since ions of the same polarity accumulate at the surface of the droplet, there comes a point when the electrostatic repulsion of these like charges overcomes the surface tension of the liquid. The surface of the liquid expands to form a Taylor cone [47].

The onset of ES - or the electric field, E_{ON}, which leads to instability of the Taylor cone - is satisfied by the equation given by E_{ON} [48].

$$E_{ON} = (2\gamma\cos\phi/\varepsilon_O r_C)^{1/2}$$

where: γ = surface tension, ϕ = half-angle of the Taylor cone, ε_O = permittivity of vacuum and r_C = radius of the capillary

The potential (applied to the capillary) which is required for the onset of ES is given by V_{ON} [48].

$$V_{ON} = (r_C\gamma\cos\phi/2\varepsilon_O)^{1/2} \ln(4d/r_C)$$

Every parameter in this equation is the same as in the previous equation. These two equations include a term for the surface tension, γ, of the solvent. This illustrates that the surface tension of the solvent is important in determining the

voltage required for the onset of ES. It is observed that lower onset voltages are required for acetonitrile relative to water. This is in direct correlation with the surface tension of these two solvents because water has a higher surface tension than acetonitrile. Therefore, it is more difficult to 'pull' or 'distort' the surface of water relative to acetonitrile.

Once the initial droplet separates from the capillary, the hot drying gas induces evaporation of the solvent in the droplet. Desolvation of the droplets results in an increase in repulsion between like charges. This results because the charges on the droplet are closer to each other. When the electrostatic repulsion exceeds the surface tension, the droplet "explodes". The phenomenon is referred to as Coulomb explosion [7]. This model entails solvent evaporation from the charged droplets until the charge density increases to the Rayleigh limit [49]. At this point, electrostatic repulsion surpasses surface tension and the parent droplet breaks into smaller droplets.

$$q_{Ry} = 8\pi(\varepsilon_O \gamma R^3)^{1/2}$$ - the Rayleigh limit

To date, there are two models for the escape of ions from the charged droplets. Dole et al. [45a], including Hines, proposed the charged-residue mechanism for ES. The charged-residue model suggests that Coulomb explosions continue until there is only one ion per droplet. Iribarne and Thompson [50] proposed the ion evaporation model. In this model, there is desolvation until the droplet is 10-20 nm large, at which time the ions in the droplet may evaporate and be mass analyzed. The limitations of both models have been addressed in the first chapter of Reference 8a. Descriptions of droplet

formation, droplet disintegration and desolvation, as well as the escape of ions were given. Figure 1-1 shows a representation of the ES process.

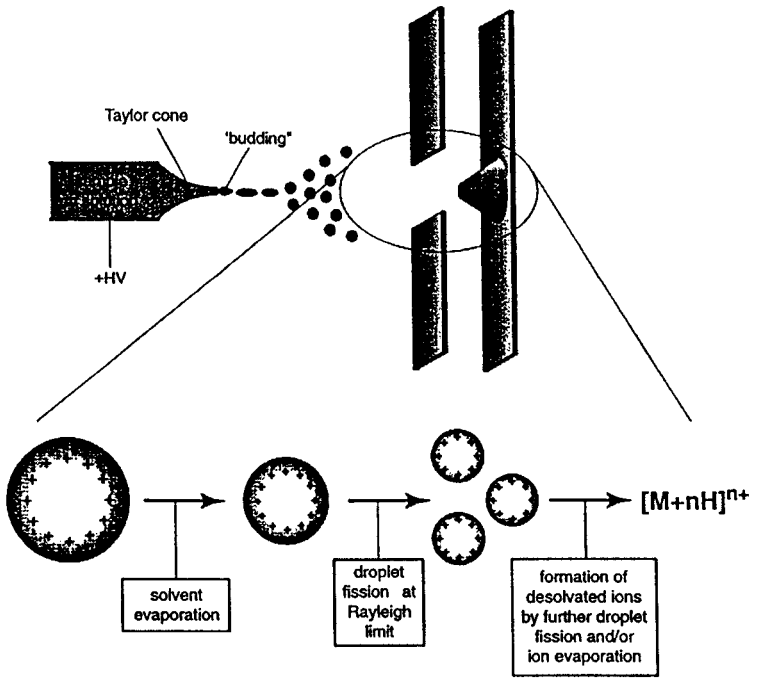

Figure 1-1. Droplet production in the electrospray interface. Reprinted with permission from S.J. Gaskell, *J. Mass Spectrom.*, **1997**, *32*, 677. © John Wiley and Sons Limited. Reproduced with permission.

As mentioned, desorption of pre-formed ions is one mechanism by which ions are transferred from the solution-phase to the gas-phase in FAB. This is also the case for ES ionization. A review of the contribution of solution- and gas-phase chemistry to the ions observed in an ES mass spectrum has been prepared [8d]. Some of these processes are discussed here.

3.iv.a. Contribution of gas-phase chemistry to ESMS

Fenn and co-workers observed that aqueous solutions of proteins are observed as multiply protonated ions by ESMS [51a]. This characteristic of

proteins makes them suitable models for investigating the effect of *gas-phase* reactions, under ESI conditions, on the formation of multiply protonated protein ions [51b]. The hypothesis is as follows. If the ES mass spectrum of a protein reflects its gas-phase chemistry, then reacting a base with the protein in the gas-phase will result in the protein appearing at a mass-to-charge (m/z) ratio, that is, at higher mass (lower charge state), relative to when no base is added. McLuckey et al. [51b] observed a reduction in the charge state of cytochrome c when dimethylamine was present in the gas-phase. The presence of a proton-bridged complex between cytochrome c and dimethylamine provided evidence for a mechanism whereby dimethylamine de-protonates a multiply charged cytochrome c ion.

Kebarle et al. [52] also obtained evidence for the contribution of gas-phase reactions to the appearance of an ES mass spectrum. In their study, an equimolar mixture of a pair of hydrochloride salts of bases, having different gas-phase proton affinity (PA) values were analyzed by ES. These ionic compounds are suitable models for studying gas-phase reactions in ES ionization because their formation is not dependent on solution-phase protonation. The authors observed that the $[M+H]^+$ ion corresponding to the base with higher PA was more intense than that of the other base. These investigations provide evidence that gas-phase reactions contribute to the ions observed in an ES mass spectrum.

3.iv.b. Contribution of solution-phase chemistry to ESMS

The previous section provided a discussion about the contribution of gas-phase chemistry to the types of ions appearing in an ES mass spectrum. There

have also been studies which investigate the relationship between solution-phase chemistry and the ions observed in an ES mass spectrum. The formation of complexes in solution, have traditionally been studied using condensed-phase techniques such as titration [53]. However, the low energy imparted to ions generated by ES ionization makes it a suitable technique for analyzing complexes formed in the solution-phase.

Investigating the relationship between solution-phase chemistry and the ions observed in an ES mass spectrum have included: a) the influence of solvent polarity on the ES response of the analyte dissolved in it; b) the effect of analyte concentration on its ES response; c) the effect of ion-pairing on the ES response of the analyte; d) the solution-phase equilibrium of complexes formed in the solution-phase, and their transfer to the gas-phase; and e) the pH of the solution. Point d) is important to the work presented in this thesis.

Complexation reactions are the basis of the work described in Chapters 2 to 6, inclusively. Competing reactions affect the solution-phase equilibrium of non-covalent, as well as covalent complexes. As competing reactions deplete the complexed species in solution, it is expected that there is a concomitant decrease in the intensity of the ion corresponding to the complex of interest.

There are a few tenets which should be considered when differentiating between complexes formed as an artefact of the desolvation process, and complexes originating in the solution-phase [54]. The subject of these tenets is to differentiate between specific and non-specific interactions. If the interface conditions are adjusted so that the intensity of the ion corresponding to the complex dominates the intensity of the dissociated species, then the complex

resulted from the solution-phase. If changing the components of the complex changes the intensity of the ion corresponding to the complex relative to its components, then the complex is derived from the solution-phase.

It is clear that between the time that an initially neutral sample solution is pumped into the ES capillary, and the moment that the ions are displayed on the monitor, a complex series of events has occurred. These events include both gas-phase and solution-phase reactions. The relative contribution from these reactions to the ions observed in an ES mass spectrum is not known and will probably vary with the analyte.

A major part of the thesis describes the use of ESMS for structural analysis of complexes formed with sugars and ginsenosides. The complexing agents employed are metal ions, including VO^{++}, and boric acid. Analysis of sugar-metal ion complexes [55] by ES has been reviewed. A review of boric acid, and VO^{++} complexation to sugars is given in the introductory pages to Chapters 5 and 6, respectively.

3.v. Matrix-assisted laser desorption ionization (MALDI)

Laser desorption (LD) [24] is the process where laser pulses from 10^6 to 10^{10} W/cm^2 and pulsewidths in the range 1-100 ns, are focussed onto a sample plate. The sample is irradiated with laser wavelengths either in the infrared (IR) or the ultraviolet (UV) range. One drawback of this technique is that laser beam irradiation of the sample results in sample decomposition. The radiation damage to the sample results in a reduction in sensitivity. Furthermore, it was observed

that if the sample is dissolved in a matrix before analysis [9d], then the sensitivity of this ionization method increases.

Laser desorption from solid samples wherein the analyte is interspersed in a matrix is called matrix-assisted laser desorption ionization (MALDI) [9]. The matrix is present in 10^3:1 excess relative to the analyte. The two common structural features of MALDI matrices are the presence of: 1) a chromophore, and 2) functional groups which can form hydrogen bonds. The matrix has a chromophore and is present in large excess relative to the analyte. Therefore, the matrix absorbs a large part of the laser's energy. Relative to LD, MALDI reduces radiation damage of the analyte. Nevertheless, between MALDI and ES, the former imparts more energy to the analyte. This is evidenced by the phenomenon referred to as post-source decay (PSD) [56]. This term refers to the phenomenon where ions dissociate en route to the detector.

The status of MALDI-MS has been reviewed [9c]. The article encompasses the factors influencing the MALDI process. These factors include laser wavelength and pulse width, and matrix identity [57]. As with laser desorption mass spectrometry, wavelengths at both the infrared (IR) and ultraviolet (UV) wavelengths have been used in MALDI experiments. While there is less fragmentation in IR-MALDI mass spectra, the *general* appearance is similar to that obtained with UV-MALDI [58].

There are a number of proposed mechanisms for the formation of ions by MALDI [9c]. These mechanisms are characterized as primary and secondary processes. One combination of primary and secondary mechanisms is presented. The energy available from irradiation with a N_2 laser at 337 nm is

about 4 eV. The ionization energy of a typical organic molecule is approximately twice this value. Therefore, a mechanism which can accumulate the energy absorbed by the laser is required. Such a mechanism may be fulfilled via pooling the energy [59] from adjacent excited matrix molecules; see Scheme 1.ii. This is a reasonable assumption because the matrix is present in large excess relative to the analyte. Thus, there is a high probability of finding two excited matrix molecules adjacent to each other.

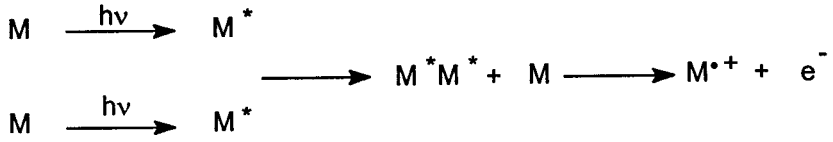

Scheme 1.ii. A schematic for an energy-pooling mechanism between excited matrix molecules.

As described for FAB and ES, solution-phase chemistry is accompanied by secondary reactions in the gas-phase. These chemical ionization-type reactions are inferred from comparative MALDI mass spectra obtained using 2,5-dihydroxybenzoic acid (DHBA), and 2,5-dimethoxybenzoic acid [60]. The ratio of the intensity of $[M+H]^+$ to $M^{\bullet+}$ is less for 2,5-dimethoxybenzoic acid, relative to DHBA. Therefore, the hydroxyl protons are the major suppliers of the proton in protonated DHBA. These observations support a gas-phase mechanism for protonation. In the same vein, it has been proposed that metal ion attachment occurs in the gas-phase [61].

The pulsed nature of MALDI required that it be coupled to a mass analyzer which can record the entire mass spectrum at any one time. The time-of-flight (TOF) [62] mass analyzer accomplishes this task. A more detailed description of this mass analyzer is given in section 4.ii. The ions generated by

MALDI and which are subsequently accelerated into the TOF mass analyzer, have both velocity and spatial distribution. One method of reducing velocity distribution is delayed extraction (DE). This technique not only improves mass resolving power, but also improves the instrument's sensitivity for detecting fragmentations reactions; see the discussion below.

Carbohydrate analysis by MALDI-MS has recently been reviewed [63]. The review discussed MALDI-MS of free sugars as well their conjugates. In general, positive ion MALDI-MS of oligosaccharides yielded the $[M+Na]^+$ ion. The MALDI mass spectrum of sugars also provides structural information. Different types of fragmentation reactions occur at specific rates. The ion corresponding to loss of CO_2 (from uronic acids) may be identified by prompt extraction. Additionally, it was observed that cross-ring cleavages are detected by prompt extraction. These fragmentations provide linkage information. By contrast, glycosidic cleavages require more time to occur, thus these fragmentations are more easily observed using delayed extraction. These bond cleavages provide sequence information.

4. Mass Analyzers: Instrumentation used in this work

Several forms of mass analyzers exist. These include the magnetic sector analyzer (double-focussing instruments), the time-of-flight mass analyzer, and the quadrupole mass filter. A triple quadrupole mass spectrometer, a (MALDI) time-of-flight mass analyzer, and a double-focussing instrument are used in the experiments described in the thesis.

4.i. Magnetic and electric sector instruments

The alkylation reactions of N-ethyl- and ring-ethylanilines with iodomethane, and N-methylaniline and the toluidines with iodoethane were done on a VG Analytical ZAB-R mass spectrometer; see Figure 1-2.

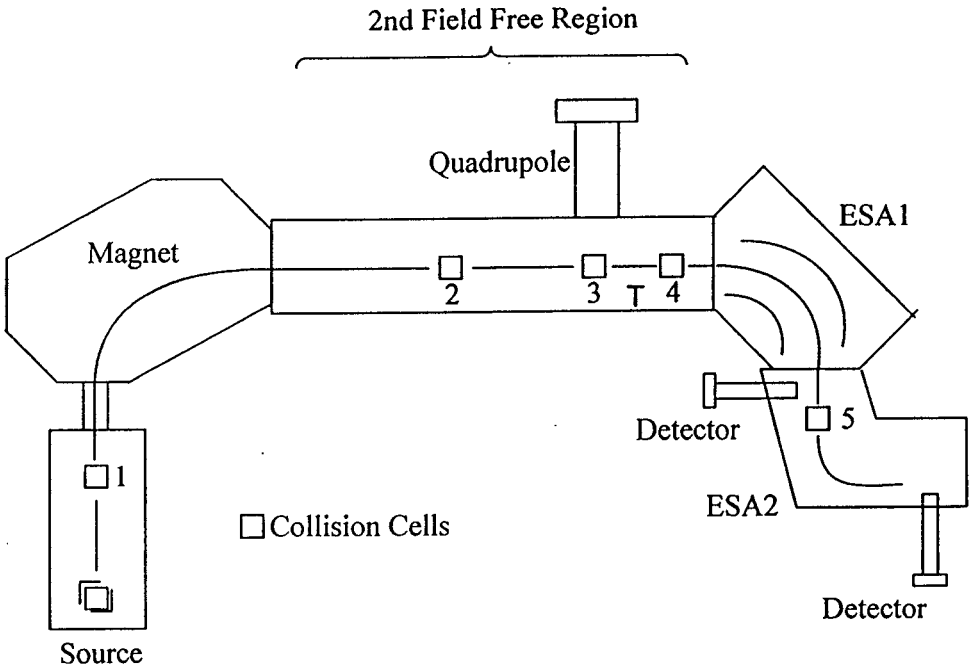

Figure 1-2. Schematic diagram of the VG Analytical ZAB-R instrument.

The alkylation products generated in the ion source are extracted by means of a repeller electrode located in the ionization chamber. As the ions exit the source, they are accelerated by application of a potential difference, 6-8 kV. The fall in potential energy is equal to the gain in kinetic energy or translational energy and is given by, $zeV = \frac{1}{2} mv^2$. In this equation, m is the mass of the ion, v is its

terminal velocity, e is the charge of a single electron and z is the charge of the ion. Therefore, ions possessing the same charge will also have the same kinetic energy.

The ZAB-R instrument is a double-focussing instrument which has the geometry, BE_1E_2 (B = magnetic analyzer, E = electric sector). Double-focussing instruments have both direction and velocity focussing. These instruments may either have forward or Nier-Johnson geometry [64], EB, or they may have reversed geometry, BE, such as the ZAB-R.

In a magnetic sector analyzer, the ion travels a path of radius, r, through a magnetic field, B, and velocity, v. The magnetic field deflects the ions in a curved trajectory. The motion of the ion is described by, $mv^2/r = Bzev$. This equation describes the balance between angular momentum and the centrifugal force caused by the field, B. The equation shows that the smaller ions are deflected to a greater extent than the larger ions. It is on this basis that mass analysis occurs. Rearranging the equation, $mv^2/r = Bzev$, to the form, $mv = Bzer$, illustrates that the magnetic sector is a momentum analyzer. The overall equation which describes the operation of a magnetic sector analyzer is given by, $m/z = B^2r^2e/2V$, where V is the accelerating voltage.

The ZAB-R is comprised of two electric (E) sectors. The ions in an electrostatic analyzer (ESA) experience an electric field which coerces them to travel a circular path. The path an ion travels is dependent on a balance between the electrostatic force acting on it and the centrifugal force. The motion of the ions is described by: $mv^2/r = ezE$, where r is the radius of the ion path in the electric sector, E is the field strength of the ESA, and the other parameters are

as defined for the magnetic sector analyzer. Therefore, the radius of the path travelled by the ion is dependent on its energy and not its mass.

4.ii. Time-of-flight instruments

In 1946, Stephens [62a] introduced time-of-flight (TOF) mass spectrometry [62]. Ions are separated based on their different arrival times at the detector. The arrival time of an ion is dependent upon its mass, which is in turn dependent on its velocity; $t = (m/2zeV)^{1/2}L$, where V is the acceleration voltage and L is the flight path length.

In short, the entire mass spectrum is obtained in every single cycle of the measurement without the need for scanning voltages or currents. As such, the TOF mass analyzer is suited with ionization methods which produce ions in bursts of pulses. These ionization methods include MALDI. Furthermore, because of the use of few ion optical elements, there is higher transmission of ions relative to other mass analyzers.

One drawback of the early TOF instruments is their low achievable resolution. This results from the fact that there is spatial, temporal, and velocity distributions of the ion population. Techniques have been implemented to reduce the contribution from each of spatial, temporal, and velocity distribution of the ions, but few that address them simultaneously. The development of time-lag focussing [65a], a reflecting electrostatic field (reflectron) [65b,c], and orthogonal acceleration [65d] were key stages in improving the resolution achievable with TOF instruments.

Time-lag focussing [65a] imposes a time delay between ion formation and ion extraction. The time delay accommodates re-aligning of the ions according to their kinetic energies. However, the required time delay is specific for ions of different mass.

The resolution that may be reached with TOF instruments was increased with the advent of the reflectron [65b,c]. This ion mirror reduces the spatial and velocity distribution of the ions. The reflectron decelerates ions and then re-accelerates them in the reverse direction before detection. The idea is that, for ions of a specific mass, the ones with higher kinetic energy penetrate deeper into the reflection field than the slower moving ions. Therefore, by the time the ions arrive at the detector, they would be detected at the same time.

Off-axis TOF mass spectrometry of ions from continuous ion-beams was known in the 1960s [65c]. The design was used to couple TOF mass spectrometry with an atmospheric pressure source. In the late 1980s [65e], orthogonal acceleration was described as a specific method for introducing ions into a TOF mass spectrometer. This technique provides simultaneous correction for velocity and spatial ion dispersion.

It is now common that commercially available TOF mass spectrometers are fitted with a reflectron. Researchers at Micromass Ltd. (United Kingdom) [62g] have reported that the MH^+, m/z 1758.933, of renin substrate was resolved to 4000.

The TOF instrument used for the MALDI experiments presented in Chapter 4 is a Bruker Reflex II instrument. It is equipped with a reflectron mirror.

4.iii. Quadrupole instruments

Paul [66a] invented the quadrupole mass filter. Dawson [66b] described the theory of operation of the quadrupole mass filter. These mass analyzers are compact, accommodate fast scanning, and the source operates close to ground potential. The latter characteristic makes for easy application of quadrupoles as the mass analyzer in hybrid techniques such as liquid chromatography / mass spectrometry; see Section 6.

The quadrupole mass filter is comprised of four parallel rods. The rods in the quadrupole assembly are arranged such that opposite rods, in the x-y direction, are electrically connected. Therefore, a two-dimensional quadrupole field is generated in the x-y direction. Ions enter and travel in the z-direction; see Figure 1-3.

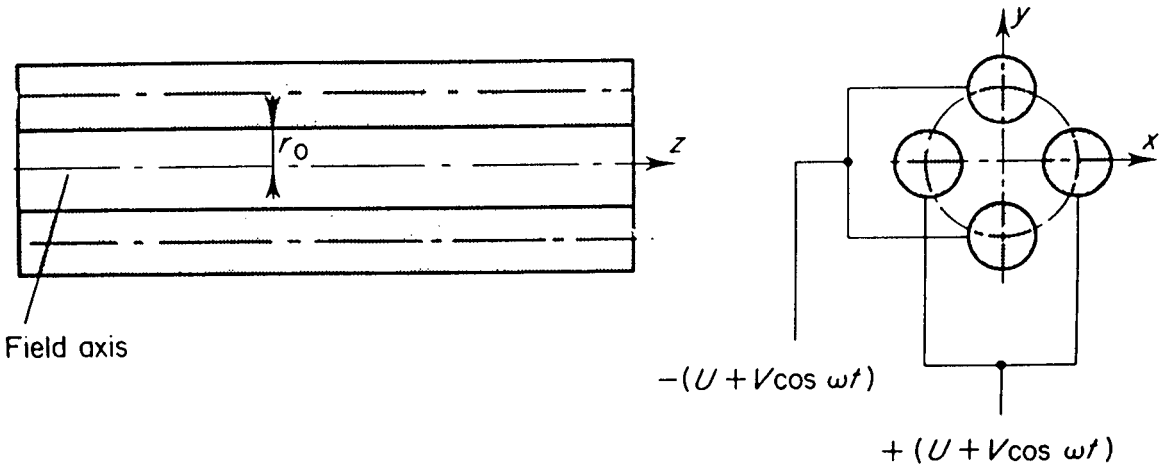

Figure 1-3. Schematic of the rod assembly in a quadrupole mass analyzer. (The schematic on the right shows four circles which represent the front face of the rods.)

The field is established by application of a radio-frequency (RF), V, and a DC, U, potential to the rods of the quadrupole assembly. The applied voltage, ϕ, is given

by, $\phi_{x\text{-}z} = +(U+V\cos\omega t)$, and $\phi_{y\text{-}z} = -(U+V\cos\omega t)$, where ω is the angular frequency of the RF potential.

Mass scanning is accomplished by increasing the values of the RF (V) and DC (U) voltages while maintaining a constant ratio of the two. The ions oscillate in the x-y plane due to the potentials applied to the rods. The oscillation is a property of the mass-to-charge (m/z) ratio of the ions. Therefore, the mass filters separate ions directly, i.e., by their m/z ratio.

The two potentials have different effects on ions with different mass. The x-z direction is considered a high-mass pass filter and the y-z direction a low-mass pass filter. In practice, setting the appropriate mass range implies that a certain ratio of RF to DC is set. The values of these voltages are such that they correspond to the low end of the mass range. During the experiment, the RF and DC voltages are increased to maintain the initial ratio while scanning to the high end of the prescribed mass range.

The ions have stable trajectories over a range of values for U and V. These values are obtained by solving the Mathieu equation [66b],

$$\frac{d_2u}{d\xi^2} + (a_u - 2q_u\cos 2\xi)u = 0$$

In this equation, u is a dimensionless parameter and represents the Cartesian x, y, and z coordinate axes in the quadrupole mass filter. The trapping parameters a_u and q_u are also dimensionless and they relate the ions having stable trajectories, with U and V.

$$a_x = -a_y = \frac{8eU}{mr_o^2\omega^2} \qquad q_x = -q_y = \frac{-4eV}{mr_o^2\omega^2}$$

The work described in Chapters 2-6 is performed on a Micromass Quattro LC triple quadrupole instrument. Although it is referred to as a triple quadrupole only the first and third quadrupoles are mass analyzers. The second quadrupole is operating in RF-only mode and is the collision cell; see Section 5.

5. Dissociation of Ions

5.i. Unimolecular Dissociation

Ions generated via 70 eV electrons have a range of internal energies [5c,d]. This means that there are ions which may have sufficient energy to dissociate (unimolecularly) in the source, or en route to the detector. If these dissociations occur in the field-free region of the instrument, then the dissociation products are focussed and detected as 'metastable ions' [5d].

Metastable ion (MI) mass spectra can only be obtained on sector instruments having reversed-geometry. The precursor ion is selected with the magnetic sector, while the electric sector is scanned for the dissociation products.

5.ii. Tandem Mass Spectrometry

Tandem mass spectrometry (MS/MS) is a technique which delineates bond connectivity within a molecule [5d,10]. A term that is used synonymously with MS/MS is collision-induced dissociation (CID). In general, CID involves two stages that are temporally separated.

These stages are represented by the following equations.

$$M_1^+ + N \rightarrow M_1^{+*} + N'$$
$$M_1^{+*} \rightarrow M_2^+ + M_3$$

where: M_1^+ = precursor ion, N = collision gas, M_1^{+*} = excited precursor ion
M_2^+ = product ion, M_3 = neutral lost

The first equation represents collision between the mass-selected ion M_1^+ and the collision gas, N, to form excited M_1^{+*} ions and collision gas molecules with different translational energy, N'. The second equation represents dissociation of M_1^{+*} to the product ions, M_2^+ and the neutral M_3.

CID is used for providing structural information for the mass-selected ion when: a) its fragment ions are obscured by the presence of other compounds, or b) *it* is obscured by other ions generated from the matrix during ionization, or c) the ionization method chosen yields relatively few structurally diagnostic fragments. A brief overview of the instrumentation used for tandem mass spectrometry experiments is given.

As the acronym MS/MS implies, tandem mass spectrometry requires that there are two mass analyzers placed in tandem. The first MS/MS instrument comprised of a magnetic sector followed by an electric sector [5d,10a]. There are two (general) types of MS/MS instruments: a) those where the mass analyzers are arranged in tandem; and b) those capable of storing ions, e.g., the ion-trap [67a] and the ion cyclotron-resonance [67b]. Hybrid instruments, where different mass analyzers are combined, e.g., sector mass spectrometers and quadrupole mass filters, have also seen considerable use. Cooks et al. [68] built the first

hybrid instrument. It comprised of a magnetic sector (B), followed by an RF-only quadrupole (q), and finally a mass-analyzing quadrupole (Q).

When recording product ion scans [10e,f] using a triple quadrupole instrument, a precursor ion is selected in the first mass analyzer and then after collision in a radio-frequency (RF)-only quadrupole, the products of the collision process are mass-analyzed in the third quadrupole. In precursor ion scans [69], the first mass analyzer is scanned while the second is held at a fixed mass. In hybrid instruments, low-energy collisions are performed via decelerating the ions before they reached the collision cell. In these instruments, high-energy experiments are performed in the region between the ion source and the magnetic sector.

In general, high-energy CID experiments are performed on sector instruments while low-energy experiments are done on quadrupole instruments [10a]. The maximum amount of energy that may be imparted on an ion in a collision is given by the *relative* kinetic energy in the centre-of-mass coordinate system, E_{CM} [70a],

$$E_{CM} = E_{LAB}[(m_N + m_{ION})/m_N]$$

where: E_{LAB} = ion kinetic energy, m_N = mass of neutral, m_{ION} = mass of target ion

E_{LAB} can be directly related to the accelerating voltage employed. High-energy CID experiments are performed with E_{LAB} values in the kiloelectronvolt (keV) range, whereas in low-energy experiments E_{LAB} is less than 100 eV [70a]. With reference to the two stages of CID, excitation and re-distribution of internal energy, the first stage involves transfer of a fraction of E_{CM} into internal energy.

A fraction of the ion translational energy is converted into internal energy. The internal mode that is excited – vibrational versus electronic – is dependent on whether the interaction time between the ion and the neutral is comparable to the period of the internal mode [70]. When the interaction time between the neutral and the ion is short (10^{-14} s), as in high-energy experiments, electronic excitation occurs. Evidence that high-energy collisions are responsible for electronic excitation is obtained from comparative experiments with 50 eV EI mass spectra of a number of aromatic compounds [10b]. The internal energy deposition associated with keV CID experiments ranges from 1-10 eV, but the average is only a few eV [71a].

In the second stage of CID, re-distribution of internal energy, electronic excitation is re-distributed into vibrational-rotational excitation modes. Re-distribution of energy into vibrational-rotational modes ultimately leads to bond cleavage reactions. In keV CID mass spectra, fragmentation processes requiring large critical energies are observed. The latter is attainable because there is a high-energy tail (up to 10 eV) in the internal energy distribution.

Low-energy CID experiments (in an RF-only quadrupole) are characterized by multiple collisions between the neutral and the ion as well as a longer-lived collision complex. The interaction time (10^{-13} s) between the ion and neutral in low-energy collisions is comparable to the period of vibrational excitation. As with high-energy collisions, the average internal energy deposition is also on the order of a few eV [71b,c]. In contrast, there is no high-energy tail and the distribution of internal energy in low-energy CID is narrower than in keV CID. This means that although the molecular ion is often absent or of low

abundance in low-energy CID, fragmentation processes requiring a large critical energy are not observed. The latter processes are not accessible because there is no high-energy tail in the internal energy distribution curve.

High-energy CID experiments are presented in Chapter 7. These high-energy experiments are performed on the VG Analytical ZAB-R mass spectrometer by: a) mass-selecting the precursor ion with the magnet; b) colliding these ions with O_2 in the second field free region (see Figure 1-2); and c) acquiring the CID mass spectrum by scanning the first electric sector.

Low-energy CID experiments, < 100 eV, are presented in Chapters 2 to 6. These experiments are performed on a Micromass Quattro LC triple quadrupole mass spectrometer. The precursor ion is selected by the first quadrupole, which then undergoes collisions with Ar in the collision cell (the RF-only quadrupole), and finally, the third quadrupole acquires the product ion spectrum.

5.iii. Tandem mass spectrometry of sugars

A major part of the fundamental studies of tandem mass spectrometric analysis of sugars was done using FAB-MS [72] and ESMS [73]. The past ten years, witnessed an increase in the use of MALDI-MS in conjunction with post-source decay (PSD) and CID [63] for obtaining structural information on sugars and glycoconjugates.

Very soon after its inception, FAB-MS [25] became the method of choice for analyzing sugars [36]. As mentioned, both proton- and metal-attachment ions of sugars are formed under FAB-MS conditions. However, for the purposes of

this thesis, the focus will be on the metal ion adducts. In general, it has been found that FAB MS/MS on metal ion adducts of sugars reveal linkage information, sequence, and to a lesser extent branching information [72].

A select number of reports on ES MS/MS analysis of metal adducts of sugars is referenced [73]. These studies involved the analysis of sugar adducts with alkali metal ions [73a,b], alkaline earth metal ions [73c], and transition metal ions [73d-h]. These experiments provide information on sequence, linkage, branching, as well as ring size. It has also been shown that tandem mass spectrometry experiments of complexes formed between Zn (II)-triethyleneamine and sugars, provide the anomeric configuration [73g].

Structural analysis of sugars using MALDI-MS is becoming increasingly popular. Both PSD and CID experiments have been employed [63a]. The PSD experiments provided information on the sequence of sugars since *O*-glycosidic bond cleavage dominates. CID experiments on ions generated by MALDI were performed on a magnetic sector mass spectrometer fitted with a MALDI source, a collision cell, and an orthogonal time-of-flight mass analyzer [63b]. These experiments provided information on both the sequence and the linkage between sugar residues.

6. Hyphenated Techniques

The principles of chromatography were described by Michael Tswett [74a,b]. In general terms, it is the separation of a mixture into its components via differential partitioning between two phases. The distribution of a component

between the two phases is given by the distribution coefficient, $K = C_1/C_2$, where the subscripts represent the two phases and C the concentration [74c].

One type of chromatography is liquid chromatography (LC) [74c]. In this technique, both the analyte and the eluting or mobile phase are liquids. The phase to which the components of the mixture selectively partition is solid. High-pressure liquid chromatography (HPLC) [11] is performed at high pressures. Classical LC utilizes columns with inner diameters of 1 cm (or larger) and particles with diameters of 100 to 200 mm. HPLC is performed using more narrow columns, 1-10 mm, and particles with diameters of about 3-10 μm. The dimensions of the column provide increased pressure under which the separation takes place. The experimental design of HPLC systems provides more control over the separation than LC. The characteristics of HPLC instrumental designs which provide control of the separation include: 1) ease with which columns may be inter-changed; 2) control of the temperature of the column; 3) use of single, binary or ternary solvent composition; 4) gradient or isocratic elution; and 5) compatibility with a number of detector systems.

The composition of the mobile phase may either be constant (isocratic) throughout the separation, or it may change according to a prescribed gradient. A gradient elution is especially suited to analyzing a mixture that has widely separated chromatographic peaks, or a mixture which has components that are strongly retained to the stationary phase of the column.

The HPLC separation may either be normal phase or reversed-phase. The reversed-phase mode is used for separating mixtures of polar compounds. These compounds include pharmaceutical, environmental, and biologically active

compounds. A variety of applications exist due to the number of solvents and stationary phases that can be combined. The stationary phase of the columns used in reversed-phase (RP) HPLC is non-polar. The columns that are most often used in RP HPLC have their silica support derivatized with the alkyl chains $-C_{18}H_{37}$ and $-C_8H_{17}$. The solvents used in RP HPLC include H_2O, CH_3OH, and CH_3CN.

Detectors commonly employed in HPLC instruments include the ultraviolet diode array detector (UV-DAD), the fluorescence detector, refractive index (RI) detector, evaporative light-scattering detector (ELSD), and the mass spectrometer. The mass spectrometer is suited for analyzing compounds that do not fluoresce or that do not absorb UV light.

The mass spectrometer most frequently interfaced with HPLC instruments is equipped with an atmospheric pressure ionization source (API). The electrospray (ES) mass spectrometer, described in section 3.vii, is one API technique used as a detector for HPLC instruments. As mentioned, ESMS is a powerful method for analyzing neutral, polar, involatile, and thermally labile compounds.

The technique where an HPLC is combined with a mass spectrometer is referred to as liquid chromatography mass spectrometry (LC/MS) [8d,12d]. In addition to molecular mass and structural characterization, mass spectrometry accommodates detection with high sensitivity and high selectivity. Structural characterization and selectivity is improved with the technique liquid chromatography / mass spectrometry / mass spectrometry (LC/MS/MS). This technique is especially suited to analyzing compounds such as triterpene

glycosides, from complex matrices such as root extracts. Analysis of neutral sugars by LC/MS and LC/MS/MS requires a post-column additive [8a]. Since sugars from complexes with metal ions such as Na^+, its acetate salt is a suitable post-column additive.

7. Scope of the thesis

The main focus of the work described in this thesis is the development of mass spectrometry-based methods to characterize the structure of sugars and an important class of triterpene glycosides, the ginsenosides. Ginsenosides, the active constituents of the ginseng root, are complex molecules consisting of a triterpene core and one or more sugar moieties.

Chapter 2 describes a methodology based on electrospray mass spectrometry (ESMS) and subsequent collision experiments (MS/MS) to characterize ginsenosides via their complexes with alkali metal ions and the transition metal ions Co^{++}, Ni^{++}, and Zn^{++}. This work also describes the complementary structure information obtained from ESMS and MS/MS experiments on the de-protonated ginsenoside ion. The results presented in Chapter 2 show that substantial structure information can be obtained from such experiments on positive and negative ions.

The structure information that can be obtained concerns: i) the molecular mass; ii) the nature of the triterpene core; iii) the type of sugar (pentose, hexose, deoxyhexose) attached to the core; iv) the sequence of the sugar moieties; v) the points of attachment of the sugar to the core; and vi) the linkage between the sugar residues.

The methodology described in Chapter 2 is used to develop a separation and structure characterization procedure of ginsenosides in root extracts as well as 'over-the-counter' ginseng preparations. These experiments are described and discussed in Chapter 3. The LC/MS based analytical procedure led to the identification of eight ginsenoside standards in a mixture of ten. The ginsenoside mixture studied comprised three classes of isomers. Of these, a pair of isomeric ginsenosides of MW = 1078 Da co-eluted and could not be differentiated by MS/MS experiments. These ginsenosides are different in that one of the isomers contains a pentose sugar having all hydroxyl groups in a *trans* orientation, while the other features a pair of the pentose hydroxyl groups in the *cis* orientation.

The analysis of a root extract by the above procedure showed that ginsenosides with known structures can readily be identified. In addition, several new ginsenosides were found and characterized. Structure proposals for ten of these new compounds are presented.

Chapter 4 presents a study of a family of naturally occurring sulfated polysaccharides, the κ-carrageenans. The techniques of ES and MALDI (matrix-assisted laser desorption/ionization) mass spectrometry were used, in conjunction with alkali metal ion exchange reactions, to probe the structure analysis of these compounds.

From the work described in Chapters 2 and 3, it became clear that isomeric ginsenosides whose only structural difference concerns the nature of the sugar moiety cannot be differentiated by MS/MS experiments. The work described in Chapters 5 and 6 deals with two new approaches for differentiating

stereoisomeric polyols and geometric isomeric sugars based on selective complexation to boric acid or oxovanadium(IV).

Finally, in Chapter 7, results are presented of a brief study of the protonation and alkylation of a series of model compounds, the N-alkylated anilines, in both the condensed phase and the gas-phase. This project is not immediately related to the analytical method development described in the previous Chapters. However, the key ionization method of the thesis, electrospray mass spectrometry, involves both solution- and gas-phase chemistry. Thus, the results of this Chapter may serve to gain a better understanding of the behaviour of ions in the condensed phase versus the gas-phase.

References

[1] a. T.A. Springer, *Nature*, **1990**, *346*, 425. b. L.A. Laskey, *Science*, **1992**, *258*, 964. c. S. Ratner, *Invasion Metastasis*, **1992**, *12*, 61.

[2] P. Velupillai, D.A. Harn, *Proc. Natl. Acad. Sci. USA*, **1994**, *91*, 18.

[3] R.A. Laine, *Glycobiology*, **1994**, *4*, 759.

[4] L.M. Teesch and J. Adams, *Org. Mass Spectrom.*, **1992**, *27*, 931.

[5] a. A.J. Dempster, *Phys. Rev.*, **1921**, 18, 415. b. A.O. Nier, *Rev. Sci. Instrum.*, **1947**, 18, 398. c. F.W. McLafferty and F. Tureček, *Interpretation of Mass Spectra*, 4th Ed., University Science Books, California, **1993**. d. R.G. Cooks, J.H. Beynon, R.M. Caprioli and G.R. Lester, *Metastable Ions*, Elsevier Scientific Publishing Company, Amsterdam, **1973**.

[6] a. M.S.B. Munson and F.H. Field, *J. Am. Chem. Soc.*, **1966**, *88*, 2621. b. M.S.B. Munson, *Int. J. Mass Spectrom.*, **2000**, *200*, 243. c. A.G. Harrison, *Chemical Ionization Mass Spectrometry*, 2nd Ed., CRC Press, London, **1997**.

[7] J.B. Fenn, M. Mann, C.K. Meng, S.F. Wong and C.W. Whitehouse, *Mass Spectrom. Rev.*, **1990**, *9*, 37.

[8] a. R.B. Cole, *Electrospray Ionization Mass Spectrometry Fundamentals, Instrumentation and Applications*, John Wiley & Sons, Inc., New York, **1997**. b. R.B. Cole, *J. Mass Spectrom.*, **2000**, *35*, 763. c. P. Kebarle, *J. Mass Spectrom.*, **2000**, *35*, 804. d. G. Wang and R.B. Cole, Solution, Gas-phase, and Instrumental Parameter Influences on Charge-state Distributions in Electrospray Ionization

Mass Spectrometry. In: *Electrospray Ionization Mass Spectrometry Fundamentals, Instrumentation and Applications*, R.B. Cole, (Ed.), John Wiley & Sons, Inc., New York, **1997**, p137.

[9] a. K. Tanaka, H. Waki, Y. Ido, S. Akita, Y. Yoshida and T. Yoshida, *Rapid Commun. Mass Spectrom.*, **1988**, *2*, 151. b. M. Karas and F. Hillenkamp, *Int. J. Mass Spectrom. Ion Proc.*, **1987**, *78*, 53. c. R. Zenobi and R. Knochenmuss, *Mass Spectrom. Rev.*, **1998**, *17*, 337. d. L.G. Wright, R.G. Cooks and K.V. Wood, *Biomed. Mass Spectrom.*, **1985**, *12*, 159.

[10] a. K.L. Busch, G.L. Glish and S.A. McLuckey, *Mass Spectrometry/Mass Spectrometry: Techniques and Applications of Tandem Mass Spectrometry*, VCH Publishers, Inc., New York, **1988**. b. K.R. Jennings, *Int. J. Mass Spectrom. Ion Phys.*, **1968**, *1*, 227. c. J.H. Beynon, R.M. Caprioli and T. Ast, *Int. J. Mass Spectrom. Ion Phys.*, **1971**, *7*, 88. d. P.F. Bente III and F.W. McLafferty, Analytical Applications of Two Dimensional Mass Spectrometry. In: *Mass Spectrometry*, V3 PtB, C. Merrit Jr. and C.N. McEwen (Eds.), Marcel Dekker, Inc., New York, **1980**, p253. e. R.A. Yost and C.G. Enke, *J. Am. Chem. Soc.*, **1978**, *100*, 2274. f. R.A. Yost and C.G. Enke, *Anal. Chem.*, **1979**, *51*, 1251A. g. K. Levsen and H. Schwarz, *Mass Spectrom. Rev.*, **1983**, *2*, 77.

[11] L.R. Synder, J.J. Kirkland and J.L. Glajch, *Practical HPLC Method Development*, 2nd Ed., John Wiley & Sons, Inc., New York, **1997**.

[12] a. M.L. Vestal, *Methods Enzymol.*, **1990**, *193*, 107. b. F.A. Mellon, *VG Monographs*, **1991**, *2*, 1. c. E. Gelpi, *J. Chromatogr. A*, **1995**, *703*, 59. d. R.D. Voyksner, Combining Liquid Chromatography with Electrospray Mass Spectrometry. In: *Electrospray Ionization Mass Spectrometry Fundamentals, Instrumentation and Applications*, R.B. Cole, (Ed.), John Wiley & Sons, Inc., New York, **1997**, p323.

[13] a. B. Jezowska-Trzebiatowska, The Role of Oxygen in Coordination Compounds. In: *Theory and Structure of Complex Compounds*, B. Jezowska-Trzebiatowska (Ed.), Wydawnictwa Naukowo-Techniczne, Warsaw, **1964**, p1. b. T.-L. Ho, *Hard and Soft Acids and Bases Principle in Organic Chemistry*, Academic Press, New York, **1977**.

[14] a. J.F. Robyt, *Essentials of Carbohydrate Chemistry*, Springer-Verlag New York, Inc., New York, **1998**, p48. b. U. Piarulli and C. Floriani, *Prog. Inorg. Chem.*, **1997**, *45*, 393. c. J.-F. Verchere, S. Chapelle, F. Xin and D.C. Crans, *Prog. Inorg. Chem.*, **1998**, *47*, 837. d. S.J. Angyal and R.J. Hickman, *Aust. J. Chem.*, **1975**, *28*, 1279.

[15] F. Vögtle and E. Weber, *Host Guest Complex Chemistry Macrocycles Synthesis, Structures and Applications*, Springer-Verlag, Berlin, **1985**.

[16] a. R. Montgomery, *Adv. Chem. Ser.*, **1973**, *117*, 197. b. K. Bock, C. Pedersen and H. Pedersen, *Adv. Carbohydr. Chem. Biochem.*, **1984**, *42*, 193.

[17] a. J.J. Thomson, *Rays of Positive Electricity and Their Applications to Chemical Analyses, Longmans*, Green and Co., London, **1913**. b. Thomson, J.J., *Phil. Mag.*, **1909**, *18*, 821.

[18] A.J. Dempster, *Phys. Rev.*, **1918**, *11*, 316.

[19] F.W. Aston, *Phil. Mag.*, **1919**, *38*, 707.

[20] R.J. Beuhler, E. Flanigan, L.J. Greene and L. Friedman, *J. Am. Chem. Soc.*,

1974, *96*, 3990.

[21] M.A. Baldwin and F.W. McLafferty, *Org. Mass Spectrom.*, **1973**, *7*, 1353.

[22] A. Dell, D.H. Williams, H.R. Morris, G.A. Smith, J. Feeney and G.C.K. Roberts, *J. Am. Chem. Soc.*, **1975**, *97*, 2497.

[23] a. R.D. Macfarlane and D.F. Togerson, *Science*, **1976**, *191*, 920. b. R.D. Macfarlane, *Anal. Chem.*, **1983**, *55*, 1247A. c. B. Sundqvist and R.D. Macfarlane, *Mass Spectrom. Rev.*, **1985**, *4*, 421.

[24] a. F. Hillenkamp, Laser Induced Ion Formation from Organic Solids. In: *Ion Formation from Organic Solids*, A. Benninghoven (Ed.), Springer-Verlag, Berlin, **1983**, p190. b. M. Karas and U. Bahr, *Tr. Anal. Chem.*, **1986**, *5*, 90. c. R.J. Cotter, *Anal. Chim. Acta.*, **1987**, *195*, 45.

[25] a. M. Barber, R.S. Bordoli, R.D. Sedgwick and A.N. Tyler, *Chem. Commun.*, **1981**, 325. b. D.J. Surman and J.C. Vickerman, *Chem. Commun.*, **1981**, 324.

[26] a. E.W. Müller, *Z. Phys.*, **1951**, *131*, 136. b. M.G. Inghram and R. Gomer, *J. Chem. Phys.*, **1954**, *22*, 1279. c. F.W. Röllgen, Principles of Field Desorption Mass Spectrometry. In: *Ion Formation From Organic Solids*, A. BenningHoven (Ed.), Springer-Verlag, Berlin, **1983**, p2.

[27] a. M.L. Vestal, *Mass Spectrom. Rev.*, **1983**, *2*, 447. b. G. Schmelzeisen-Redeker, L. Bütfering and F.W. Röllgen, *Int. J. Mass Spectrom. Ion Proc.*, **1989**, *90*, 139.

[28] G.O. Aspinall, Chemical Characterization and Structural Determination of Polysaccharides. In: *The Polysaccharides*, G.O. Aspinall (Ed.), Academic Press, Inc., New York, **1982**, p36.

[29] E.P.L. Hunter and S.G. Lias, *J. Phys. Chem. Ref. Data 27*, **1998**.

[30] R.I. Reed, *J. Chem. Soc.*, **1958**, 3432.

[31] a. J. Longren and S. Svennson, *Adv. Carbohydr. Chem. Biochem.*, **1974**, *29*, 42. b. T. Radford and D.C. DeJongh, Carbohydrates. In: *Biochemical Applications of MS* (Suppl.), G.R. Waller and O.C. Dermer (Eds.), John Wiley & Sons, New York, **1980**, p256. c. S.B. Levery and S. Hakomori, *Methods Enzymol.*, **1987**, *138*, 13. d. C.G. Hellerqvist, *Methods Enzymol.*, **1990**, *193*, 554. e. C.G. Hellerqvist and B.J. Sweetman, *Biomed. App. Mass Spectrom.*, **1990**, *34*, 91.

[32] a. R.J. Cotter and C. Fenselau, *Biomed. Mass Spectrom.*, **1979**, *6*, 287. b. D.I. Carrol, J.G. Nowin, R.N. Stillwell and E.C. Horning, *Anal. Chem.*, **1981**, *53*, 2007. c. V.N. Reinhold and S.A. Carr, *Anal. Chem.*, **1982**, *54*, 499. d. U. Rapp, G. Dielmann, D.E. Games, J.L. Gower and E. Lewis, *Adv. Mass Spectrom.*, **1980**, *8B*, 1660. e. K. Harada, S. Ito, N. Takeda, M. Suzuki and A. Tatematsu, *Biomed. Mass Spectrom.*, **1983**, *10*, 5. f. R. Geyer, H. Geyer, S. Kuhnhardt, W. Mink and S. Stim, *Anal. Biochem.*, **1983**, *133*, 197. g. E.G. de Jong, W. Heerma and C.A.X.G.F. Sicherer, *Biomed. Mass Spectrom.*, **1979**, *6*, 242.

[33] A. Benninghoven, D. Jaspers and W. Sichtermann, *Appl. Phys.*, **1976**, **11**, 35.

[34] a. W. Aberth, K.M. Straub and A.L. Burlingame, *Anal. Chem.*, **1982**, *54*, 2029. b. J. Sunner, *Organic Mass Spectrom.*, **1993**, *28*, 805.

[35] a. C. Fenselau and R.J. Cotter, *Chem. Rev.*, **1987**, *87*, 501. b. E. Schröder, H. Münster and H. Budzikiewicz, *Org. Mass Spectrom.*, **1986**, *21*, 707. c. B.D. Musselman, J.T. Watson, C.K. Chang, *Org. Mass Spectrom.*, **1986**, *21*, 215. d. G.M. Lancaster, F. Honda, Y. Fukuda and J.W. Rabalais, *J. Am. Chem. Soc.*,

1979, *101*, 1951.

[36] a. H. Egge and J. Peter-Katalinic, *Mass Spectrom. Rev.*, **1987**, *6*, 331. b. A. Dell, A.J. Reason, K.-H. Khoo, M. Pianco, R.A. McDowell and H.R. Morris, *Methods Enzymol.*, **1994**, *230*, 108.

[37] a. G. Puzo and J.-C. Prome, *Org. Mass Spectrom.*, **1984**, *19*, 448. b. K. Harada, M. Suzuki and H. Kambara, *Org. Mass Spectrom.*, **1982**, *17*, 386.

[38] S.A. Carr, V.N. Reinhold, B.N. Green and J.R. Hass, *Biomed. Mass Spectrom.*, **1985**, *12*, 288.

[39] A.P. Bruins, T.R. Covey and J.D. Henion, *Anal. Chem.*, **1987**, *59*, 2642.

[40] R. Tilney and H.W. Peabody, *Brit. J. Appl. Phys.*, **1953**, *4*, S51.

[41] J. Zeleny, *Phys. Rev.*, **1917**, *10*, 1.

[42] a. P. Lenard, *Weid. Ann.*, **1892**, *46*, 584. b. A. Coehn and H. Mozer, *Ann. Phys.*, **1914**, *43*, 1048.

[43] S. Chapman, *Phys. Rev.*, **1937**, *52*, 184.

[44] R.L. Hines, *J. Appl. Phys.*, **1966**, *37*, 2730.

[45] a. M. Dole, I.L. Mack, R.L. Hines, R.C. Mobley, L.D. Ferguson and M.B. Alice, *J. Chem. Phys.*, **1968**, *49*, 2240. b. M. Yamashita and J.B. Fenn, *J. Phys. Chem*, **1984**, *88*, 4451. c. M. Yamashita and J.B. Fenn, *J. Phys. Chem*, **1984**, *88*, 4671. d. M.L. Aleksandrov, L.N. Gall, V.N. Krasnov, V.I. Nikolaev, V.A. Pavlenko and V.A. Shkurov, Dokl. Akad. Nauk. *SSSR*, **1984**, *277*, 379.

[46] a. L.B. Loeb, A.F. Kip, G.G. Hudson and W.H. Bennett, *Phys. Rev.*, **1941**, *60*, 71A. b. R.J. Pfeifer and G.D. Hendricks, *AIAAJ*, **1968**, *6*, 496.

[47] G.I. Taylor, *Proc. R. Soc. London A*, **1964**, *A280*, 383.

[48] D.P.H. Smith, *IEEE Trans. Ind. Appl.*, **1986**, *IA-22*, 527.

[49] Lord Rayleigh, *Philos. Mag.*, **1882**, *14*, 184.

[50] a. J.V. Iribarne and B.A. Thomson, *J. Chem. Phys.*, **1976**, *64*, 2287. b. B.A. Thomson and J.V. Iribarne, *J. Chem. Phys.*, **1979**, *71*, 4451.

[51] a. J.B. Fenn, M. Mann, C.K. Meng, S.F. Wong and C.M. Whitehouse, *Science*, **1989**, *246*, 64. b. S.A. McCluckey, G.J. van Berkel, G.L. Glish, *J. Am. Chem. Soc.*, *1990*, *112*, 5668.

[52] M.G. Ikonomou, A.T. Blades and P. Kebarle, *Anal. Chem.*, **1990**, *62*, 957.

[53] D.C. Harris, *Quantitative Chemical Analysis*, 2nd Ed., W.H. Freeman and Company, New York, **1987**, p272.

[54] R.D. Smith and K.J. Light-Wahl, *Biol. Mass Spectrom.*, **1993**, *22*, 493.

[55] a. V.N. Reinhold, B.B. Reinhold and C.E. Costello, *Anal. Chem.*, **1995**, *67*, 1772. b. V.N. Reinhold, B.B. Reinhold and S. Chan, *Methods Enzymol.*, **1996**, *271*, 377. c. V.N. Reinhold and B.B. Reinhold, Carbohydrate Mass Spectrometry. In: *Fundamentals and Applications of Gas Phase Ion Chemistry*, Ed. K.R. Jennings, Kluwer Academic Publishers, The Netherlands, **1999**, p181.

[56] a. B. Spengler, D. Kirsch and R. Kaufmann, *J. Phys. Chem.*, **1992**, *96*, 9678. b. R. Kaufmann, P. Chaurand, D. Kirsch and B. Spengler, *Rapid Commun. Mass Spectrom.*, **1996**, *10*, 1199. c. M. Takayama and A. Tsugita, *Int. J. Mass*

Spectrom., **1998**, *181*, L1. d. J. Franzen, R. Frey, A. Holle and K.-O. Kraüter, *Int. J. Mass Spectrom.*, **2001**, *206*, 275.

[57] M. Karas and U. Bahr, Steps Towards A More Refined Picture of the Matrix Function in UV MALDI. In: *Large Ions: Their Vaporization, Detection and Structural Analysis*, T. Baer, C.Y. Ng and J. Powis (Eds), John Wiley & Sons Ltd., New York, **1996**, p27.

[58] S. Niu, W. Zhang and B.T. Chait, *J. Am. Soc. Mass Spectrom.*, **1998**, *9*, 1.

[59] a. M. Karas, H. Ehring, N. Eckhard, B. Stahl, K. Strupart, F. Hillenkamp, M. Grehl and B. Krebs, *Org, Mass Spectrom.*, **1993**, *28*, 1476. b. R.E. Johnson, *Int. J. Mass Spectrom. Ion. Proc.*, **1994**, *139*, 25. c. H. Ehring and B.U.R. Sundqvist, *J. Mass Spectrom.*, **1995**, *30*, 1303. d. H. Ehring and B.U.R. Sundqvist, *Appl. Surf. Sci.*, **1996**, *96-98*, 577.

[60] H. Ehring, M. Karas and F. Hillenkamp, *Org. Mass Spectrom.*, **1992**, *27*, 472.

[61] M. Karas, M. Glückmann and J. Schäfer, *J. Mass Spectrom.*, **2000**, *35*, 1.

[62] a. W.E. Stephens, *Phys. Rev.*, **1946**, *69*, 691. b. C. Weickhardt, F. Moritz and J. Grotemeyer, *Mass Spectrom. Rev.*, **1996**, *15*, 139. c. M. Guilhaus, V. Mlynski and D. Selby, *Rapid Commun. Mass Spectrom.*, **1997**, *11*, 951. d. R.J. Cotter, *Anal. Chem.*, **1999**, *71*, 445A.. e. K.G. Standing, *Int. J. Mass Spectrom.*, **2000**, *200*, 597. f. B.A. Mamyrin, *Int. J. Mass Spectrom.*, **2001**, *206*, 251. g. R. Bateman, J. Brown, J. Hoyes, T. Williams, T. Kosaka, T. Kinoshita and T. Nakamura, *Micromass UK Ltd. Technical Note 107*, **1997**.

[63] a. D.J. Harvey, *Mass Spectrom. Rev.*, **1999**, *18*, 349. b. E. Clayton and R.H. Bateman, *Rapid Commun. Mass Spectrom.*, **1992**, *6*, 719.

[64] E.G. Johnson and A.O. Nier, *Phys. Rev.*, **1953**, *91*, 10.

[65] a. W.C. Wiley and I.H. McLaren, *Rev. Sci. Instrum.*, **1955**, *26*, 1150. b. S.G. Alikanov, *Sov. Phys. JETP*, **1957**, *4*, 452. c. G.O. O'Halloran, R.A. Fluegge, J.F. Betts and W.L. Everett, *Technical Report No. ASD-TDDR-62-644 Part I & II* prepared under contract Nos AF33(616)-8374 and AF33(657)-11018 by the Bendix Corporation Research Laboratories Division, Southfield, Michigan, **1964**. d. B.A. Mamyrin, D.V. Karatev, D.V. Shmikk and V.A. Zagulin, *Sov. Phys. JETP*, **1973**, *37*, 45. e. J.H.J. Dawson and M. Guillhaus, *Rapid Commun. Mass Spectrom.*, **1989**, *3*, 155.

[66] a. W. Paul, H.P. Reinhard and U. von Zahn, Z. Phys., 1958, 152, 143. b. P.H. Dawson, *Quadrupole Mass Spectrometry and Its Applications*, Elsevier, New York, **1976**.

[67] a. R.E. March and J.F.J. Todd, *Practical Aspects of Ion Trap Mass Spectrometry*, Vol. 1, CRC Press, New York, **1995**. b. A.G. Marshall, C.L Hendrickson and G.S. Jackson, *Mass Spectrom. Rev.*, **1998**, *17*, 1.

[68] G.L. Glish, S.A. McCluckey, T.Y. Ridley and R.G. Cooks, *Int. J. Mass Spectrom. Ion Phys.*, **1982**, *65*, 141.

[69] D. Zakett, P.H. Hemberger and R.G. Cooks, *Anal. Chim. Acta*, **1980**, *119*, 149.

[70] a. E. de Hoffman, *J. Mass Spectrom.*, **1996**, *31*, 129. b. R.H. Haynes and M.L. Gross, *Methods Enzymol.*, **1990**, *193*, 237.

[71] a. M.S. Kim and F.W. McLafferty, *J. Am. Chem. Soc.*, **1978**, *100*, 3279. b. V.H. Wysocki, H.I. Kenttämaa and R.G. Cooks, *Int. J. Mass Spectrom. Ion Proc.*, **1987**,

75, 181. c. H.I. Kenttämaa and R.G. Cooks, *Int. J. Mass Spectrom. Ion Proc.*, **1985**, *64*, 79.

[72] a. R.A. Laine, *Methods Enzymol.*, **1989**, *179*, 157. b. B.L. Gillece-Castro and A.L. Burlingame, *Methods Enzymol.*, **1990**, *193*, 689. c. R. Orlando, C. Allen Bush and C. Fenselau, *Biomed. Environ. Mass Spectrom.*, **1990**, *19*, 747. d. Z. Zhou, S. Ogden and J.A. Leary, *J. Org. Chem.*, **1990**, *55*, 5444. e. G.E. Hofmeister, Z. Zhou and J.A. Leary, *J. Am. Chem. Soc.*, **1991**, *113*, 5964. f. J. Lemoine, B. Fournet, D. Despeyroux, K.R. Jennings, R. Rosenberg and E. de Hoffman, *J. Am. Soc. Mass Spectrom.*, **1993**, *4*, 197. g. J.A. Carroll, D. Willard and C.B. Lebrilla, *Anal. Chim. Acta*, **1995**, *307*, 431.

[73] a. M. Kohler and J.A. Leary, *Anal. Chem.*, **1995**, *67*, 3501. b. M.R. Asam and G.L. Glish, *J. Am. Soc. Mass Spectrom.*, **1997**, *8*, 987. c. A. Fura and J.A Leary, *Anal. Chem.*, **1993**, *65*, 2805. d. E.M. Sible, S.P. Brimmer and J.A. Leary, *J. Am. Soc. Mass Spectrom.*, **1997**, *8*, 32. e. G. Smith and J.A. Leary, *J. Am. Chem. Soc.*, **1998**, *120*, 13046. f. S. Konig and J.A. Leary, *J. Am. Soc. Mass Spectrom.*, **1998**, *9*, 1125. g. S.P. Gaucher and J.A. Leary, *J. Am. Soc. Mass Spectrom.*, **1999**, *10*, 269. h. H. Desaire and J.A. Leary, *Anal. Chem.*, **1999**, *71*, 1997.

[74] a. M. Tswett, *Travl. Soc. Naturalistes Varisovic*, **1903**, *14*, 1903. b. M. Tswett, *Ber. Deut. Botan. Geo.*, **1906**, *24*, 385. c. C.F. Simpson, *An Introduction to Liquid Chromatography and Some Fundamental Relationships*. In: Techniques in Liquid Chromatography, C.F. Simpson (Ed.), John Wiley & Sons, Chichester, **1982**.

Chapter 2

Characterization of ginseng saponins using electrospray mass spectrometry and collision-induced dissociation experiments of metal-attachment ions

Chapters 2 and 3 describe a strategy for structure characterization of ginsenosides, as well as its application to the separation and structure analysis of new ginsenosides from complex ginseng root extracts.

Electrospray mass spectrometry (ESMS) and collision-induced dissociation (CID) methodologies have been developed for the structural characterization of ginseng saponins (ginsenosides). Ginsenosides are terpene glycosides containing a triterpene core to which one to four sugars may be attached. They are neutral molecules which readily form molecular metal-attachment ions in positive ion ESMS experiments. In the presence of ammonium hydroxide intense deprotonated ions are generated. Both positive and negative ion ESMS experiments were found to be useful for molecular mass and structure determination of ten ginsenoside standards. Negative ion experiments made possible the determination of the molecular mass of each ginsenoside standard, the mass of the triterpene core and the masses and sequences of the sugar residues. Positive ion ESMS experiments with the alkali metal cations Li^+ or Na^+ and the transition metal cations Co^{2+}, Ni^{2+} and Zn^{2+} were also useful in determining molecular masses. These alkali and transition metal cations form strongly bonded attachment ions with the ginsenosides. As a result, the CID mass spectra of the metal attachment ions show a variety of (structure characteristic) fragmentations. These experiments can be used to determine the identity of the triterpene core, the types and attachment points of sugars to the core and the nature of the *O*-glycosidic linkages in the appended disaccharides. Combining the results from the negative and positive ion experiments provides a promising approach to the structure analysis of this class of natural products.

The work in this Chapter has been published previously in an article under the same title: S.Z. Ackloo, R.W. Smith, J.K. Terlouw, and B.E. McCarry, The Analyst, 2000, 125, 591.

Introduction

The therapeutic effects of ginseng have long been known in Asia and its use in North America has become increasingly popular in recent years. Demand for American ginseng in Asia has led to its increased plantings in North America

[1]. The pharmacologically active components of ginseng are believed to be ginsenosides, a class of distinctive triterpene glycosides, see Scheme 1. In recent years, there has been a large increase in reports on their biological activity [2-12]. Some are central nervous system stimulants and hypotensive agents [2-4]; for example, ginsenoside Rf inhibited voltage-dependent Ca^{2+} channels in sensory neurons [5-7]. The growth rate of human ovarian cancer expressed in mice was reduced after feeding the mice with ginsenoside Rh_2 [8], while ginsenosides Rb_1 and Rg_1 reduced the inflammatory response in asthmatic patients [9-12].

Of the sixty-four reported ginsenosides [13], only seven are commercially available, see Scheme 1. The majority of known ginsenosides consist of a triterpene core which can be either protopanaxadiol or protopanaxatriol. Sugars are attached to the triterpenes *via* *O*-glycosidic linkages; diol cores have sugars attached to C3 and C20 while triol cores have sugars attached to C6 and C20, respectively.

The overall goal of the present work is the development of ESMS methods for structural characterization of ginsenosides using small amounts of material and minimal chemical derivatization. Up to 1985, the mass spectrometric techniques available required chemical derivatization prior to analysis, a time-consuming process. These methods included electron impact mass spectrometry of acetate, trimethyl silyl ether and methyl derivatives of ginsenosides [14], field desorption mass spectrometry [15], and secondary ion mass spectrometry [16]. Definitive structural assignments have relied primarily

on nuclear magnetic resonance spectroscopy [17] which requires a considerably larger amount of analyte than any mass spectrometric approach.

In 1995, van Breemen *et al.* demonstrated that ginsenoside sodium-attachment ions could be formed and analyzed by liquid chromatography/mass spectrometry (LC/MS) [18]. Compared to traditional methods of analysis, we found this approach attractive since it does not require a time-consuming derivatization prior to analysis. Reports on the mass spectrometric analysis of structurally related saponins provided further useful information [19,20], confirming that the fragmentation patterns of triterpene glycosides are determined by their sugar moieties. From the vast body of literature on the mass spectrometry of sugars, references 21-34 are of immediate interest to this study. The studies reported in these papers demonstrate that underivatized sugars yield excellent ESMS spectra in the presence of metal ions. In three of these studies [26,27,29] it is shown that CID experiments of sugar metal-attachment ions with transition metal ions [26,27] as well as Li^+ and Na^+ [29], provide information on the nature of the *O*-glycosidic linkage. In particular, the method reported by Asam *et al.* [29] appeared to hold considerable promise for deriving useful information on the nature of *O*-glycosidic linkages in the disaccharides from ginsenosides.

Very recently, Wang *et al.* [35] proposed an LC/MS method in which protonated ginsenosides are subjected to CID experiments. This approach provides information on the types of sugars, the *O*-glycosidic linkages and the triterpene cores. Metal-attachment ions with sodium and potassium were also briefly examined in this study. However, these species were not further

investigated, possibly because their CID mass spectra showed fewer fragment ions than the protonated species.

Based upon the pioneering studies of van Breemen *et al.* [18] and those in refs. 26, 27 and 29, we report an ESMS based approach to the structural characterization of ginsenosides complementary to that of Wang *et al.* [35]. Using ten ginsenoside standards as model compounds, we find our method to be useful for molecular mass and structure determination, isomer differentiation and determination of *O*-glycosidic linkages in ginsenosides. The approach involves both positive and negative ion ESMS and CID experiments.

The longer term goal of this work is the development of a routine LC/MS methodology for the structure analysis and quality control of ginsenosides in complex mixtures (root extracts) and the refinement of structure determination methods for isolated ginsenosides.

Experimental

Ginsenosides Rb_1, Rb_2, Rc, Rd, Re, Rf, and Rg_1 were purchased from Indofine Chemical Company Inc. (New Jersey, U.S.A.), while ginsenosides Rb_3 and Rg_3 and gypenoside XVII were obtained from Agriculture Canada (Delhi, Canada). Glucose disaccharides having α-1,2-, α-1,6-and β-1,6-*O*-glycosidic linkages were obtained from Sigma (St. Louis, U.S.A.). Acetonitrile (HPLC grade) was obtained from Caledon Laboratories (Georgetown, Canada) and water was obtained from a Milli-Q water purification system (Millipore, Mississauga, Canada).

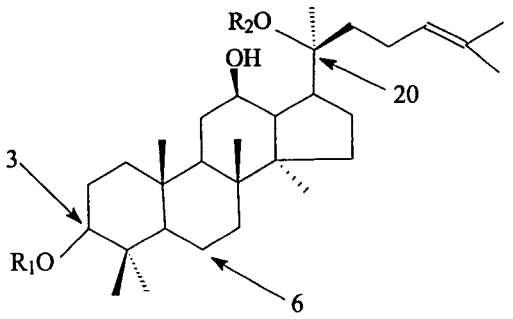

	R_1	R_2	MW
Protopanaxadiol	H	H	460
Ginsenoside			
Rb_1	Glc^1-O-^{2}Glc-	Glc^1-O-^{6}Glc-	1108
Rb_2	Glc^1-O-^{2}Glc-	Ara^1-O-^{6}Glc-	1078
Rb_3	Glc^1-O-^{2}Glc-	Xyl^1-O-^{6}Glc-	1078
Rc	Glc^1-O-^{2}Glc-	$Ara(f)^1$-O-^{6}-Glc-	1078
Rd	Glc^1-O-^{2}Glc-	Glc-	946
Gypenoside XVII	Glc-	Glc^1-O-^{6}Glc-	946
Rg_3	Glc^1-O-^{2}Glc-	H	784

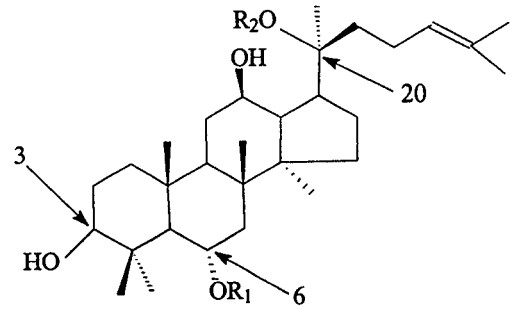

	R_1	R_2	MW
Protopanaxatriol	H	H	476
Ginsenoside			
Re	Rhm^1-O-^{2}Glc-	Glc-	946
Rf	Glc^1-O-^{2}Glc-	H	800
Rg_1	Glc-	Glc-	800

Scheme 1: Structures of the ginsenoside standards used. Glc= glucose; Ara= arabinose; Xyl= xylose; Rhm= rhamnose; f =furanose (unless otherwise specified the sugars are in their pyranose form).

A.C.S. reagent grade metal salts were purchased from Aldrich (Milwaukee, U.S.A.). Li^+, Na^+, K^+ and Rb^+ were introduced as their acetate salts while Cs^+ was introduced as its iodide salt. Transition metal cations (Co^{2+}, Ni^{2+} and Zn^{2+}) were introduced as their chloride salts.

Mass spectrometry experiments were performed on a Micromass Quattro LC triple quadrupole mass spectrometer (Manchester, England) equipped with a "pepper-pot". The solvent delivery system was a Brownlee Labs Microgradient System syringe pump which introduced the mobile phase at a flow rate of 5 μL/min.

The mobile phase was a 1:1 solution of water and acetonitrile. Solutions containing 40 mM of a ginsenoside and 65 mM of a metal salt were introduced by infusion in positive ion experiments, whereas negative ion experiments were performed by infusion of solutions containing 100 mM ginsenoside with 0.1% NH_4OH. The yield of metal-attachment ions was highest at a cone voltage of 120 V. In CID experiments on the alkali metal attachment ions, argon (at an indicated pressure of 2×10^{-3} mBar) was used as the collision gas at a collision energy of 50 eV. CID experiments on the transition metal attachment ions were performed using a collision energy of 30 eV.

Results and Discussion

The structures of the ten ginsenoside standards used in this work are listed in Scheme 1. While the triterpene cores have either three or four hydroxyl groups, sugars are attached to the triterpene at only two positions, C3 and C20 in the case of protopanaxadiol-based ginsenosides and C6 and C20 in the case

of the protopanaxatriol-based ginsenosides. Variations in the types of sugars, their sequence and type of glycosidic linkages can lead to a variety of structures, including isomeric ginsenosides. Carbon 20, a common attachment point for both triterpene series, is a tertiary centre while C3 and C6 are secondary carbons; it was anticipated that fragmentation under positive ion conditions would occur more readily at C20 than at C3 or C6, due to the greater stability of tertiary cations (at C20) compared to the corresponding secondary species at either C3 or C6.

At the outset of this work we realized that in order to propose a structure for a ginsenoside, various mass spectrometric techniques would be necessary to obtain some or all of the following data: 1) the molecular mass of the ginsenoside, 2) the type of triterpene core, 3) the number and types of sugars attached to the core, 4) the points of attachment of the sugars, 5) the sequence of sugar residues attached to the core and 6) the stereochemistry of each sugar-sugar linkage. The combination of triterpenes, sugar moieties and glycosidic linkages in ginsenosides affords structures with molecular ions and fragment ions that may (or may not) be unique or common to a number of ginsenosides. For example, differentiation between the triterpene cores (protopanaxadiol and protopanaxatriol) is often important because their mass difference is only 16 Da; this mass difference is reflected in two otherwise identical ginsenosides, ginsenoside Rg_3 (diol core, MW = 784 Da, Scheme 1) and ginsenoside Rf (triol core, MW = 800 Da, Scheme 1). If a deoxyhexose such as rhamnose is substituted for a hexose such as glucose, the resulting mass difference is also 16 Da. Thus, the diol-based ginsenoside Rd with three glucose sugars has a

molecular mass, 946 Da, (and elemental composition) identical to that of the triol-based ginsenoside Re, which contains two glucose sugars and one rhamnose sugar.

Negative ion experiments : infusion of ginsenosides in the presence of NH_4OH

Infusion of a solution containing a ginsenoside in the presence of 0.1 % NH_4OH, yielded spectra containing a wealth of data that provided information on the molecular mass, the triterpene core, the nature of the sugars and their sequence in each ginsenoside. First, all ginsenosides show intense $[M-H]^-$ ions, confirming their molecular masses as exemplified by the spectra of ginsenosides Rc and Re in Figure 2-1.

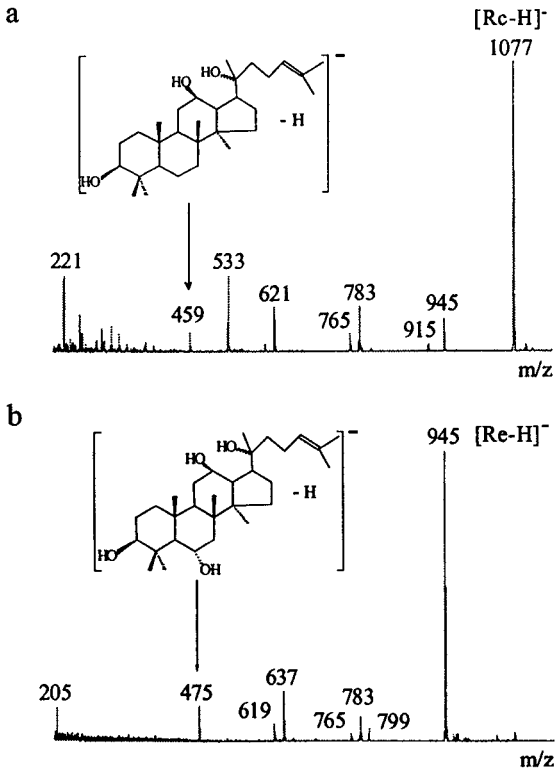

Figure 2-1: Negative ion ES mass spectra of ginsenoside Rc, item a), and ginsenoside Re, item b).

Second, each ginsenoside shows a fragment ion at either m/z 459 or at m/z 475, clearly identifying the triterpene core as protopanaxadiol (Figure 2-1a) or protopanaxatriol (Figure 2-1b), respectively. Third, fragment ion masses in the full scan mass spectrum provide structure characteristic information which was verified by MS/MS experiments. For example, ginsenoside Rc has four sugar residues attached to a diol core, see Scheme 1, and it gives a strong $[Rc\text{-}H]^-$ ion at m/z 1077 (Figure 2-1a). Ions at m/z 945 and 915 arise from losses of a 5-carbon sugar and a 6-carbon sugar, respectively, indicating that these sugars are likely the terminal sugars of each of the two disaccharides. Loss of sugar moieties continues sequentially until only the triterpene core remains; see m/z 459 in Figure 2-1a. These observations are in line with negative ion fast-atom bombardment (FAB) MS/MS results on saponins from black bean [20].

Positive ion experiments : infusion of ginsenosides in the presence of metal ions

Preliminary experiments probed the formation of ginsenoside metal-attachment ions with the alkali metal ions (Li^+ to Cs^+). Infusion ESMS experiments showed that all ginsenoside standards contained endogenous amounts of sodium and potassium salts in the lower percentage range, with sodium predominating. Infusing solutions containing a cation:ginsenoside molar ratio of 1.5:1 ensured that the added alkali metal ion was in excess of the endogenous Na^+ and K^+ ions. This step allowed a better assessment of adduct ion formation with the added metal ions.

A series of ES experiments with ginsenoside Rc (MW=1078 Da) serves to illustrate observations typical for all ginsenoside standards. In the presence of Li^+, the lithiated molecular ion $[Rc+Li^+]^+$ was observed at m/z 1085; see Figure 2-2a. This mass spectrum also shows molecular metal-attachment ions with Na^+ and K^+ at m/z 1101 and m/z 1117, respectively, due to the sodium and potassium salts in the standard. CID experiments performed on these ginsenoside metal-attachment ions revealed a preferred fragmentation pathway. Scheme 2 shows a stylized diagram of a ginsenoside structure, together with the full structure of ginsenoside Rc, which shows the principal dissociations that the molecular metal-attachment ions undergo.

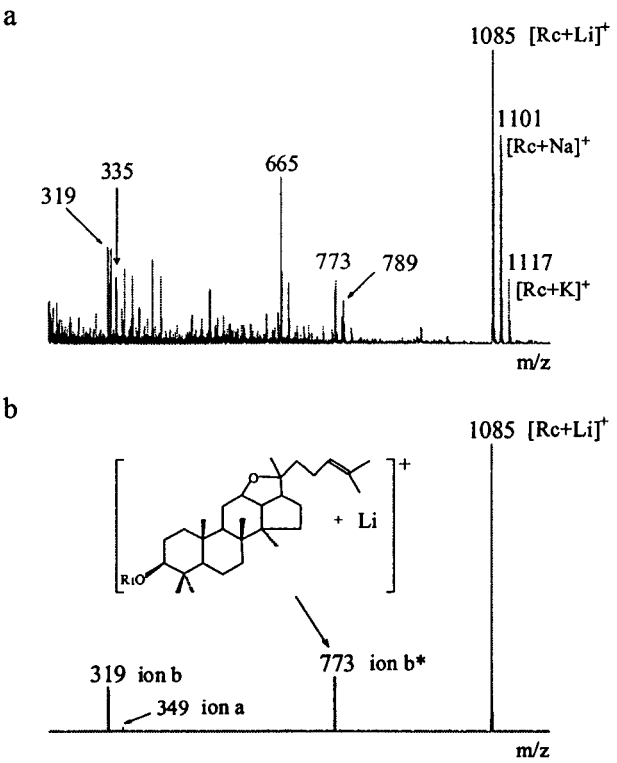

Figure 2-2: Positive ion ES mass spectrum of ginsenoside Rc and Li^+, item a), and the CID mass spectrum of the $[Rc+Li^+]^+$ ion at m/z 1085, item b).

The cleavage reactions occur predominantly at the glycosidic linkage at C20 of the triterpene core and further at C3 (diol core) or C6 (triol core); all molecular ions and fragment ions are metallated ions. Fragment ions **a** and **a*** result from bond cleavages of glycosidic linkages at the C3 or C6 glycosidic linkage. Fragment ion **a** is a metallated saccharide species while fragment ion **a*** is a metallated triterpene-saccharide species. The key fragment ions **b** and **b*** result from cleavage at the C20 glycosidic linkage; fragment ion **b** represents the metallated saccharide while fragment ion **b*** is a metallated triterpene-saccharide species. The **a*** and **b*** ions can also lose the saccharide(s) attached to the triterpene core to yield a metallated triterpene species, denoted as ion **c** in Scheme 2.

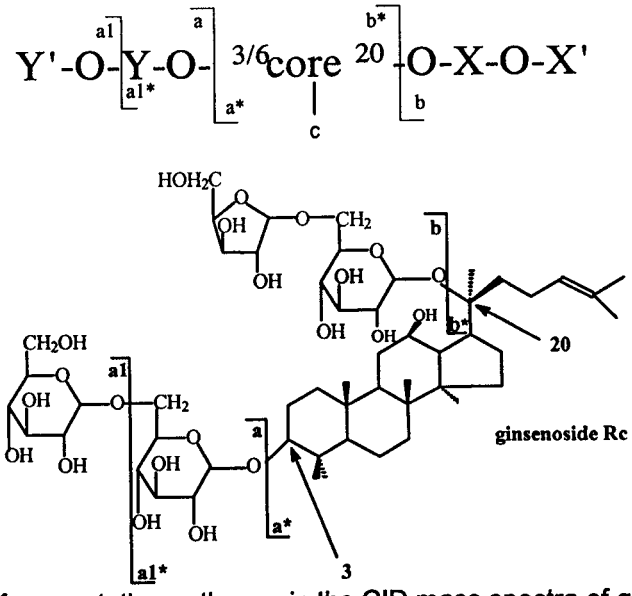

Scheme 2: Main fragmentation pathways in the CID mass spectra of ginsenoside metal-attachment ions (see text and Table 1).

A CID experiment on the $[Rc+Li]^+$ ion yielded a simple spectrum with two major fragment ions, at m/z 319 and 773; see Figure 2-2b. These ions likely

correspond to the lithiated disaccharide and core-disaccharide fragment ions resulting from bond cleavage at C20. Using the nomenclature in Scheme 2, the m/z 319 ion is a **b** type ion while the m/z 773 ion is a **b*** type ion. Infusion of ginsenoside Rc in the presence of Na^+ or K^+ yielded $[Rc+Na]^+$ or $[Rc+K]^+$ adduct ions. Upon collision these attachment ions generated the metallated disaccharide and core-disaccharide fragment ions **b** and **b***. Experiments with Rb^+ or Cs^+ also yielded intense attachment ions but their MS/MS spectra only showed Rb^+ and Cs^+ cations, at m/z 85 and m/z 133 respectively. The ginsenosides examined all showed a pronounced degree of fragmentation in the presence of Li^+ and Na^+, less so in the presence of K^+ while little or no fragmentation occurs in the presence of Rb^+ and Cs^+. This trend suggests that the interaction of a ginsenoside with an alkali metal cation decreases with an increase in the size of the ion. Kohler *et al.* [26] noted a similar trend in a study of carbohydrates.

In the presence of Co^{2+}, Ni^{2+} or Zn^{2+} ions, the ginsenosides do not generate molecular metal-attachment ions but rather $[M\text{-}H^+ + metal^{2+}]^+$ ions. Thus, adduct ion formation with transition metal cations involves deprotonation, presumably of a hydroxyl group of a saccharide unit. The resulting alkoxide site provides a strong electrostatic interaction for the transition metal ion which is not available to the alkali metal ions. Increasing the internal energy of these ions in a CID experiment results in a large number of fragmentations.

Ginsenoside Rc is used to illustrate the trends: its ES mass spectrum in the presence of Co^{2+} is shown in Figure 2-3a. The spectrum displays an intense $[M\text{-}H^+ + metal^{2+}]^+$ ion at m/z 1136 while the peak at m/z 1173 represents an

adduct ion with $CoCl^+$. Figure 2-3b shows the CID mass spectrum of the $[Rc\text{-}H^+ + Co^{2+}]^+$ ion which shows a higher degree of dissociation than any alkali metal ion, even Li^+, compare Figure 2-2b.

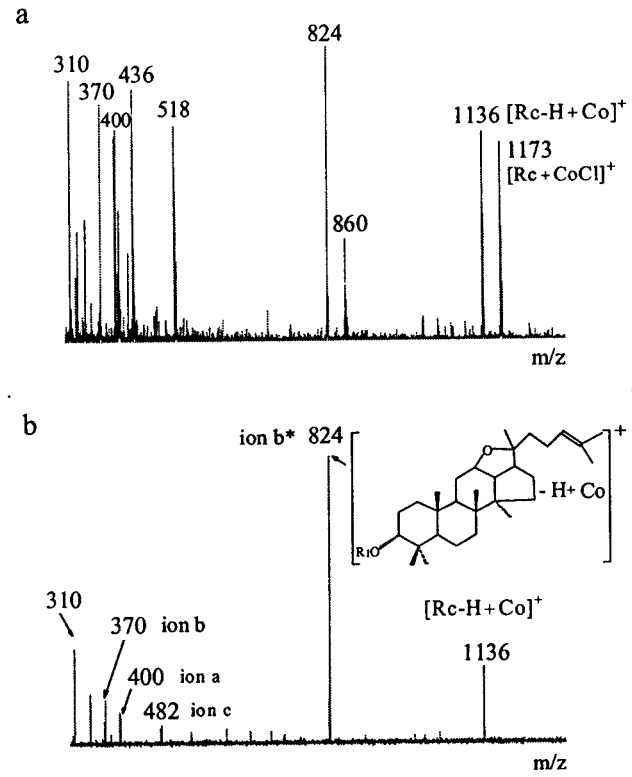

Figure 2-3: Positive ion ES mass spectrum of ginsenoside Rc and Co^{2+}, item a), and the CID mass spectrum of the $[Rc\text{-}H^+ + Co^{2+}]^+$ ion at m/z 1136, item b).

The normalized fragment ion abundances observed in MS/MS experiments on the metallated molecular ions of the ten ginsenoside standards are reported in Table 1. Table 1a lists the data for those ginsenosides containing four or three saccharides while Table 1b deals with ginsenosides containing two saccharides. The data only refer to the metal ions Li^+, Na^+, K^+, Co^{2+} and Ni^{2+} : adducts with Rb^+ and Cs^+ showed little or no fragmentation, while those with Zn^{2+} fragmented similarly to Co^{2+}.

Table 1a: Normalized fragment ion abundances derived from the CID mass spectra of ginsenoside metal-attachment ions. (a "blank" space indicates a relative intensity ≤ 1%, while "-" indicates that the ion in question cannot be formed)

Ginsenoside	Metal ion	a	a*	b	b*	c
Rc	Li^+	12	13	100		
	Na^+	2	67	100	50	
	K^+			100	19	
	Co^{2+}		5	15	100	5
	Ni^{2+}		100	22	91	
Rb_2	Li^+	64	26	100	84	
	Na^+	4	4	100	51	
	K^+	3	4	100	47	
	Co^{2+}		6	40	100	1
	Ni^{2+}		30	60	100	58
Rb_3	Li^+	6	41	85	100	
	Na^+	5	7	100	90	
	K^+			100	23	
	Co^{2+}		15	11	100	15
	Ni^{2+}		100	30		
Rb_1	Li^+	100	3	100	19	
	Na^+	100		100	20	
	K^+	100		100	20	
	Co^{2+}	31	5	31	100	2
	Ni^{2+}	100		100	78	22
Rd	Li^+	16	5	16	100	
	Na^+	17	8	17	100	
	K^+	25	11	25	100	
	Co^{2+}		16		100	13
	Ni^{2+}		25		100	21
Gypenoside XVII	Li^+	-	9	100		
	Na^+	-		100		
	K^+	-		100		
	Co^{2+}	-		100	23	
	Ni^{2+}	-		100	70	
Re	Li^+	9	68	9	100	14
	Na^+		25	3	100	3
	K^+		23	67	100	29
	Co^{2+}				37	100
	Ni^{2+}				100	

The first part of Table 1a lists data for ginsenosides Rc, Rb_1, Rb_2 and Rb_3 which contain diol cores and four sugars in the form of two disaccharide units attached at C3 and C20.

All sugars in ginsenoside Rb_1 (MW = 1108) are glucose while ginsenosides Rb_2, Rb_3 and Rc (MW = 1078) each have a 5-carbon sugar in the terminal position of the disaccharide attached to C20. Since the masses of the disaccharide units attached to C20 in the latter three ginsenosides are 30 Da less than the glucose disaccharide in ginsenoside Rb_1, differentiation of these ginsenosides from ginsenoside Rb_1 is straightforward (Table 1a). The predominant fragmentation route for all four metallated ginsenosides was bond cleavage at C20, a tertiary centre, to afford **b** and **b*** ions; fragmentation at C3 to afford ions **a** and **a*** was less abundant (Table 1a). Ginsenoside Rb_1 has identical disaccharide units at C3 and C20, therefore fragment ion **a** is indistinguishable from fragment ion **b**.

The smaller alkali metal cations afforded more intense **b** ions, implying a greater association with the departing disaccharide. However, adduct ions with transition metals gave more intense **b*** ions. Hard acids like these transition metal ions tend to associate strongly with hard bases like the hydroxyl group. Therefore, transition metal ions prefer to be associated with the portion of the molecule containing more hydroxyl groups; in these cases it is the triterpene-saccharide portion.

The ginsenosides containing three sugars showed fragmentation patterns very similar to those with four sugars; that is, the major fragment ions were **b** and **b*** type ions resulting from cleavage at C20, see Table 1a (bottom part). These

three ginsenosides have the same molecular mass and each contains a monosaccharide unit and a disaccharide unit (Scheme 1). MS/MS data for these isomeric ginsenosides showed that fragmentation at C20 predominates and that metal cations tend to be retained preferentially on disaccharide units rather than on monosaccharide units. These observations allowed for easy differentiation of ginsenoside Rd and gypenoside XVII. Both are diol-based ginsenosides with a disaccharide at C20 (gypenoside XVII) and a monosaccharide at C20 (ginsenoside Rd). The major fragment ion in the CID mass spectrum of lithiated gypenoside XVII was type **b** while for ginsenoside Rd it was type **b***. Ginsenoside Re is triol-based with a similar arrangement of sugars around the triterpene core to ginsenoside Rd. The **b*** fragment ion was predominant in the CID mass spectrum of ginsenoside Re. This is consistent with the proposal that metal cations prefer to be associated with fragments containing a disaccharide.

Three ginsenoside standards contained only two sugars, see Table 1b. Ginsenoside Rg_1 with a single sugar attached to both C6 and C20 showed predominant fragment ions of the **a/b** and **a*/b*** type, indicative of cleavage at C3 or C20. In light of the previous discussion it is probable that the ions observed result from bond cleavage at C20 but this cannot be confirmed. The remaining ginsenosides (Rf and Rg_3) are unusual in that they contain disaccharides at C3 or C6 and no sugar substituent at C20; thus fragment ions **b** and **b*** cannot be formed. Only **a** type fragment ions are observed (Table 1b).

In summary, ginsenosides with three and four sugar units fragment in a readily interpretable fashion. Based on these observations, the assignment of a basic structure of an unknown ginsenoside with three or four sugars should be

straightforward. Ginsenosides with two (or fewer) sugars have less predictable fragmentation pathways and their structural assignments may be more challenging.

Table 1b: Normalized fragment ion abundances derived from the CID mass spectra of ginsenoside metal-attachment ions, continued.

Ginsenoside	Metal ion	a1	a	a1*	b	b*	c
Rg_1	Li^+	-	100	-	100	40	40
	Na^+	-	100	-	100	46	3
	K^+	-	76	-	76	100	31
	Co^{2+}	-		-		100	6
	Ni^{2+}	-		-		100	
Rf	Li^+	9	100		-	-	9
	Na^+	5	100		-	-	3
	K^+				-	-	
	Co^{2+}		100	60	-	-	95
	Ni^{2+}				-	-	
Rg_3	Li^+	45	11	100	-	-	2
	Na^+	77	18	100	-	-	
	K^+	100	45	87	-	-	
	Co^{2+}	10		100	-	-	10
	Ni^{2+}			100	-	-	

(a "blank" space indicates a relative intensity ≤ 1%, while "-" indicates that the ion in question cannot be formed)

Identification of the triterpene core

The diol and triol triterpene cores were identified by both negative and positive ion ESMS experiments. Full scan negative ion ESMS experiments showed ions corresponding to the two core types. Ginsenosides containing diol cores showed an ion at m/z 459 (Figure 2-1a), while ginsenosides containing triol cores showed an ion at m/z 475 (Figure 2-1b). CID experiments confirmed that the m/z 459 and m/z 475 ions are generated from their respective $[M-H]^-$ precursor ions (results not shown). Negative ion ESMS data from the ten

ginsenoside standards provided unambiguous identification of the triterpene core.

From the results presented in Table 1, it follows that metallated core ions, **c** type ions, are generated in MS/MS experiments on the various metal-attachment ions but their intensity varies considerably and is highly dependent on both the ginsenoside structure and the nature of the metal ion. One trend is that the triol-containing ginsenosides yield more intense metallated core ions than their diol-containing counterparts. The results tabulated in Table 1 further indicate that the nature of the triterpene core could be established by *combining* the information from the Li, Co and Ni experiments but the negative ion data clearly provide a better diagnostic tool.

Determination of the *O*-glycosidic linkage

One major challenge is the determination of the nature of the glycosidic linkages between the sugar units. Most of the ginsenosides contain disaccharides with 1,2- and 1,6-*O*-glycosidic linkages [13]. Recent studies of saccharides aimed to establish the nature of the linkage using Li^+ and Na^+ [29] or transition metal cations [27] prompted us to explore these approaches in the present work. We infused Li^+ with three glucose disaccharide standards having α-1,6-, β-1,6- and α-1,2-*O*-glycosidic linkages and obtained results very similar to those of Asam and Glish [29]; see the first three entries in Table 2. CID experiments on the lithiated α-1,2-linked glucose disaccharide molecular ion showed loss of a single neutral of mass 120. In contrast, the CID mass spectra

of the α- and β-1,6-linked glucose disaccharides were characterized by neutral losses of 60, 90 and 120 Da, the loss of 60 yielding the base peak.

Table 2: Normalized neutral loss abundances for glucose disaccharide standards and disaccharides derived from ginsenoside lithium-attachment ions.

Compound		Abundance of Neutral Losses		
		120 Da	90 Da	60 Da
α-1,2-glucose disaccharide		100		
α-1,6-glucose disaccharide		31	91	100
β-1,6-glucose disaccharide		50	68	100
ginsenoside Rg_3	6C6C (1,2-linked)	100		
ginsenoside Rf	6C6C (1,2-linked)	100		
ginsenoside Re	6C6C (1,2-linked)	100		
ginsenoside Rd	6C6C (1,2-linked)	100		
gypenoside XVII	6C6C (1,6-linked)	43	75	100
ginsenoside Rb_2	5C6C (1,6-linked)	18	48	100
	6C6C (1,2-linked)	100		
ginsenoside Rb_3	5C6C (1,6-linked)	21	50	100
	6C6C(1,2-linked)	26	52	100
ginsenoside Rc	5C6C (1,6-linked)	26	54	100
	6C6C (1,6-linked)	100		30

(α = hydroxyl group on C1 is below the plane; 5C6C = disaccharide unit containing a five carbon sugar and a six carbon sugar; 6C6C = disaccharide unit containing two six carbon sugars; 1,2-linked = sugars in the disaccharide are linked via a 1,2-O-glycosidic linkage; a "blank" space indicates a relative intensity ≤ 1%)

However, the CID mass spectra of the α- and β- anomers are not sufficiently different to permit an unambiguous differentiation between the α- and β-anomers of an unknown saccharide.

The disaccharides present in the various ginsenosides were isolated for structural analysis *via* in-source CID [36]. The relative fragment ion intensities for the three disaccharide reference compounds and those derived from the eight

ginsenoside standards that contain disaccharides, are presented in Table 2. The glycosidic linkages listed (left column in Table 2) for the ginsenosides are taken from the literature [13]. The first three entries in Table 2 show the normalized neutral loss abundances of the three glucose disaccharide standards. The remaining entries are the normalized neutral loss abundances for disaccharide species derived from ginsenosides containing disaccharide units. The pattern of neutral losses in the ginsenoside-derived disaccharides is very similar to those of the glucose disaccharide standards. Nine of the eleven *O*-glycosidic linkages in the ginsenosides examined are correctly identified using this approach. However, two glucose-glucose disaccharides – the 6C6C entries for ginsenosides Rb_3 and Rc - yielded neutral loss data which are not consistent with the literature assignments [13]. This method has a high probability of success in differentiating 1,2-linked from 1,6-linked disaccharides in these complex molecules but analysis of more reference compounds is required to establish its full potential.

Differentiation of isomers

The differentiation of isomeric substances is a good test of the usefulness of this methodology. Among the available standards were three isomeric ginsenosides with molecular mass 946 Da (Rd, Re and gypenoside XVII), three with molecular mass 1078 Da (Rb_2, Rb_3 and Rc) and two with molecular mass 800 Da (Rf and Rg_1); see Scheme 1. Ginsenoside Re, one of the 946 Da isomers, has a triol core and so is easily differentiated from ginsenoside Rd and gypenoside XVII using negative and positive ion ESMS

approaches. The positive ion CID mass spectrum of the lithiated molecular ion of ginsenoside Re clearly showed the triol core (m/z 447, Figure 2-4a) whereas the lithiated molecular ions of the other two isomers did not afford $[core+Li^+]^+$ ions (Table 1).

Ginsenoside Rd and gypenoside XVII differ in the arrangements of the sugars attached to the core. Gypenoside XVII, with a glucose disaccharide at C20, showed preferential bond cleavage at C20 and the formation of a lithiated disaccharide ion (**b** type ion, m/z 349, Figure 2-4b). On the other hand, the isomeric ginsenoside Rd with a single glucose at C20 showed a major fragment ion at m/z 773 (**b*** type ion, Figure 2-4c), corresponding to the loss of a glucose molecule.

The 1078 Da isomers could not be differentiated by our ESMS methods. This is perhaps not too surprising, considering that their structures are closely similar. The only difference between ginsenosides Rb_2 and Rc, see Scheme 1, is the conformation of the terminal pentose in the C20 disaccharide; arabinose has the pyranose form in ginsenoside Rb_2 and the furanose form in ginsenoside Rc. In ginsenoside Rb_3 the terminal pentose in the C20 disaccharide is xylose, not arabinose. On the other hand, the 800 Da ginsenosides Rf and Rg_1 were easily differentiated because Rg_1 has a glucose at C20 whereas Rf has no sugar at C20; loss of glucose from ginsenoside Rg_1 is a predominant pathway. Overall, the combination of ESMS methods is useful for differentiating ginsenosides belonging to two of three groups of isomers.

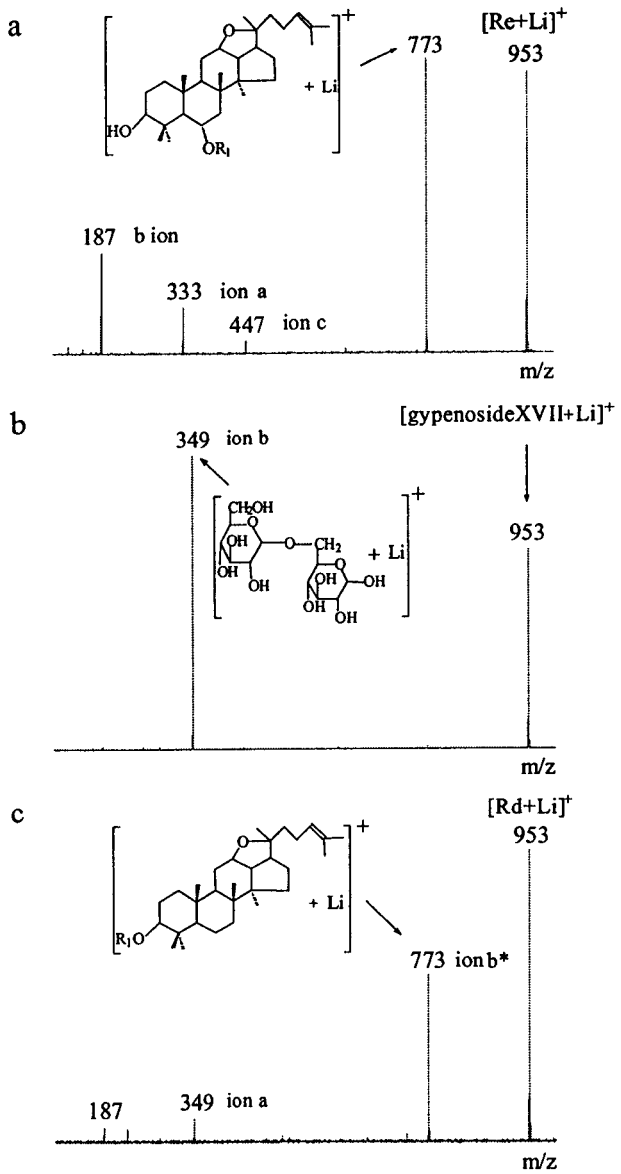

Figure 2-4: CID mass spectra of the m/z 953 ion generated by Li^+ attachment to: ginsenoside Re, item a), gypenoside XVII, item b), and ginsenoside Rd, item c).

Conclusions

Under ESMS conditions ginsenosides readily form molecular attachment ions with small alkali metal and transition metal ions. These adduct ions provided molecular mass information which is consistent with results from negative ion

experiments. Structural information was obtained from MS/MS experiments on the ginsenoside metal-attachment ions which includes the nature of the triterpene core, the types of sugars (pentose or hexose) attached to the ginsenoside and the types of attachment points of the sugars to the core (secondary *vs.* tertiary centres). The nature of the *O*-glycosidic linkage present in the disaccharides could be obtained from CID experiments on the Li^+ adducts of source-generated disaccharides from the ginsenosides.

Negative ion experiments allowed for the determination of the molecular mass and the type of triterpene core of each ginsenoside. Furthermore, negative ion mass spectra allowed determination of the sequence of the sugar moieties. The results presented show that structural characterization of ginsenosides by these mass spectrometric techniques is feasible and that these approaches are amenable to future applications in the LC/MS and LC/MS/MS analyses of complex mixtures of ginsenosides such as in root extracts.

The methodology for providing a structure for a ginsenoside, using the approach presented in the thesis, is summarized in Section I of the Appendix.

References

[1] J. Schriener, *Canadian Geographic*, **1994**, *114*, 43.

[2] H. Saito, Y. Yoshida, K. Takagi, *Jpn. J. Pharmacol.*, **1974**, *24*, 119.

[3] T. Kaku, T. Miyata, T. Urono, I. Sako, A. Kinoshita, *Arzneim.-Forsch.*, **1975**, *25*, 539.

[4] T. Kita, T. Hata, Y. Kawashima, T. Kaku, E. Itoh, *J. Pharm. Dyn.*, **1981**, *4*, 381.

[5] M. Yamamoto, A. Kumagai, Y. Yamamura, *Arzneim.-Forsch.*, **1975**, *25*, 1240.

[6] J.S. Mogil, Y.H. Shin, E.W. McCleskey, S.C. Kim, S.Y. Nah, *Brain Res.*, **1998**, *792*, 218.

[7] S.Y. Nah, H.J. Park, E.W. McCleskey, *Proc. Natl. Acad. Sci.* U S A, **1995**, *92*, 8739.

[8] H. Nakata, *Jpn. J. Cancer Res.*, **1998**, *89*, 733.

[9] J. Subiza, J.L. Subiza, P.M. Escribano, M. Hinojosa, R. Garcia, M. Jerez, E.J.

Subiza, *Allergy Clin. Immunol.*, **1991**, *88*, 731.

[10] D.A. Moneret-Vautrin, G. Kanny, A. Lagrange, *Rev. Med. Interne*, **1994**, *15*, 216.

[11] T.Y. Chan, *Vet. Hum. Toxicol.*, **1995**, *37*, 156.

[12] K. Shichinohe, M. Shimizu, K. Kurokawa, *J. Vet. Med. Sci.*, **1996**, *58*, 55.

[13] J. Shoji, Recent Advances in the Chemical Studies on Ginseng. In: *Adv. In Chinese Medicinal Materials Research*, H.M. Chang, H.W. Yeung, W.-W. Tso, A. Koo (Eds.), **1985**, p455.

[14] R. Kasai, K. Matsuura, O. Tanaka, S. Sanada, J. Shoji, *J. Chem. Pharm. Bull.*, 1977, **25**, 3277.

[15] T. Komori, M. Kawamura, K. Miyahara, T. Kawasaki, O. Tanaka, S. Yahara, H. R. Schulten, *Z. Naturforsch.*, **1979**, *34*, 1094.

[16] I. Kitagawa, T. Taniyama, T. Hayashi, M. Yoshikawa, *Chem. Pharm. Bull.*, **1983**, *31*, 3353.

[17] O. Tanaka, Chemical analysis of Ginseng. In: *Recent Studies on Ginseng*, H. Oura, Kumagai, S. Shibata, K. Takagi (Eds.), Kyoritsu Publ. Co., **1981**, p42.

[18] R.B. van Breemen, C. Huang, C. Lu, H. Rimando, H.S. Fong, J.F. Fitzloff, *Anal. Chem.*, **1995**, *67*, 3985.

[19] S. Fang, C. Hao, W. Sun, Z. Liu, S. Liu, *Rapid Commun. Mass Spectrom.*, **1998**, *12*, 589.

[20] M.-R. Lee, C.-M. Chen, B.-H. Hwang, L.-M. Hsu, *J. Mass Spectrom.*, **1999**, *34*, 804.

[21] Z. Zhou, S. Ogden, J.A. Leary, *J. Org. Chem.*, **1990**, *55*, 5444.

[22] J. Lemoine, B. Fournet, D. Despeyroux, K. R. Jennings, R. Rosenberg, E. de Hoffman, *J. Am. Soc. Mass Spectrom.*, **1993**, *4*, 197.

[23] G. E. Hofmeister, Z. Zhou, J.A. Leary, *J. Am. Chem. Soc.*, **1991**, *113*, 5964.

[24] A. Staempfli, Z. Zhou, J.A. Leary, *J. Org. Chem.*, **1992**, *57*, 3590.

[25] A. Fura, J.A. Leary, *Anal. Chem.*, **1993**, *65*, 2805.

[26] M. Kohler, J.A. Leary, *Anal. Chem.*, **1995**, *67*, 3501.

[27] E. M. Sible, S. P. Brimmer, J. A. Leary, *J. Am. Soc. Mass Spectrom.*, **1997**, *8*, 32

[28] M.T. Cancilla, S.G. Penn, J.A. Carroll, C.B. Lebrilla, *J. Am. Chem. Soc.*, **1996**, *118*, 6736.

[29] M. R. Asam, G. L. Glish, *J. Am. Soc. Mass Spectrom.*, **1997**, *8*, 987.

[30] L.P. Brull, V. Kovacik, J.E. Thomas-Oates, J. Haverkamp, *Rapid Commun. Mass Spectrom.*, **1998**, *12*, 1520.

[31] H. Desaire, J.A. Leary, *Anal. Chem.*, **1999**, *71*, 1997.

[32] M.T. Cancilla, A.W. Wong, L.R. Voss, C.B. Lebrilla, *Anal. Chem.*, **1999**, *71*, 3206.

[33] S.P. Gaucher, J.A. Leary, *J. Am. Soc. Mass Spectrom.*, **1999**, *10*, 269.

[34] S. Konig, J.A. Leary, *J. Am. Soc. Mass Spectrom.*, **1999**, *11*, 1125.

[35] X. Wang, T. Sakuma, E. Asafu-Adjaye, G. Shiu, *Anal. Chem.*, **1999**, *71*, 1579.

[36] A.P. Bruins, ESI Source Design and Dynamic Range Considerations. In: Electrospray Ionization Mass Spectrometry: Fundamentals, Instrumentation and Applications, R.B. Cole (Ed.), John Wiley and Sons Inc., **1997**, p130.

Chapter 3

LC/MS and LC/MS/MS of *Panax quinquefolium* L. (American Ginseng) root extracts: Separation and structure characterization of new ginsenosides

Using ten standards, liquid chromatography mass spectrometry (LC/MS) and LC/MS/MS methodologies for the separation and structural characterization of ginsenosides have been developed. The structural information provided by this approach includes molecular mass, sequence and composition of sugars, triterpene identification, and isomer differentiation.

The LC/MS method employs post-column addition of either NH_4OH and sodium acetate, with analysis in negative ion and positive ion modes, respectively. Ginsenosides readily form metal ion adducts, which are detected by mass spectrometry, and in the presence of NH_4OH, intense deprotonated ions are generated. LC/MS analysis of a mixture of ten standards revealed that LC separates some isomers; those which co-eluted and have indistinguishable MS/MS spectra cannot be differentiated by either LC/MS or LC/MS/MS. Co-eluting, non-isomeric ginsenosides are readily differentiated by LC/MS.

In general, triol-ginsenosides eluted earlier than their diol-containing counterparts under reversed-phase LC conditions. The 946 Da ginsenosides, Rd and Re, have different cores and elution times. Ginsenoside Re, which has a triol core, eluted seven minutes earlier than the diol-containing ginsenoside Rd. The diol-ginsenosides eluted according to the number of sugar moieties they contain. Therefore, the diol-ginsenoside with the most sugar residues, and thus the highest molecular mass, eluted first.

The LC/MS and LC/MS/MS characterization of the mixture of standards, have led to an approach for the separation and structural characterization of ginsenosides from ginseng root extracts. Analysis of an American ginseng root extract revealed that the mixture is very complex and that there are more ginsenosides than is listed in the literature cited. Structure proposals are discussed for ten of the new ginsenosides. These new compounds included a malonic acid ester, a succinic acid ester, two acetic acid esters, two trisaccharide-containing ginsenosides, and isomers of known ginsenosides.

This LC/MS/MS approach has provided a means by which mixtures of ginsenosides may be analyzed. Trends in the elution characteristics as well as the mass spectrometric behaviour of ginsenosides are addressed.

Introduction

In Chapter 2, positive and negative ion ESMS and MS/MS methodologies were developed for structure characterization of ginsenosides. In this Chapter,

LC/MS and LC/MS/MS approaches based on these methodologies are extended to structure characterization of *new* ginsenosides.

There are 64 ginsenosides reported up to 1985 [1a] and at least 31 reported between 1986 and 2001 [1b-j]. The majority consists of a triterpene core, which can be either protopanaxadiol (diol) or protopanaxatriol (triol). Sugars are attached to the triterpenes via *O*-glycosidic linkages; diol cores have sugars attached to C3 and C20, while triol cores have sugars attached to C6 and C20, respectively (see Scheme 1 and Section A of the Appendix).

Mass spectrometry [2] and other conventional analytical techniques have been used to analyze ginsenosides. These techniques include: 1) TLC [3]; 2) colourimetry [4]; 3) nuclear magnetic resonance (NMR) spectroscopy [5]; 4) gas chromatography (GC) [6]; and 5) liquid chromatography (LC) [7]. Although definitive structural assignments have relied primarily on NMR analyses [5], this technique requires a considerably larger amount of analyte than any mass spectrometric approach.

Early mass spectrometric analyses of ginsenosides included chemical ionization mass spectrometry (CIMS) [2b], field desorption mass spectrometry [2c,d], fast-atom bombardment mass spectrometry (FAB) [2e], and ^{252}Cf-plasma desorption mass spectrometry (PDMS) [2f]. Many of the latter approaches required derivatization prior to analysis. Of these methods, only FDMS analysis has yielded the metal ion adduct of ginsenosides.

More recently, ESMS approaches based on the formation of adducts between metal ions and ginsenosides have been described [2h-j]. Analysis by ESMS did not require a time-consuming derivatization step. This observation is

not without precedent because it is a well-established fact that sugars form complexes with metal ions [8a], and that these complexes may be detected by mass spectrometry [8b].

HPLC in conjunction with mass spectrometry – a technique popularly referred to as LC/MS – has been employed to analyze mixtures of ginsenosides [9]. This hybrid technique is a powerful tool for the separation and structural analysis of large, polar, involatile compounds such as ginsenosides. FAB [9b,c], thermospray (TS) [9d], and ES [1j,10] are ionization methods that have been employed in these LC/MS approaches. As with ES, TS does not require that the ginsenosides be derivatized prior to analysis. We are interested in using electrospray ionization (ESI) in the LC/MS method and thus these articles are discussed.

In 1995, van Breemen et al. [10a] observed that underivatized ginsenosides could be analyzed by LC/MS using ESMS. Under these conditions, ginsenosides formed complexes with Na^+ ions. The formation of Na^+ adducts was exciting since it provided a facile route to analyzing ginsenosides without derivatization. Moreover, the formation of the Na^+ attachment ion, with background concentrations of Na^+, showed the high affinity of ginsenosides for Na^+.

Recently, Wang et al. [10b] reported an LC/MS/MS method in which H^+ and Na^+ attachment ions of ginsenosides were subjected to CID experiments. It was concluded that more structurally useful product ions were obtained from CID experiments on the H^+ attachment ions of ginsenosides, relative to the Na^+ attachment ions. MS/MS experiments on the proton attachment ions of

ginsenosides allowed the types of sugars, i.e., hexose versus pentose, the *O*-glycosidic linkage, and the mass of the triterpene core to be determined.

In the same year, Fuzzati et al. [10c] developed two LC methodologies for analyzing mixtures of ginsenosides. The first employed evaporative light scattering detection (ELSD) and the second, negative ion ESMS detection. A comparison of the two methodologies was presented. The idea was to demonstrate that an LC/MS method is as sensitive as an LC/ELSD method. ELSD was chosen because ginsenosides exhibit low UV absorbance (~203 nm). The LC/ELSD method and the LC/MS method have independently identified 25 ginsenosides from Korean ginseng. Quantification of ginsenosides by the two methods showed similar results. These researchers also reported new ginsenosides, which are isomers of ginsenosides Ra_1 and Ra_2 [1]; structures were not provided.

In two independent studies, Chan et al. [10d] and van Breemen et al. [10e] used LC/MS and LC/MS/MS, respectively, to differentiate between Asian ginseng and American ginseng. Chan et al. [10d] proposed that Asian ginseng might be differentiated from American ginseng because 24-(*R*)-pseudoginsenoside F11 (MW = 800 Da) is unique to American ginseng, whereas its isomer ginsenoside Rf is only found in Asian ginseng. However, van Breemen et al. [10e] reported that both these ginsenosides are present in Asian ginseng whereas American ginseng only contains 24-(*R*)-pseudoginsenoside F11 (MW = 800 Da). The latter authors also proposed that the ratio of the two isomers may be used to identify Asian ginseng and determine whether it was contaminated with American ginseng.

In our work, LC/MS as well as LC in conjunction with tandem mass spectrometry (MS/MS) techniques were explored. These experiments were performed on a triple quadrupole mass spectrometer equipped with an ES source. Scan functions such as product ion, precursor ion, and neutral loss are accessible with this instrument [11]. Product and precursor ion scans were addressed in Chapter 1. Neutral loss scans are useful for identifying compound classes. For example, under positive ion ES MS/MS conditions, ginsenosides lose a neutral corresponding to the sugar bonded to the triterpene core [2h]. If the sugar is a hexose disaccharide, then the neutral species lost has a mass of 342 Da. Therefore, a neutral loss scan of 342 Da, may aid in identification of ginsenosides containing this disaccharide. The hybrid technique LC/MS in conjunction with the different scan functions are suited for analysis of complex mixtures such as ginseng root extracts, and also enable identification of new compounds.

The ginsenoside standards shown in Scheme 1 in conjunction with the approach of Chapter 2 will be used to develop an LC/MS approach for the analysis of ginsenosides. The infusion ES MS/MS experiments reported in Chapter 2 [2h], have showed that the most useful structural information was obtained from ginsenoside-Li^+ attachment ions. Additionally, aqueous solutions of ginsenosides give ES mass spectra which show both the $[M+Na]^+$ and the $[M+K]^+$ adduct ions [2h]. Because Na^+ is present in samples as well as common laboratory solvents, post-column addition of Na^+ (rather than Li^+) was chosen for the positive ion LC/MS experiments. Furthermore, the mass difference between Li^+ and Na^+ is 16 Da, and there are ginsenosides differing in mass by 16 Da; see

Section A of the Appendix for a list of known ginsenosides. Thus, the 16 Da difference between Li^+ and Na^+ could easily result in misleading interpretations; it would be very difficult to differentiate between the Li^+ and Na^+ attachment ions of a single ginsenoside, and ginsenosides differing in mass by 16 Da.

The ten ginsenoside standards are grouped in five molecular mass classes, of which three have isomeric compounds. The LC/MS method is evaluated – using the ten standards – for its ability to differentiate isomeric and co-eluting ginsenosides. The latter points are important in the development of LC/MS separations of complex mixtures. Once the new LC/MS method has been evaluated, it is applied to the separation of ginsenosides from an American ginseng root extract as well as over-the-counter ginseng preparations. LC/MS using selected-ion monitoring (SIM) of the Na^+ adducts of ginsenosides, as well as LC/MS/MS experiments are employed to identify ginsenosides of known structure. Full scan acquisition methods are used for identifying new ginsenosides. The structures of new ginsenosides are probed using both positive and negative ion LC/MS/MS experiments.

Experimental

Ginsenosides Rb_1, Rb_2, Rc, Rd, Re, Rf, and Rg_1 were purchased from Indofine Chemical Company Inc (N.J., U.S.A.), while ginsenosides Rb_3 and Rg_3 and gypenoside XVII were donated by Agriculture Canada (Delhi, Canada); see Scheme 1. A 'crude extraction' of ginsenosides from a sample of dried American ginseng root – donated by Mr Jeffrey Rice of J.C.K. Farms Limited in Brantford, Ontario – was accomplished by sonication in CH_3OH by Dipa Patel, a past

undergraduate student at McMaster University. Further sonication in 95%:5% C_2H_5OH:H_2O (v/v) and refluxing in 95%:5% C_2H_5OH:H_2O (v/v) was done to obtain the ginsenoside extract used in these experiments. The over-the-counter preparations – 'Certified' Korean Red Panax ginseng and 'Nature Made' Korean White ginseng – were extracted by refluxing in 95%:5% C_2H_5OH:H_2O (v/v). In both cases, the extract was subjected to a clean-up step using a solid-phase extraction cartridge.

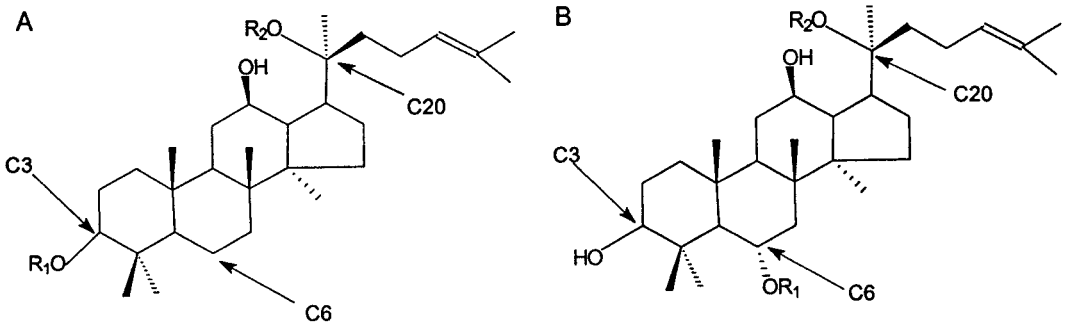

	R_1	R_2	MW
A. Protopanaxadiol	H	H	460
Ginsenoside			
Rb_1	Glc^1-O-^{2}Glc-	Glc^1-O-^{6}Glc-	1108
Rb_2	Glc^1-O-^{2}Glc-	Ara^1-O-^{6}Glc-	1078
Rb_3	Glc^1-O-^{2}Glc-	Xyl^1-O-^{6}Glc-	1078
Rc	Glc^1-O-^{2}Glc-	$Ara(f)^1$-O-^{6}-Glc-	1078
Rd	Glc^1-O-^{2}Glc-	Glc-	946
Gypenoside XVII	Glc-	Glc^1-O-^{6}Glc-	946
Rg_3	Glc^1-O-^{2}Glc-	H	784
B. Protopanaxatriol	H	H	476
Ginsenoside			
Re	Rhm^1-O-^{2}Glc-	Glc-	946
Rf	Glc^1-O-^{2}Glc-	H	800
Rg_1	Glc-	Glc-	800

Scheme 1: Structures of ten ginsenoside standards.

The cartridge used in these experiments was a Mega Bond Elut from Varian, Inc. (Walnut Creek, CA); 10g C_{18} stationary phase. The cartridge was conditioned with 200 mL of each of C_2H_5OH : H_2O (v/v), and 20% C_2H_5OH : 80% H_2O. The extract was dissolved in 20% C_2H_5OH : 80% H_2O at a concentration of 30 mg/mL. From this mixture, 60 mL were loaded onto the cartridge. The cartridge was washed with 200 mL 20% C_2H_5OH: 80% H_2O. The ginsenoside fraction was eluted with 120-200 mL 95%:5% C_2H_5OH:H_2O (v/v) and subjected to LC/MS analysis.

LC separations were performed on a Hewlett-Packard 1090 liquid chromatograph (Hewlett-Packard, Canada) equipped with a 1040A ultraviolet diode-array detector (UV-DAD) at 204 nm. Ten microliter injections were made onto a Restek Pinnacle PAH reversed-phase 3 μm C_{18} column (4.6 x 200 mm) with a column temperature of 40°C. The solvent gradient used: A = H_2O and B = ACN. The gradient followed the profile: 0 min, 80% A + 20% B; 20 min, 50% A + 50% B; 24 min, 0% A + 100% B; 29 min, 0% A + 100% B; 31 min, 80% A + 20% B; the flow rate was 600 μL/min.

Mass spectrometry experiments were performed on a Quattro LC triple quadrupole mass spectrometer (Micromass, England). The cone voltage was set at 120 V for positive ion experiments and 110 V for negative ion experiments. MS/MS experiments used Argon (collision cell pressure = 2 x 10^{-3} mBar) at collision energies between 30 eV and 40 eV.

Negative ion LC/MS experiments were performed with post-column addition of 0.1% ammonium hydroxide, and positive ion experiments with 10^{-5} M sodium acetate.

Results and Discussion

I. LC/MS analysis of a mixture of ginsenoside standards

a. Differentiating co-eluting and isomeric ginsenosides

There are 64 ginsenosides listed in the review published in 1985 [1a] and, to our knowledge, 31 additional compounds reported between 1986 and 2001 [1b-j]. The structures are provided in Section A of the Appendix. These ginsenosides are grouped into 47 molecular mass classes with a number of isomeric structures. Three molecular mass classes, for which there are isomers, are 800 Da (Rf and Rg_1), 946 Da (Rd, Re, and gypenoside XVII), and 1078 Da (Rb_2, Rb_3, and Rc); see Scheme 1. Using these eight ginsenosides as examples, we observed that isomeric ginsenosides differ in the type of triterpene core, the sugars attached to the triterpene core, and if they are comprised of the same core and saccharides, then their point of attachment to the core is different.

The advantages and limitations of our LC/MS approach were evaluated by separating a mixture of ten standards; see Scheme 1. Trends in the LC/MS analysis of the ten standards were applied to the interpretation of a similar analysis of reported and new ginsenosides in complex mixtures.

The method presented is a LC-UV/MS method. The UV chromatogram has provided indirect information about the presence of ginsenosides. Most ginsenosides contain only one chromophore, an alkene bond, thus limiting absorption to the lower end (~200 nm) of the UV spectrum. Some ginsenosides contain an isolated carbonyl group [1]. Therefore, UV diode array detection (UV-DAD) is not a conclusive method for identifying and differentiating ginsenosides.

On the other hand, UV detection is useful for identifying compounds which are not ginsenosides, i.e., those components which have distinct UV chromophores.

Figure 3-1 shows the UV and MS chromatograms for the reversed-phase LC separation of the mixture of ten ginsenoside standards. The assignment of ginsenosides to specific peaks in this UV chromatogram was done by comparison with the retention times observed in the UV chromatograms for individual ginsenoside standards (data not shown). The UV chromatogram, at 204 nm, shows eight peaks for the ten standards; see Figure 3-1. There are two pairs of co-eluting ginsenosides at the retention times 13 and 24 min. The first co-eluting pair is ginsenosides Rg_1 (800 Da) and Re (946 Da). LC/MS and LC/MS/MS experiments have confirmed the identities of these ginsenosides; see Figures 3-2 and 3-3.

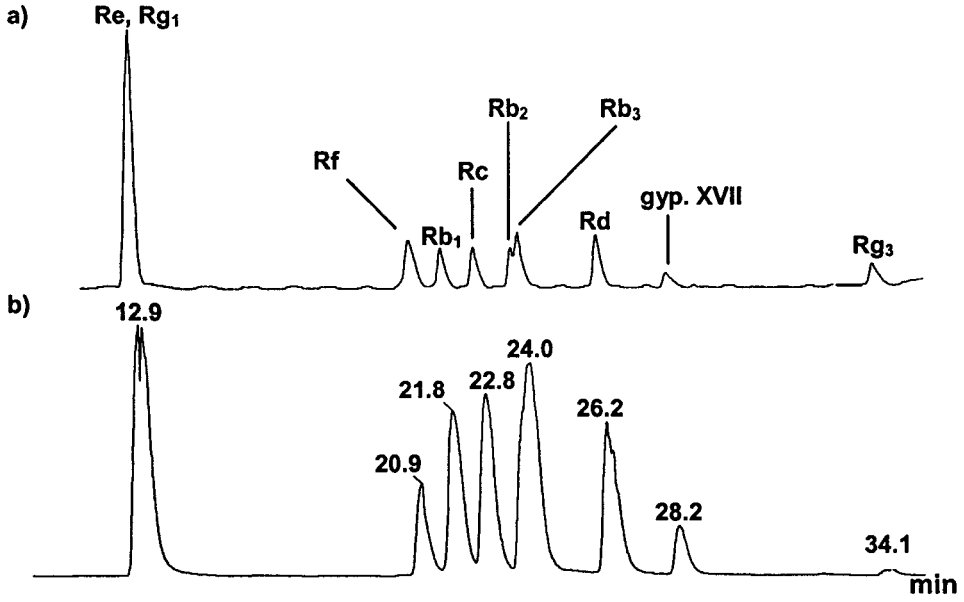

Figure 3-1: Reversed-phase LC/MS separation of 10 ginsenoside standards: UV chromatogram (204 nm), item a); and MS chromatogram, item b).

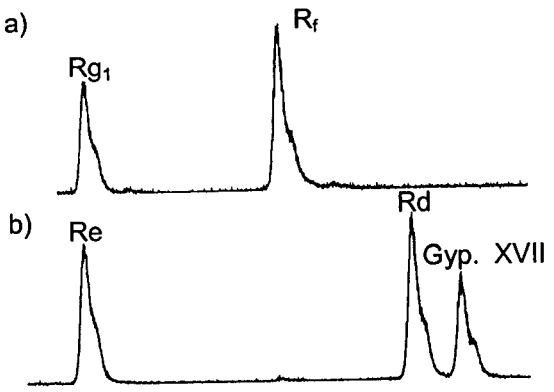

Figure 3-2: Ion chromatograms for m/z 823, ginsenosides Rg_1 and Rf, item a); and m/z 969, ginsenosides Rd, Re and gypenoside XVII, item b).

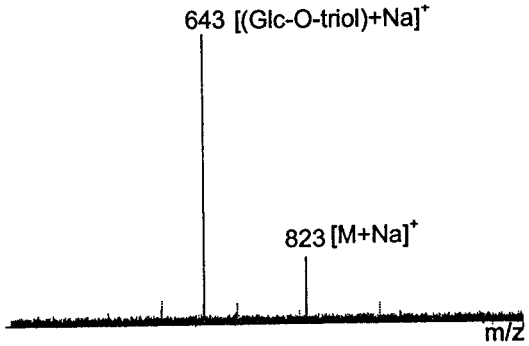

Figure 3-3: LC/MS/MS mass spectrum of the $[M+Na]^+$ ion, m/z 823, from the MS chromatogram shown in Figure 1b and the ion chromatogram in 2a; M = ginsenoside Rg_1.

The second co-eluting pair, ginsenosides Rb_2 and Rb_3, could not be differentiated by either LC/MS or LC/MS/MS since they differ by only one isomeric sugar moiety. Ginsenoside Rb_2 has an arabinose sugar, while ginsenoside Rb_3 has a xylose sugar; see Scheme 1. Arabinose has a pair of *cis* hydroxyl groups, while these hydroxyl groups have a *trans* relationship in xylose. This seemingly insignificant difference results in the two ginsenosides having identical MS/MS mass spectra and closely similar elution times.

The UV and MS chromatograms of Figure 3-1 and the ion chromatograms of Figure 3-2 illustrated that this LC/MS method is suitable for

separating the isomers in two of the three molecular mass groups examined; the 800 Da and 946 Da isomers. The third group of isomeric ginsenosides, with molecular mass 1078 Da, were not completely resolved.

b. Trends observed in the RP LC/MS analysis of ginsenoside standards

Based on the elution profile displayed in Figure 3-1 and the structures shown in Scheme 1, trends were observed. These trends along with the experimental evidence, which verify the trends and general observations, is also provided.

1. The more polar triol-ginsenosides eluted earlier than their diol-containing counterparts; see Figure 3-1 and Scheme 1.

2. It was observed that the polarity of the core and not the sugars, determined the retention time of triol-ginsenosides.

3. Triol-ginsenosides having a free C20 hydroxyl were retained longer on the column than their isomers which had sugar residues at C20.

4. Diol-ginsenosides eluted according to the number of sugar moieties they contained. This implied that these ginsenosides eluted according to decreasing molecular mass.

In general, diol-ginsenosides eluted later than triol-ginsenosides. Ginsenoside Re has a triol core whereas its isomers ginsenoside Rd and gypenoside XVII have diol cores; see Scheme 1. Each of these isomers has three sugar moieties attached to the core. The chromatograms of Figure 3-1 show that ginsenoside Rd eluted ~ 2 min earlier than gypenoside XVII, but the

triol-containing ginsenoside Re eluted 13 min earlier than Rd! Confirmatory evidence that the sugar residues did not play a major role in determining the polarity of triol-ginsenosides was obtained by comparing the retention times for ginsenosides Re, Rf and Rg_1. Ginsenosides Re, MW = 946 Da, and Rg_1, MW = 800 Da, co-elute at 13 min but ginsenoside Rf, MW = 800 Da, eluted 8 min later. Ginsenoside Re has three sugars attached to it, one more than either of ginsenosides Rf or Rg_1. Therefore, the sugar moieties do not seem to play a significant role in determining the polarity of triol-ginsenosides. The observations presented above were used to define a retention time window for elution of diol- and triol-ginsenosides.

Triol-ginsenosides tend to elute before 20 min while diol-ginsenosides elute after 22 min. This 'rule' is derived from the observed retention times for triol- and diol-ginsenoside standards (see Scheme 1 and Figure 3-1) and is not applicable to ginsenosides containing a carboxylic acid functional group. Therefore, if the identity of the core is not obtained from negative ion ESMS experiments, the retention time may be used to assign the core type.

Evidence supporting the third trend was obtained by comparison of the retention times for the triol-ginsenosides Rf and Rg_1; the former was retained longer on the column. The only structural difference between these isomeric compounds is the point of attachment of the sugar residues to the core; see Scheme 1. Ginsenoside Rg_1 has glucose moieties attached to C6 and C20, whereas ginsenoside Rf has a glucose disaccharide attached to C6. Therefore, ginsenoside Rf has a free hydroxyl at C20. A longer retention time for ginsenoside Rf is attributed to more facile access of the alkyl chain at C20 to the

C_{18} stationary phase. This fostered increased partitioning of the alkyl chain with the stationary phase, and thus longer retention time. These observations were consistent with chromatographic separation. In the analysis of a mixture by LC, compounds close in structure with the stationary phase have a higher affinity for the stationary phase and thus will be retained for a longer period. A similar observation was made for the retention times of ginsenoside Rd and gypenoside XVII.

The elution time for ginsenoside Rd differed from that of gypenoside XVII by two minutes. Ginsenoside Rd has a hexose disaccharide at C3, and a hexose at C20; the reverse is true for gypenoside XVII (see Scheme 1). This observation was rationalized by proposing that the C20 position of ginsenoside Rd has a smaller radius than that of gypenoside XVII. Thus, ginsenoside Rd spent a shorter time partitioning with the stationary phase than does gypenoside XVII.

In general, diol-ginsenosides eluted in order of decreasing number of sugar units; see Figure 3-1 and Scheme 1. The elution order of the diol-ginsenosides is also correlated to molecular mass (*vide supra*). The order of elution for the diol-containing ginsenosides was: 1) ginsenoside Rb_1, MW = 1108 Da, which contains two hexose disaccharides; 2) the 1078 Da isomers which contain a hexose disaccharide and a pentose/hexose disaccharide; 3) the 946 Da isomers which contain three hexose sugars; and 4) ginsenoside Rg_3, MW = 784 Da, which contains one hexose sugar. Therefore, the number and type of sugar units played a major role in determining the elution order of diol-containing ginsenosides.

The dominant role that the sugar moieties played in determining the polarity of diol-containing ginsenosides was evidenced by two observations. Ginsenosides differing by a –CHOH group, and ginsenosides differing in the conformation of one sugar moiety were chromatographically separated. Ginsenosides Rb_1 and Rc, which differ by a –CHOH group, have elution times that differ by one minute; see Scheme 1 and Figure 3-1. Furthermore, of the 1078 Da isomers, ginsenoside Rc eluted earlier than the co-eluting pair ginsenosides Rb_2 and Rb_3. The pentose sugar in ginsenoside Rc has the *furanose* form, whereas the pentose sugars in ginsenosides Rb_2 and Rb_3 have the *pyranose* form. These latter observations showed that this LC separation was sensitive to the size of the sugar (pentose versus hexose) as well as its conformation (*furanose* versus *pyranose*).

II. LC/MS and LC/MS/MS analysis of ginseng extracts and commercial preparations

a) Complexity of the American ginseng root extract

Before LC/MS analysis, the ginsenoside-containing fraction from the root extract was analyzed by infusion ESMS. This experiment provided the molecular mass range for ginsenosides present in the root extract. Positive ion mode infusion ESMS of this fraction yielded the mass spectrum shown in Figure 3-4. The spectrum is dominated by four peaks (m/z 789, m/z 969, m/z 1101, m/z 1131) and about eight additional peaks of lower intensity. This sample of ginsenoside extract was then analyzed by LC/MS.

The UV and MS chromatograms from the LC/MS separation of the ginsenoside extract are shown in Figure 3-5. Many more peaks were observed in

the MS chromatogram relative to the infusion ESMS experiment, compare Figures 3-4 and 3-5b. The larger number of peaks in the MS chromatogram illustrated the complexity of the root extract.

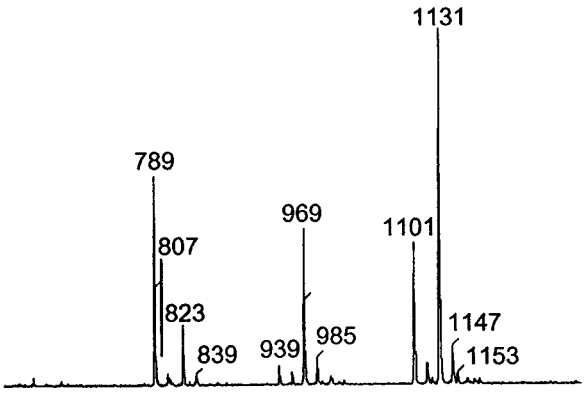

Figure 3-4: Analysis of the ginsenoside fraction from American ginseng roots by infusion ESMS; positive ion ES mass spectrum shown.

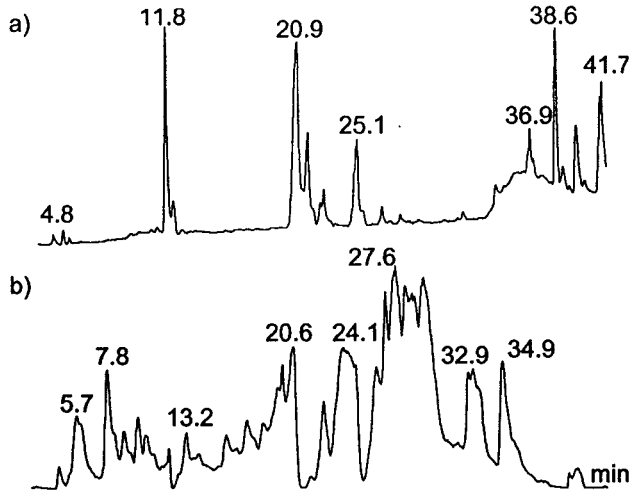

Figure 3-5: Separation of ginsenosides from American ginseng root extracts: the LC chromatogram (204 nm), item a) and the MS chromatogram, item b).

The LC-UV chromatogram of Figure 3-5a provided useful information. The early-eluting compounds (0-30 min) mainly displayed absorption in the range of 200-210 nm, while the compounds eluting in the range 30-40 min,

showed absorption at longer wavelengths. Those components exhibiting high-UV absorption are not ginsenosides.

The sensitivity of mass spectrometry as a detector for ginsenosides relative to UV was evident in the LC-UV and MS chromatograms shown in Figure 3-5. These two chromatograms show that even when a signal was not present in the UV chromatogram, e.g., between 12 and 21 min, ginsenosides were present. The MS chromatogram corresponded to data collected in the selected-ion monitoring (SIM) mode. The mass values used in the SIM experiment corresponded to the Na^+ adducts of the molecular masses presented by Shoji [1a]; see Section A.i. of the Appendix for this list.

Figure 3-6 shows ion chromatograms for five ions observed in the infusion experiment (Figure 3-4) which also correspond to the five molecular masses of the standards used (see Scheme 1). In the spectrum of Figure 3-4, the intensities of m/z 807 and m/z 823 relative to any of m/z 969, m/z 1101 and m/z 1131 are low. Nevertheless, the quality of all ion chromatograms in Figure 3-6 is an excellent attestment to the sensitivity of the MS method.

A primary goal of this work was to develop an LC method capable of separating as many ginsenosides as possible, particularly isomeric ginsenosides. The ion chromatograms of Figure 3-6 are those of isomeric ginsenosides and illustrate that the LC method accomplished the separation of many isomeric ginsenosides. Ion chromatograms corresponding with the Na^+ attachment ion of the reported ginsenosides [1] are provided in Section A of the Appendix. The peak widths in these mass chromatograms are variable,

consistent with the partial resolution of isomeric compounds. These observations indicate the complexity of this root extract.

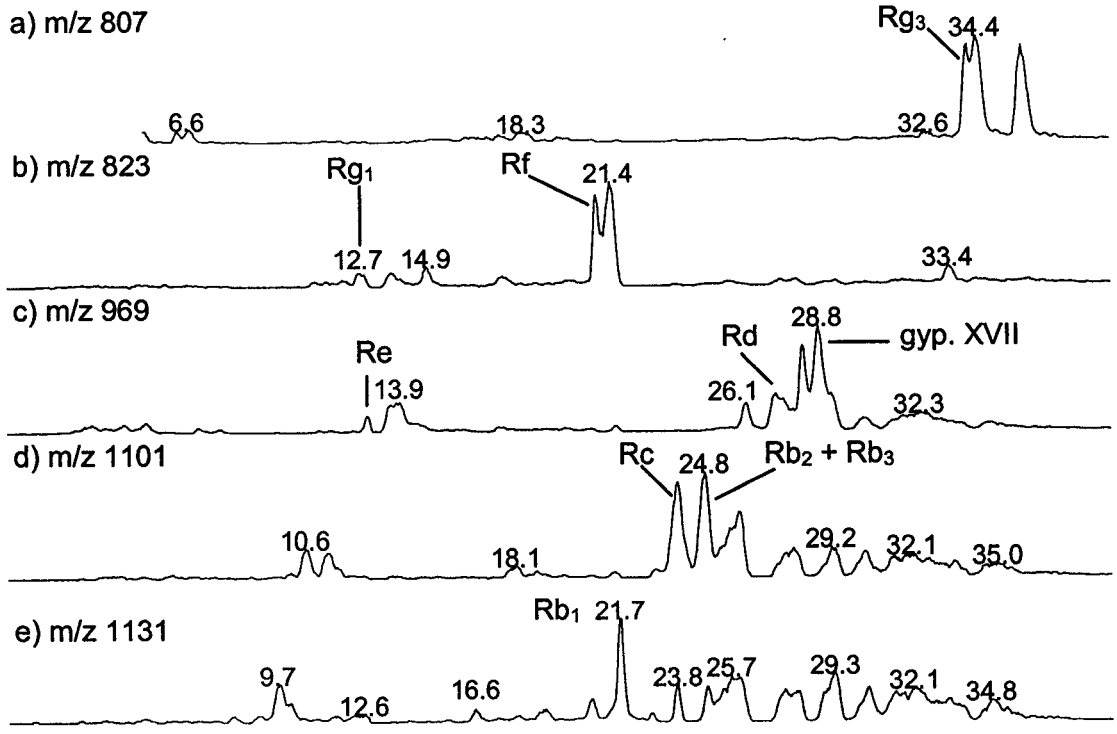

Figure 3-6: Ion chromatograms for m/z 807, item a); m/z 823, item b); m/z 969, item c); m/z 1101, item d); and m/z 1131, item e) from an American ginseng root extract.

It well known that metal ion adducts of sugars are detected by mass spectrometry [8], and that the stereochemistry of the hydroxyl groups on the sugar influences metal ion complexation to sugars [12]. There are two concerns that resulted from these facts. Firstly, isomeric ginsenosides may display different Na^+ complexation efficiencies and therefore give different responses under MS analysis. Secondly, it is of interest to investigate whether the number of sugars that a ginsenoside contains enhances its complexation with Na^+. The

with Na^+. The ginsenosides chosen to address these concerns were the 946 Da isomers, ginsenosides Re and Rd and gypenoside XVII, and the 1108 Da ginsenoside Rb_1; see Scheme 1. The 946 Da isomers differ in their core type as well as the type and arrangement of sugars on the core. Meanwhile, ginsenoside Rb_1 was chosen because it has four sugars attached to the core whereas ginsenoside Rd and gypenoside XVII have three sugars. Digitoxin, MW = 764 Da, with three 2,6-dideoxy ribose moieties attached to a steroid core, was used as the internal standard.

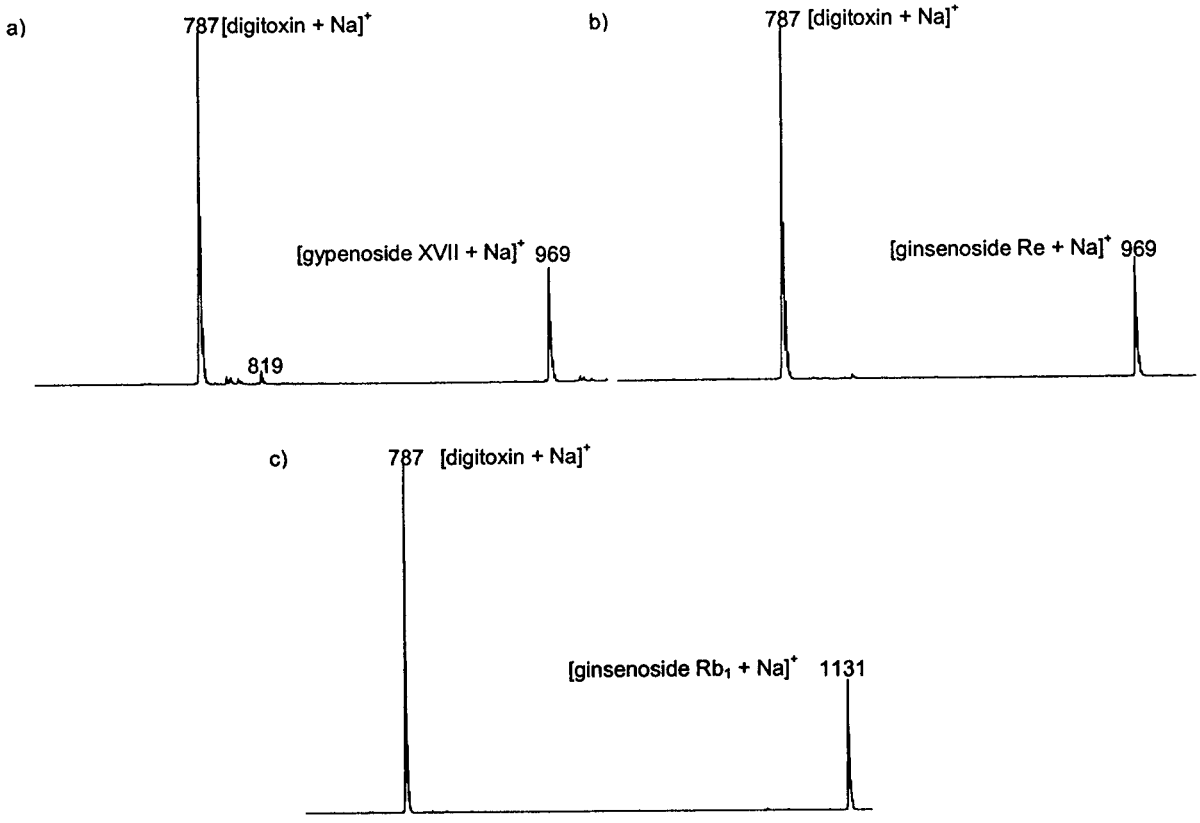

Figure 3-7: Positive ion infusion ESMS analysis of solutions containing a 1:1:3 molar ratio of: gypenoside XVII:digitoxin:Na^+, item a); ginsenoside Re:digitoxin:Na^+, item b); and ginsenoside Rb_1:digitoxin:Na^+, item c).

Each ginsenoside was mixed with sodium acetate and digitoxin so that the molar ratio of Na^+ : ginsenoside : digitoxin was 3:1:1. This molar ratio ensured that there was sufficient Na^+ for complexation to both digitoxin and the ginsenoside.

An aliquot of each of the analyte solutions was analyzed by ESMS, and the intensity of the Na^+ adduct ions was monitored. It was observed that the intensity ratios of the peaks corresponding to the $[M+Na]^+$ ions of the ginsenosides to digitoxin was similar for the isomeric ginsenosides as well as for ginsenoside Rb_1. These observations suggested that under ESMS conditions, formation of the Na^+ attachment ions of ginsenosides is independent of the arrangement of sugars on the triterpene core and the number of sugar moieties attached to the ring; see Figure 3-7 and Scheme 1. Thus, the response factors for all ginsenosides (under these ESMS conditions) were assumed to be similar.

The next section provides an evaluation of the ginsenoside content of over-the-counter ginseng preparations relative to that of an American ginseng root extract.

b) Comparison of American ginseng root extract with Korean Red and Korean White ginseng preparations

The purpose of this comparison was to evaluate the ability of LC/MS and LC/MS/MS methods to examine these complex mixtures and to determine the relative ratios of ginsenosides present within the over-the-counter preparations relative to that in an American ginseng root. Extracts from an American ginseng root and from two over-the-counter preparations were analyzed by LC/MS; the mass chromatograms are shown in Figure 3-8.

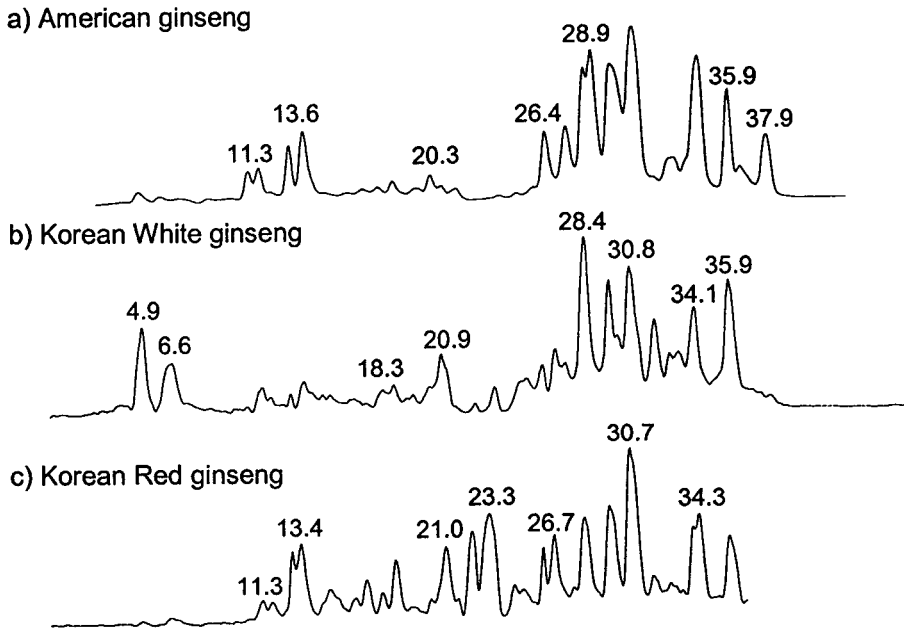

Figure 3-8: Mass chromatograms of an LC/MS separation of extracts from American ginseng root, item a), Korean White ginseng preparation, item b), Korean Red ginseng preparation, item c).

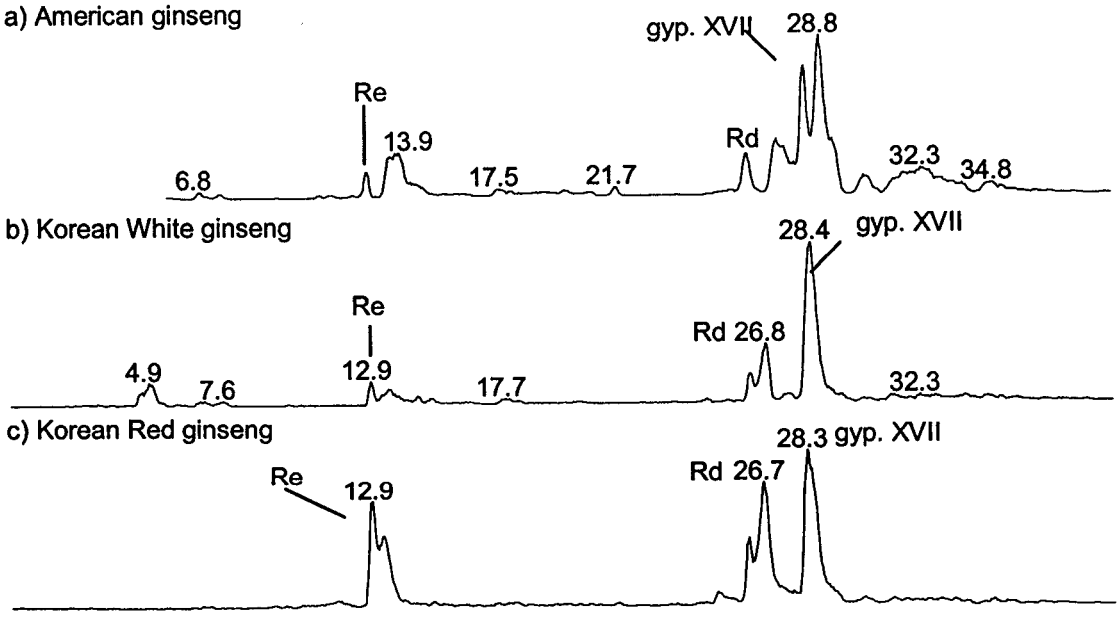

Figure 3-9: Ion chromatograms of the 946 Da isomers from American ginseng, item a), Korean White ginseng, item b), Korean Red ginseng, item c).

The composition and relative ratios of ginsenosides *within* the Korean Red, Korean White, and American ginseng extracts are different. This became more evident when the ion chromatograms for the 946 Da ginsenosides were compared; see Figure 3-9. Additional ion chromatograms for each of American, Korean Red and Korean White ginsengs are provided in Sections B to G of the Appendix. The latter chromatograms illustrated that, among three species of ginseng, the relative concentration of ginsenosides in a specific molecular mass class is different.

The complexity of these ginseng extracts is captured more completely in Table 1. The data are compiled from the ion chromatograms corresponding to Na^+ adduct ions of reported ginsenosides [1], and which are presented in Sections B to G of the Appendix. An approximation of the number of sodiated ginsenosides were prepared by comparing the ion chromatograms of each of these ginseng extracts, and identifying correlations between the retention times of the peaks among the ion chromatograms. Table 1 summarizes these observations.

For each molecular mass class is included the mass of the $[M+Na]^+$ ion used to generate the ion chromatogram, along with the number of ginsenosides in each extract, and the total number of ginsenosides in that mass class compared to the number of reported ginsenosides. In summary, of the 47*molecular mass classes* reported [1], 40 are found for American ginseng, 38 for Korean White ginseng, and 36 for Korean Red ginseng. For American ginseng, there were 167 ginsenosides grouped into 40 molecular mass classes, for Korean White ginseng 127 ginsenosides were grouped within 38 molecular

mass classes, and for Korean Red ginseng 124 ginsenosides were grouped into 36 molecular mass classes.

Table 1: The numbers of ginsenosides observed in an American ginseng root extract and Korean Red and Korean White 'over-the-counter' preparations. The 95 reported ginsenosides, categorized in 47 molecular mass classes are also presented. Ginsenosides with peak intensities ≥ 1 x 10^5 are reported.

Molecular mass (Da)	$[M+Na]^+$	**Number of reported ginsenosides**	**Number of observed ginsenosides**		
			American ginseng	**Korean White ginseng**	**Korean Red ginseng**
622	645	**1**	0	0	1
636	659	**4**	1	6	3
638	661	**4**	5	4	7
652	675	**1**	1	0	1
654	677	**6**	3	1	5
670	693	**1**	1	0	1
672	695	**1**	0	0	0
724	747	**1**	0	0	0
754	777	**1**	2	1	2
770	793	**3**	0	4	3
782	805	**2**	7	4	4
784	807	**5**	8	4	5
786	809	**3**	5	3	8
794	817	**1**	4	2	0
800	823	**5**	6	4	5
802	825	**1**	5	1	5
814	837	**1**	2	1	0
816	839	**1**	4	3	0
828	851	**1**	1	4	1
842	865	**1**	2	1	1
902	925	**1**	0	2	0
916	939	**3**	4	2	4
926	949	**2**	2	0	0
***930**	953	**1**	3	2	3
932	955	**1**	9	5	9
944	967	**1**	4	1	2
946	969	**3**	7	6	5
948	971	**2**	8	5	5
956	979	**1**	3	4	2
962	985	**7**	7	5	5
974	997	**1**	0	0	1
980	1003	**1**	6	4	7
***988**	1011	**3**	7	3	2

* Structure proposals are provided for new ginsenosides from these molecular mass classes; see section d).

Molecular mass (Da)	$[M+Na]^+$	**Number of reported ginsenosides**	**Number of observed ginsenosides**		
			American ginseng	**Korean White ginseng**	**Korean Red ginseng**
1014	1037	**1**	2	1	0
1078	1101	**4**	6	5	4
***1032**	1055	**1**	3	4	1
1046	1069	**1**	2	0	0
***1108**	1131	**1**	5	3	2
1120	1143	**3**	4	5	3
1122	1145	**1**	6	5	5
***1150**	1173	**1**	3	4	2
1164	1187	**2**	3	2	3
1194	1217	**1**	2	3	3
1210	1233	**3**	3	4	2
1232	1255	**1**	1	1	0
1240	1263	**3**	4	5	2
1270	1293	**1**	6	3	0
Total		**95**	**167**	**127**	**124**

* Structure proposals are provided for new ginsenosides from these molecular mass classes; see section d).

We have presented a cursory comparison between two species of Asian ginseng and American ginseng. One point that was raised in the introduction to this Chapter was differentiating between Asian ginseng and American ginseng. Two recent articles reported [10d,e] that American ginseng may be differentiated from Asian ginseng based on the presence of ginsenosides unique to each species. Chan et al. [10d] concluded that pseudoginsenoside F11 (MW = 800 Da) was unique to American ginseng and ginsenoside Rf (MW = 800 Da) was unique to Asian ginseng. Van Breemen et al. [10e] confirmed that pseudoginsenoside F11 is unique to American ginseng, but reported that Asian ginseng contained both isomers.

During the process of identifying the reported ginsenosides in our sample of American ginseng, ginsenosides consistent with the molecular mass,

triterpene type, and disaccharide of pseudoginsenoside F11 as well as ginsenoside Rf was identified in our sample of American ginseng.

Although we have an authentic standard for ginsenoside Rf, this is not the case for pseudoginsenoside F11. Therefore, its identification is based on the following. Pseudoginsensoside F11 and ginsenoside Rf are 800 Da isomers which differ because their core type, and the attached disaccharide are different; see Section A.i. of the Appendix. Ginsenoside Rf contains a hexose disaccharide attached to a core with elemental composition $C_{30}H_{52}O_5$, whereas pseudoginsenoside F11 has a core with elemental composition $C_{30}H_{52}O_6$, and a deoxyhexose/hexose disaccharide. These ginsenosides were identified by 'extracting' the summed positive ion LC/MS/MS ion chromatogram corresponding to the Na^+ attachment ion of their (unique) disaccharides, and the precursor ion. The ion chromatograms, shown in Figure 3-10, illustrate that the two ginsenosides had retention times which were different by about 0.2 min.

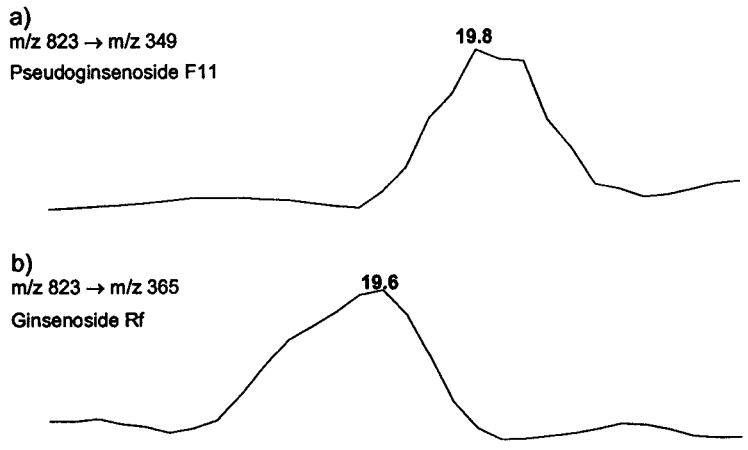

Figure 3-10: Ion chromatograms for m/z 349, item a), and m/z 365, item b). The ion chromatograms are generated from the LC/MS/MS experiment on the $[M+Na]^+$ ion of ginsenosides with molecular mass 800 Da.

These findings support the proposal that this sample of American ginseng contained both ginsenoside Rf and pseudoginsenoside F11.

c) Identification of known and new ginsenosides in American ginseng root

A comprehensive list of reported ginsenosides and their structures from a number of species of ginseng are provided in Section A of the Appendix. These varieties included American ginseng, Red ginseng, Chikusetsu ginseng, San-chi ginseng, Zu Tziseng, *Panax pseudoginseng*, Chinese *Panax Japonicus*, *Panax ginseng*, *Panax vietnamensis* Ha *et* Grushv, [1]. Of these 95 ginsenosides, there are 21 compounds which are known to have isomers.

LC/MS of the ginsenoside fraction of an American ginseng root extract was used to detect the Na^+ adduct ions of the reported ginsenosides [1]. The ion chromatograms for these sodiated ginsenosides are provided in Sections B and E of the Appendix. The molecular masses of many reported ginsenosides – including malonyl ginsenosides – were detected. The ginsenoside standards used in this work were identified by comparison to their LC/MS chromatograms. Sodium attachment ions of molecular masses corresponding to ginsenoside Ro (956 Da), quinquenoside R1 (1150 Da) and pseudoginsenoside F11 (800 Da) were detected by LC/MS and their structures were confirmed by LC/MS/MS experiments of their $[M+Na]^+$ ions (not shown).

Malonic acid esters of ginsenosides Rb_1, Rd and one of Rc, Rb_2, or Rb_3 were more readily identified – by both positive and negative ion LC/MS – in the room temperature C_2H_5OH (95%) extract of American ginseng root. In order for these ginsenosides to be observed in negative ion LC/MS, sodium acetate was

used as the post-column additive. The weakly basic solution, 0.1% (v/v) NH_4OH, which was normally employed as the post-column additive in negative ion LC/MS, was sufficiently alkaline to promote decarboxylation of the malonyl ginsenosides. The LC/MS/MS spectra of the identified malonyl ginsenosides are given in Section H of the Appendix.

The LC/MS experiment, with the mass spectrometer recording full-scan spectra in the mass range 600 Da to 1300 Da, is also used to identify the ginsenosides having molecular masses that were not, to our knowledge, previously reported. A list of the masses for these new ginsenosides is provided in Table 2.

Table 2: A list of ginsenosides with new molecular masses from our sample of American ginseng root. (These molecular masses were obtained from the LC/MS experiment where full scan spectra were acquired. Only those masses which had an intensity > 1x 10^5 were recorded.)

$[M+Na]^+$	Molecular mass	Retention window (min)
707, 1049	684, 1026	3.5-5.5
995, 1001, 1017	972, 978, 994	5.5-7.5
841, 1247	818, 1224	7.5-9.5
1165, 1247	948, 1142, 1224	9.5-11.5
801, **1165**	778, **1142**	11.5-13.5
1117, 1133, **1147**, 1163, 1179, **1231**	**1094**, 1110, **1124**, 1140, 1156, **1208**	13.5-15.5
1117, 1147, 1149	1094, 1124, 1126	15.5-17.5
841, 1001, 1017	818, 978, 994	17.5-19.5
801, 983, 1129	778, 960, 1106	19.5-21.5
767, 1117, 1147	744, 1094, 1124	21.5-23.5
831, 1117, 1123, 1189	808, 1094, 1100, 1166	23.5-25.5
831	808, 842	25.5-27.5
857, 993, 1199	834, 970, 1176	27.5-29.5
831	808	29.5-31.5

*Structure proposals are provided for these ginsenosides.

The list in Table 2 contains a total of 39 ginsenosides categorized into 26 molecular mass groups. When taken together with the ginsenosides of known masses in Table 1, a total of 111 new compounds have been identified in American ginseng.

In Chapter 2, we reported that metal ion adducts of ginsenosides undergo preferential cleavage at C20 of the triterpene to afford a sodiated saccharide ion. This dissociation can be used as the basis for neutral loss scans to detect ginsenosides which contain a specified sugar at C20 of the core.

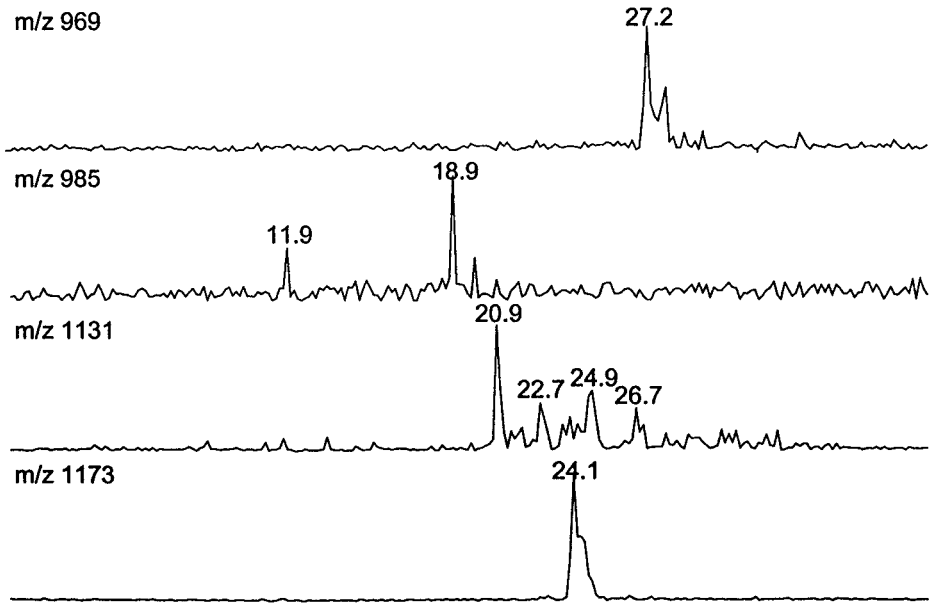

Figure 3-11: Ion chromatograms for known ginsenosides from four molecular mass classes, and which contain a glucose disaccharide at C20 of the core. These ginsenosides were detected via a neutral loss scan of 342 Da; a glucose disaccharide.

Therefore, we explored the use of neutral loss scans to identify ginsenosides comprising of hexose and pentose/hexose disaccharides. Using this technique, we detected 4 of 7 ginsenosides from Reference 1a, which should undergo loss

of a hexose disaccharide. These ion chromatograms are provided in Figure 3-11. Neutral loss scans may be used as a complementary technique for identifying ginsenosides.

The next section discusses structure proposals for ten new ginsenosides from an American ginseng root extract.

d) Structural characterization of new ginsenosides from American Ginseng roots using LC/MS/MS experiments

An ES MS/MS approach for structural characterization of ginsenosides based on analysis of metal ion adducts and deprotonated ginsenoside ions have been reported [2h]. This methodology was used in combination with the trends described in section I to propose structures for ten new ginsenosides. A number of reasons prevented structure characterization of additional compounds. For many of the new ginsenosides, it was not possible to obtain reliable positive ion or negative ion LC/MS/MS spectra. While injecting larger concentrations of extract onto the column may have helped to overcome this problem for some compounds, this approach would have resulted in poorer chromatographic separations and a dirtier ion source. Finally, some new ginsenosides afforded intense LC/MS/MS spectra which were not readily interpreted, and thus new structures could not be proposed with any confidence. Therefore, structures were proposed for ten new ginsenosides; six from the molecular mass classes in bold font in Table1 and the four compounds in bold font in Table 2. Before describing the structures of new ginsenosides, a brief summary of the previous work [2h] is warranted.

In general, positive ion MS/MS experiments on metal ion adducts of ginsenosides showed preferential bond cleavage (of the sugar) at C20 of the core. This dissociation resulted in two signals representing complementary parts of the ginsenoside. The trends identified in the positive ion MS/MS experiments were best represented by the nomenclature system in Scheme 2. Negative ion ESMS experiments corroborated and complemented structural information obtained from positive ion experiments. Negative ion ESMS experiments were performed in the presence of 0.1% (v/v) NH_4OH. The resulting mass spectra provided molecular mass, triterpene identification, and saccharide composition and sequence.

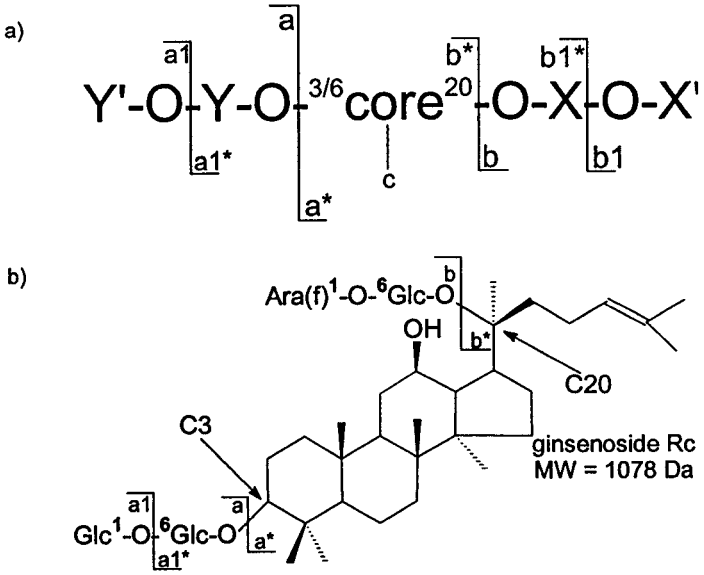

Scheme 2: Schematic representation of the nomenclature used to assign structures to ginsenosides, item a), and a model compound ginsenoside Rc, item b).

Unless otherwise stated, the structures proposed for the ten new ginsenosides were deduced from structural information inferred from both

positive and negative ion ESMS and MS/MS experiments. The intensity ratios of the fragment ions corresponding with 9 of 10 new ginsenosides are presented in Table 3. The ginsenosides are arranged according to their elution from the reversed-phase column. The structure of the ginsenoside in entry **9** cannot be represented by the nomenclature depicted in Scheme 2.

Table 3: New ginsenosides, M, and the relative intensity ratio of their product ions (a blank space indicates a relative intensity of ≤1%).

Entry	$[M+Na]^+$	M	Retention time (min)	a	a*	b	b*	b1	b1*
1	1055	**1032**	5.7		21	49	15	100	35
2	1165	**1142**	12.1			100	25		
3	1147	**1124**	14.2			100	30		
4	1231	**1208**	14.2	37	20	100			
5	1117	**1094**	14.7	11		100	41		
6	1011	**988**	18.7	9		100	35		
7	1173	**1150**	25.3	70	33	100	6		
8	1131	**1108**	25.5			100	17		
9	1131	**1108**	27.8			43		100	35
10	953	**930**	32.8	See the text for a discussion					

The retention times are provided in Table 3 because it helped in assigning the type of triterpene core, i.e., diol versus triol. As discussed in Section I, diol-ginsenosides eluted later than their triol counterparts. Although, the triterpene core may be identified *directly* from negative ion ES MS/MS experiments [2h], sufficient material was necessary to do these experiments successfully. Negative ion experiments of ginsenosides are at least 10-fold less sensitive than positive ion experiments. Therefore, in cases when the negative ion LC/MS/MS experiments could not provide conclusive results, retention times were used to assign core types to new ginsenosides.

Proposed structures of ten new ginsenosides are presented in Scheme 3. The triterpene is the backbone to which the substituents R_1 to R_4 are attached. The saccharides are described as being deoxyhexose, hexose, or pentose. The approach described in this work cannot differentiate between isomeric sugars, such as glucose and galactose.

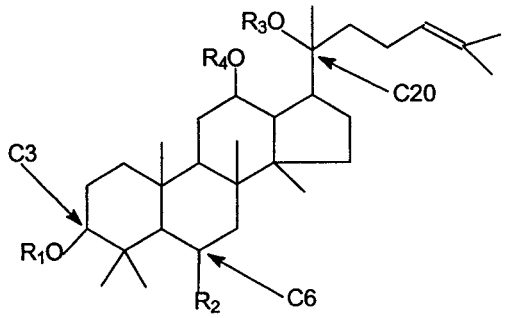

Entry	M	Assigned name	Core	R_1	R_2	R_3	R_4
1	1032	malonyl ginsenoside Re_1	Triol	H	hex-O-	HO_2C-CH_2-C(=O)-O-hex-O-deoxyhex-	H
2	1142	ginsenoside Rb_1A	New	See text for a discussion			
3	1124	ginsenoside Rb_4	Triol	H	hex-O-hex-O-	hex-O-hex-	H
4	1208	succinyl ginsenoside Rb_1	Diol	hex-O-hex-	H	HO_2C-$(CH_2)_2$-C(=O)-O-hex-O-hex-	H
5	1094	ginsenoside Rb_5	Triol	H	hex-O-hex-O-	pent-O-hex-	H
6	988	acetyl ginsenoside Re_2	Triol	H	hex-O-deoxyhex-O-	CH_3CO-hex-	H
7	1150	quinquenoside R2	Diol	hex-O-hex-	H	CH_3CO-hex-O-hex-	H
8	1108	ginsenoside Rb_6	Diol	hex-	H	hex-O-hex-	hex
9	1108	ginsenoside Rb_7	Diol	hex-	H	hex-O-hex-O-hex-	H
10	930	chikusetsusaponin IV	Diol	H	H	deoxyhex-O-hex-O-hex-	H

hex = hexose sugar; pent = pentose sugar; deoxyhex = deoxyhexose sugar

Scheme 3: Proposed structures for 10 new ginsenosides.

Another limitation to our approach was that it was not possible to assign (*absolutely*) *O*-glycosidic linkages between sugar moieties. In Chapter 2 [2h], an approach reported by Glish et al. [13] was used in order to assign *O*-glycosidic linkages in sugar residues from ginsenoside standards. The latter authors

reported that the Li^+ and Na^+ attachment ions of disaccharides undergo unique dissociations under ES MS/MS conditions. These dissociations are dependent on the *O*-glycosidic linkage in the disaccharide, and involve characteristic losses of 60 Da, 90 Da or 120 Da. A pseudo-MS/MS/MS experiment was employed to identify the *O*-glycosidic linkages in the disaccharides from ginsenoside standards[2h]. These pseudo-MS/MS/MS experiments were accomplished via in-source CID [14] in conjunction with an MS/MS experiment. In the analysis of a complex mixture of ginsenosides, such pseudo-MS/MS/MS experiments may not provide *O*-glycosidic linkage information as reliably as one would obtain with pure single compounds. Co-eluting, isomeric ginsenosides differing *only* in the type of *O*-glycosidic linkage would not be readily differentiated. This is because pseudo-MS/MS/MS experiments of ginsenosides differing in an *O*-glycosidic linkage would probably reflect a dissociation pattern characteristic of both linkages. Nevertheless, whenever it was possible to examine isolated components from the complex mixture, ions corresponding to losses of 60 Da, 90 Da and 120 Da were identified in the LC/MS/MS spectrum. These latter ions were used to assign a tentative *O*-glycosidic linkage.

The procedures used for the structure characterization of these new ginsenosides involve both negative ion and positive ion MS/MS experiments. The triterpene core was assigned based on negative ion LC/MS/MS experiments in combination with retention time information. The LC/MS/MS data is definitive, whereas the retention times are interpretive. The triol-ginsenoside standards eluted before 20 min and the diol standards eluted after ca. 22 min. Clearly, this guideline is not applicable to ginsenosides containing polar functionalities such

as a carboxylic acid functional group; see the discussion of the new ginsenoside in entry **4** of Table 3 and Scheme 3. The remainder of this section discusses the structure proposals.

*d).i. Entry **1** – **malonyl ginsenoside Re_1** **MW = 1032 Da***

Entry **1** of Table 2 and Scheme 3 is a member of the family of malonyl ginsenosides. The CID spectra of this class of ginsenosides are characterized by peaks corresponding to loss of 44 Da (CO_2) – not necessarily from the precursor ion – see Figure 3-12 and Section H of the Appendix.

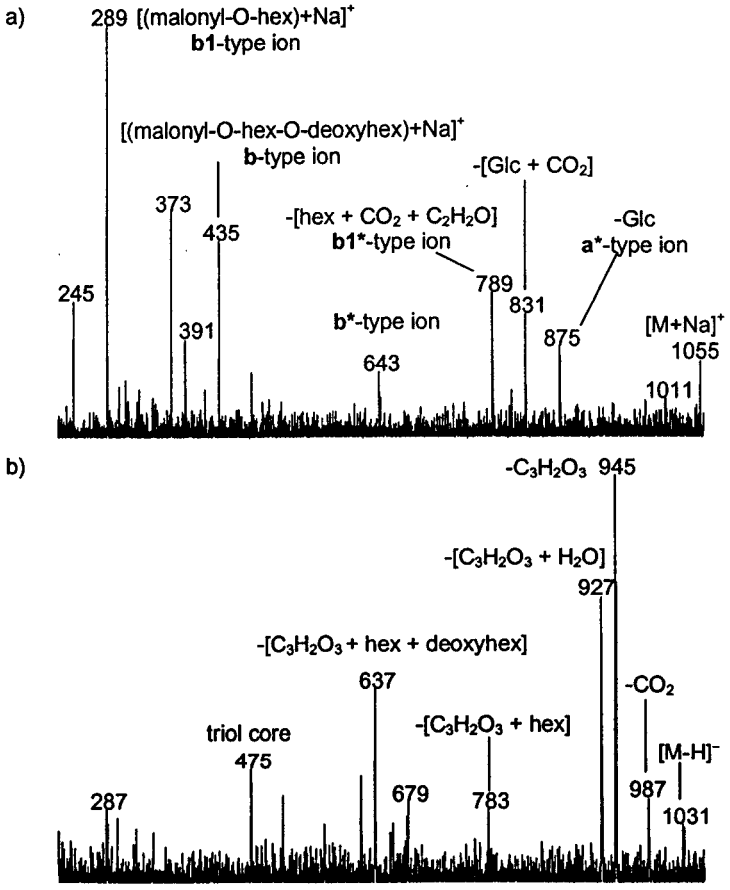

Figure 3-12: Entry **1** (5.7 min) - Positive ion LC/MS/MS mass spectrum of an $[M+Na]^+$ ion at m/z 1055, item a); and a negative ion LC/MS/MS mass spectrum of an $[M-H]^-$ ion at m/z 1031, item b).

The spectrum of Figure 3-12a contains peaks at m/z 435 and at m/z 643. Using the nomenclature given in Scheme 2, these peaks were assigned as **b**-type and **b***-type ions, respectively. The complementary pair of ions m/z 289 and m/z 789, were assigned as **b1**-type and **b1***-type ions. The m/z 289 and m/z 435 ions (nominally) correspond to Na^+ attachment ions of malonic acid esters of a hexose and a deoxyhexose/hexose disaccharide, correspondingly.

The negative ion LC/MS/MS spectrum of Figure 3-12b yielded peaks at m/z 987, m/z 945, m/z 783, m/z 637 and m/z 475. The peak at m/z 987 corresponds to loss of 44 Da, CO_2, from the mass-selected ion. This dissociation is not surprising for this –COOH containing compound. The peak at m/z 945 nominally corresponds to loss of 86 Da which may occur via consecutive losses of [44 Da + 42 Da] or loss of $C_3H_2O_3$ from m/z 1031.

The m/z 475 peak is characteristic of a triol-containing ginsenoside; see Scheme 1. The retention time for this ginsenoside fell within the range estimated for elution of the triols. The peaks at m/z 945, m/z 783, m/z 637 and m/z 475 indicated that this ginsenoside comprised of two hexose (162 Da) moieties and one deoxyhexose (146 Da) moiety. The m/z 435 ion in the positive ion LC/MS/MS mass spectrum showed that the ginsenoside is comprised of a malonyl deoxyhexose/hexose disaccharide. While positive ion experiments did not reveal the sequence of the sugars, negative ion LC/MS/MS experiments were very useful for this [2h]. Thus, it was proposed that a hexose residue is attached to the C6 hydroxyl of the triol core, and that the [malonyl-hexose-*O*-deoxyhexose-] moiety is attached to the C20 hydroxyl via the deoxyhexose

residue. This ginsenoside was given the structure illustrated in entry **1** of Scheme 3, and assigned the name **malonyl ginsenoside Re_1**.

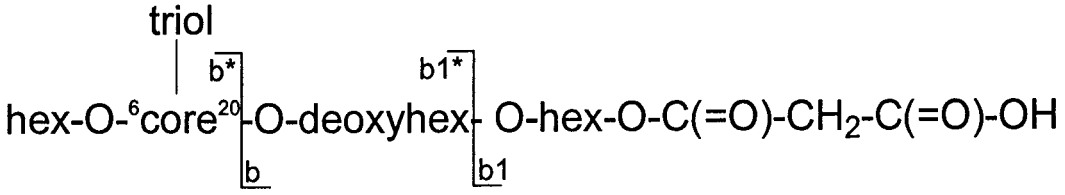

malonyl ginsenoside Re MW = 1032 Da

*d).ii. Entry **2** – **ginsenoside Rb_1A MW = 1142 Da***

Entry **2** cannot be represented by the triterpene in Scheme 3 because it is proposed to have a core with mass 494 Da.

The positive ion spectrum, shown in Figure 3-13a, comprises of a **b**-type ion m/z 365 and a **b***-type ion m/z 821. The m/z 365 ion is assigned as the Na+ attachment ion of a hexose disaccharide. At this point, no further structural information could be obtained from this spectrum so we turned to the negative ion MS/MS spectrum; see Figure 3-13b.

In the mass range 400-1145 Da, this spectrum contained peaks at m/z 1141, m/z 979, m/z 817, m/z 799, m/z 655 and m/z 493. The increments between the peaks m/z 1141, m/z 979, m/z 817, m/z 655 and m/z 493 is 162 Da. Therefore, this ginsenoside comprised of four hexose moieties. The core is assigned to m/z 493 and thus the mass of the core is 494 Da, $C_{30}H_{54}O_5$, with one possible structure shown below.

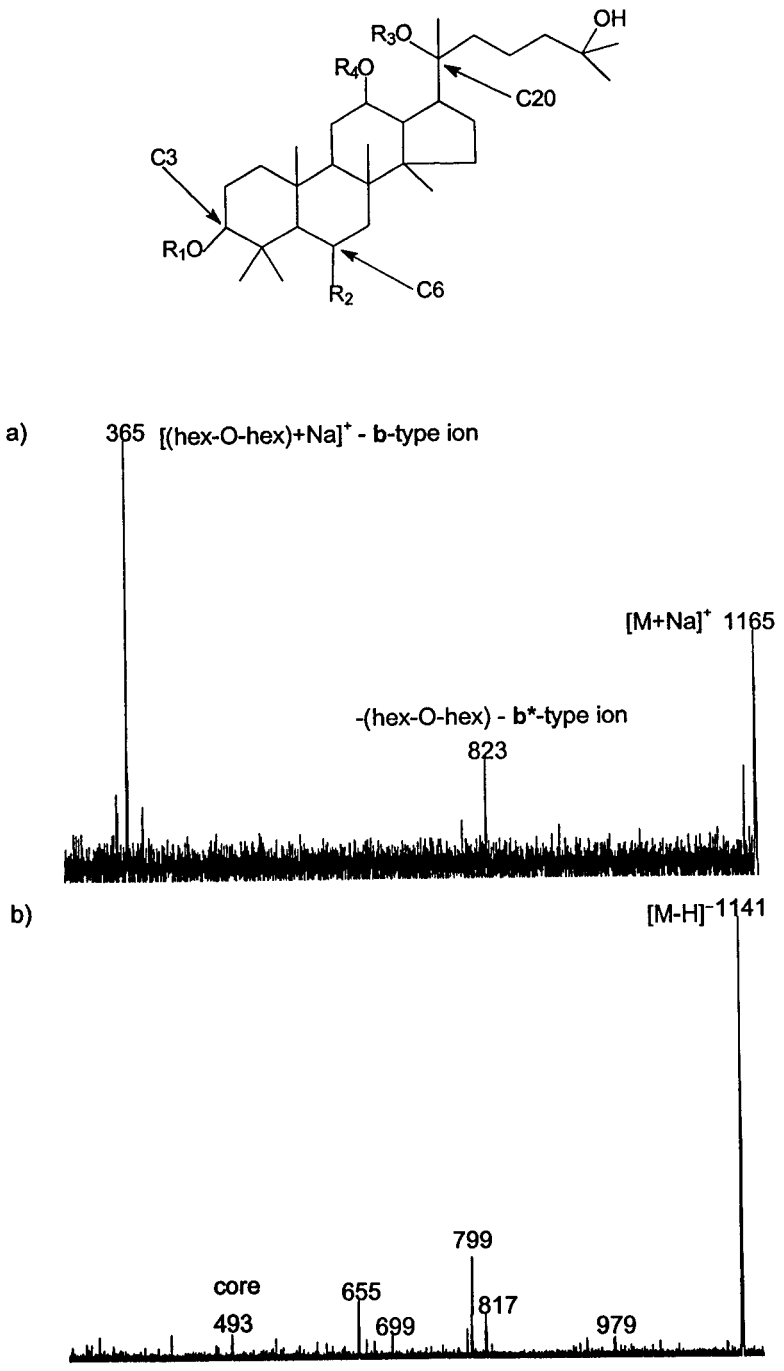

Figure 3-13: Entry **2** (12.1 min) - Positive ion LC/MS/MS mass spectrum of an $[M+Na]^+$ ion at m/z 1165, item a); and a negative ion LC/MS/MS mass spectrum of an $[M-H]^-$ ion at m/z 1141, item b).

With a core of this mass the **b***-type ion at m/z 821 in Figure 3-13a comprises of a hexose disaccharide. Although it is likely that this ginsenoside may have saccharides attached to either of R_1 to R_4 in the triterpene, it is proposed that the hexose disaccharides are attached to R_2 and R_3. This results from the fact that the known triol-ginsenosides have sugars attached to these positions.

Entry **2** is named ginsenoside Rb_1A.

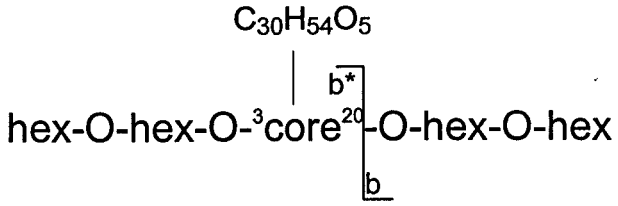

ginsenoside Rb_1A MW = 1142 Da

*d).iii. Entry **3** – **ginsenoside Rb_4 MW = 1124 Da***

The ginsenoside in entry **3** has a molecular mass of 1124 Da, which is 16 Da larger than ginsenoside Rb_1. The base peak in the positive ion LC/MS/MS mass spectrum is m/z 365, a **b**-type ion; see Figure 3-14a. This ion (nominally) corresponds to a Na^+ attachment ion of a hexose disaccharide. The peak at m/z 805 is assigned as the **b***-type ion. Based on observations presented in Chapter 2, it was proposed that this new ginsenoside contained at least one hexose disaccharide, and that it was attached to the C20 hydroxyl. The point of attachment of the hexose disaccharide to the core was inferred from the observation that its Na^+ attachment ion, m/z 365, was the base peak in Figure 3-14a.

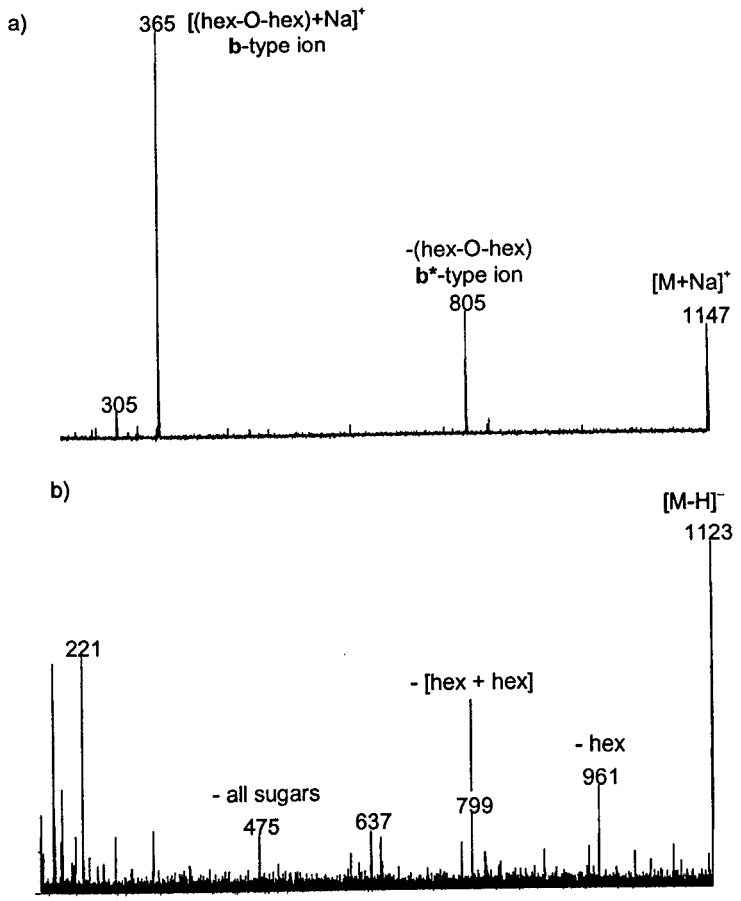

Figure 3-14: Entry **3** (14.2 min) - Positive ion LC/MS/MS mass spectrum of an $[M+Na]^+$ ion at m/z 1147, item a); and a negative ion LC/MS/MS mass spectrum of an $[M-H]^-$ ion at m/z 1123, item b).

The negative ion LC/MS/MS experiment revealed that the ginsenoside was comprised of four hexose sugars, as evidenced by the incremental mass difference between the peaks m/z 1123, m/z 961, m/z 799, m/z 637 and m/z 475; see Figure 3-14b. The ion at m/z 475 indicated that the ginsenoside in entry **3** of Table 2 and Scheme 3 contained a triol core. Thus, it was proposed that the ginsenoside with molecular mass 1124 Da has the same number of hexose moieties, as does ginsenoside Rb_1, except that it has a triol core. This new

ginsenoside is proposed to have a hexose disaccharide bonded to hydroxyl groups at C6 and C20 of the triol core.

These hexose disaccharides may not have the same *O*-glycosidic linkage. Nevertheless, we assigned 1,6-*O*-glycosidic linkages to both disaccharides based on the following observations. Low intensity peaks were observed at m/z 305, m/z 275 and m/z 245. The m/z 245 : m/z 275 : m/z 305 was ca. 0.25 : 0.4 : 1. A similar ratio [2h] has been observed for the 1,6-linked glucose disaccharide from ginsenoside Rb_3. Entry **3** was assigned the name **ginsenoside Rb_4**.

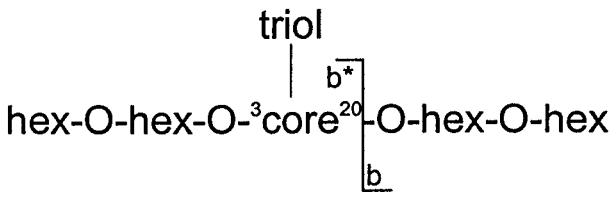

ginsenoside Rb_4 MW = 1124 Da

*d).iv. Entry **4** – **succinyl ginsenoside Rb_1** **MW = 1208 Da***

The positive ion LC/MS/MS spectrum of the ginsenoside in entry **4** yielded a **b**-type ion at m/z 465, an **a**-type ion at m/z 365, and an **a***-type ion at m/z 889; see Figure 3-15a. The **a**-type and **a***-type ions are complementary parts of the $[M+Na]^+$ ion at m/z 1231. The 100 Da difference between m/z 365, which corresponds to a Na^+ attachment ion of a hexose disaccharide, and m/z 465 was attributed to a succinyl functional group. Hence, one hydroxyl group on a hexose moiety was esterified with succinic acid. This was a reasonable suggestion since known ginsenosides [1], as well as new ginsenosides (see above) have undergone esterification with acetic acid and malonic acid. Acetic

acid, malonic acid, and succinic acid are *C*-atom carriers in the Kreb's cycle [15], and as such are likely to be present in ginseng root extracts.

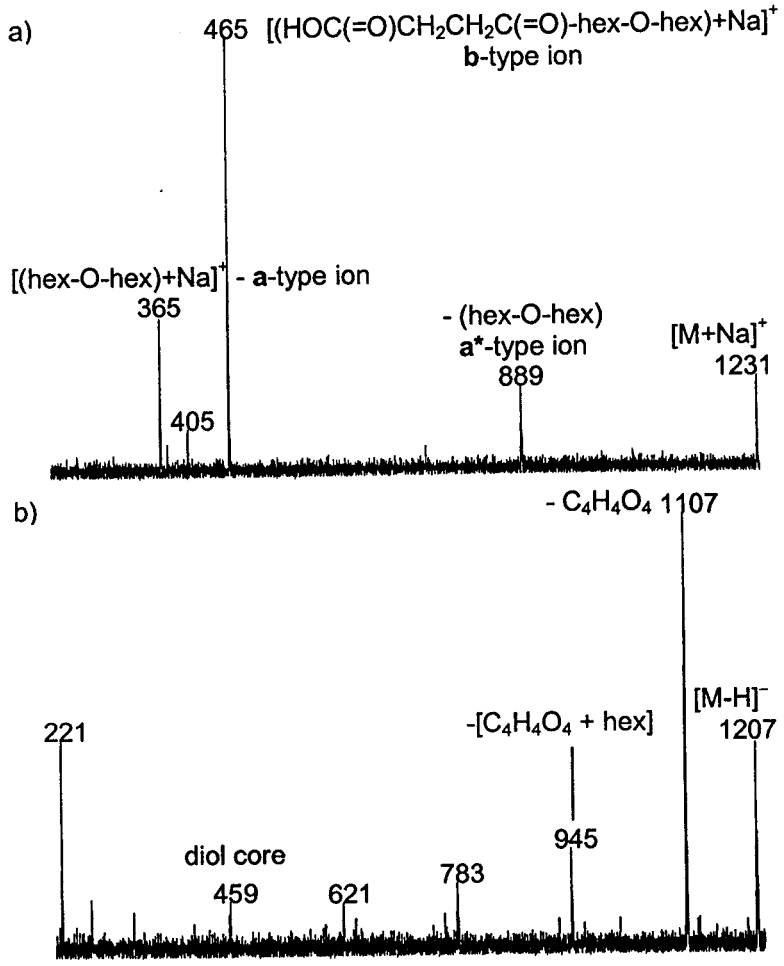

Figure 3-15: Entry **4** (14.2 min) - Positive ion LC/MS/MS mass spectrum of an $[M+Na]^+$ ion at m/z 1231, item a); and a negative ion LC/MS/MS mass spectrum of an $[M-H]^-$ ion at m/z 1207, item b).

The negative ion LC/MS/MS spectrum of this proposed succinic acid ester showed loss of 100 Da ($C_4H_4O_3$) from the $[M-H]^-$ ion (m/z 1207); see Figure 3-15b. This loss provided evidence that the ginsenoside of entry **4** may be a

succinic acid ester. This spectrum contained peaks which indicated that the ginsenoside was comprised of four hexose sugars attached to a diol core. Since the **b**-type ion corresponded to a monosuccinyl hexose disaccharide, it was proposed that the latter disaccharide was attached to the C20 hydroxyl, and the hexose disaccharide was attached to the C3 hydroxyl of the core.

This new ginsenoside was named **succinyl ginsenoside Rb_1**. It is also worth mentioning that although this ginsenoside contained a diol core, it eluted at 14.1 min. Therefore, the use of the retention time as a guide for assigning core type is not applicable to ginsenosides containing a carboxylic acid group.

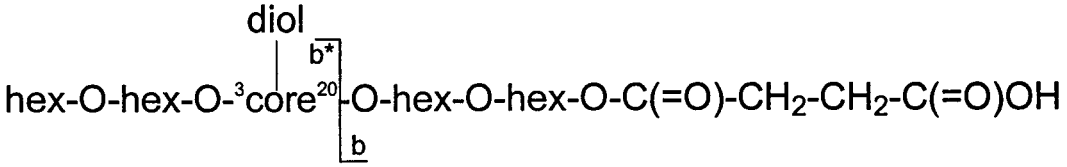

succinyl ginsenoside Rb_1 MW = 1208 Da

d).v. Entry ***5– ginsenoside Rb_5 MW = 1094 Da***

The positive ion MS/MS mass spectrum of the ginsenoside in entry **5** contained peaks at m/z 335 and m/z 365; see Figure 3-16a. Analysis of the Na^+ attachment ions of the standards ginsenosides Rb_2, Rb_3, and Rc by ES MS/MS also yielded peaks at m/z 335 and m/z 365 (data not shown). These latter ions corresponded to the Na^+ adducts of a pentose/hexose disaccharide, and a hexose disaccharide, respectively. Using the nomenclature provided in Scheme 2, the m/z 335 and m/z 365 ions were assigned as the **b**-type and **a**-type ions, correspondingly. The m/z 335 ion was assigned as the **b**-type ion because it was the base peak in Figure 3-16a. It therefore follows that the pentose/hexose

disaccharide was attached to the C20 hydroxyl of the core. The signal at m/z 805 is the **b***-type ion, and thus is complementary to m/z 335.

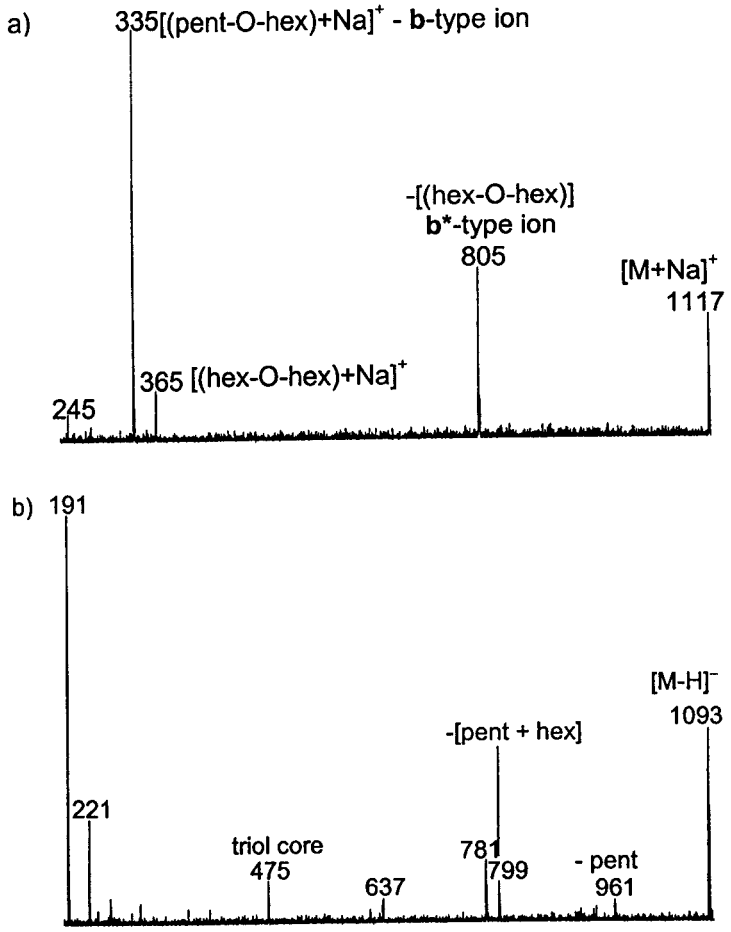

Figure 3-16: Entry **5** (14.7 min) - Positive ion LC/MS/MS mass spectrum of an $[M+Na]^+$ ion at m/z 1117, item a); and a negative ion LC/MS/MS mass spectrum of an $[M-H]^-$ ion at m/z 1093, item b).

The negative ion MS/MS spectrum of the $[M-H]^-$ ion, m/z 1093, contained a peak at m/z 475; see Figure 3-16b. Therefore, this ginsenoside has a triol core. Furthermore, this spectrum showed that the ginsenoside is comprised of a pentose and three hexose sugars. This was consistent with the assignment from

positive ion experiments. The observed dissociation leading to the generation of m/z 961 in Figure 3-16b indicated that the pentose/hexose disaccharide was attached to the C20 hydroxyl via the pentose sugar.

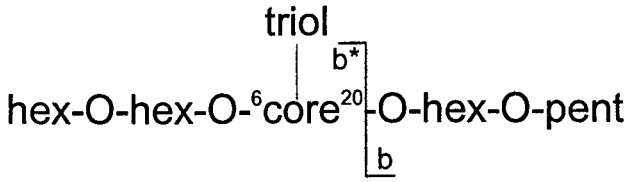

ginsenoside Rb_5 MW = 1208 Da

The structural information obtained from the spectra shown in Figure 3-16 provided evidence for a structure which has a pentose/hexose disaccharide attached to the C20 hydroxyl (via the pentose sugar), and a hexose disaccharide attached to the C6 hydroxyl of the triol core. This triol-containing relative of the diol-ginsenosides Rb_2, Rb_3 and Rc, was assigned the name **ginsenoside Rb_5**.

*d).vi. Two acetyl ginsenosides – entries **6** and **7** of Table 3 and Scheme 3*

Entries **6** and **7** appeared to be monoacetyl ginsenosides. Since decarboxylation of malonic acid esters can yield acetyl acid esters, it was important to establish whether malonyl ginsenosides were undergoing decarboxylation during LC/MS to form these compounds. Section H in the Appendix and Figure 3-12 contain spectra which provide evidence that malonic acid esters can decarboxylate to generate the acetic acid esters.

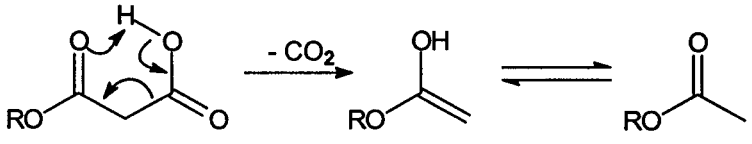

Scheme 4: Decarboxylation of a malonic acid ester, R = ginsenoside.

Precursor ion experiments of the Na^+ attachment ions of acetyl ginsenosides were performed. These spectra are not presented, but they showed that acetyl ginsenosides were not formed from malonyl ginsenosides during LC/MS analysis.

d).vi.1. Entry ***6 – acetyl ginsenoside Re$_2$ MW = 988 Da***

The ginsenosides in entries **5** and **6** are isomers. The positive ion LC/MS/MS spectrum of the ginsenoside in entry **6** contained a **b**-type ion at m/z 245 and a **b***-type ion at m/z 789; see Figure 3-17a.

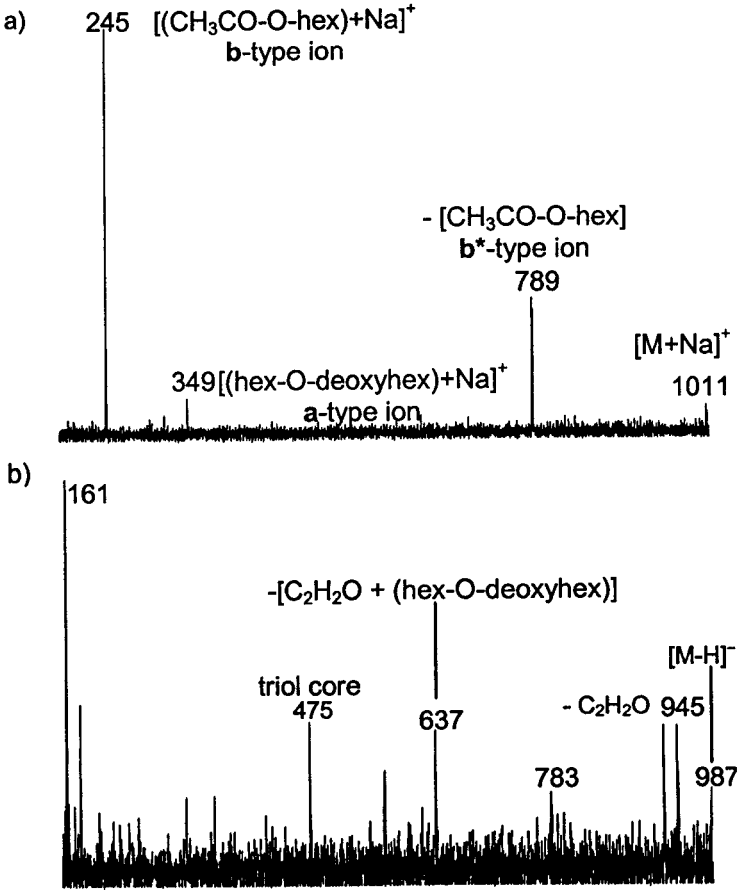

Figure 3-17: Entry **6** (18.7 min) - Positive ion LC/MS/MS mass spectrum of an $[M+Na]^+$ ion at m/z 1011, item a); and a negative ion LC/MS/MS mass spectrum of an $[M-H]^-$ ion at m/z 987, item b).

The **b**-type ion corresponds to an acetic acid ester of a hexose moiety. The relative intensities of the **b**-type and **b***-type ions indicate that the acetyl hexose residue is attached to the C20 hydroxyl group. The **a**-type ion at m/z 349 corresponds to a Na^+ attachment ion of a deoxyhexose/hexose disaccharide.

The negative ion LC/MS/MS spectrum of $[M-H]^-$ (m/z 987) contained a signal at m/z 475 which indicated that the ginsenoside is comprised of a triol core; see Figure 3-17b. This spectrum also contained a peak at m/z 945 which corresponded to loss of 42 Da (C_2H_2O) from the m/z 987 ion. This loss provided evidence for esterification with acetic acid. There were also peaks corresponding to loss of 162 Da, 146 Da and 162 Da (in that order) from m/z 945. The order in which the saccharides were lost, indicated that the deoxyhexose in the deoxyhexose/hexose disaccharide was bonded to the C6 hydroxyl group of the triol core; see Scheme 3. In summary, entry **6**, named **acetyl ginsenoside Re_2**, contained an acetyl hexose moiety attached to the C20 hydroxyl group and a deoxyhexose/hexose disaccharide attached to the C6 hydroxyl group.

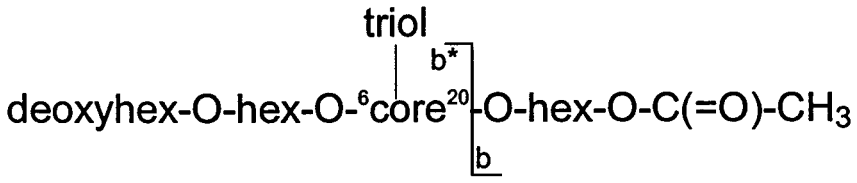

acetyl ginsenoside Re_2 MW = 988 Da

*d).vi.2. Entry **7** – **quinquenoside R2 MW = 1150 Da***

Entry **7** of Table 2 and Scheme 3 is the second of two new compounds which were identified as monoacetyl ginsenosides. This new compound is

proposed to be a positional isomer of a known ginsenoside quinquenoside R1 whose structure is shown below.

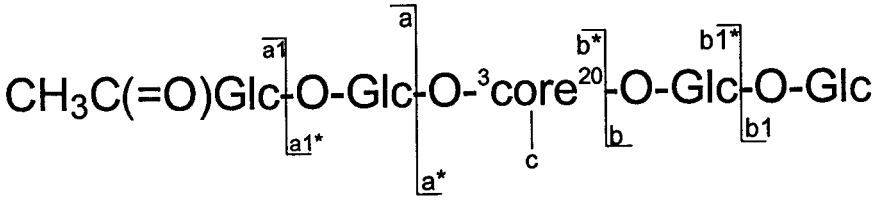

quinquenoside R1 MW = 1150 Da

During detection and identification of known ginsenosides [1], it became clear that a ginsenoside consistent with the structure of quinquenoside R1 was identified by positive and negative ion LC/MS/MS experiments; see Figure 3-18 and Section A.i. of the Appendix. The dissociations observed in these LC/MS/MS spectra are used to interpret the dissociation observed in the LC/MS/MS spectra of the ginsenoside in entry **7**.

The positive ion LC/MS/MS spectrum of quinquenoside R1 (Figure 3-18a) contained **b**-type and **b***-type ions at m/z 365 and m/z 831, respectively. The m/z 365 ion is the Na^+ attachment ion of the glucose disaccharide. The peak at m/z 407, an **a**-type ion, confirmed the presence of the acetyl glucose disaccharide; see Figure 3-18a. The m/z 831 ion corresponds to the Na^+ adduct of a triol core attached to an acetyl hexose disaccharide. The presence of an acetyl group was confirmed by the negative ion LC/MS/MS spectrum of Figure 3-18b. This spectrum contained a peak at m/z 1107 which corresponded to loss of 42 Da from the mass-selected ion, m/z 1149. Additionally, the spectrum also provided evidence that the ginsenoside contained four glucose disaccharides and a diol

core. This is consistent with the structure of the known compound quinquenoside R1.

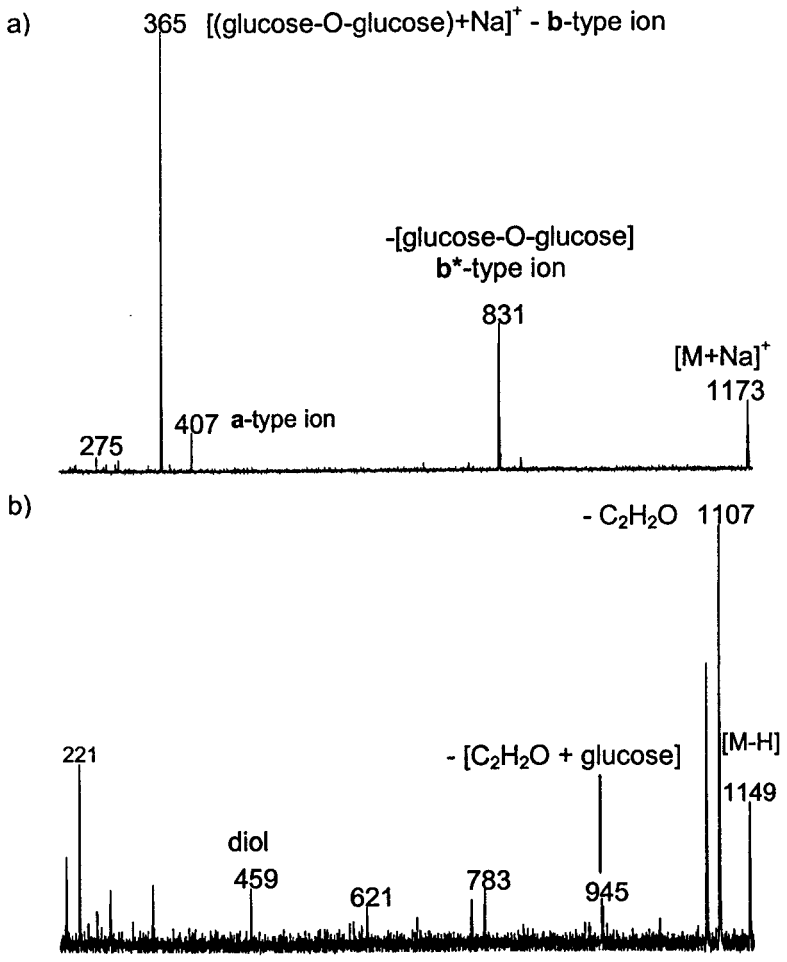

Figure 3-18: Quinquenoside R1 (24.8 min) - Positive ion LC/MS/MS mass spectrum of the $[M+Na]^+$ ion of at m/z 1173, item a); and negative ion LC/MS/MS mass spectrum of its $[M-H]^-$ ion at m/z 1149, item b).

Entry **7**, in Table 3, is an isomer of quinquenoside R1. The positive ion LC/MS/MS spectrum of this new compound is provided in Figure 3-19a. The base peak at m/z 407 was assigned as the **b**-type ion, while m/z 789 was

assigned as the **b***-type ion. The peaks at m/z 365 and m/z 831 are **a**-type and **a***-type ions, respectively. These four peaks are consistent with a ginsenoside comprised of an acetyl-hexose/hexose disaccharide and a hexose disaccharide. The ratio of the intensities of peaks at m/z 407 and m/z 789 indicated that the acetyl-hexose/hexose disaccharide is attached to the C20 hydroxyl.

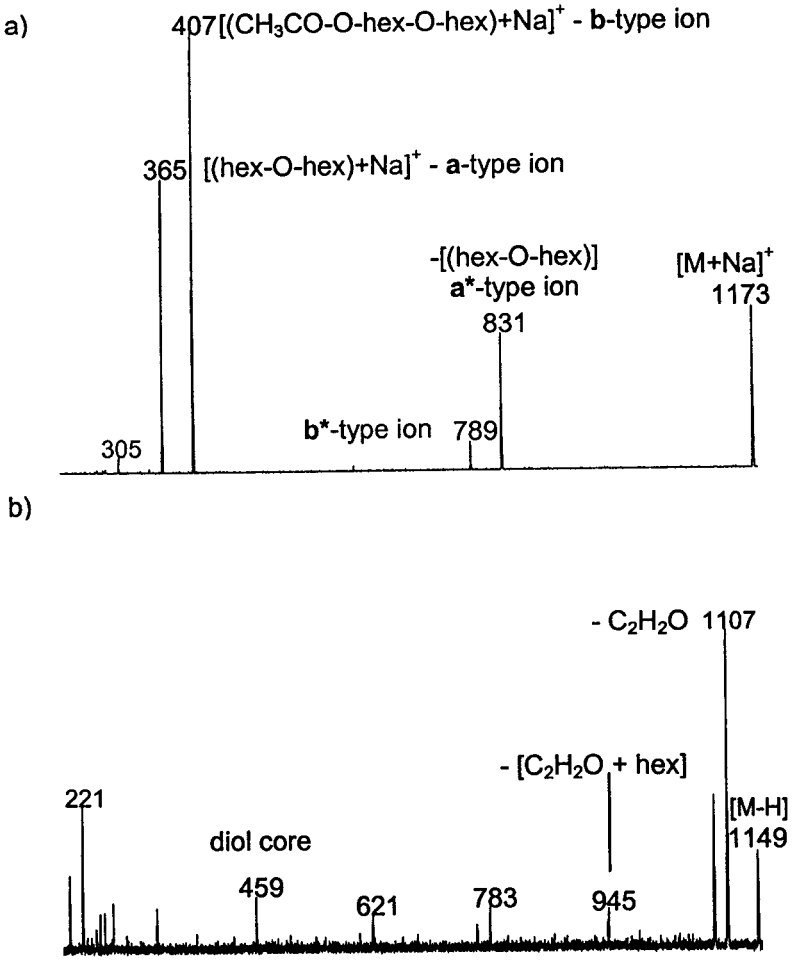

Figure 3-19: Entry 7 (25.3 min) - Positive ion LC/MS/MS mass spectrum of an $[M+Na]^+$ ion at m/z 1173, item a); and a negative ion LC/MS/MS mass spectrum of an $[M-H]^-$ ion at m/z 1149, item b).

The negative ion LC/MS/MS spectrum of this acetyl ginsenoside was similar to that of quinquenoside R1; compare Figures 3-18b and 3-19b. The spectrum of Figure 3-19b contained peaks which provided evidence that the ginsenoside was comprised of a diol core, four hexose disaccharides and an acetyl group. Therefore, the complete structure – illustrated in Scheme 3 – has the hexose disaccharide attached to the C3 hydroxyl, and the acetyl-hexose/hexose disaccharide attached to the C20 hydroxyl of the diol core. Entry **7** was named **quinquenoside R2**.

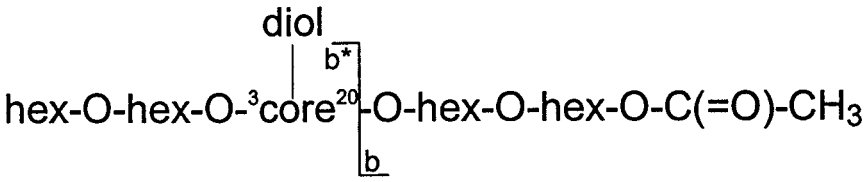

quinquenoside R2 MW = 1150 Da

d).vii. Two isomers of ginsenoside Rb_1

*d).vii.1. Entry **8** – **ginsenoside R_6** **MW = 1108 Da***

The next two ginsenosides, entries **8** and **9** of Table 2 and Scheme 3, are isomers of ginsenoside Rb_1. The positive ion LC/MS/MS spectrum of the ginsenoside in entry **8** yielded a **b**-type ion, m/z 365, corresponding to the Na^+ attachment ion of a hexose disaccharide; see Figure 3-20a. This spectrum also showed a **b***-type ion at m/z 789. Therefore, it was proposed that the hexose disaccharide was attached to the C20 hydroxyl of the core. The peak at m/z 951 corresponded to loss of a hexose moiety from the mass-selected ion, m/z 1131. This dissociation was not observed for the $[M+Na]^+$ ion of ginsenoside Rb_1. We

turned to the negative ion experiments for information about core type, sugar composition and sequence.

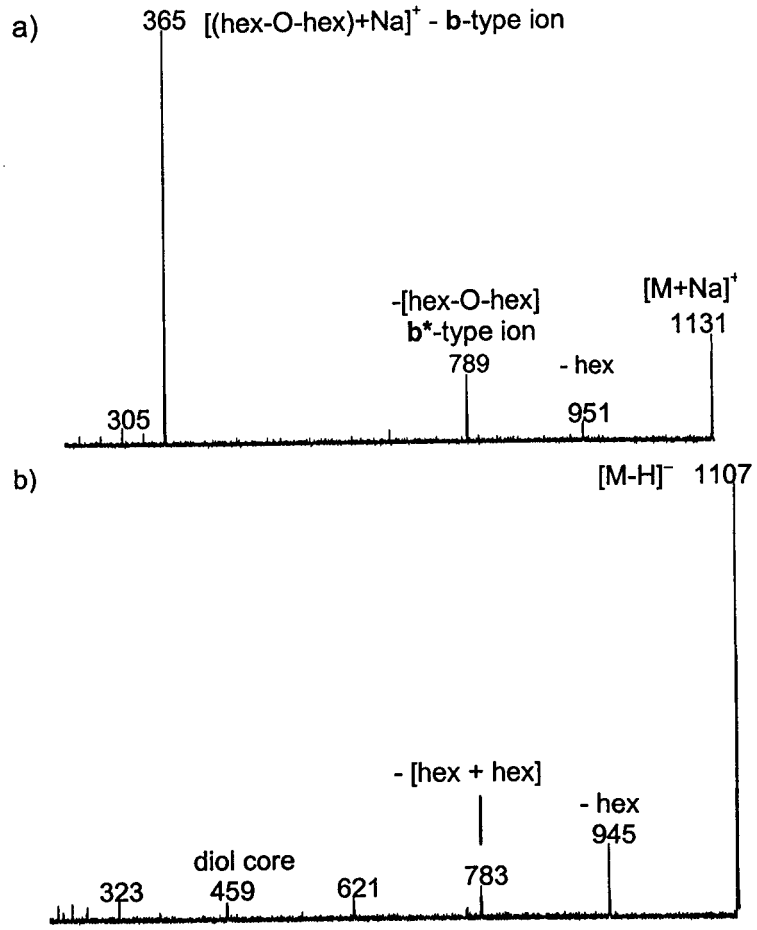

Figure 3-20: Entry **8** (25.5 min) - Positive ion LC/MS/MS mass spectrum of an $[M+Na]^+$ ion at m/z 1131, item a); and a negative ion LC/MS/MS mass spectrum of an $[M-H]^-$ ion at m/z 1107, item b).

The negative ion LC/MS/MS spectrum of Figure 3-20b confirmed that this ginsenoside did indeed comprise of four hexose monosaccharides and a diol core. Since this ginsenoside had a diol core, we suggested a structure that had a

hexose disaccharide attached to the C20 hydroxyl, and hexose moieties attached to the C3 and C12 hydroxyl groups; see Scheme 3. A structure such as this is not without precedent since known ginsenosides contain sugars attached to the C12 hydroxyl of the core; see Section A of the Appendix. Entry **7** was named **ginsenoside Rb_6**.

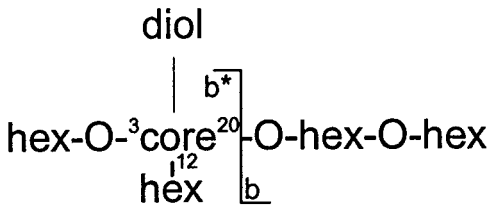

ginsenoside Rb_6 MW = 1108 Da

*d).vii.2. Entry **9** – **ginsenoside R_7** **MW = 1108 Da***

A second isomer of ginsenoside Rb_1, entry **9** in Scheme 3, eluted at 27.8 min. The positive ion LC/MS/MS mass spectrum of this ginsenoside, given in Figure 3-21a, contained a base peak at m/z 365, and additional peaks at m/z 527 and m/z 789. The signal at m/z 527 was not observed for any of the standards studied. Nevertheless, it was assigned as the **b**-type ion, and proposed to be the Na^+ attachment ion of a hexose trisaccharide. In order to explain the rationale for this assignment, we need to consider the positive ion MS/MS spectrum of a known ginsenoside. None of the ginsenoside standards contain a trisaccharide. However, in the list of reported ginsenosides, there are three isomeric ginsenosides of MW = 1240 Da, and which comprised of a trisaccharide; see Section A.i. of the Appendix.

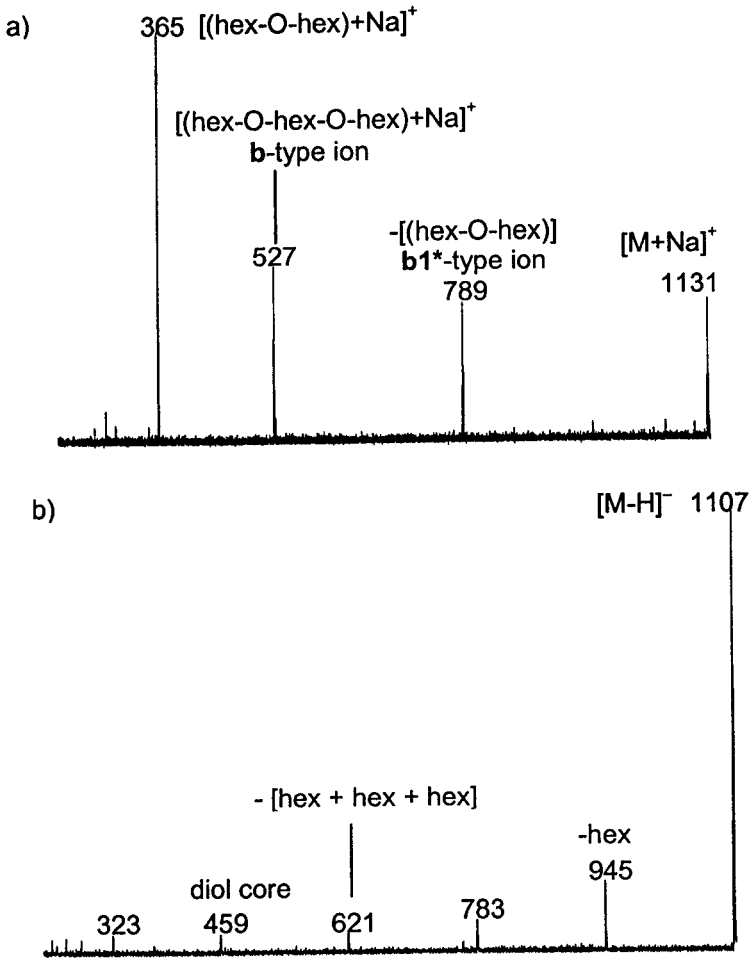

Figure 3-21: Entry **9** (27.8 min) - Positive ion LC/MS/MS mass spectrum of an $[M+Na]^+$ ion at m/z 1131, item a); and a negative ion LC/MS/MS mass spectrum of an $[M-H]^-$ ion at m/z 1107, item b).

The positive ion MS/MS spectrum of one of these isomers is provided in Figure 3-22. This spectrum contains a base peak at m/z 497 which corresponds to a Na^+ adduct of a pentose/hexose/hexose trisaccharide. Based on the findings reported in Chapter 2, ginsenosides undergo predominant fragmentation at C20 of the triterpene. Thus, it is proposed that the spectrum of Figure 3-22 may represent two of the three 1240 Da isomers; the two which contain a trisaccharide at C20. The latter isomers cannot be absolutely differentiated by

our approach, but the for the purposes of this discussion, it is proposed that Figure 3-22 is representative of the (abbreviated) structure of notoginsenoside R4 shown below.

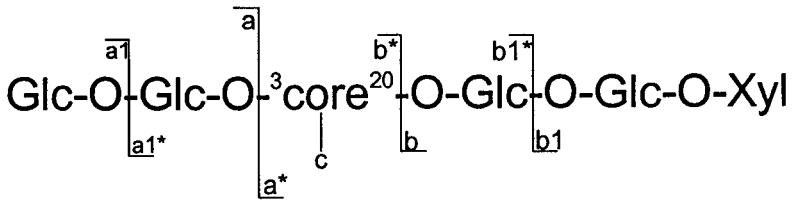

Notoginsenoside R4 MW = 1240 Da

The base peak in the spectrum of Figure 3-22, m/z 497, was assigned as the **b**-type ion. The peak at m/z 789 corresponded to a Na^+ adduct of a hexose disaccharide attached to a diol core and was assigned as the **b***-type ion. The peak at m/z 335 corresponds to a Na^+ adduct of a pentose/hexose disaccharide. The fact that product ions corresponding to a pentose/hexose disaccharide and a pentose/hexose/hexose trisaccharide are formed from notoginsenoside R4, see above, is used to complete the structure proposal of entry **9** in Table 3 and Scheme 3.

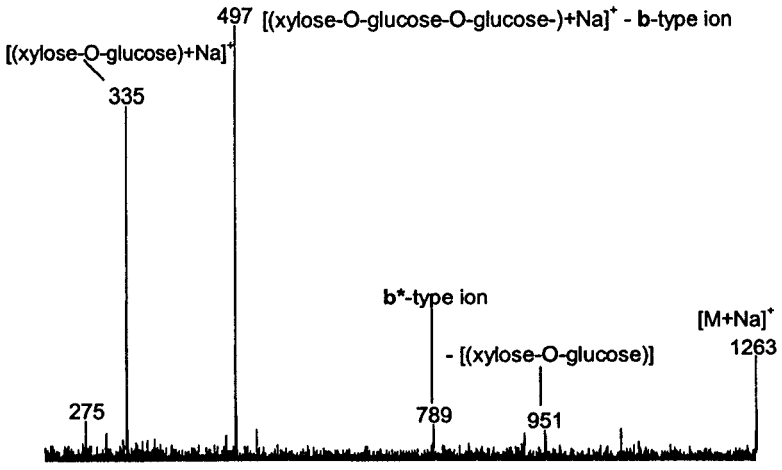

Figure 3-22: Positive ion LC/MS/MS mass spectrum of an $[M+Na]^+$ ion at m/z 1263. This ginsenoside is presumed to be Notoginsenoside R4.

The spectrum of Figure 3-21a contained peaks at m/z 365 and m/z 789. These peaks are complementary and were assigned as the **b1**-type, and **b1***-type ions, respectively. From analysis of the standards, the m/z 365 ion was proposed to be the Na^+ attachment ion of a hexose disaccharide. The negative ion LC/MS/MS spectrum of Figure 3-21b provided evidence that the ginsenoside in entry **9** had a diol core (m/z 459) attached to four hexose sugars. Considering the dissociation pattern depicted in Figure 3-22, a ginsenoside known to have a trisaccharide, we proposed a structure where a hexose trisaccharide was attached to the C20 hydroxyl, and a hexose monosaccharide attached to the C3 hydroxyl. Entry **9** was named **ginsenoside Rb_7**.

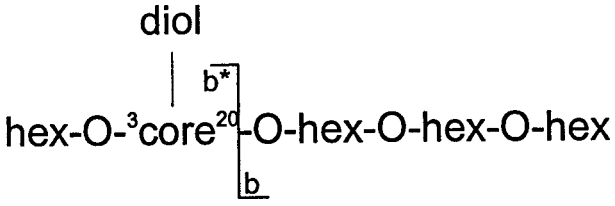

ginsenoside Rb_7 MW = 1108 Da

*d).viii. Entry **10** – **chikusetsusaponin IV** **MW = 930 Da***

The positive and negative LC/MS/MS spectra of the ginsenoside in entry **10** are shown in Figure 3-23. The structure proposed for this ginsenoside could not be represented by the nomenclature provided in Scheme 2. The spectrum of Figure 3-23a contained peaks at m/z 203, m/z 349, m/z 365 and m/z 789. It is proposed that m/z 789 is generated via loss of a deoxyhexose moiety from the precursor ion, m/z 953. The peaks at m/z 349 and m/z 365 corresponded to the Na^+ attachment ion of a deoxyhexose/hexose disaccharide and a hexose

disaccharide, respectively. The rationale for the presence of both m/z 349 and m/z 365 in this spectrum followed from the observed dissociations for the trisaccharide-containing notoginsenoside R4; see Figure 3-22. The spectrum of Figure 3-22 showed peaks which corresponded with the Na^+ attachment ions of a xylose/glucose disaccharide as well as of a pentose/hexose/hexose trisaccharide. Therefore, the trisaccharide had undergone a dissociation to yield the pentose/hexose disaccharide. This observation was used to interpret the spectrum of Figure 3-23a.

We proposed that m/z 349 and m/z 365, in Figure 3-23a, are generated by dissociation of a trisaccharide comprising of two hexose moieties and a deoxyhexose moiety. Considering that m/z 365 is the base peak, then it is likely that the trisaccharide from which this ion originated is probably attached to the C20 hydroxyl. The negative ion LC/MS/MS experiment was used to obtain core type and obtain saccharide composition and sequence of this new ginsenoside.

The spectrum of Figure 3-23b showed peaks at m/z 929, m/z 783, m/z 621 and m/z 459. Thus the ginsenoside contained a diol core. Moreover, the increments between these four peaks correspond with the presence of two hexose sugars and a deoxyhexose sugar. The order in which these sugars were lost, i.e., the deoxyhexose followed by the hexose moieties, indicated that the deoxyhexose sugar was not attached (directly) to the ring. One of the hexose residues was attached to the ring. The structure of this ginsenoside is depicted in Scheme 3.

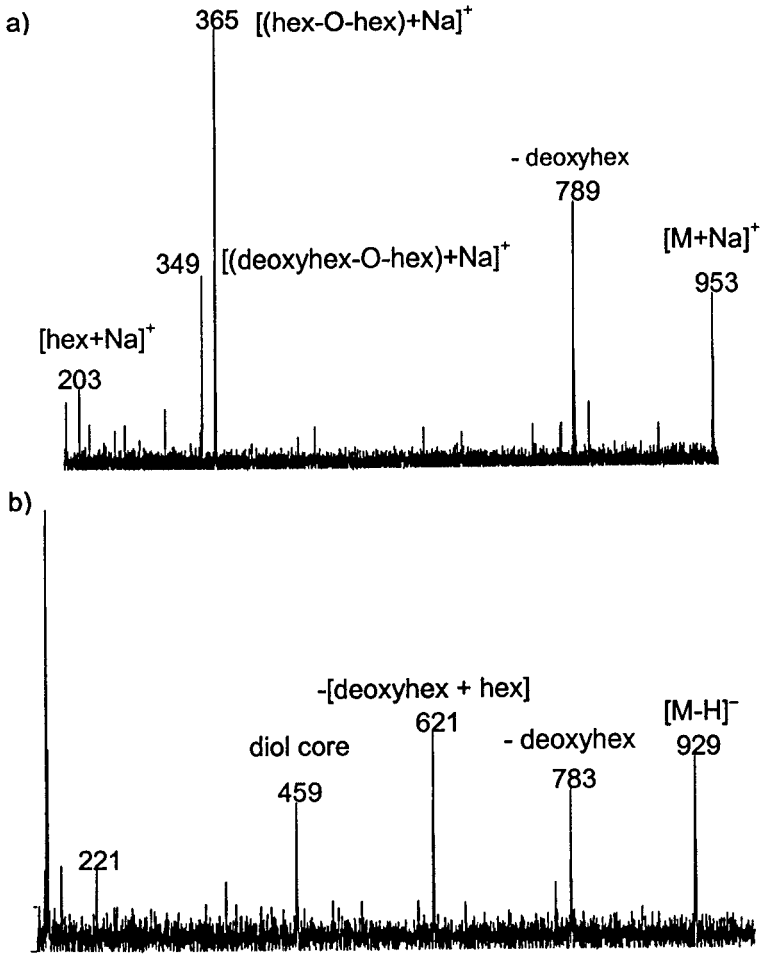

Figure 3-23: Entry **10** (32.9 min) - Positive ion LC/MS/MS mass spectrum of an $[M+Na]^+$ ion at m/z 953, item a); and a negative ion LC/MS/MS mass spectrum of an $[M-H]^-$ ion at m/z 929, item b).

Entry **10** was assigned the name **chikusetsusaponin IV**.

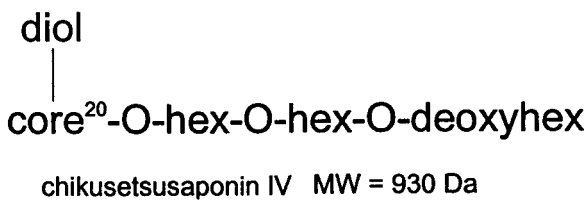

chikusetsusaponin IV MW = 930 Da

Conclusions

The retention times of 10 ginsenoside standards, separated by reversed-phase LC/MS, revealed clear trends. Triol-containing ginsenosides eluted earlier than diol-containing ginsenosides. Ginsenoside Rf, which has a glucose disaccharide at the C3 hydroxyl and a free hydroxyl group at C20, is retained longer than its isomer ginsenoside Rg_1, which has single sugar residues, attached to the C6 as well as C20 hydroxyl groups.

As the number of sugar units attached to diol-ginsenosides increased, there was a concomitant decrease in their retention time. For example, ginsenoside Rb_1, which has four hexose sugars, eluted earlier than either ginsenosides Rd and gypenoside XVII, which have three hexose sugars. This trend was not observed for the triols; two triol-ginsenosides comprising of a different number of sugar units, ginsenosides Re and Rg_1, co-eluted.

Complex mixtures of ginsenosides were analyzed by LC/MS using a 40-minute long reversed-phase acetonitrile/water gradient. These mixtures included an American ginseng extract and two 'over-the-counter' preparations, Korean Red and Korean White ginseng. Analysis of these mixtures provided evidence that the relative concentrations of ginsenosides within a specific species are different. These LC conditions afforded the opportunity to resolve many new ginsenosides. The ginsenosides detected included isomers of known ginsenosides, and those whose masses were not previously reported. A list of these compounds for an American ginseng root is presented in Table 4.

In general, within a molecular mass class that was previously reported, the same number or more ginsenosides were detected. This list also contains

ginsenosides with molecular masses that were not previously reported; these molecular masses are in bold font. The extensive list provided in Table 4 and the fact that both Korean Red and Korean White ginsengs contained 26 more ginsenosides than were reported [1] illustrate the highly complex nature of these mixtures. Structure proposals for new ginsenosides from American ginseng were presented.

Table 4: A list of the molecular masses and numbers of reported ginsenosides as well as new ginsenosides from an American ginseng root. The new molecular masses are in bold font.

MW (Da)	Reported	This work	MW (Da)	Reported	This work	MW (Da)	Reported	This work
622	1	0	**834**	-	**1**	1078	3	6
636	1	1	842	1	1	**1094**	-	**4**
638	4	5	902	1	0	**1100**	-	**1**
652	1	1	916	3	4	**1106**	-	**1**
654	6	3	926	2	2	1108	1	5
670	1	1	930	1	2	**1110**	-	**1**
672	1	0	932	1	9	1120	3	4
684	-	**1**	944	1	4	1122	1	6
724	1	0	946	3	7	**1124**	-	**3**
744	-	**1**	948	2	8	**1126**	-	**1**
754	1	2	956	1	3	**1140**	-	**1**
770	3	0	**960**	-	**1**	**1142**	-	**2**
778	-	**2**	962	7	7	1150	1	3
782	2	7	**970**	-	**1**	**1156**	-	**1**
784	5	8	**972**	-	**1**	1164	2	3
786	3	5	974	1	0	**1166**	-	**1**
794	1	4	**978**	-	**1**	**1176**	-	**1**
800	5	6	980	1	6	1194	1	2
802	1	5	988	3	7	**1208**	-	**1**
808	-	**3**	**994**	-	1	1210	3	3
814	1	2	1014	1	2	**1224**	-	**2**
816	1	4	**1026**	-	**1**	1232	1	1
818	-	**2**	1032	1	3	1240	3	4
828	1	4	1046	1	2	1270	1	6

Using the trends observed in the LC/MS separation of ten standards and those outlined in Chapter 2, structures were proposed for 10 new ginsenosides

from the American ginseng root extract. The new ginsenosides, whose proposed structures are shown in Scheme 3, included acetic acid esters, a malonic acid ester of ginsenoside Re, and a succinic acid ester of ginsenoside Rb_1. Structure characterization of nine of the ginsenosides in Scheme 3 employed both positive ion and negative ion LC/MS/MS experiments. As was observed for entry **5** in Scheme 3, negative ion experiments were not always practical. As such there are several other ginsenosides for which negative ion LC/MS/MS spectra were not practical and thus structure proposals were not possible.

References

[1] a. J. Shoji, *Recent Advances in the Chemical Studies on Ginseng.* In: Adv. In Chinese Medicinal Materials Research, H.M. Chang, H.W. Yeung, W.-W. Tso, A. Koo (Eds.), **1985**, p. 455. b. T. Namba, K. Matsushige, T. Morita and O. Tanaka, *Chem. Pharm. Bull.*, **1986**, *34*, 730. c. S. Zhang, X. Yao, Y. Chen, C. Cui, Y. Tezuka and T. Kikuchi, *Chem. Pharm. Bull.*, **1989**, *37*, 1966. d. T. Morita, Y.-C. Kong, P.-H. But, K.-H. Ng, T.-T. Yip, R. Kasai and O. Tanaka, *Chem. Pharm. Bull.*, **1986**, *34*, 4368. e. N.M. Duc, N.T. Nham, R. Kasai, A. Ito, K. Yamasaki and O. Tanaka, *Chem. Pharm. Bull.*, **1993**, *41*, 2010. f. N.M. Duc, R. Kasai, K. Ohtani, A. Ito, N.T. Nham, K. Yamasaki and O. Tanaka, *Chem. Pharm. Bull.*, **1994**, *42*, 115. g. N.M. Duc, R. Kasai, K. Ohtani, A. Ito, N.T. Nham, K. Yamasaki and O. Tanaka, *Chem. Pharm. Bull.*, **1994**, *42*, 634. h. M. Yoshikawa, T. Murakami, K. Yashiro, J. Yamahara, H. Matsuda, R. Saijoh and O. Tanaka, *Chem. Pharm. Bull.*, **1998**, *46*, 647. i. D.-Q. Dou, Y.-J. Chen, L.-H. Liang, F.-G. Pang, N. Shimizu and T. Takeda, *Chem. Pharm. Bull.*, **2001**, *49*, 442. j. Q. Le Tran, I.K. Adnyana, Y. Tezuka, T. Nagaoka, Q.K. Tran and S. Kadota, *J. Nat. Prod.*, **2001**, *64*, 456.

[2] a. T. Komori, O. Tanaka and Y. Nagai, *Org. Mass Spectrom.*, **1974**, *9*, 744. b. R. Kasai, K. Matsuura, O. Tanaka, S. Sanada and J. Shoji, *Chem. Pharm. Bull.*, **1977**, *25*, 3277. c. B.Y. Kim and M.Y. Lee, *Arch. Pharmacol. Res.*, **1992**, *15*, 328. d. T. Komori, M. Kawamuru, K. Miyahara, T. Kawasaki, O. Tanaka, S. Yahara and H.R. Schulten, *Z. Naturforsch.*, **1979**, *34C*, 1094. e. H.R. Schulten and F. Soldati, *J. Chromatogr.*, **1981**, *211*, 37. f. Y.N. Elkin and V.V. Makhankov, *Acta. Pharmacol. Sin.*, **1993**, *14*, 97. g. M. Yamamoto and K. Sugiyama, *Shoyakugaku Zasahi*, **1992**, *46*, 394. h. S.Z. Ackloo, R.W. Smith, J.K. Terlouw and B.E. McCarry, *The Analyst*, **2000**, *125*, 291. M.A. Tawab, U. Bahr, B. Danieli, S. Gebhardt, M. Karas, S. Riva and M. Schubert-Zsilavecz, *Helv. Chim. Acta*, **2000**, *83*, 739. i. M. Cui, F. Song, Z. Liu and S. Liu, *Rapid Commun. Mass Spectrom.*, **2001**, *15*, 586.

[3] a. I. Kitagawa, M. Yoshikawa, M. Yoshihara, T. Hayashi, T. Taniyama, *Yakugaku Zasshi*, **1983**, *103*, 612. b. T.M. Lee and A.D. Marderosian, *J. Pharm. Sci.*, **1981**,

70, 89. c. S. Sanada, J. Shoji and S. Shibata, *Yakugaku Zasshi*, **1978**, *98*, 1048. d. S. Shibata, O. Tanaka, T. Ando, M. Sado, S. Tsushima and T. Ohsawa, *Chem. Pharm. Bull.*, **1979**, *27*, 147.

[4] a. S. Hiai, H. Oura, Y. Odaka and T. Nakajima, *Planta. Med.*, **1975**, *28*, 363. b. J.L. Hon-Chiu and E.J. Staba, *J. Nat. Prod.*, **1980**, *43*, 340.

[5] a. O. Tanaka, Chemical analysis of Ginseng. In: *Recent Studies on Ginseng*, H. Oura, A. Kumagai, S. Shibata, K. Takagi (Eds.), Kyoritsu Publ. Co., **1981**, p. 42. b. Y.N. Shukla and R.S. Thukar, *Phytochem.*, **1990**, *29*, 239.

[6] a. T. Tani, M. Kubo, T. Katsuki, M. Higashino, T. Hayashi and S. Arichi, *J. Nat. Prod.*, **1981**, *44*, 401. b. E. Bombardelli, A. Bonati, B. Gabetta and E.M. Martinelli, *J. Chromatogr.*, **1980**, *196*, 121.

[7] a. O. Sticher and F. Soldati, *Planta Med.*, **1979**, *36*, 30. b. H. Besso, Y. Saruwatari, K. Futamura, K. Kunihiro, T. Fuwa and O. Tanaka, *Planta Med.*, **1979**, *37*, 226. c. O. Sticher and F. Soldati, *Planta Med.*, **1980**, *39*, 348. d. W.A. Court, J.G. Hendel and J. Elmi, *J. Chromatogr. A*, **1996**, *755*, 11 (and references sited within).

[8] a. D.M. Whitfield, S. Stojkovski and B. Starker, *Coord. Chem. Rev.*, **1993**, *122*, 171. b. L.M. Teesch and J. Adams, *Org. Mass Spectrom.*, **1992**, *27*, 931.

[9] a. K. Hostettman and A. Marston, *Saponins: Chemistry and Pharmacology of Natural Products*, Cambridge University Press, Cambridge, **1995**. b. M. Hattori, Y. Kawata, N. Kakiuchi, K. Matsuura, and T. Namba, *Shoyakugaku Zasshi*, **1988**, *42*, 288. c. M. Hattori, Y. Kawata, N. Kakiuchi, K. Matsuura, T. Tomimori and T. Namba, *Chem. Pharm. Bull.*, **1988**, *36*, 4467. d. M. K. Park, J.H. Park, S.B. Han, Y.G. Shin, I.H. Park, *Korio Insam Hakhoechi*, **1995**, *19*, 134.

[10] a. R.B. van Breemen, C.-R. Huang, Z.-Z. Lu, A. Rimando, H.H.S. Fong and J.F. Fitzloff, *Anal. Chem.*, **1995**, *67*, 3985. b. X. Wang, T. Sakuma, E. Asafu-Adjaye and G.K. Shiu, *Anal. Chem.*, **1999**, *71*, 1579. c. N. Fuzzati, B. Gabetta, K. Jayakar, R. Pace and F. Peterlongo, *J. Chromatogr. A*, **1999**, *854*, 69. d. T.W.D. Chan, P.P.H. But, S.W. Cheng, I.M.Y. Kwok, F.W. Lau and H.X. Xu, *Anal. Chem.*, **2000**, *72*, 1281. e. W. Li, C. Gu, H. Zhang, D.V.C. Awang, J.F. Fitzloff, H.H.S. Fong and R.B. van Breemen, *Anal. Chem.*, **2000**, *72*, 5417.

[11] K.L. Busch, G.L. Clish and S.A. McCluckey, *Mass Spectrometry/Mass Spectrometry: Techniques and Applications of Tandem Mass Spectrometry*, VCH Publishers, Inc., New York, **1988**.

[12] a. U. Piarulli and C. Floriani, *Prog. Inorg. Chem.*, **1997**, *45*, 393. b. J.-F. Verchere, S. Chapelle, F. Xin and D.C. Crans, *Prog. Inorg. Chem.*, **1998**, *47*, 837.

[13] M. R. Asam, G. L. Glish, *J. Am. Soc. Mass Spectrom.*, **1997**, *8*, 987.

[14] A.P. Bruins, ESI Source Design and Dynamic Range Considerations. In: Electrospray Ionization Mass Spectrometry: Fundamentals, Instrumentation and Applications, R.B. Cole (Ed.), John Wiley and Sons Inc., **1997**, p130.

[15] B. Alberts, D. Bray, J. Lewis, M. Raff, K. Roberts and J.D. Watson, *Molecular Biology of the Cell* (2^{nd} Ed.), Garland Publishing, Inc., **1989**.

Chapter 4

Carrageenan Analysis by Matrix-assisted Laser Desorption/ Ionization and Electrospray Ionization Mass Spectrometry I. *kappa*-Carrageenans

This Chapter describes a mass spectrometric study of κ-carrageenans, members of a family of sulfated polysaccharides. As with the ginsenosides these polysaccharides present a complex structural problem.

Matrix-assisted laser desorption/ionization (MALDI) and electrospray ionization (ESI) mass spectra of small *kappa*-carrageenans are reported and discussed. MALDI spectra can be obtained in both the positive and negative ion mode. In the absence of extraneous metal ions, positive ions are formed by the attachment of one Na^+ ion to the carrageenan, whereas for negative ions one Na^+ ion is detached from the sulfate group. Multiply charged species are not observed in MALDI. Intense ESI spectra can be obtained in the negative ion mode and now multiply charged species are seen. Alkali exchange experiments show that in these small carrageenan anions one, but only one, alkali metal ion is bound in a bidentate coordination with two ionic sulfate groups. G2-type *ab initio* calculations on model ions HO^- $[M^+]$ ^-OH (M = Li, Na, K, Cs) as well as arguments based on a simple Coulombic interaction model show that the bidentate stabilization energy drops rapidly as the size of the alkali cation increases. Exchange of Na^+ with Li^+ leads to expulsion of the Na^+ ion generating, in ESI, intense multiply charged anions. An attempt is made to rationalize this behaviour in terms of hydration effects.

The work in this Chapter has been recently published in an article under the same title: S.Z. Ackloo, J.K. Terlouw, P.J.A. Ruttink and P.C. Burgers, Rapid Commun. Mass Spectrom., 2001, 15, 1152.

Introduction

Carrageenan is the generic name for a family of natural, water-soluble, partially sulfated galactans isolated from red seaweed (*Rhodophyta*) [1]. They are isolated as salts where the major counter-ion is usually Na^+. One of the basic properties of carrageenans is their ability to induce gelation of solutions - particularly in the presence of K^+ and Ca^{++} - and carrageenans are therefore used as high value food ingredients [2]. The total world production of seaweeds

for carrageenan extraction is c. 120 million kg, yielding c. 25 million kg of carrageenans with an estimated value of c. $265 million [2]. The carrageenan family has three main branches named *kappa* (κ), *iota* (ι) and *lambda* (λ) which are differentiated by the number of sulfate groups per monomer. The repeating monomer structures of κ- and ι-carrageenans are shown in Figure 1a and 1b respectively and we note that the repeating unit is a disaccharide.

Commercial carrageenan products are rarely pure and contain varying amounts of impurities. We and others [3] have found that carrageenans can be efficiently separated by Capillary Electrophoresis (CE). We wished to identify the separated carrageenans off-line by either Matrix-Assisted Laser Desorption/Ionization / Time-of-Flight (MALDI-TOF) or Electrospray Ionization (ESI) mass spectrometry, without the need for additional derivatization steps which might degrade the polymer.

During the course of this study we found that MALDI and ESI are excellent techniques to probe metal ion interactions with the charged carrageenan back-bone. Such metal ion-carrageenan interactions undoubtedly play a key role in the mechanism for gelation and so we decided to investigate these matters in some detail.

Knutsen et al. [4] have proposed an alternative nomenclature for red seaweed polysaccharides which is based on logical abbreviations and IUPAC nomenclature. For the present study all compounds are pure κ-carrageenans and for simplicity we use the abbreviation DP_n to designate a *kappa*-carrageenan with Degree of Polymerization n; for example *kappa*-DP_2 is a tetrasaccharide containing two sulfate groups.

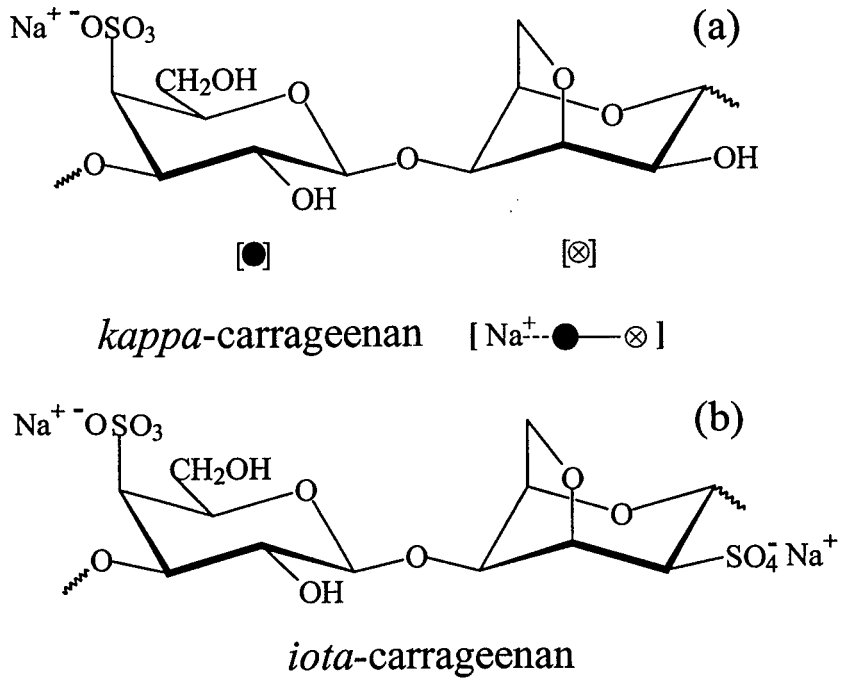

Figure 4-1: Neutral repeating unit of a *kappa*-carrageenan, item a), and an *iota*-carrageenan, item b).

Experimental

The following κ-carrageenans were purchased from Dextra Laboratories Ltd. (UK) : DP_1 (M = 426.10, item C1002), DP_2 (M = 834.18, item C1003), DP_3 (M = 1242.26, item C1010) and DP_4 (M = 1650.35, item C1011). The counter ion is Na^+ and thus the neutral repeating unit has a mono-isotopic mass of 408.084, see Figure 4-1a. The endgroup is water. The M values are the calculated mono-isotopic molecular masses including Na^+.

MALDI-TOF mass spectra were obtained using the Hercules Bruker Reflex II instrument operated either in the positive or negative ion mode. Ions were generated by a nitrogen laser (337 nm) and were accelerated to 20 keV. Between 200 and 1000 laser shots were averaged to generate the mass spectra.

In the spectra of Figures 4-2 – 4-9 the masses are given as nominal mono-isotopic masses. The samples were prepared as follows: 10 mg of the matrix, 2,5-dihydroxy benzoic acid (DHBA), was dissolved in 1 mL of ultrapure water. Carrageenan stock solutions of 10^{-2} mol/L in water were prepared. 90 μL of the matrix solution and 10 μL of the carrageenan solution were mixed and 0.5 μL of this solution was pipetted onto the MALDI target and dried under a stream of ambient air. No additional cationizing agent was added.

Negative ion ESI-MS and MS/MS experiments were performed on the Micromass Quattro LC triple quadrupole instrument at McMaster University. Stock solutions were prepared at a concentration of 7.5×10^{-4} mol/L in water. The analytes were infused via a pneumatically assisted Rheodyne 7010 injector equipped with a 20 μL injection loop at a flow rate of 10 μL/min. Normal mass spectra were acquired with the cone set at 30 V, the capillary at 4 kV, the high voltage lens at 0.2 kV, and the multiplier at 700 V. Product ion spectra were obtained with argon as collision gas (2.5×10^{-3} mBar) at a collision energy of 40 - 50 eV and the multiplier at 800 V.

Results and discussion

MALDI-TOF experiments: molecular integrity and concentration effects

It appeared that in MALDI-TOF experiments a carrageenan having mass M can become positively charged by the attachment of an additional Na^+ (leading to M + 23 cations) or it may become negatively charged by shedding a Na^+ (leading to M - 23 anions). First we will discuss spectra recorded in the positive

ion mode. In Figure 4-2a is shown the molecular region of the MALDI mass spectrum of DP_4 which contains four Na^+.

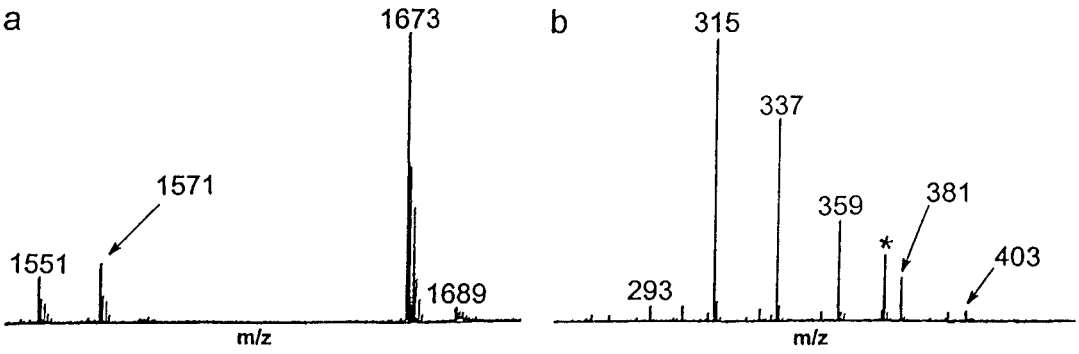

Figure 4-2. Positive ion MALDI spectra of DP_4, item a) and the tetra sodium salt of EDTA, item b). * denotes matrix signal.

The sodiated molecular ion appears at m/z 1673 with a weak K^+ adduct at m/z 1689. Now it is in principle possible that exchange reactions occur between the carrageenan molecules and the matrix molecules, whereby protons furnished by the acidic matrix exchange with one or more Na^+ ions of the carrageenan. The fact that these exchange reactions can readily occur is shown by the MALDI mass spectrum of the tetra sodium salt of EDTA (MW = 380), see Figure 4-2b. Significant Na^+/H^+ exchange reactions of the type [-COONa $\rightarrow$ -COOH] have taken effect as evidenced by the presence of peaks separated by 22 mass units. However, such Na^+/H^+ exchange signals appear to be absent for the DP_4 carrageenan. It will be shown below that exchange reactions do occur for carrageenans, i.e. [$-OSO_3Na \rightarrow -OSO_3H$], but that they are immediately followed by loss of a stable SO_3 molecule (ΔH_f = - 400 kJ/mol [5]). The carrageenan would appear to "lose" 102 mass units, that is the sulfate functionality is formally

lost via the sequence $X\text{-}OSO_3^-\ [Na^+] \rightarrow X\text{-}OSO_3^-\ [H^+] \rightarrow X\text{-}O^-\ [H^+] + SO_3$. For DP_4 such a process leads to anions at m/z 1571. The peak at m/z 1551 ("loss" of 120 mass units), we propose arises from a similar process whereby Na^+/H^+ exchange is now followed by loss of a stable H_2SO_4 molecule (ΔH_f = - 735 kJ/mol [5]).

As stated above, MALDI mass spectra of carrageenans can also be obtained in the negative ion mode. From preliminary experiments it quickly appeared that metal ion interactions with the charged carrageenan backbone could best be studied by observing negative ions and so all the following experiments were performed in the negative ion mode. First we will address concentration effects. The MALDI mass spectrum of DP_3 using a stock concentration of 10^{-2} mol/L is given in Figure 4-3a. The desodiated molecular anion is present at m/z 1219, together with peaks corresponding to the above "losses" of 102 mass units; also at this high stock concentration a weak signal is present for the dimer species, i.e. the ion $1219^-\ [Na^+]\ 1219^-$ at m/z 2461. No signals, and this goes for all carrageenans studied, could be detected for multiply charged (i.e. multiply desodiated) anions $[M\text{-}nNa]^{n-}$ ($n > 1$) whereas such species are readily formed by ESI, see below.

When the stock concentration was reduced to 10^{-4} mol/L, the mass spectrum in Figure 4-3b was obtained and this spectrum may be compared with that of Figure 4-3a. It is immediately seen that the "sulfate" eliminations are more prominent at the lower concentration; this is to be expected since at these lower analyte concentrations the matrix molecules will be present to a great excess (5000 : 1 compared to 50 : 1 at the higher analyte concentration). Secondly, and surprisingly, it follows from a comparison of the molecular region

around m/z 1219 at high and low concentrations, (Figures 4-3c and 4-3d), that at low concentrations additional signals appear at 16 mass units higher and at 6 mass units lower.

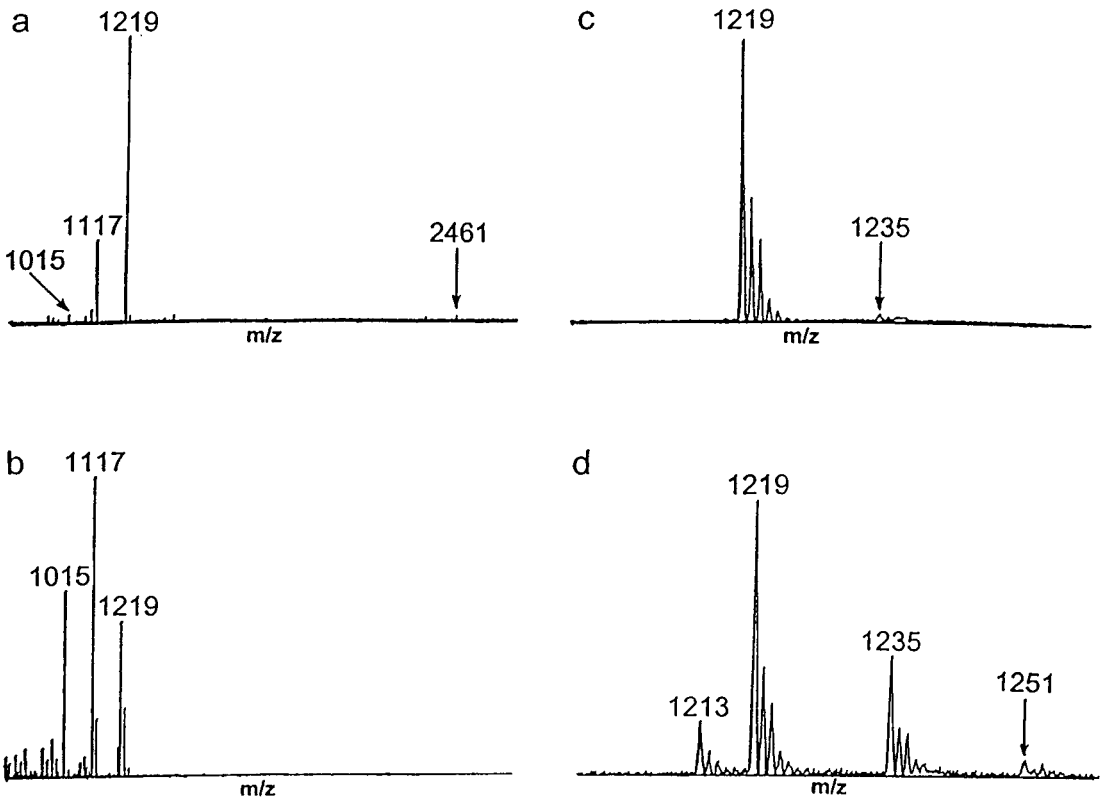

Figure 4-3. Negative ion MALDI spectra of DP_3 at a stock concentration of 10^{-2} mol/L and 10^{-4} mol/L, items a) and b) respectively and an expansion of the molecular mass region of the spectra shown in a) and b), items c) and d) respectively.

Metal ion exchange experiments, see below, indicate that the [+16] peaks arise by the exchange of one Na^+ ion with one K^+ ion and that the [-6] signals arise by exchange of two Na^+ ions with one Ca^{++} ion, thus maintaining a net charge of minus one.

Analysis of the matrix solution by Inductively Coupled Plasma-Atomic Emission Spectroscopy (ICP-AES) leads to the conclusion that the minor K^+/Ca^{++}

impurity originates from the carrageenan sample. We tentatively propose that the observed incorporation of K^+ and Ca^{++} into the carrageenan may be attributed to a solvent effect. Thus at lower concentrations of the carrageenan, hydration of Na^+ relative to that of K^+ and Ca^{++} competes more efficiently with attachment of the alkali cation to the carrageenan, see below.

Metal cation complexation with carrageenans

In the following discussion, we will represent the non-sulfated moiety of a carrageenan by a 'crossed' circle and the sugar unit carrying the SO_4^- functionality by a filled circle, see Figure 4-1a.

Metal ion - saccharide interactions play a key role in many biological processes and the intrinsic chemical properties of metal ion complexes of saccharides can be studied in the solvent free environment of the mass spectrometer [6,7]. For example, from Na^+ affinity measurements, it was concluded that Na^+ binds itself to saccharides in a multidentate coordination of the Na^+ with the neutral oxygen sites of the saccharides [7]. It is therefore entirely possible that for carrageenans the sodium ions also bind themselves in a bidentate or multidentate fashion to the negatively charged SO_4^- groups. That such complexation reactions indeed occur follows from the following experiments. The MALDI mass spectrum of DP_2 is, not unexpectedly, very similar to that of DP_3, compare Figures 4-4a and 4-3a. Note that the signal for the dimer species at m/z 1645 is virtually absent. In Figure 4-4b is shown the MALDI mass spectrum of DP_1. Apart from the molecular anion at m/z 403 there are now two other intense signals at m/z 829 and at m/z 579.

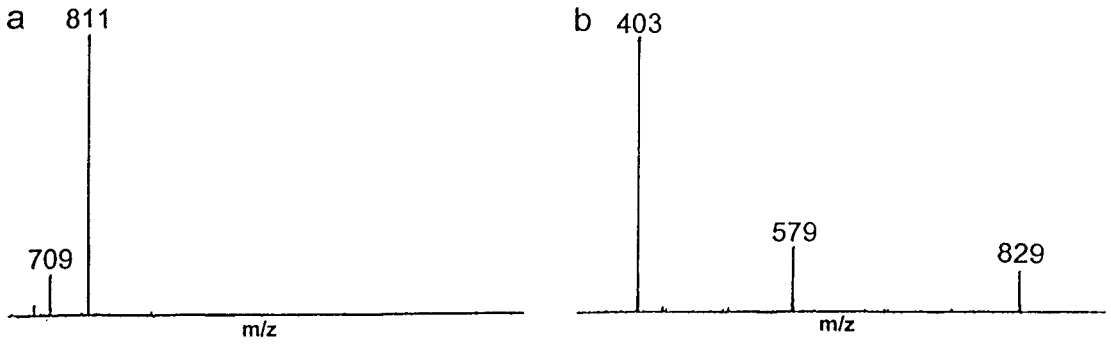

Figure 4-4: Negative ion MALDI spectra of DP_2, item a) and DP_1, item b).

We propose that these signals correspond to association of DP_1 with itself and with a DHBA matrix molecule, respectively, as illustrated :

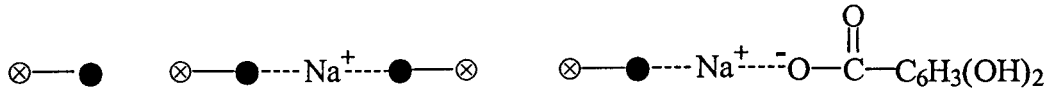

m/z 403 m/z 829 m/z 579

The dotted lines designate electrostatic interactions. We propose that the reason why only DP_1 abundantly undergoes association reactions is that the higher carrageenan anions already exist as very stable bidentate structures, for example structure **1** for DP_2.

Further evidence for the occurrence of such bidentate structures comes from alkali ion exchange experiments

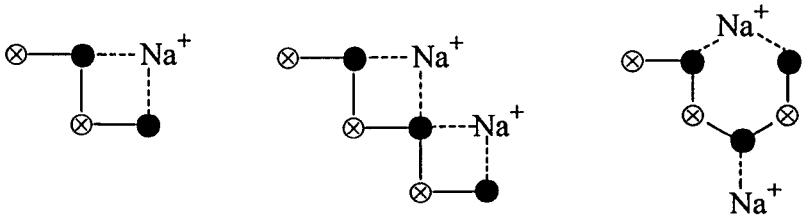

1 **2** **3**

A solution of 0.01 mol/L of DP_2 furnishes 0.02 mol/L of Na^+ and so equimolar exchange reactions were performed by adding 0.02 mol/L solutions of LiCl, KI or CsI to an equal volume of a 0.01 mol/L solution of DP_2. The negative ion MALDI mass spectrum resulting from such an exchange experiment using Cs^+ is given in Figure 4-5a.

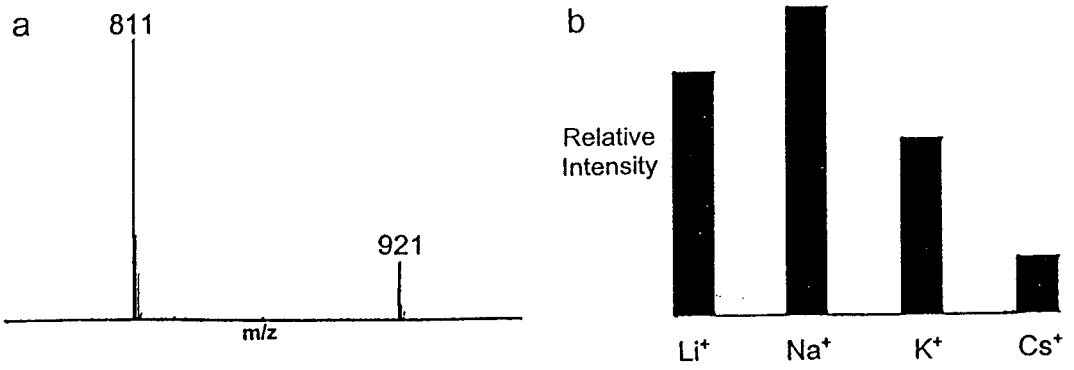

Figure 4-5. Negative ion MALDI spectrum of DP_2 exchanged with Cs^+, item a) and a bar-graph representation of the relative intensity ratios of the molecular ions corresponding with DP_2 exchanged with Li^+, K^+ and Cs^+, item b).

It is seen that the signal for the Cs^+ containing ion is c. 5 times less intense than that for the Na^+ containing ion. This, we argue, is due to the lower charge density of the Cs^+ ion compared to that of the Na^+ ion (by a factor of 5.6) leading to a less stable bidentate structure. The results for equimolar exchange experiments with Li^+, K^+ and Cs^+ are compiled in Figure 4-5b as a bar graph.

It can be seen that the intensity of the K^+ containing ions lies between those of the Cs^+ and Na^+ containing ions, as predicted on the basis of the intermediate charge density of the K^+ ion. Since the charge density of the Li^+ cation is much greater than that of Na^+ (by a factor of 4.1) it may reasonably be

expected that the Li^+ bidentate is more stable than the Na^+ bidentate and so, in an equimolar exchange experiment, the peak for the Li^+ containing ions would be expected to be significantly more intense than that for the Na^+ containing ions. However, the spectrum presented in Figure 4-5b indicates that this is not the case : equimolar exchange with Li^+ leads to a signal which has about the same intensity as that for the Na^+ containing ions. A possible rationalization for this behaviour is given in the next section.

For larger carrageenans the possibility exists that multiple bidentate structures are formed. For example the singly charged negative ion of DP_3 may exist as double or as single bidentates; possible structures for a single (**2**) and a double bidentate (**3**) are shown above.

An equimolar Cs^+ exchange experiment yielded the MALDI mass spectrum shown in Figure 4-6a. If the anion exists as the double bidentate structure **2**, then the calculated intensity ratio for ions containing two sodium ions [2Na], one sodium and one cesium ion [1Na, 1Cs], and two cesium ions [2Cs] becomes: [2Na] : [1Na, 1Cs] : [2Cs] = 1 : 0.4 : 0.04, which corresponds with $(1 : 0.2)^2$. However, the observed intensity distribution, see Figure 4-6a, more closely matches the ratio 1 : 1 : 0, expected if one Na^+ ion in the carrageenan can be freely exchanged, whereas the other cannot. This indicates that the anion of DP_3 is better described as **3** - where it is assumed that the non-bidentate sodium ion can be freely exchanged - rather than as **2**, perhaps because of the lesser ring strain associated with **3**. Similar results were obtained for Cs^+ exchange of the anion of DP_4 which contains three sodium ions, see Figure 4-6b. The observed intensity distribution closely matches that for random exchange of two sodium

ions (calculated ratio = 1 : 2 : 1). This indicates that for DP_4 too, only one bidentate bridge exists.

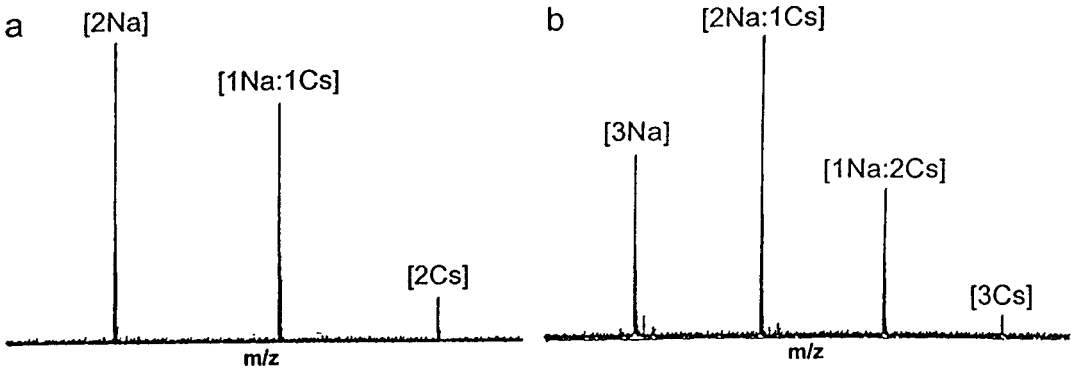

Figure 4-6: Negative ion MALDI spectra of DP_3 exchanged with Cs^+, item a) and DP_4 exchanged with Cs^+, item b).

Similar exchange experiments were performed using the alkaline earth elements Mg^{++}, Ca^{++} and Ba^{++} whose relative charge densities are : 5.2 : 1.5 : 1 [8]. It was observed that in these cases two Na^+ ions are exchanged by one alkaline earth element; thus exchange of the anion of DP_3 with Ca^{++} yielded a signal six mass units lower than that for the ion containing two Na^+ ions as indicated below :

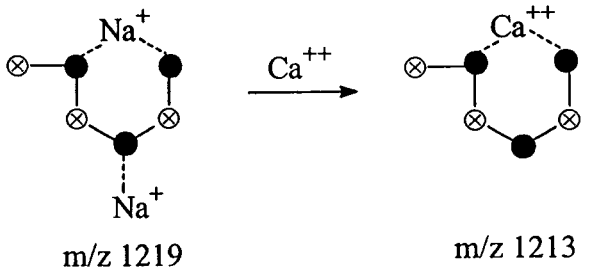

m/z 1219 m/z 1213

Thus the M-6 peak observed in the MALDI spectra of carrageenans at low stock concentrations results from exchange of two Na^+ ions with one Ca^{++} ion. For the

alkaline earth elements the affinity appeared to be highest for Ca^{++}. This parallels the results obtained for the alkali ion family where the element with largest charge density (i.e. Li^{+}) did not produce the most intense signal.

Finally, exchange experiments were performed with the transition metal ion Cu^{++}. If Cu^{++} behaves in a way similar to that of the alkaline earth elements, then exchange of DP_3 should lead to structure **4**, see below. In Figure 4-7b is given the MALDI mass spectrum of DP_3 exchanged with Cu^{++} and this mass spectrum may be compared with that of DP_3 itself (Figure 4-7a).

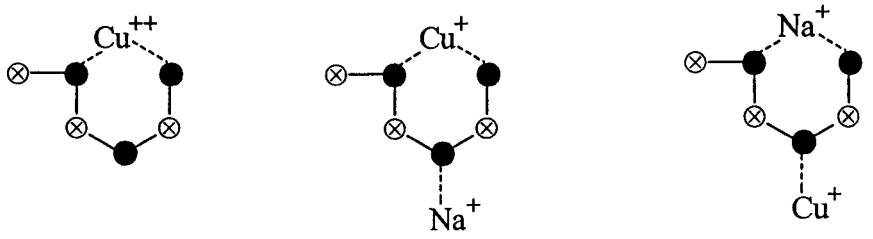

4 m/z 1236 **5a** m/z 1259 **5b** m/z 1259

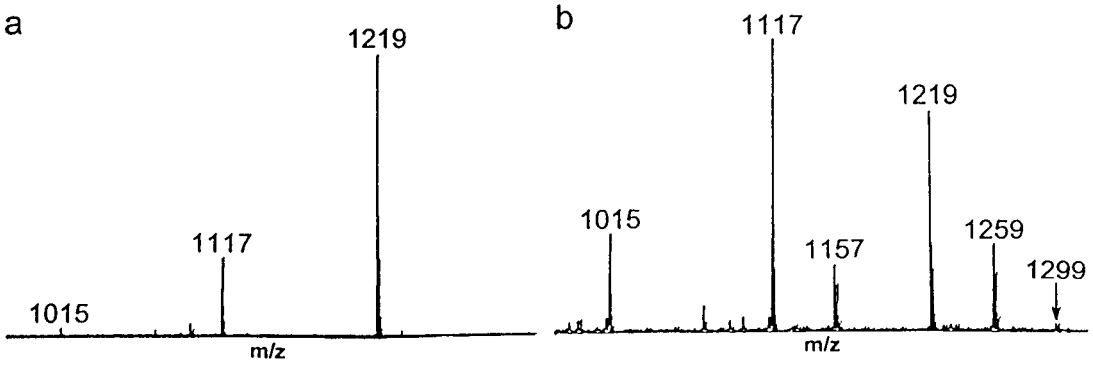

Figure 4-7: Negative ion MALDI spectrum of DP_3, item a) and DP_3 exchanged with Cu^{++}, item b).

It can be seen that there is no signal at the expected mass for incorporation of Cu^{++}, *viz.* at m/z 1236, but instead an intense signal is observed 23 mass units higher, namely at m/z 1259 (from the isotope pattern it is clear that this ion contains one Cu atom). We conclude that the ions at m/z 1259 are ions **5a** and/or **5b**, where the Cu^{++} has been reduced to Cu^{+}. A weak signal is also present for the incorporation of two Cu^{+} ions at m/z 1299. Reduction of Cu^{++} has been observed previously in the MALDI spectra of polystyrenes [9-11]. It has been suggested that the large energy gain for reduction of Cu^{++} to Cu^{+} (12.56 eV) as opposed to only 5.76 eV for reduction of Ca^{++} to Ca^{+}, is the driving force for this process. Presumably, the electron is furnished by the matrix or analyte in a collision as the ions become desolvated during desorption [11]. It can also be seen from Figure 4-7b that the "sulfate" eliminations become more pronounced when Cu^{++} is added to the carrageenan solution. However, this does not appear to be unique for Cu^{++} as intense "sulfate" eliminations are also seen in exchange experiments with the alkaline earth elements.

Bidentate stabilization energies: ab initio calculations

To assess ionic bidentate bond strengths we have performed *ab initio* calculations at the G2 level of theory [12]. Such high level calculations are restricted to relatively small molecules and thus we have taken as a model for the bidentate, the structure HO^{-} $[M^{+}]$ ^{-}OH (**6**), where M is the alkali cation. The Bidentate Stabilization Energy (BSE) is defined as the energy needed to separate the components of **6** to infinity : HO^{-} $[M^{+}]$ ^{-}OH (**6**) $\rightarrow$ $[M^{+}]$ + ^{-}OH + ^{-}OH (Eqn. 1).

Standard methods such as the G2 method are incapable of treating third row atoms. Therefore it was decided to adapt it in the following way. Geometries were calculated using MP2(Full)/6-311+G(d,p). The triple zeta valence AO set is needed to treat K properly, the diffuse functions are needed because we are dealing with anions and a single set of polarization functions is necessary to obtain reasonably accurate bond lengths. The ZPE was calculated in the same way and the result was scaled by a factor of 0.9427. An estimate of the electronic energy was then obtained by combining the results from CCSD(T)6-311+G(d,p), MP4SDTQ/6-311+G(2df,p) and MP2/6-311+ G(3df,2p) calculations :

$$E_c = E[CCSD(T)/6\text{-}311+G(d,p)] + \Delta E_1 + \Delta E_2$$

$$\Delta E_1 = E[MP4SDTQ/6\text{-}311+G(2df,p)] - E[MP4SDTQ/6\text{-}311+G(d,p)]$$

$$\Delta E_2 = E[MP2/6\text{-}311+G(3df,2p)] - E[MP2/6\text{-}311+G(2df,p)]$$

In these calculations partially frozen cores were used, that is, $N_C = 1$ for O and Na, and $N_C = 5$ for K. Test calculations showed that the correlation effects due to the n = 2 shell cannot be neglected. Analogously the n = 3 shell correlations for K are quite important.

Finally a higher level correlation contribution was added as in the G2 method:

$$\Delta E_3 = n_{pair}\,\Delta E_p - [n_\alpha\,\Delta E_\alpha + n_\beta\,\Delta E_\beta],$$

where n_α and n_β represent the number of valence α and β electrons respectively, n_{pair} refers to the number of valence electron pairs; ΔE_p = 0.00114 H, ΔE_α = 0.00019 H, ΔE_β = 0.00595 H.

The final energy is then obtained by using $E_f = E_c + \Delta E_3 + E_{ZPE}$(scaled).

The accuracy of the additivity assumption yielding E_c was checked by a CCSD(T)/6-311+G(3df,2p) calculation on HO^- $[K^+]$ ^-OH. This calculation yielded an energy of – 750.93895 H, which differs by only 0.00001 H from the value derived from the additivity scheme. The results obtained by our procedure are given in Table 1. A comparison of the results for some reactions involving the species at hand to experimental data [5] indicates that the calculated energies are accurate to about 20 kJ/mol.

From these calculations the Bidentate Stabilization Energies (BSE) can be assessed, see Table 1.

Table 1. Total electronic energies (E_f) of HO^- $[M^+]$ ^-OH and its dissociation products, bidentate stabilization energies (BSE), and hydration energies (HE) of M^+.

Species	E_f [H]	BSE [a]	BSE [b]	HE [c]
$Li^+ + 2\ ^-OH$	-158.67042			
$HO^-[Li^+]\ ^-OH$	-159.07249	1060	1040	515 $[Li^+]$
$Na^+ + 2\ ^-OH$	-313.23308			
$HO^-[Na^+]\ ^-OH$	-313.58002	910	880	400 $[Na^+]$
$K^+ + 2\ ^-OH$ [d]	-750.67721			
$HO^-[K^+]\ ^-OH$	-750.97778	790	765	335 $[K^+]$
$HO^-[Cs^+]\ ^-OH$			680	280 $[Cs^+]$

[a] BSE (kJ/mol) derived from the ab initio calculations
[b] BSE (kJ/mol) from the Coulombic model described in the text
[c] HE (kJ/mol) from Ref. 17, see text
[d] E_f for OH^- is - 75.70729 H

We have also calculated BSE values using a simple electrostatic model based on Coulomb's law which yields the expression :

$$\Delta E \text{ (kJ/mol)} = -\frac{3}{2R} \times 1390 \qquad R \text{ in } \mathring{A}$$

where R is the bond length of the $[M^+]$ ^-OH bond, for which we have taken the sum of the ionic radius of M^+ and the van der Waals radius of a (neutral) oxygen atom. It can be seen that the agreement is quite good and so the Coulombic model was used to estimate the BSE for HO^- $[Cs^+]$ ^-OH for which the *ab initio* value could not be assessed.

From the results in Table 1, it follows that for gaseous HO^- $[M^+]$ ^-OH ions, the bidentate stabilization energy drops rapidly as the size of M^+ increases. Extending these findings to the carrageenan DP_2 anion, bidentate formation with K^+ and Cs^+ should be less efficient than complexation with Na^+, as is observed, see Figure 5b.

Our calculations also predict that complexation with Li^+ should be even more efficient than complexation with Na^+, but this seems to be at odds with the results shown in Figure 5b. However, although the environment of the analyte in the matrix is very different to that in solution, recent reports indicate that MALDI mass spectra, acquired under certain experimental conditions (such as choice of matrix and pH of solution [13-16]), may reflect solution phenomena. In solution, for carrageenans one competitive process is hydration of the alkali cation, as indicated for DP_2 in Eqn. (2) :

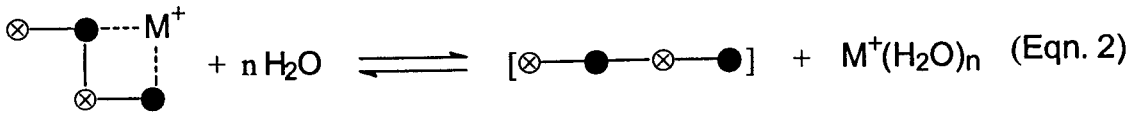

7 **8** (M = 394)

The hydration energy of the alkali cations in the gas phase, i.e. the energy gain associated with the reaction $M^+(H_2O)_{n-1} + H_2O \rightarrow M^+(H_2O)_n$, has been measured [17] for n = 1 - 6. The total energy change, that is the energy gain for the process $M^+ + 6\ H_2O \rightarrow M^+(H_2O)_6$,is taken as being closest to the Hydration Energy (HE) in solution [18] and these values are also listed in Table 1. From these data it follows that solvation of the alkali cation cannot compete with bidentate formation, not even in the case of Li^+. Why then is it so hard to incorporate Li^+ into the carrageenan? One other consideration in determining the true selectivity in an aqueous solution is the extent to which the bidentate structure **7** is also solvated. It may well be that the bidentate bond lengths for Na^+, K^+ and Cs^+ are large enough so that complexation with the carrageenan does not completely block access to surrounding water molecules. In other words, in the case of Li^+, structure **7** would *not* be stabilized by solvent interactions. In any event, we propose that when Li^+ is added to an aqueous solution of a carrageenan where the counter ion is Na^+ (or an alkali cation of higher atomic weight), the equilibrium of Eqn. (2) will shift to the right. As a result, more alkali-free carrageenan anions of structure **8** are produced and this is precisely what is observed in our ESI experiments.

ESI experiments

All ESI experiments were performed in the negative ion mode using stock solutions having a concentration of 7.5 x 10^{-4} mol/L. The ESI mass spectra of DP_2 and of DP_3 are given in Figures 4-8a and 4-8b respectively. In both cases the singly desodiated anion is clearly present at m/z 811 and at m/z 1219. Also present are peaks corresponding to "losses" of 102, at m/z 709 and m/z 1117 respectively, as was observed in the MALDI spectra discussed in the previous section. ESI-MS/MS experiments show that for DP_2 the ions at m/z 709 originate from m/z 789 (loss of SO_3) which itself is only a weak signal in the ESI and MALDI mass spectra. Thus in both ESI and MALDI experiments, the Na^+ ion in the anion of DP_2 apparently can be exchanged with a proton followed by expulsion of SO_3.

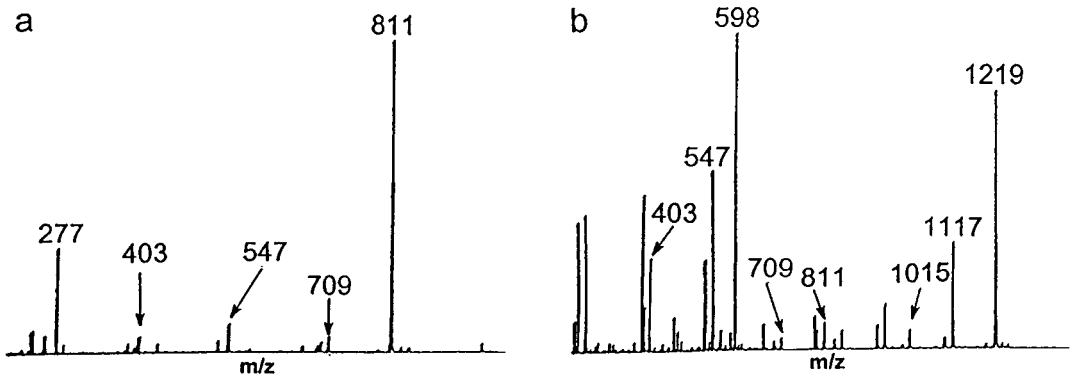

Figure 4-8. Negative ion ESI spectra of solutions containing DP_2, item a) and DP_3, item b).

Additional peaks are seen for elimination of a galactose-4-sulfate moiety, depicted as [●] in Figure 4-1, at m/z 547 and at m/z 955 for DP_2 and DP_3 respectively (these processes are also seen in the MS/MS mass spectra of m/z

811 and m/z 1219 respectively). However, a major difference between the ESI spectra of DP_2 and DP_3 is that for DP_2 there are no doubly charged (i.e. doubly desodiated) anions at m/z 394, whereas for DP_3 the corresponding peak at m/z 598 is the base peak. We attribute this remarkable all-or-nothing effect to the bidentate structures **1** and **3** : the bidentate sodium cation in these structures is securely sequestered and cannot easily be removed from the anion.

By contrast, the non-bidentate sodium ion in structure **3** can be expelled easily. These findings are in complete agreement with our Cs^+ exchange MALDI experiments, see above, where it was found that the anion of DP_2 is more accurately described by structure **3** rather than by structure **2**.

We also performed Cs^+ and Li^+ exchange ESI experiments. Again, these measurements appeared to be in full agreement with our MALDI data, but they reveal an additional important phenomenon which is not apparent from our MALDI results. DP_2 was exchanged with a 28.6 fold excess of Cs^+ and the ratio of Cs^+ and Na^+ containing ions (m/z 921 : m/z 811) was found to be 4.8, indicative of a discrimination against Cs^+ incorporation into the carrageenan by a factor of 6. This is gratifyingly close to the factor of 5 calculated from the intensity ratios observed in the MALDI mass spectra. It should also be noted that in the Cs^+ exchange experiment no doubly charged species could be detected. The ESI mass spectrum of DP_2 exchanged with a 2.6 fold excess of Li^+ is shown in Figure 4-9a (these experiments were performed using $^6LiCO_3$).

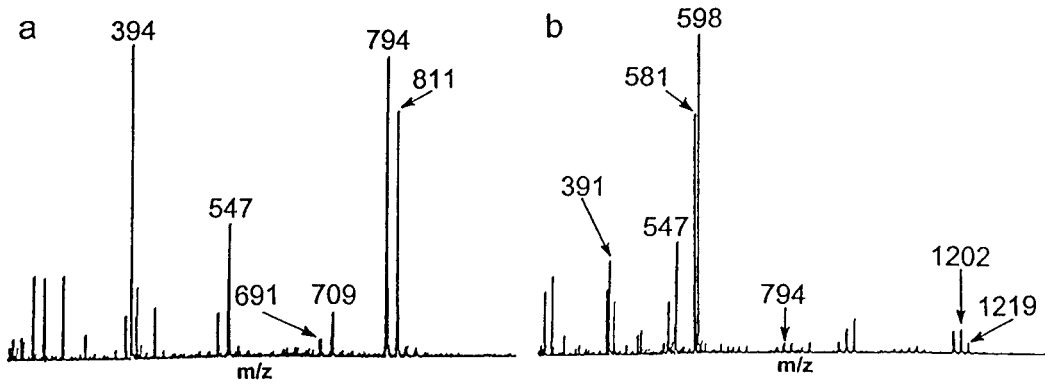

Figure 4-9: Negative ion ESI spectra of solutions of DP_2 exchanged with Li^+, item a) and DP_3 exchanged with Li^+, item b).

Now, from the MALDI experiments it appeared that incorporation of Li^+ was not favoured over complexation with Na^+, despite the fact that Li^+ has a much larger charge density than Na^+. This behaviour appears to be even more pronounced in our ESI experiments from which it would follow that it is about 2.5 times *less* likely to incorporate Li^+ into the carrageenan, see Figure 4-9a. However, it is also seen that the doubly charged signal (structure **8**) is now almost the base peak, whereas it was absent when the counter ions were Na^+ (see Figure 4-8a) or Cs^+ and so again an all-or nothing effect presents itself. Thus, the equilibrium shown in Eqn. (2) lies completely to the left in the case of Na^+ and Cs^+, but shifts to the right when Li^+ is added. This behaviour becomes even more pronounced when the carrageenan anion contains a sodium cation which is not bound in a bidentate fashion and which can therefore readily be removed from the carrageenan as for example in structure **3** for DP_3, see above. Exchange with Li^+ now leads to the spectrum shown in Figure 4-9b. This

spectrum is dominated by the doubly charged species **9** and **10** whereas the singly charged anions (m/z 1185, 1202 and 1219) are now weak signals only.

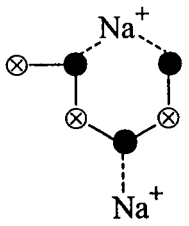

9 (M = 598)

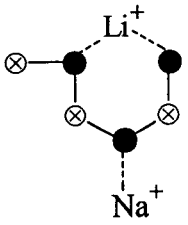

10 (M = 581)

Similarly, for DP_4, exchange with Li^+ leads to an ESI mass spectrum in which the *triply* charged anions represent the most intense peaks, while the singly charged anions are now very weak signals. Thus for all carrageenans studied the relative intensity of the multiply charged anions in the ESI spectra can be greatly enhanced by adding Li^+ to the carrageenan stock solution.

Conclusions

The application of MALDI-MS and ESI-MS to the analysis of carrageenan samples has proven relatively straightforward, provided that dilution effects of the carrageenan solutions are recognized and appreciated. In MALDI-MS these effects manifest themselves in the following ways. At analyte concentrations below 10^{-3} mol/L, matrix induced expulsion of sulfate groups becomes an important process and such eliminations should be recognized for what they are. As will be shown in a future publication on *iota*-carrageenans, identification of such processes may not be a trivial matter at all : loss of a sulfate group from an

iota part leads to a mass peak which could, mistakenly, be identified as belonging to a component containing a *kappa* moiety. Secondly, dilute carrageenan solutions show a notable degree of exchange between the dominant Na^+ ion with K^+ / Ca^{++} ions, present as minor impurities in the carrageenan samples. Such exchange reactions lead to signals 16 Da higher and 6 Da lower respectively than the expected mass. As will be shown in our future publication, these signals dominate the spectra obtained from very dilute solutions and if they are not recognized as such, an unknown carrageenan may remain unidentified.

References

[1] H.H. Shelby and R.L. Whistler. In *Industrial Gums: Polysaccharides and Their Derivatives*, 3rd Ed. R.L. Whistler and J.L. BeMiller (Eds.), Academic Press, **1993**, p87.

[2] G.A. De Ruiter and B. Rudolph, *Trends Food Science Techn.* **1997**; *8*, 389.

[3] J. Hau and M. Roberts, *Anal. Chem.*, **1999**, *71*, 3977.

[4] S.H. Knutsen, D.E. Myslabodski, B. Larsen and A.L. Usov, *Bot. Mar.*, **1994**, *37*, 163.

[5] S.G. Lias, J.E. Bartmess, J.F. Liebman, J.L. Holmes, R.O. Levin and W.G. Mallard, *J. Phys. Chem.*, Ref. Data *17* Supplement 1, **1988**.

[6] B.A. Cerda, S. Hoyau, G. Ohanessian and C. Wesdemiotis, *J. Am. Chem. Soc.*, **1998**, *120*, 2437.

[7] B.A. Cerda and C. Wesdemiotis, *Int. J. Mass Spectrom.*, **1999**, *189*, 189.

[8] J.W. Eichinger Jr. In: *The Encyclopedia of Chemistry*, 2nd Ed. G.L. Clark and G.G. Hawley (Eds.), Reinhold Publishing Corporation, **1966**, p205.

[9] E. Lehmann, R. Knochenmuss and R. Zenobi, *Rapid Commun. Mass Spectrom.*, **1997**, 11, 1483.

[10] P.C. Burgers and J.K. Terlouw, *Rapid Commun. Mass Spectrom.*, **1998**, *12*, 801.

[11] R. Zenobi and R. Knochenmuss, *Mass Spectrom. Rev.*, **1998**, *17*, 337.

[12] L.A. Curtiss, K. Raghavachari, G.W. Trucks and J.A. Pople, *J. Chem. Phys.*, **1991**, *94*, 7221.

[13] C. Masselon, B. Salih and R. Zenobi, *J. Am. Soc. Mass Spectrom.*, **1999**, *10*, 19.

[14] A.S. Woods, J.C. Buchsbaum, T.A. Worrall, J.M. Berg and R.J. Cotter, *Anal. Chem.*, **1995**, *67*,4462.

[15] T.B. Farmer and R.M. Caprioli, *J. Mass Spectrom.*, **1998**, *33*, 697.

[16] F. Dubois, R. Knochenmuss and R. Zenobi, *Eur. Mass Spectrom.*, **1999**, *5*, 267.

[17] I. Dzidic and P. Kebarle, *J. Phys. Chem.*, **1970**, *74*, 1466.
[18] M.B. More, D. Ray and P.B. Armentrout, *J. Am. Chem. Soc.*, **1999**, *121*, 417.

Chapter 5

Structure Analysis of Diols by Electrospray Mass Spectrometry on Boric Acid Complexes

The previous three Chapters described structure characterization of a class of triterpene glycosides and sulfated polysaccharides. It became clear that triterpene glycosides differing only in an isomeric sugar cannot be differentiated by MS/MS experiments. The work described in Chapters 5 and 6 describe two approaches for differentiating stereoisomeric polyols and geometric isomeric sugars based on selective complexation to boric acid and oxovanadium(IV).

A method is presented to characterize diols using negative ion electrospray (ES) mass spectrometry in combination with collision induced dissociation (MS/MS). The analyte diol is added to a solution containing an ethylene glycol/boric acid [2:1] complex and then subjected to infusion ES. The following boric acid complexes are formed : (i) a complex with two ethylene glycol molecules, (ii) a mixed ethylene glycol/analyte complex, and (iii) a complex with two analyte molecules. The first complex serves as reference for the assessment of the extent of complex formation with the analyte.

The ES mass spectra of acyclic vicinal diols all feature intense mixed complex signals, indicative of efficient complex formation. Chemical fine tuning is achieved by MS/MS experiments. Thus, although the (2*R*,3*R*)-(-)-2,3-butanediol and *meso*-2,3-butanediol stereo-isomers show the same complexation efficiency, MS/MS experiments revealed pronounced structure characteristic differences. By contrast, 1,3- and 1,4-diols are less prone to complex formation as they give only weak signals relative to the reference. For cyclic vicinal diols only the *cis* isomer produces an intense mixed complex, whose MS/MS spectrum is characteristically different from that of the *trans* form. The above procedure does not permit an unambiguous differentiation of acyclic polyhydroxy compounds like mannitol and sorbitol. However, structurally related methyl glycosides show characteristic MS/MS spectra.

Our findings indicate that the above simple procedure may be useful to probe the presence and structure of diols and other polyols in aqueous solutions.

The work in this Chapter has been published previously in an article under the same title: S.Z. Ackloo, P.C. Burgers, B.E. McCarry, and J.K. Terlouw, Rapid Commun. Mass Spectrom., 1999, 13, 2406.

Introduction

Boron has 3 valence electrons and forms planar, tricovalent derivatives that are electron deficient. These derivatives act as Lewis acids by accepting two

electrons from bases to complete the outer shell octet of boron ; the two reactants (the boron derivative and the Lewis base) form stable coordinate covalent complexes, many of which are commercially available. For example, boron trifluoride diethyl etherate $(C_2H_5)_2O^+$-BF_3^- is widely used as a catalyst for esterifications and acylations. Any substance having free electron pairs can accommodate a proton and so Lewis bases are identical with the BrØnsted-Lowry bases. By contrast, Lewis acids are not necessarily proton donors. A case in point is boric acid $B(OH)_3$ [1]. An aqueous solution of boric acid is weakly acidic, but not because boric acid deprotonates by itself ; rather it can only generate protons after hydration has taken effect :

$$B(OH)_3 + H_2O \rightleftharpoons B(OH)_4^- + H^+$$

In fact, the intermediate complex $B(OH)_3OH_2$ [2] acts as the BrØnsted acid.

It has long been known that boric acid reacts efficiently with certain hydroxy compounds in aqueous solution, leading to a decrease in pH [3]. Over 150 years ago, Biot reported that a solution of boric acid became acidic to litmus upon the addition of sugar [4,5]. In fact, the extent to which the pH of solutions containing boric acid decreased upon addition of a polyhydroxy compound has been used as an indication of the ease of chelate formation. In 1949, Deutsch and Osoling [5] investigated the boric acid–mannitol system. Mannitol (compound **14** in Scheme 1) contains six hydroxyl groups of which two pairs (C2 and C3, and C4 and C5) are *cis* to each other, allowing easy formation of the complex. In solution mannitol does not have restricted movement so it is likely that the terminal hydroxyl groups rotate to a position that allows easy complex

formation. This increases the number of combinations of hydroxyl groups which can complex with boric acid. Deutsch and Osoling [2,6] described the formation of two types of complexes :

(i) a 1 : 1 [1M] complex, also referred to as a B^-L complex
(ii) a 2 : 1 [2M] complex, also referred to as a B^-L_2 complex

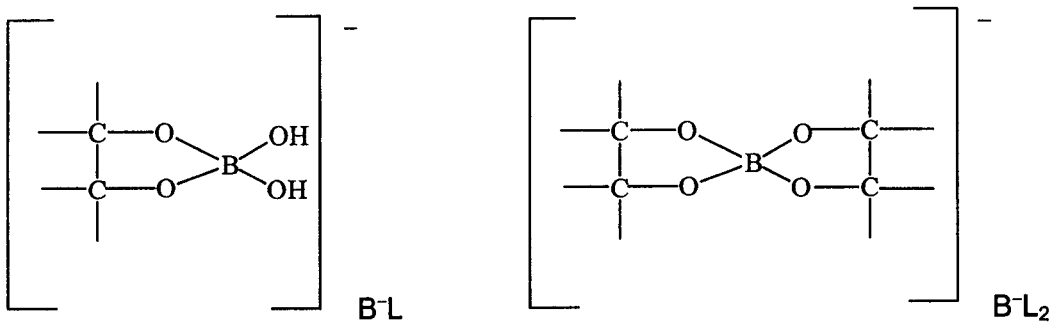

Titration of a boric acid/mannitol solution with sodium hydroxide showed that the [1M] complex ($K = 3 \times 10^2$) predominates when there is excess boric acid while the [2M] complex ($K = 5 \times 10^4$) is the principal species when there is excess mannitol.

Although potentiometry provided initial evidence for the existence of these complexes, conductometry, polarimetry, electrophoresis, refractometry, nuclear magnetic resonance (NMR) spectroscopy [1] and circular dichroism [7] have also been used for their characterization. NMR spectroscopy is one technique that has often been used to characterize borate esters. Carbon-13 (^{13}C), proton (^{1}H), and boron-11 (^{11}B) NMR spectroscopy have been used either in conjunction with each other, or separately to analyze the complexes. In particular, association constants for many [1M] and [2M] borate esters, including those of 1,2-ethanediol and 1,2-propanediol, have been obtained [6,7]. Further, Chapelle and Verchere used ^{11}B and ^{13}C NMR spectroscopy to show that sugars

of the *ribo* series have a higher affinity for boric acid relative to the *xylo* series [8]. In solution, sugars equilibrate between the α/β-furanose and α/β-pyranose forms. *Xylo* sugars exist mainly in the pyranose form which implies that the hydroxyl groups are in a *trans* orientation. As a result chelate formation between *xylo* sugars and boric acid is less facile.

Several applications based on affinity chromatography have been reported wherein (stereo) isomeric polyols have been separated. One example is the use of affinity chromatography to separate sugars by using an anion-exchange stationary phase [9,10].

Mass spectrometry has also been used in studies of boric acid complexes of polyols and carbohydrates using negative ion ES and fast atom bombardment [11], thermospray [12] and matrix-assisted laser desorption [13] techniques. In addition, Bayer et al., in a recent communication [14] on coordination-ionspray-MS (CIS-MS), have reported that under the conditions selected for CIS-MS, fructose produces a stable [2M] complex whereas glucose does not.

In this contribution we have applied the concept of boric acid complexation to explore structure analysis of isomeric polyols using negative ion ES in conjunction with collion-induced dissociation of the complexes. The selected group of (stereo) isomeric polyhydroxy compounds is listed in Scheme 1.

Experimental

Boric acid was obtained from CP Baker while ^{10}B-boric acid was purchased from Sigma-Aldrich. For all experiments HPLC-grade methanol and

distilled de-ionised water was used. The compounds listed in Scheme 1, 1,2-ethanediol (ethylene glycol) (**1**), 1,2-propanediol (**2**), 1,3-propanediol (**3**), 1,2-butanediol (**4**), 1,3-butanediol (**5**), 1,4-butanediol (**6**), *meso*-2,3-butanediol (**7**), (2*R*,3*R*)-(-)-2,3-butanediol (**8**), 1,3-cyclopentanediol [mixture of *cis* and *trans* isomers] (**9**), *cis*-1,2-cyclopentanediol (**10**), *trans*-1,2-cyclopentanediol (**11**), *cis*-1,2-cyclohexanediol (**12**), *trans*-1,2-cyclohexanediol (**13**), D-mannitol (**14**), D-sorbitol (**15**), α-methyl-D-glucopyranoside (**16**) and α-methyl-D-mannopyranoside (**17**) were purchased from Sigma-Aldrich and used without further purification. The deuterium labelled 1,2-propanediol isotopologues were a gift from Dr A. Milliet (Ecole Polytechnique, Palaiseau, France).

Negative ion ESMS and MS/MS experiments were performed on the McMaster Quattro LC (Micromass, England) triple quadrupole instrument. Normal mass spectra were acquired with the cone set at 30 V, the capillary at 4 kV, the high voltage lens at 0.2 kV, and the multiplier at 700 V. Product ion spectra were obtained using Argon as the collision gas. Typically, a collision energy of 22 eV was used with a gas cell pressure of 2.5×10^{-3} mBar and the multiplier at 800 V. The analyte was infused via a pneumatically assisted Rheodyne 7010 injector equipped with a 20 μL injection loop. In all experiments a CH_3OH/H_2O (1:1) mobile phase was delivered at a flow rate of 10 μL/min via a Brownlee pump (Advanced Biosystems, Canada). All spectra were acquired for 2 minutes.

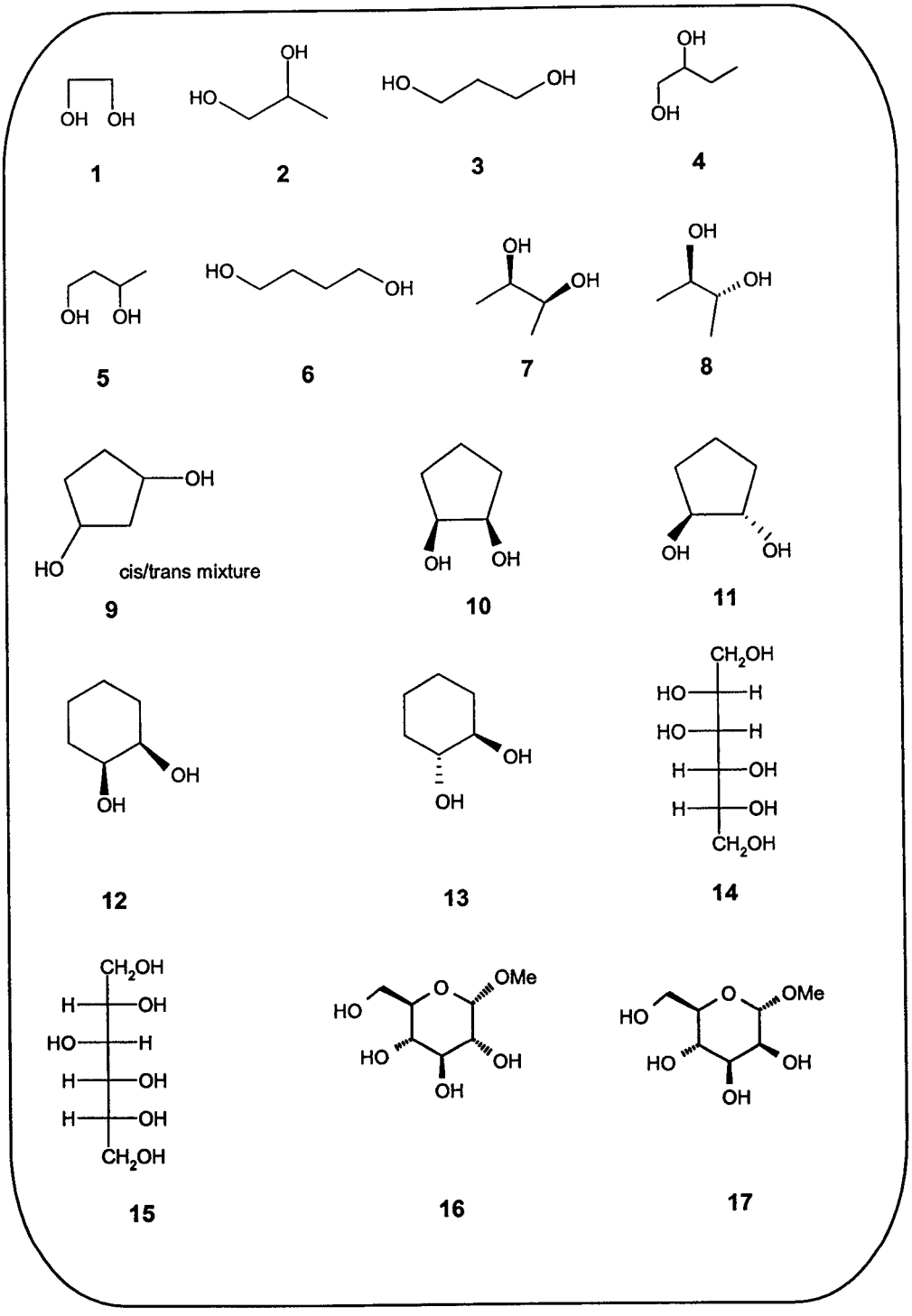
OH OH
1
OH
HO
2
HO OH
3
OH
OH
4
OH OH
5
HO OH
6
OH
OH
7
OH
OH
8
OH
HO
cis/trans mixture
9
OH OH
10
OH OH
11
OH
OH
12
OH
OH
13
CH2OH
HO H
HO H
H OH
H OH
CH2OH
14
CH2OH
H OH
HO H
H OH
H OH
CH2OH
15
HO
O
OMe
HO
OH
OH
16
HO
O
OMe
HO
OH
OH
17

Scheme 1.

Results and Discussion

Preliminary experiments

Preliminary experiments indicated that 1,2-diols such as 1,2-ethanediol (ethylene glycol), 1,2-propanediol and mannitol complexed easily with boric acid. Ethylene glycol is the simplest dihydroxy compound that can form a complex with boric acid and therefore it was chosen as an internal standard in comparative experiments. The idea was that if we mix a particular diol [B] and ethylene glycol [A] in a ratio of 1 : 1 and find a [2M] complex of boric acid and ethylene glycol [AA], a mixed complex of boric acid, the diol and ethylene glycol [AB], and a [2M] complex of boric acid and the diol [BB] in a ratio of 1 : 2 : 1, then complex formation of the diol occurs at the same rate as for ethylene glycol. In addition, MS/MS experiments on the mixed complex [AB] would allow us to obtain information as to the configuration of the hydroxyl groups of the diol [B]. Unfortunately, we found that boric acid tends to remain adsorbed in the analyte delivery system, leading to memory effects and irreproducible results. However, we also found that boric acid memory effects do not occur when the infused samples contain ethylene glycol in a two-fold excess. Therefore, in all experiments we used a molar ratio of the diol to ethylene glycol to boric acid of 1 : 2 : 1. Because borate formation is reversible, a stock solution of boric acid and ethylene glycol may be prepared and used in our comparative experiments. The analyte was prepared as follows. From 1% (w/v) solutions of boric acid or its ^{10}B isotopomer in CH_3OH/H_2O (1:1), stock solutions were prepared containing boric acid and ethylene glycol in a 1 : 2 molar ratio. To an aliquot of this solution the analyte was added such that the molar ratio of the resulting analyte/ethylene

glycol/boric acid mixture was 1 : 2 : 1. In a typical experiment 2-10 μmoles of analyte were infused.

Dissociation of the [2M] complex of boric acid and ethylene glycol, the reference diol

MS/MS experiments on the complex of boric acid and ethylene glycol at m/z 131 show that this [2M] complex dissociates largely by loss of 44 Da to form m/z 87. It will be shown below that the neutral species lost corresponds to C_2H_4O. The simplest way to envisage C_2H_4O loss is multiple simple bond cleavage without rearrangement to generate ion P in Scheme 2, where boron is doubly bonded to oxygen.

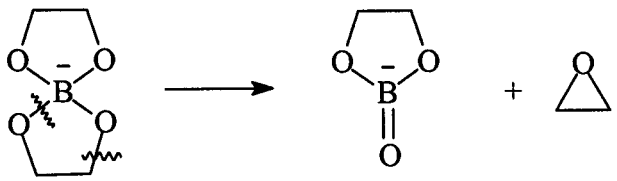

P

Scheme 2.

In this scenario the neutral lost would be ethylene oxide whose ΔH_f is -22.6 kcal/mol [15]. However, we cannot exclude the possibility that a 1,2-H shift takes effect prior to this dissociation to generate the more stable acetaldehyde isomer for which ΔH_f is -39.6 kcal/mol [15]. Such a hydrogen shift does account for the presence of a significant peak at m/z 59 in the MS/MS spectrum which, as confirmed by a ^{10}B labelling experiment, corresponds to $[C_2H_3O_2]^-$.

The vicinal diols studied competed efficiently with ethylene glycol for complex formation with boric acid. In solutions containing a straight chain vicinal

diol as the analyte, the negative ion ESMS showed peaks corresponding to the [2M] complex with ethylene glycol, the mixed complex and the [2M] complex with the analyte, in a 1 : 2 : 1 intensity ratio.

By contrast, ESMS of solutions containing a 1,3-diol as the analyte, showed a base peak corresponding to the [2M] ethylene glycol complex. A similar result was obtained when the 1,3-diol was replaced with a 1,4-diol. Therefore, as the hydroxyl groups move further apart in the diol, complex formation with boric acid and thus competition with ethylene glycol becomes more difficult. In the following, ES MS/MS experiments were performed on the mixed complexes using naturally occurring boric acid and ^{10}B-boric acid.

Propanediol series

A solution containing a 1 : 2 : 1 mole ratio of 1,2-propanediol to ethylene glycol to boric acid showed an intensity ratio of 1 : 2 : 1 for the [2M] complex with ethylene glycol (m/z 131), the mixed complex (m/z 145), and the [2M] complex with the analyte (m/z 159) respectively. However, a 1 : 0.25 : 0.05 intensity ratio was observed for the same ions when 1,2-propanediol was replaced by 1,3-propanediol, showing that complex formation for the 1,3-diol is much less efficient (by a factor of 4.5, compare the relative association constant of 3 derived from NMR experiments [6]). The MS/MS spectra of the mixed complexes of 1,2-propanediol and 1,3-propanediol are shown in Figure 5-1. The intensity differences that are observed are reproducible. It is seen that the mixed complex with 1,2-propanediol (M_1 in Scheme 3) loses C_3H_6O (methyl oxirane) more abundantly than C_2H_4O (oxirane), while the reverse is true for the mixed complex

with 1,3-propanediol (M_2 in Scheme 3). In the absence of thermochemical data it is difficult to rationalize these differences, but a brief discussion in terms of possible product structures is nevertheless useful.

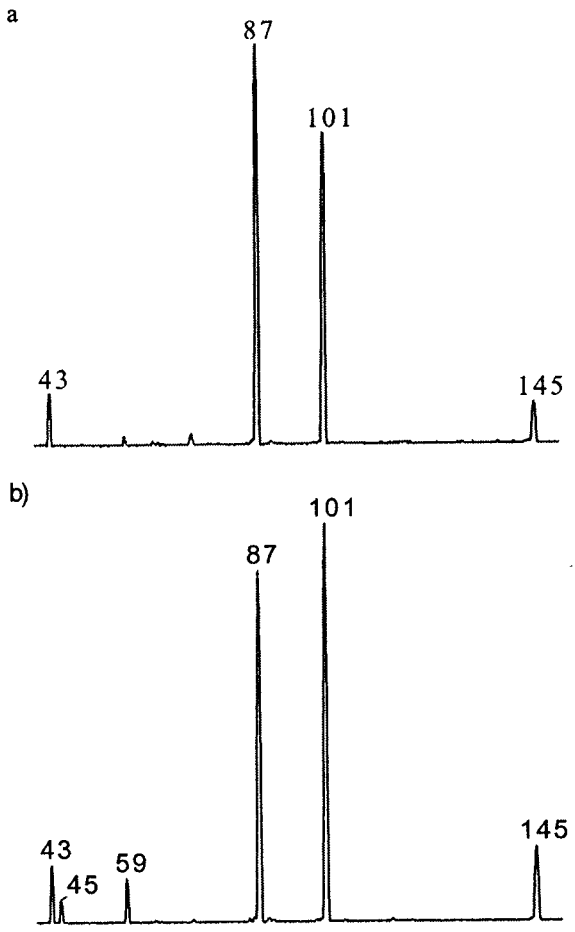

Figure 5-1. Negative ion ES MS/MS spectra of the (m/z 145) mixed complexes of 1,2-propanediol, ethylene glycol and boric acid, item a) and 1,3-propanediol, ethylene glycol and boric acid, item b).

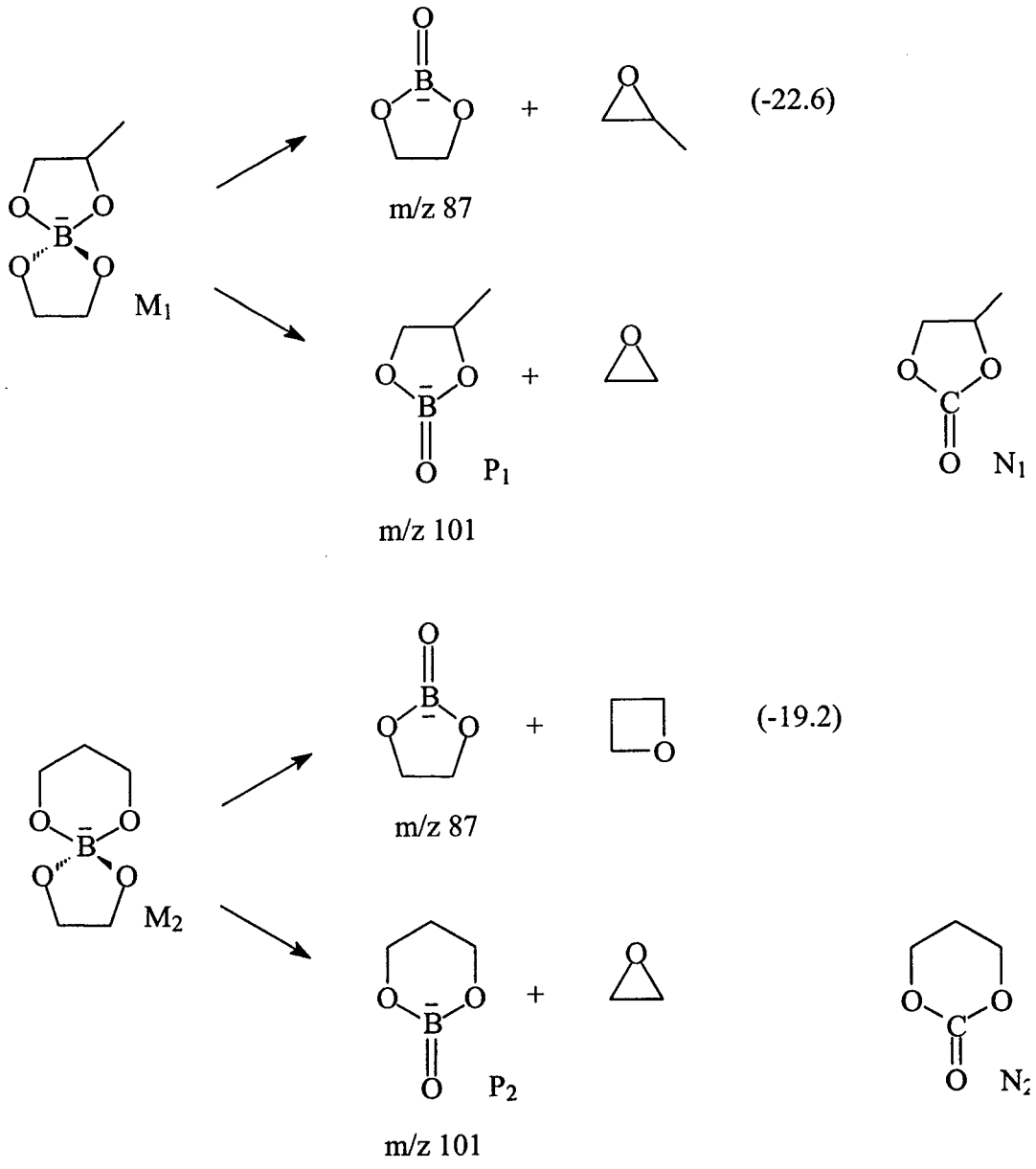

Scheme 3.

In Scheme 3 are given the product structures for the dissociations leading to m/z 87 and m/z 101, assuming that these reactions do not involve

hydrogen shifts. The numbers refer to established heats of formation (kcal/mol) from Ref. 15. There are two ways of looking at these data. The more intense m/z 87 signal in Figure 5-1a could be attributed to the formation of a more stable C_3H_6O neutral for M_1 compared to M_2 ; neutral methyl oxirane has a lower heat of formation than oxetane (note that the ring strain energies of three and four membered rings are similar [16]). Conversely, if the same neutral is formed in both these reactions, then the increased intensity of m/z 101 in Figure 5-1b indicates that the product ion P_2 is more stable than P_1. Localizing the electron on boron, the stability difference between P_1 and P_2 may be approximated by considering the isoelectronic neutrals N_1 and N_2. Although the heat of formation of N_1 has been accurately measured [15], that for N_2 is unknown. However, both heats of formation can be estimated from Benson's additivity scheme [16]. We then find that N_2 is more stable than N_1 , by 2.3 kcal/mol and equate this to the difference in the heat of formation of P_2 and P_1. Thus it is not possible to say whether formation of m/z 87 in Figure 5-1b becomes unfavourable because of a less stable neutral, or that m/z 101 becomes more favourable because of a more stable ion. It is entirely possible that there exists a delicate balance between the two.

We also examined the ESMS and MS/MS mass spectra of solutions containing 1,2-propanediol-2-d_1 and 1,2-propanediol-1,1-d_2 as the analyte. Both isotopomers cleanly generated mixed complex ions at m/z 146 and 147 respectively. Their MS/MS spectra are presented in Figure 5-2. Note that for the m/z 147 species, see Figure 5-2b, the spectrum displays a peak at m/z 103 which is two mass units higher than that observed for the unlabelled counterpart,

see Figure 5-1a, whereas m/z 87 remains unchanged. These observations confirm that the neutrals lost in these dissociations are C_2H_4O and C_3H_6O.

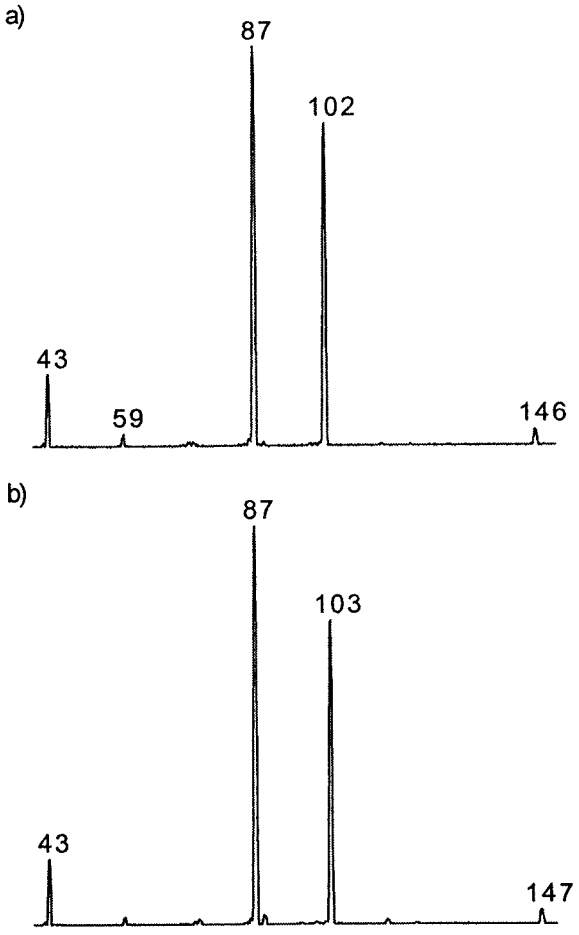

Figure 5-2. Negative ion ES MS/MS spectra of the mixed complexes of 1,2-propanediol-2-d_1, ethylene glycol and boric acid, item a) and 1,2-propanediol-1,1-d_2, ethylene glycol and boric acid, item b).

Butanediol series

A series of butanediols was also investigated by the above method. Here, too, only the vicinal diols showed ions corresponding to the [2M] ethylene glycol complex at m/z 131, [A], the mixed complex at m/z 159, [B], and the [2M] analyte complex at m/z 187, [C], with an intensity ratio of 1 : 2 : 1. For the 1,3- and 1,4-

butanediols, the normal mass spectra showed peaks corresponding to [A], [B] and [C] in an intensity ratio of 1 : 0.5 : 0.25, paralleling observations made for 1,2- and 1,3-propanediol, *vide supra*.

The ES mass spectra of solutions containing the (2*R*,3*R*)-(-)-2,3- and *meso*-2,3-butanediols as analytes are presented in Figure 5-3. These spectra are similar but not identical which becomes even more manifest when the MS/MS spectra of the mixed complexes are considered, see Figure 5-4.

The MS/MS spectra are well reproducible and spectra acquired upon alternately infusing solutions of the (2*R*,3*R*)- and *meso*-2,3- stereoisomers showed no discernable variations in the relative intensity of the MS/MS peaks. Scheme 4 shows the various reaction channels and plausible product structures. Again most heats of formation values are not available. We begin our interpretation by proposing that the stereochemistry is conserved in both the ionic and the neutral products. (This is a valid assumption for the ionic products since the reactive center is in the other ring, but for the neutral expelled stereochemical differentiation may be lost). Now it follows from Scheme 4 that for the *meso* complex both the formation of m/z 87 and m/z 115 may suffer from steric hindrance. For the formation of m/z 87 this hindrance would manifest itself in the neutral but this is not observed, only m/z 115 suffers from steric hindrance, compare Figures 5-4a and 5-4b.

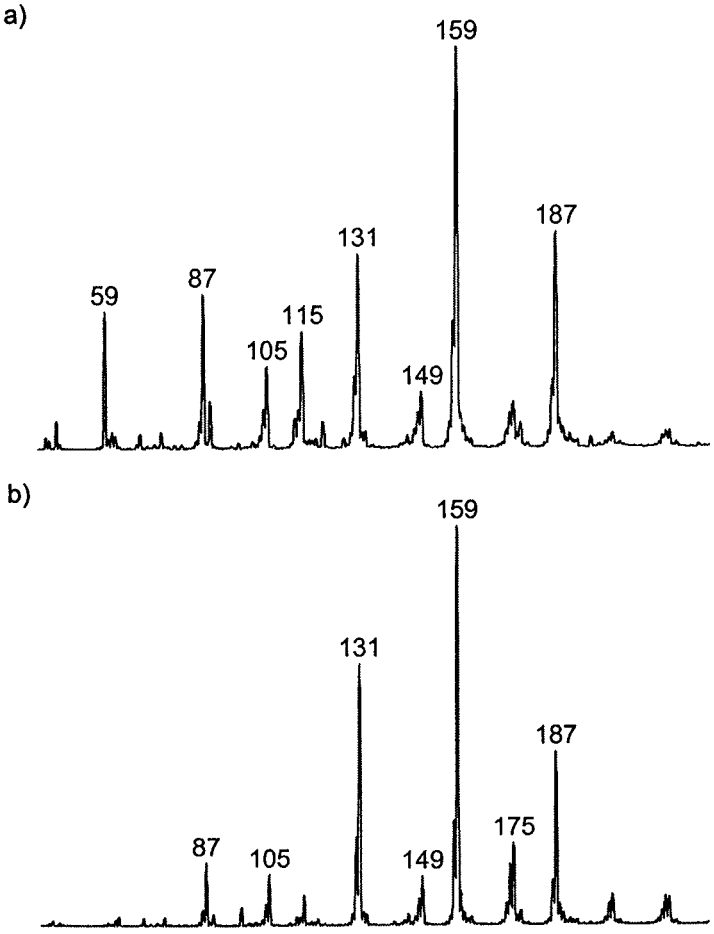

Figure 5-3. Negative ion ES mass spectra of (1 : 2 : 1) solutions of (2*R*,3*R*)-(-)-2,3-butanediol, ethylene glycol and boric acid, item a) and *meso*-2,3-butanediol, ethylene glycol and boric acid, item b).

This is entirely reasonable because, as stated above, even for the *meso* compound the neutral 1,2-dimethyl oxirane may well have the more stable *trans* configuration (and of course, if the neutral is 2-butanone, no stereoisomers exist at all). *Thus, we now have a probe for stereochemical differentiation.*

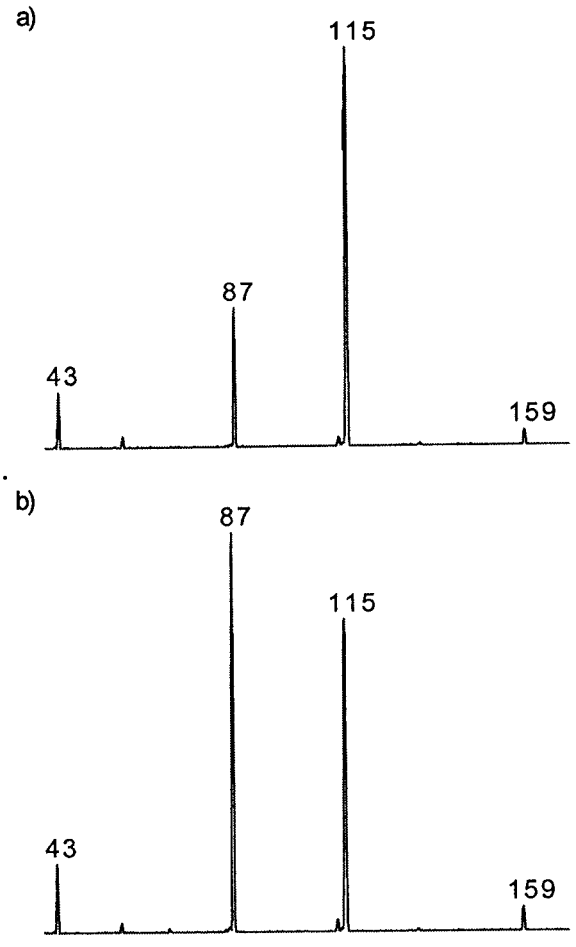

Figure 5-4. Negative ion ES MS/MS of the mixed complex (m/z 159) with (2*R*,3*R*)-(-)-2,3-butanediol, ethylene glycol and boric acid, item a) and *meso*-2,3-butanediol, ethylene glycol and boric acid, item b).

Finally, the most significant difference between the MS/MS spectra of *meso*-2,3- and 1,2-butanediol was that the mixed complex formed with 1,2-butanediol yielded a tell-tale peak at m/z 57 ($C_2HO_2^-$).

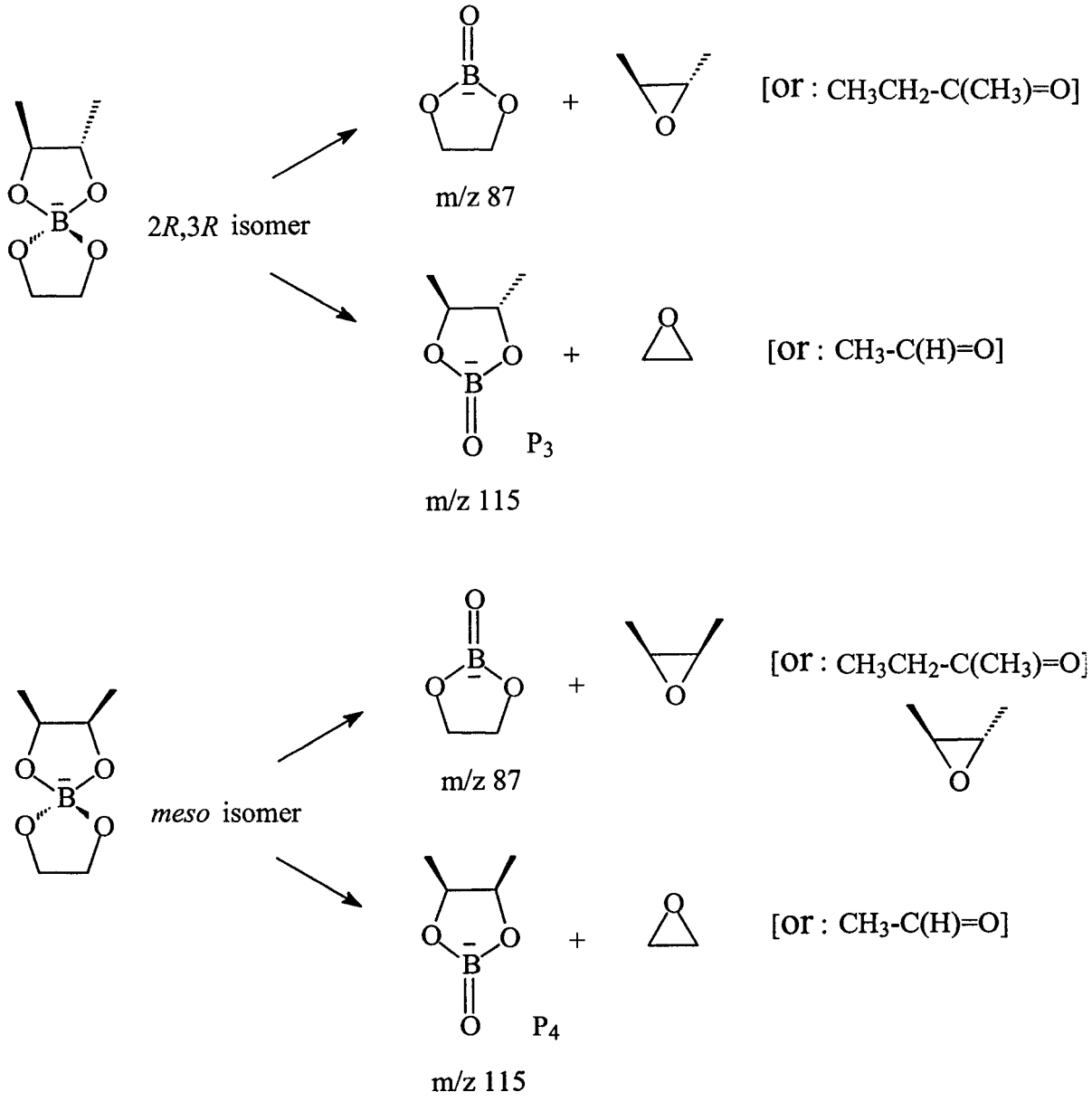
2R,3R isomer
m/z 87
[or : CH3CH2-C(CH3)=O]
P3
m/z 115
[or : CH3-C(H)=O]
meso isomer
m/z 87
[or : CH3CH2-C(CH3)=O]
P4
m/z 115
[or : CH3-C(H)=O]

Scheme 4.

Cyclopentanediols and cyclohexanediols

Next, complex formation with *cis*-1,2-, *trans*-1,2- and 1,3-cyclopentanediol (mixture of *cis* and *trans*) was investigated. Of these analytes, only *cis*-1,2-cyclopentanediol readily formed a [2M] complex with boric acid while the *trans*-1,2-cyclopentanediol and the 1,3-cyclopentanediols formed a [1M] complex.

The MS/MS spectra of the mixed complexes, see Figure 5-5, are characteristically different. Especially interesting is that the spectra of the complexes of the *cis*- and *trans*-1,2-cyclopentanediols, see Figures 5-5b and 5-5c, show an "all-or-nothing" effect in that m/z 87 is absent in the former. Thus, the mixed complex with the *cis* isomer readily loses C_2H_4O (oxirane) whereas the *trans* compound readily loses C_5H_8O. This is the opposite behaviour of that found for the 2,3-butanediols. Interestingly, the complex with 1,3-cyclopentanediol does not show a preference for loss of either oxirane or C_5H_8O. Thus, ES MS/MS allows differentiation between the *cis*- and *trans*- isomers of 1,2-cyclopentanediol and 1,3- cyclopentanediol.

Similar results were obtained for the *cis*- and *trans*- isomers of 1,2-cyclohexanediol. MS/MS experiments on the mixed complexes, see Figure 5-6, showed that the *cis* isomer loses C_2H_4O (oxirane) rather than $C_6H_{10}O_2$ while the converse is true for the *trans* isomer.

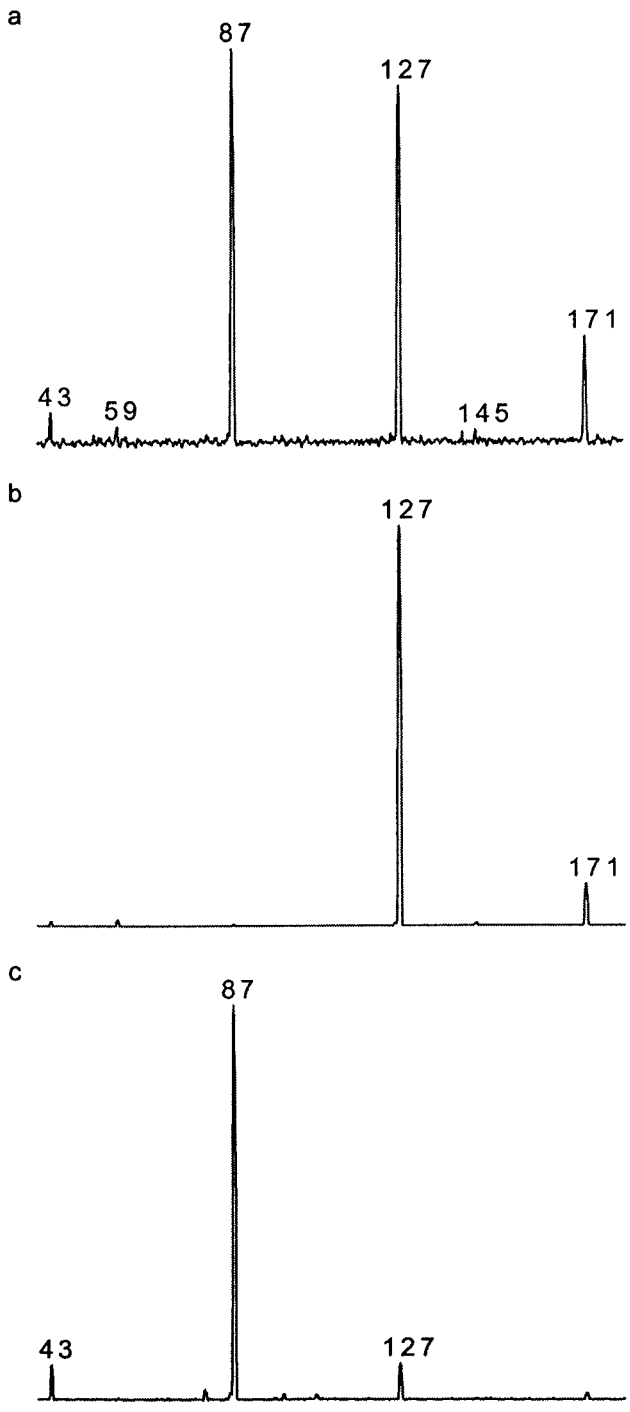

Figure 5-5. Negative ion ES MS/MS spectra of the (m/z 171) mixed complexes of ethylene glycol and boric acid with : a) (*cis*/*trans*) 1,3-cyclopentanediol, b) *cis*-1,2-cyclopentanediol and c) *trans*-1,2-cyclopentanediol.

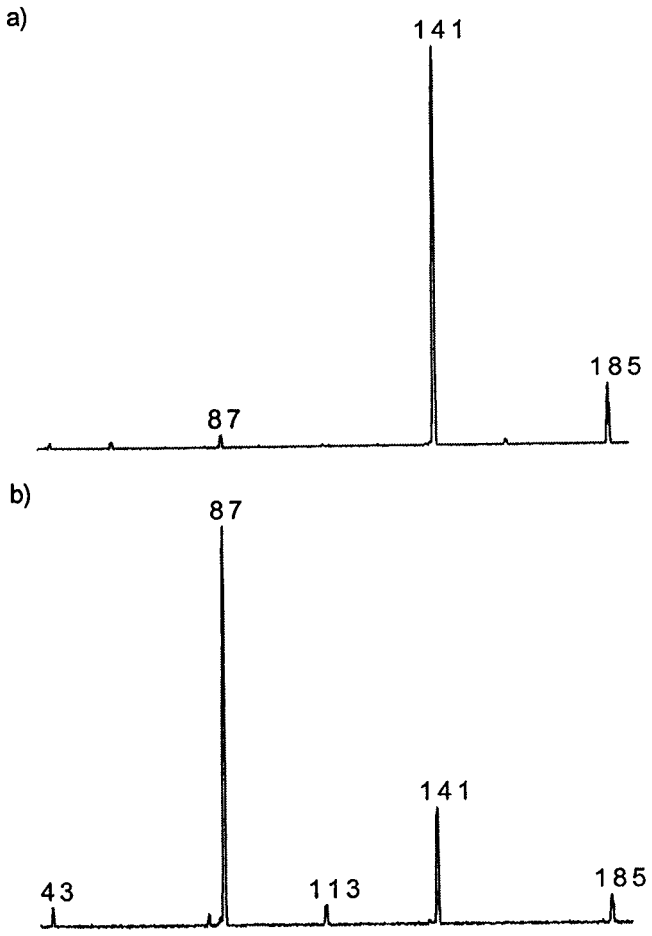

Figure 5-6. Negative ion ES MS/MS spectra of the (m/z 185) mixed complexes with *cis*-1,2-cyclohexane-diol, ethylene glycol and boric acid, item a) and *trans*-1,2-cyclohexanediol, ethylene glycol and boric acid, item b).

Mannitol and sorbitol

Mannitol was one of the first polyhydroxy compounds shown to decrease the pH of a solution of boric acid. When a solution having a 1 : 2 : 1 mole ratio of mannitol to ethylene glycol to boric acid was analyzed by ESMS, the ion corresponding to the [2M] complex between mannitol and boric acid (m/z 371) was the base peak in the spectrum, see Figure 5-7a.

This result is in keeping with the potentiometric observations which showed a substantial increase in conductance of a boric acid solution in the presence of mannitol. The fact that the [2M] complex at m/z 371 dominates the ESMS spectrum shows that mannitol competes very effectively with ethylene glycol for complexation with boric acid. This may be due in part to statistical effects, i.e. the number of vicinal hydroxyl groups available for complexation.

The stereoisomer sorbitol (**15** in Scheme 1) was similarly analyzed and again the base peak in the ESMS spectrum was the [2M] complex with boric acid, see Figure 5-7b. However, there is also a substantial signal at m/z 181 for the $[M-H]^-$ ion showing that complexation is less effective in sorbitol than in mannitol. This is not unexpected considering that mannitol, see Scheme1, has more vicinal *cis* hydroxyl groups available for efficient complexation.

The MS/MS spectra of the [2M] m/z 371 ions in Figures 5-7a and 5-7b were also obtained. The spectra appeared to be closely similar and thus the MS/MS procedure cannot differentiate these stereoisomeric sugar alcohols. This is perhaps not too surprising considering that the hydroxyl groups of these acyclic polyhydroxy compounds may freely rotate in solution allowing the vicinal hydroxyl groups of the two sugar alcohols to adopt closely similar configurations for efficient complex formation.

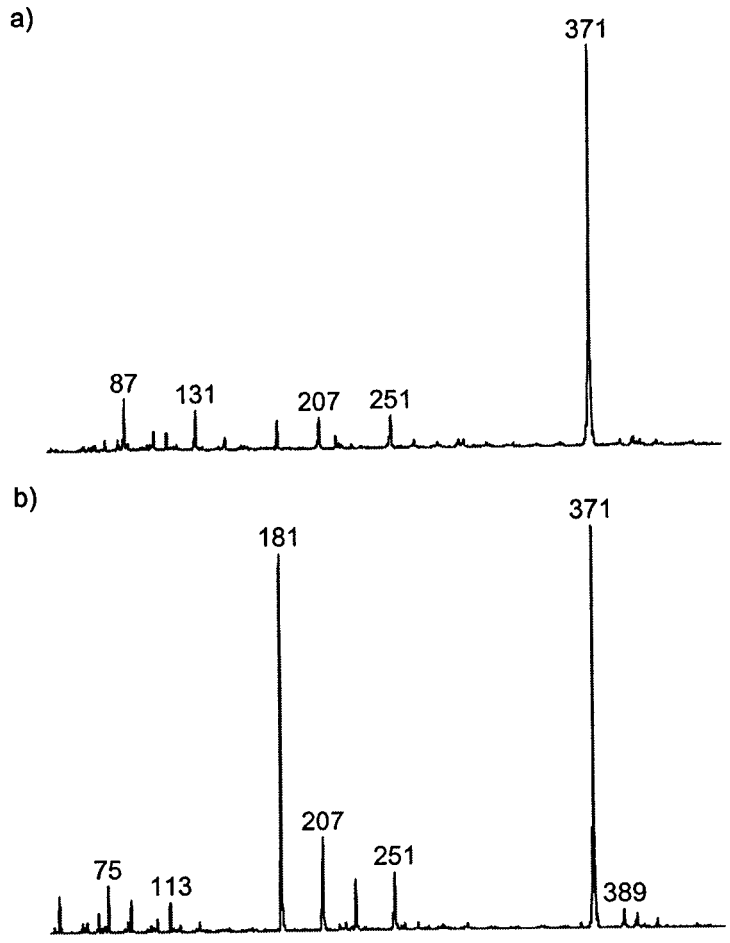

Figure 5-7. Negative ion ES mass spectrum of a (1 : 2 : 1) solution of mannitol, ethylene glycol and boric acid, item a) and sorbitol, ethylene glycol and boric acid, item b).

Methyl glycosides

Sugars in the hemiacetal/hemiketal form undergo mutarotation. This implies that they interconvert between their α/β-furanose and α/β-pyranose forms. Methylating the anomeric hydroxyl prevents mutarotation and ensures that the anomeric hydroxyl group cannot participate in complex formation. A better assessment of the use of the boric acid/ethylene glycol procedure for probing the stereochemistry of sugars is then obtained.

The normal mass spectra showed that α-methyl-mannopyranoside (**17** in Scheme 1) forms the mixed complex more readily than α-methyl-glucopyranoside (**16** in Scheme 1). The MS/MS spectrum of the ion representing the mixed complex with the α-methyl-mannopyranoside is characteristically different from that of the α-methyl-glucopyranoside, compare Figures 5-8a and 5-8b. Loss of a mass 32 neutral (CH_3OH) uniquely characterizes the mixed complex with α-methyl-mannopyranoside by the peak at m/z 231, see Figure 5-8a.

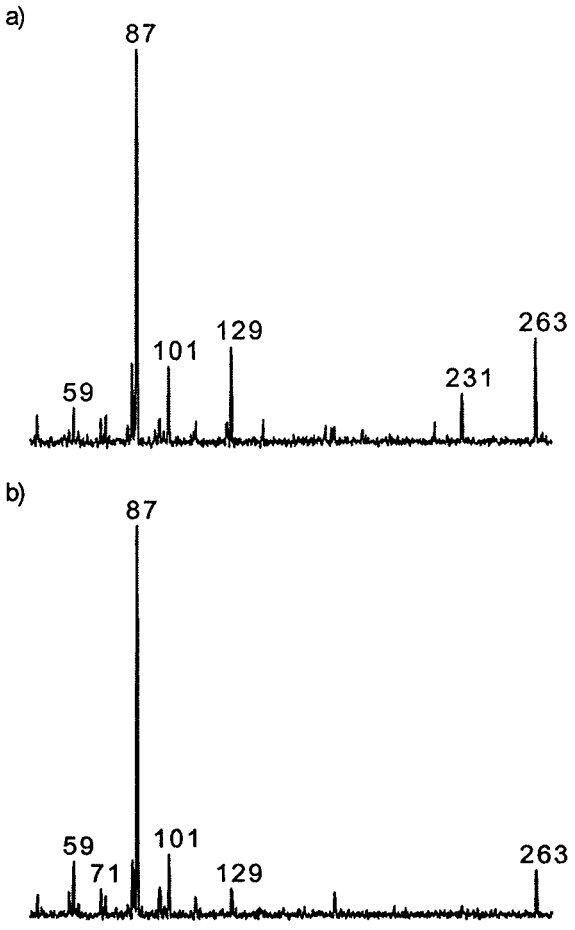

Figure 5-8. Negative ion ES MS/MS spectra of the (m/z 263) mixed complexes with α-methyl-D-mannopyranoside, ethylene glycol and boric acid, item a) and α-methyl-D-glucopyranoside, ethylene glycol and boric acid, item b).

If the complex formation involves the hydroxyl groups on C3 and C6 in the glucopyranoside and those on C2 and C3 in the mannopyranoside, the MS/MS results can be rationalized by proposing that CH_3OH represents the mass 32 neutral lost from C6 in the mixed complex with the mannopyranoside. This hydroxyl group is bonded to B in the mixed complex with a-methyl-glucopyranoside, preventing the loss of CH_3OH.

Conclusions

By adding a measured quantity of a diol of unknown composition to a methanol/water solution containing a preformed ethylene glycol/boric acid [2M] complex, the extent of complex formation between boric acid and the analyte can be assessed. The relative ease of complex-formation is derived from the relative intensity of the [2M] complex between ethylene glycol and boric acid and the [2M] complex between the analyte and boric acid.

For vicinal *cis*- and *trans*-cyclic diols it is shown that a simple ESMS experiment is sufficient to differentiate between the two isomers. MS/MS experiments show that the *cis* isomer readily loses C_2H_4O (oxirane) whereas the *trans* isomer characteristically loses the cyclic diol epoxide.

Stereoisomer differentiation between the *meso*-2,3- and (2*R*,3*R*)-(-)-2,3-butanediols is also possible but only using MS/MS experiments. Steric interactions between the two methyl groups in the mixed complex with *meso*-2,3-butanediol promote a facile loss of the butanediol portion of the mixed complex. In contrast, with (2*R*,3*R*)-(-)-2,3-butanediol, the ethanediol portion of the complex is more readily lost.

The above procedure does not permit an unambiguous differentiation of acyclic polyhydroxy compounds like the sugar alcohols mannitol and sorbitol. This is likely because these stereoisomers form structurally closely similar complexes with the boric acid/ethylene glycol mixture as witnessed by their virtually identical MS/MS spectra. However, when the structurally related sugars have been methylated on the anomeric hydroxyl group, characteristic MS/MS spectra are readily obtained.

The results obtained so far warrant a more extensive and detailed study of the use of borate complexes for the analysis of polyols in aqueous solutions.

References

[1] R. J. Ferrier, *Adv. Carbohydr. Chem. Biochem.*, **1978**, *35*, 31.

[2] M. van Duin, J.A. Peters, A.P.G. Kieboom and H. van Bekkum, *Tetrahedron,* **1984,** *40*, 2901.

[3] T. Oi, T. Takeda, and H. Kakihana, *Bull. Chem. Soc. Jpn.*, **1992**, *65*, 1903.

[4] J. B. Biot, *Compt. Rend.,* **1842**, *14*, 49.

[5] A. Deutsch and S. Osoling, *J. Am. Chem. Soc.*, **1949**, *71*, 1637.

[6] M. van Duin, J.A. Peters, A.P.G. Kieboom and H. van Bekkum, *Tetrahedron,* **1985,** *41*, 3411.

[7] Y. Shiomi, K. Kondo, M. Saisho, T. Harada, K. Tsukagoshi and S. Shinkai, *Supramol. Chem.* **2**, **1993**, 11.

[8] S. Chapelle and J. Verchere, *Carbohydr. Res.*, **1989**, *191*, 63.

[9] C.J.W. Brooks and W.J. Cole, *J. of Chromatogr.*, **1987**, *399*, 207.

[10] A. Bergold and W.H. Scouten, *Chem. Anal. (N.Y.),* **1983**, *66*, 149.

[11] M.E. Rose, D. Wycherley, S.W. Preece, *Org. Mass Spectrom.*, **1992**, *27*, 876.

[12] M. Liptak, Z. Dinya, P. Herczegh, *Org. Mass Spectrom.*, **1993**, *28*, 780.

[13] S.G. Penn, H. Hu, P.H. Brown, C.B. Lebrilla, *Anal. Chem.*, **1997**, *69*, 2471.

[14] E. Bayer, P. Gfrorer, C. Rentel, *Angew. Chem. Int. Ed.*, **1999**, *38*, 992.

[15] S. Lias, J.E. Bartmess, J.F. Liebman, J.L. Holmes, R.D. Levin, W.G. Mallard, *J. Phys. Chem. Ref. Data 17* Suppl. 1, **1988**.

[16] N. Cohen and S.W. Benson, *Chem. Rev.*, **1993**, *93*, 2419.

Chapter 6

Structure Analysis of Diols and Sugars by their Oxovanadium (VO^{++}) Complexes using Electrospray Mass Spectrometry

A method is presented to characterize diols and polyols (sugars) as oxovanadium (VO^{++}) complexes using positive ion electrospray mass spectrometry (ESMS) in combination with tandem mass spectrometry (MS/MS). The analyte is added to a solution containing a [2:1] ethylene glycol/vanadyl ion (VO^{++}) complex and then subjected to infusion ESMS analysis. The following VO^{++} complexes are formed: (i) a complex with two ethylene glycol molecules, (ii) a mixed ethylene glycol/analyte complex, and (iii) a complex with two analyte molecules. The first complex serves as a reference (or internal standard) for the assessment of the ease of complex formation with the analyte.

The ES mass spectra of acyclic vicinal diols all feature intense mixed complex signals, indicative of efficient complex formation. Structural information is obtained from MS/MS experiments. Thus, although the stereoisomers (2*R*,3*R*)-(-)-2,3-butanediol and *meso*-2,3-butanediol show a similar complexation efficiency, MS/MS experiments reveal structural differences. Isomeric cyclic vicinal diols afford intense mixed complexes, but here too the MS/MS spectra are characteristically different.

Some isomeric methyl glycosides were also examined. It was found that α-methyl-D-ribopyranoside competes more effectively with ethylene glycol than the *xylo* isomer. Similarly, α-methyl-D-mannopyranoside competes more effectively with ethylene glycol for complexation with VO^{++} than its *gluco* isomer. The MS/MS spectra of these pairs of isomers are again characteristically different. This is also true for the three isomeric disaccharides studied.

Our findings indicate that this simple complexation reaction may be useful to probe the presence and structure of diols and other polyhydroxy compounds in aqueous solutions.

Introduction

In Chapter 5 of the thesis, experiments are described on the use of boric acid complexes to aid in the structure analysis of polyhydroxy compounds, including sugars. This Chapter describes preliminary experiments aimed to explore whether complexation with VO^{++} may be an even better approach to the structure analysis of polyols.

Vanadium (V), a $3d^3 4s^2$ metal, displays a rich and varied (bio)chemistry [1,2] which includes compounds in oxidation states from + 5 to - 1. The chemistry of vanadium(IV), V^{IV}, is dominated by the formation of oxo species, and a wide range of compounds with VO^{++} is known [3].

Readily available sources of VO^{++} are the oxovanadium salts $VOSO_4$ and $VOCl_2$. The VO^{++} ion is blue and stable in air in acid solution. $VO(OH)_2$ is greyish brown and precipitates at pH 4.1 (0.01 M). It develops rapidly and redissolves in alkaline solution giving $HV_2O_5^-$ or $V_4O_9^{2-}$, reddish brown, then red. The system V^{IV} / V^V, described by the half-reaction $VO_2^+ + 2H^+ + e \leftrightharpoons VO^{++} + H_2O$ ($E^o = 1.01$ V), has redox properties similar to those of Cr^{III} / Cr^{VI}. The oxidation of vanadyl salts, slow in very acid solution, is still fairly slow at pH 1.5. It is speeded up by heating. In neutral or alkaline solution the system becomes more reducing and the oxidation is very rapid, even in the air. Chelation increases the stability of the V^{IV} oxidation state, thus slowing the oxidation process [4].

Oxovanadium complexes may, depending on the nature of the ligands, be cationic, neutral or anionic and be either 5-coordinate, where the stereochemistry is that of the square pyramid, or 6-coordinate, containing a distorted octahedron [3]. In coordinating solvents such as water, the axial and equatorial ligands rapidly exchange with a solvent molecule, at rates of $> 10^8$ sec^{-1} [5a-d] and $\sim 10^3$ sec^{-1} [5e]. In contrast, exchange of the vanadyl *O*-atom with a water molecule occurs extremely slowly, at a rate of 3×10^{-5} sec^{-1} [5f]. Thus, ligand exchange of VO^{++} complexes in aqueous solutions may be expected to occur readily and this is an important criterion in the design of our analytical procedure.

Oxovanadium(IV), VO^{++}, forms many stable complexes. One example of a neutral complex is that which is formed with two molecules of the enol form of β-diketones like the acetylacetonate shown below [2,3a].

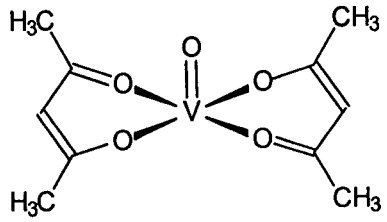

This compound has the square pyramidal structure.

The bond lengths at the equatorial position of VO^{++} complexes range from 1.90 to 2.1 Å, with *N*-atom donors showing longer bonds than the *O*-atom counterparts. The reason for this is that VO^{++} binds more strongly to *O*-donors. Amino groups do not form strong complexes with VO^{++} because they form cationic complexes that lack orbitals which can form π bonds to the "empty" d_{xz} and d_{yz} orbitals on vanadium. Thus, VO^{++} is more selective for complexation to *O*-containing than *N*-containing ligands.

The complexation of VO^{++} in aqueous solutions of tartaric acid HOOCC(H)OHC(H)OHCOOH, H_2TA, has been studied in considerable detail [3b,6-8]. The VO^{++} ion coordinates with anionic forms of the acid to give a variety of complexes whose distribution depends upon the pH of the solution and the relative amounts of VO^{++} and tartrate present [6a]. In these complexes, the tartrate anions behave as a bridging ligand, linking together monomeric units via the deprotonated carboxylic acid moiety and hydroxyl functional groups [8]. Deprotonation of the weakly acidic alcoholic hydroxyl groups of the acid can be induced by complexation to 'hard' metal ions like Na^+ and K^+, and occurs

between pH 3-5 [9]. Oxovanadium(IV), another 'hard' metal ion, may behave in the same way [10].

Of particular interest to our study is the finding that VO^{++} exhibits *selective* complexation with the *enantiomeric* forms of tartaric acid [6-8]. The crystal structures of ammonium oxovanadium(IV) complexes with D-tartrate [7a] and D,L-tartrate [7b] have also been determined. Both crystal structures illustrate that dinuclear complexes are formed. The optically active acid generates the dinuclear complex $[(VO)_2(D\text{-}TA)_2]^{4-}$ with the ligands in the *trans* orientation [7a]. On the other hand, a racemic mixture of tartaric acid formed the complex $[(VO)_2(D\text{-}TA)(L\text{-}TA)]^{4-}$, with the ligands in a *cis* geometry [7b]. Petit and Swash [6b] have used potentiometry to study the complexation between VO^{++} and the enantiomeric forms of tartaric acid. They concluded that tartaric acid in its D-, L-, and *meso*- forms, yields different complexes with VO^{++} in aqueous solutions. When *meso*-tartaric acid is the ligand, the dinuclear complex is formed to only a minor extent and this has been attributed to steric hindrance.

Recently, this system has been further studied by Kiss et al. [8] who used potentiometry, electron spin resonance (ESR) spectroscopy, and electronic absorption spectroscopy as structure probes. Their studies confirm that VO^{++} complexes selectively with the various forms of tartaric acid. These researchers also provided evidence that a trinuclear complex, $[(VO)_3(meso\text{-}TA)_3]^{4-}$, is formed with the *meso* isomer.

Among the polyols, carbohydrates are an important class of compounds, and these too form structure characteristic complexes with VO^{++}. Micera et al. [11] have employed potentiometry and spectroscopy (ESR, ^1H electron nuclear

double resonance, and electronic absorption) to study the formation of VO^{++} complexes of sugar uronic acids (containing a carboxylic acid group) as well as simple sugars. These researchers have reported [11a-c] that D-galacturonic and D-glucuronic acid complex with VO^{++} in solution. It was also reported [11c], that VO^{++} initially binds to the uronic acids via the carboxylic acid group at pH ~ 4. Once bound to the sugar molecule, VO^{++} can easily deprotonate hydroxyl groups and coordinate up to four of these. These observations suggest that simple sugars, i.e., those without a carboxylic acid group, may be able to bind VO^{++} without extra donor groups. In support of this, Micera et al. [12d] reported that VO^{++} forms complexes with simple sugars, L, to yield the structure $[VOLH]^+$ when the molar ratio of the sugar to VO^{++} is 1:1. When the molar ratio is 2:1, the complex $[VOL_2H]^+$ is formed.

Among the various analytical techniques that have been used to study vanadyl complexes, the reported mass spectrometric studies [12] largely deal with neutral complexes of β-diketones and porphyrins as well as a few structurally related compounds. In two of these studies, the ions were generated by techniques based on atmospheric pressure ionization : electrospray (ES) has been used to study complexes with Schiff bases [12a] while atmospheric pressure chemical ionization (APCI) has been used to study complexation with porphyrins [12b]. Of immediate relevance to this study, is the observation that the neutral complexes [M] are readily protonated in these ionization methods, yielding abundant $[M+H]^+$ ions.

These encouraging observations prompted us to explore the selectivity of the complexation of VO^{++} with polyhydroxy compounds and sugars, using the

strategy of Chapter 5 for the analysis of their boric acid complexes. Vanadium(IV) sulfate was used as the reagent. Two complexes are expected [12c] to be formed between VO^{++} and a polyhydroxy compound, L : (i) a 1 : 1 complex $[VOLH]^+$ and (ii) a 2 : 1 complex $[VOL_2H]^+$. Using the terminology of Deutsch and Osoling for boric acid complexes [13], these complexes are referred to as the [1M] and the [2M] complexes, respectively.

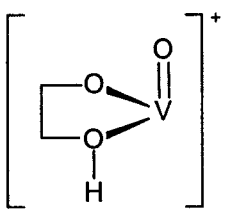

$[VOLH]^+$ or [1M]

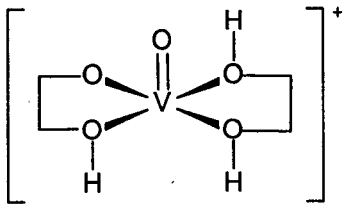

$[VOL_2H]^+$ or [2M]

The selected group of (stereo) isomeric polyhydroxy compounds is listed in Scheme 1 (in the next section).

Experimental

Vanadium (IV) sulfate was purchased from Sigma-Aldrich. For all experiments HPLC-grade methanol and distilled de-ionised water was used. The compounds listed in Scheme 1 were purchased from Sigma-Aldrich and used without further purification. They include : 1,2-ethanediol (ethylene glycol) (**1**), 1,2-propanediol (**2**), *meso*-2,3-butanediol (**3**), (2*R*,3*R*)-(-)-2,3-butanediol (**4**), *cis*-1,2-cyclopentanediol (**5**), *trans*-1,2-cyclopentanediol (**6**), *cis*-1,2-cyclohexane -diol (**7**), *trans*-1,2-cyclohexanediol (**8**), α-methyl-D-xylopyranoside (**9**), α-methyl-D-ribopyranoside (**10**), α-methyl-D-glucopyranoside (**11**), α-methyl-D-manno-pyranoside (**12**), melibiose (**13**), gentiobiose (**14**), and trehalose (**15**). The

deuterium labelled 1,2-propanediol isotopologue, 1,2-propanediol-1,1-d_2, was a gift from Dr A. Milliet (École Polytechnique, Palaiseau, France).

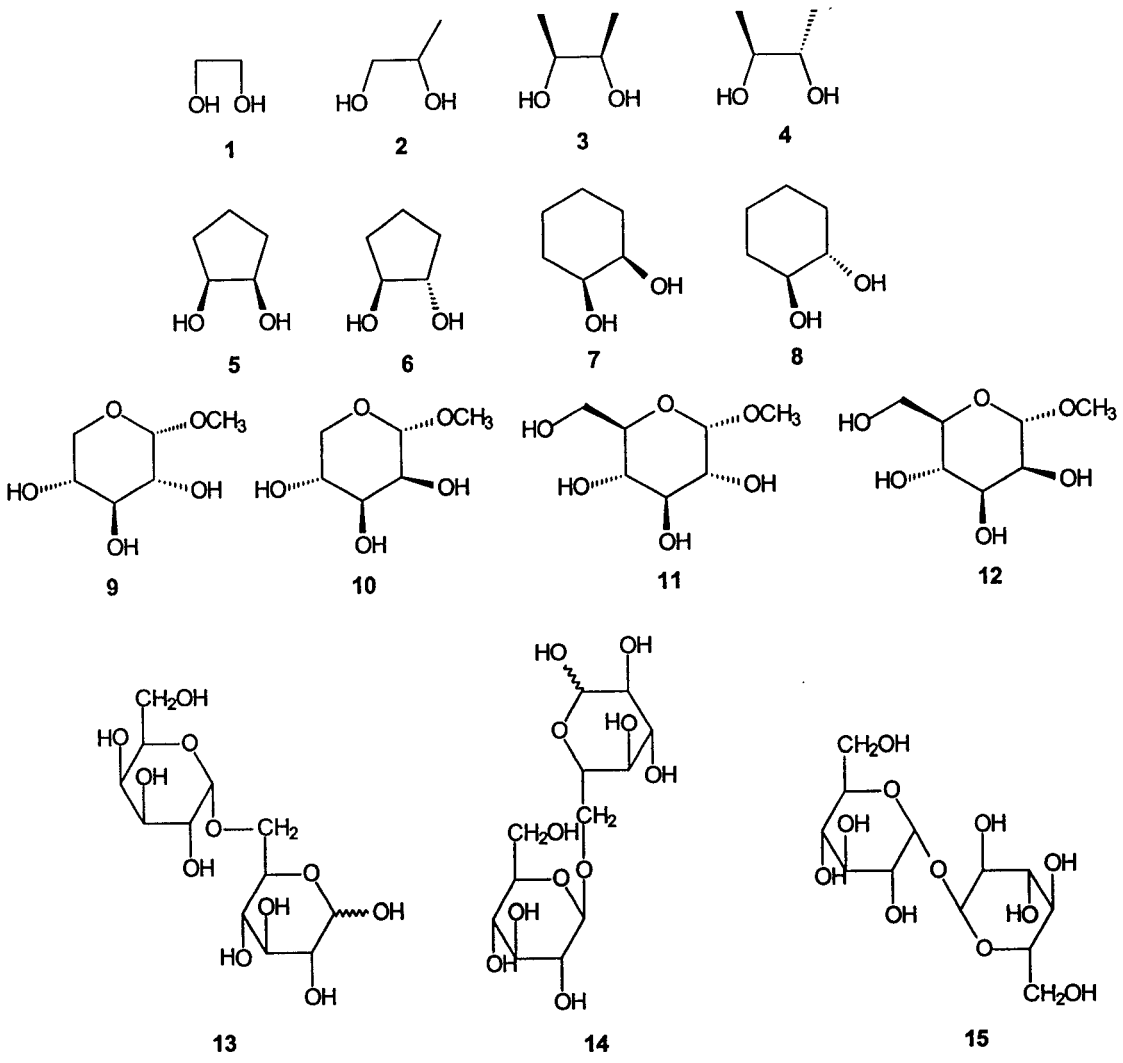

Scheme 1.

Positive ion ESMS and MS/MS experiments were performed on the McMaster Quattro LC (Micromass, England) triple quadrupole instrument. Normal mass spectra were acquired with the cone set at 15 V, the capillary at

3.2 kV, the high voltage lens at 0.2 kV, and the multiplier at 650 V. Product ion spectra were obtained using Argon as the collision gas. Typically, a collision energy of 10 eV was used with a gas cell pressure of 2.5×10^{-3} mBar and the multiplier at 650 V. The analyte was infused via a pneumatically assisted Rheodyne 7010 injector equipped with a 20 μL injection loop. In all experiments a CH_3OH/H_2O (1:1) mobile phase was delivered at a flow rate of 10 μL/min via a Brownlee pump (Advanced Biosystems, Canada). All spectra were acquired for 2 minutes.

Results and Discussion

Preliminary experiments

Preliminary experiments indicated that the 1,2-diols ethylene glycol and 1,2-propanediol complexed easily with VO^{++}. Ethylene glycol (EG) is the simplest polyhydroxy compound that can form a complex with VO^{++} and therefore it was chosen as an internal standard in comparative experiments.

Thus, if the ES spectrum of an aqueous solution containing VO^{++} and an equimolar mixture of EG and a given polyol, L, shows signals for the [2M] complexes $[VO(EG)_2H]^+$, $[VO(EG)LH]^+$ and $[VOL_2H]^+$ in a 1:2:1 ratio, the two ligands form complexes of comparable stability.

In the experimental results reported below, a molar ratio of the polyol to EG to VO^{++} of 1:2:1 was used. Such a ratio was also used in the boric acid work of Chapter 5, and it has the advantage that any residual VO^{++} that is adsorbed in the analyte delivery system will be removed. The analyte was prepared as follows. A 2.5×10^{-3} M solution of VO^{++} (pH ~ 3.2) and EG in a 1:2 molar ratio

was prepared. To an aliquot of this solution, the analyte was added such that the molar ratio of the resulting analyte/EG/VO^{++} mixture was 1:2:1. In a typical experiment 0.1 to 1 μmole of analyte was infused.

It was noted that the sensitivity of this complexation procedure was considerably higher, by a factor of ten, than that of the boric acid procedure described in the previous Chapter. This may be largely due to the fact that the oxovanadium(IV) complexes are positively charged whereas the boric acid complexes are negative : the sensitivity of the instrument is generally higher in the positive ion mode than in the negative ion mode.

Dissociation of the [2M] complex between VO^{++} and EG, the reference diol

The MS/MS spectrum of the [2M] complex of VO^{++} and EG at m/z 190 is shown in Figure 6-1. The base peak at m/z 172 in this spectrum corresponds to the loss of water. The complex also dissociates by loss of 62 Da (EG) and 44 Da (C_2H_4O), to form ions at m/z 128 and m/z 146, respectively. Note that the m/z 128 ion could also originate from the consecutive losses of H_2O and C_2H_4O. In a complementary experiment with ethylene glycol-$(OD)_2$ in D_2O, the [2M] complex cleanly shifts to m/z 193 and its MS/MS spectrum (not shown) reveals that water is specifically lost as D_2O.

Information from additional labelling experiments and computations on the product ion structures is needed to derive sound mechanistic proposals for the CID dissociations of the [2M] complexes of this study. Nevertheless, in Scheme 2 a tentative proposal is presented for the formation of the principal product ions in the spectrum of Figure 1. In this Scheme, the precursor ion at

m/z 190 is represented by a structure, A, in which the proton forms a bridge between the *O*-atoms of the ligands, but this too remains a speculative proposal.

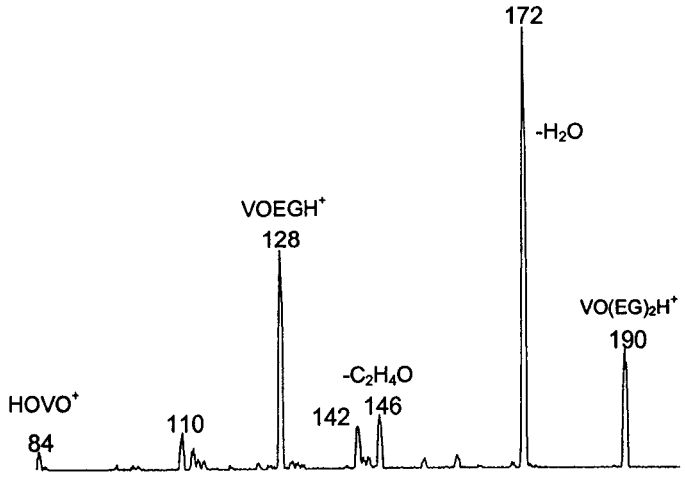

Figure 6-1. MS/MS spectrum (Ar, collision energy 10 eV) of the [2M] complex $VO(EG_2)H^+$ (EG = ethylene glycol).

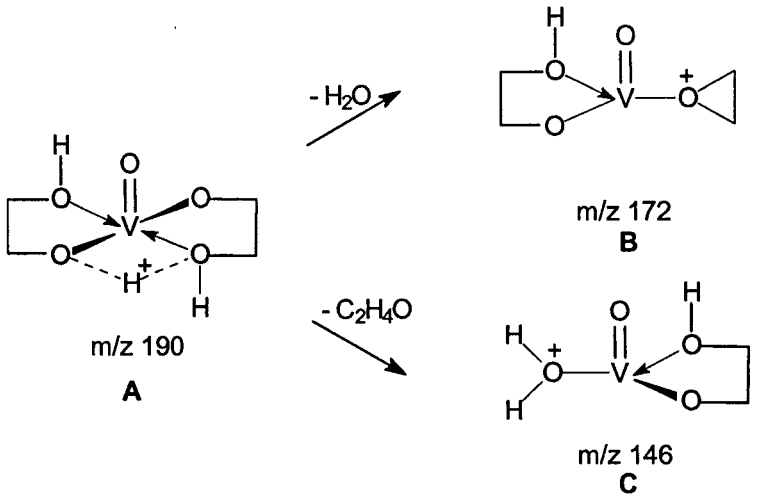

Scheme 2.

The m/z 172 ion resulting from the loss of water is represented by structure B. Its C_2H_4O moiety is proposed to have the cyclic ethylene oxide connectivity, but linear connectivities derived from acetaldehyde or vinyl alcohol

cannot be ruled out. In the same vein, the C_2H_4O molecule lost from the [2M] complex in the formation of the m/z 146 ion C is proposed to be ethylene oxide, but a viable alternative is either acetaldehyde or vinyl alcohol. These C_2H_4O isomers both have a much lower heat of formation than ethylene oxide.

Considering the heat of formation, ΔH_f, of the neutral species lost in the dissociations, it is clear that loss of H_2O is less favoured than that of EG, by 36 kcal/mol [14]. It seems reasonable to propose that loss of EG (or the consecutive loss of water and C_2H_4O) generates a complex ion that lies higher in energy than that generated by loss of H_2O. In the m/z 128 $VOEGH^+$ ion, VO^{++} has electron density donation from only two *O*-atoms, whereas H_2O loss generates a complex where VO^{++} is coordinated to three *O*-atoms.

Dissociation of the mixed complex between VO^{++} and 1,2-propanediol and 1,2-propanediol-1,1-d_2

ESMS analysis of a solution containing a 1:2:1 mole ratio of 1,2-propanediol : EG : VO^{++} yielded an intensity ratio of 0.2 : 0.6 : 1.0 for the [2M] complex with EG (m/z 190), the mixed complex (m/z 204), and the [2M] complex with 1,2-propanediol (m/z 218) respectively. Thus, 1,2-propanediol effectively competes with EG in its complexation with VO^{++}.

The structure of the mixed complex, m/z 204, was probed by a CID experiment. The CID spectrum of Figure 6-2a shows peaks of comparable intensity at m/z 142 and m/z 128, corresponding to loss of EG and 1,2-propanediol, respectively. The mixed complex also loses 58 Da to yield m/z 146,

more readily than 44 Da to give m/z 160. The mass 58 neutral is proposed to be 1,2-propylene oxide and the mass 44 neutral, ethylene oxide.

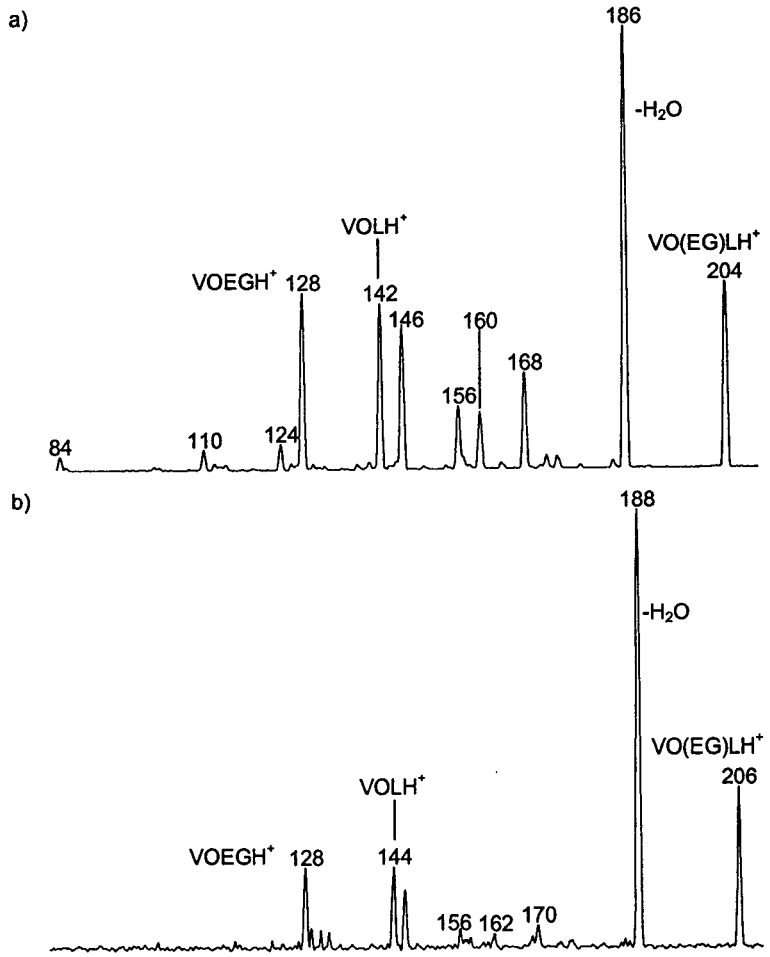

Figure 6-2. MS/MS spectra (Ar, collision energy 10 eV) of the mixed complexes $VO(EG)LH^+$ with L = 1,2-propanediol, item a) ; and 1,2-propanediol-1,1-d_2, item b).

We next examined complexation of VO^{++} to 1,2-propanediol-1,1-d_2. The full scan ES spectrum of the solution containing a 1:2:1 molar ratio of VO^{++} : EG : 1,2-propanediol-1,1-d_2 contains a peak at m/z 222. This nominally corresponds with the expected [2M] complex with 1,2-propanediol-1,1-d_2. The MS/MS spectrum of the m/z 206 mixed complex ion is given in Figure 6-2b. The

spectrum shows that the peak at m/z 186 (loss of H_2O), m/z 168 (loss of H_2O from m/z 186?), m/z 160 (loss of C_2H_4O) and m/z 142 (loss EG) of Figure 6-2a are all shifted to a higher mass by 2 Da. Therefore, these ions contain the deuterium label. If water loss involved the methylene hydrogens, then the spectrum of Figure 6-2b would have showed peaks corresponding to loss of HDO, since it is equally likely that water loss occurs from the ethylene glycol portion as well as the 1,2-propanediol portion of the complex. However, this is not observed.

Scheme 3 gives a tentative proposal for the product ion structures for the dissociations leading to m/z 162 and m/z 146 in the spectrum of Figure 6-2b.

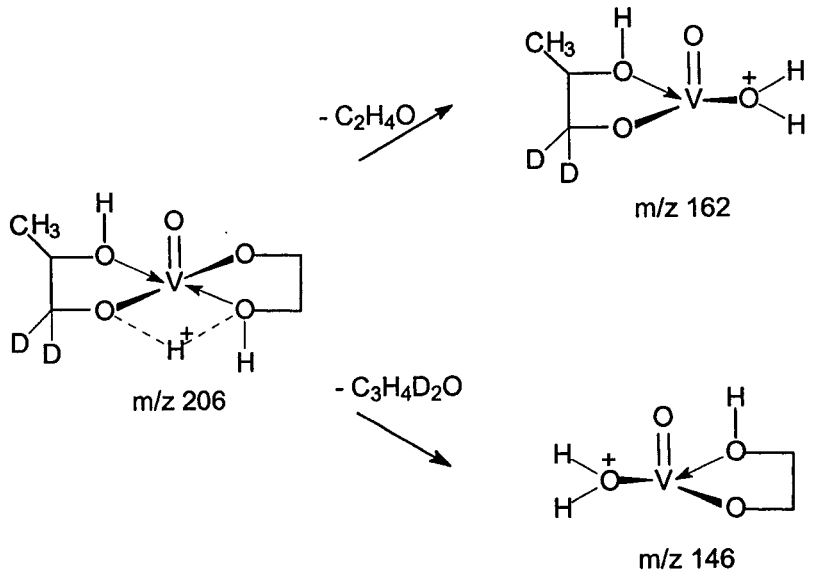

Scheme 3.

Stereoisomeric butanediols

The ES mass spectra of solutions containing the (2*R*,3*R*)-(-)-2,3- and *meso*-2,3-butanediols as analytes are presented in Figure 6-3. These spectra

are similar but not identical. The full scan mass spectra show that the ratio of the intensity of the peaks corresponding to the 2M complex with (2*R*,3*R*)-(-)-2,3-butanediol, m/z 246, and the 2M complex with EG, m/z 190, is about 3.5 times larger than that observed for the *meso* isomer. This observation provides evidence that *meso*-2,3-butanediol competes less effectively with EG for complexation to VO^{++} than (2*R*,3*R*)-(-)-2,3-butanediol and also indicates that the MS/MS spectra of the two mixed complexes will be different.

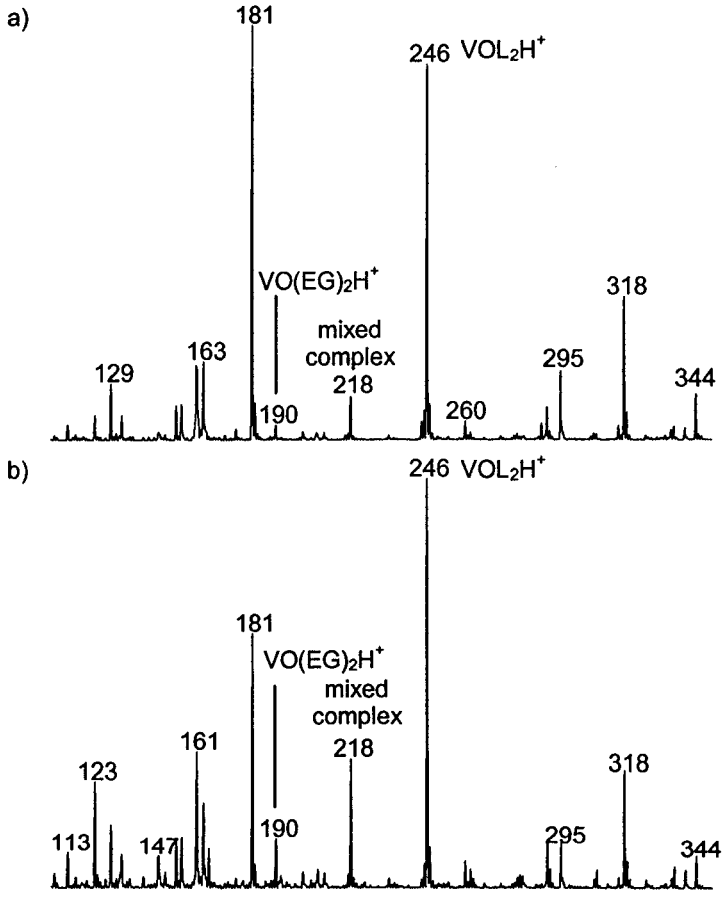

Figure 6-3. ES mass spectra of an aqueous solution of VO^{++}, EG and L (1:2:1) with L = (2*R*,3*R*)-(-)-2,3-butanediol, item a) ; and L = *meso*-2,3-butanediol, item b).

This is indeed the case. The MS/MS spectrum of the mixed complex of the *meso* isomer yields a signal at m/z 188 which corresponds to loss of a mass 30 neutral. This neutral is probably CH_2O, ΔH_f = -28 kcal/mol [14], and is not observed to a significant extent in the MS/MS spectrum of the mixed complex with the (2*R*,3*R*) isomer. Structure proposals for the ions formed upon the structure-diagnostic loss of 30 Da from the mixed complexes remain highly speculative in the absence of further deuterium-labelling experiments aimed to establish the identity of the neutral lost.

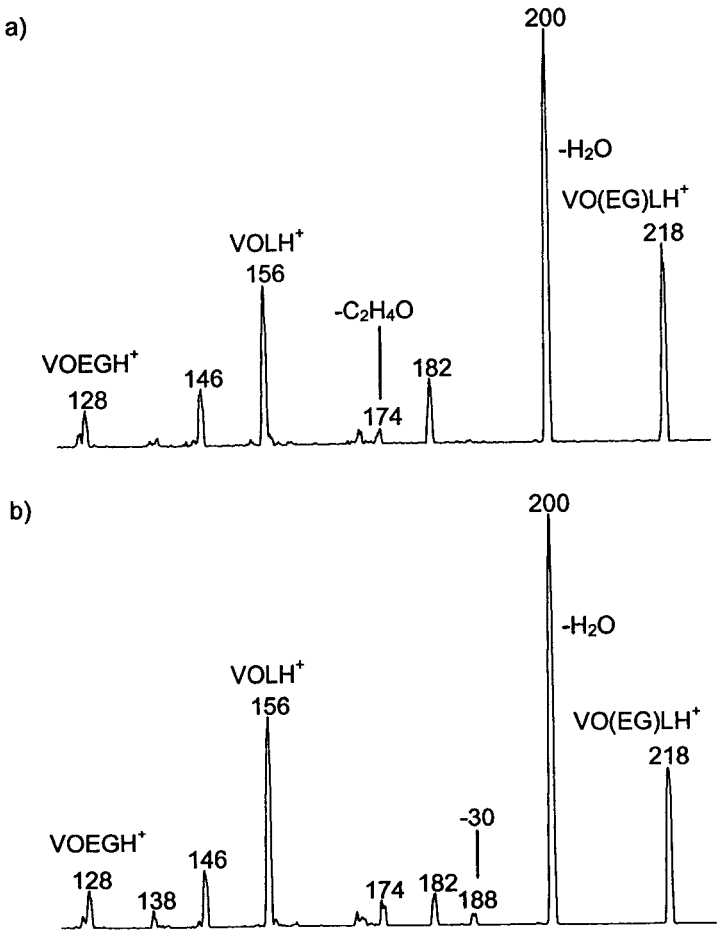

Figure 6-4. MS/MS spectra (Ar, collision energy 10 eV) of the mixed complexes $VO(EG)LH^+$ with L = (2*R*,3*R*)-(-)-2,3-butanediol, item a) ; and *meso*-2,3-butanediol, item b).

In general, the acyclic vicinal diols studied appear to compete efficiently with ethylene glycol for complex formation with VO^{++}.

Cis- and *trans*-1,2cyclopentanediols and 1,2-cyclohexanediols

Complex formation between VO^{++} and *cis*- and *trans*-1,2-cyclopentanediol was also examined. Both diols readily formed a [2M] complex with VO^{++}. However, the intensity ratios of the peaks corresponding to the [2M] complex with EG relative to that of the cyclopentanediol isomers are different. The intensity ratio for the peaks corresponding to the [2M] complexes formed with the *cis* isomer relative to that formed with EG is 9 times greater than the *trans* isomer.

The MS/MS spectra of the mixed complexes formed with the cyclopentanediols are shown in Figure 6-5. The major difference between these spectra is that the mixed complex formed with the *trans* isomer (reproducibly) loses H_2 to a larger extent than the *cis* isomer. This dissociation is also followed by loss of H_2O.

Loss of H_2 is rationalized as follows. Hydrogen molecule loss probably occurs from the cyclopentanediol portion of the mixed complex formed with the *trans* isomer because this loss is not observed for the [2M] complex with EG. If this loss involved the hydrogens of C1 and C2, then a structure that has the coordinating –OH groups closer to each other, and which may accommodate more favourable bonding with VO^{++} is formed. It is further proposed that H_2 loss does not contribute to the peaks observed in the spectrum of Figure 6-5a

because the *cis* isomer already has its –OH groups most suitably oriented for bonding with vanadium.

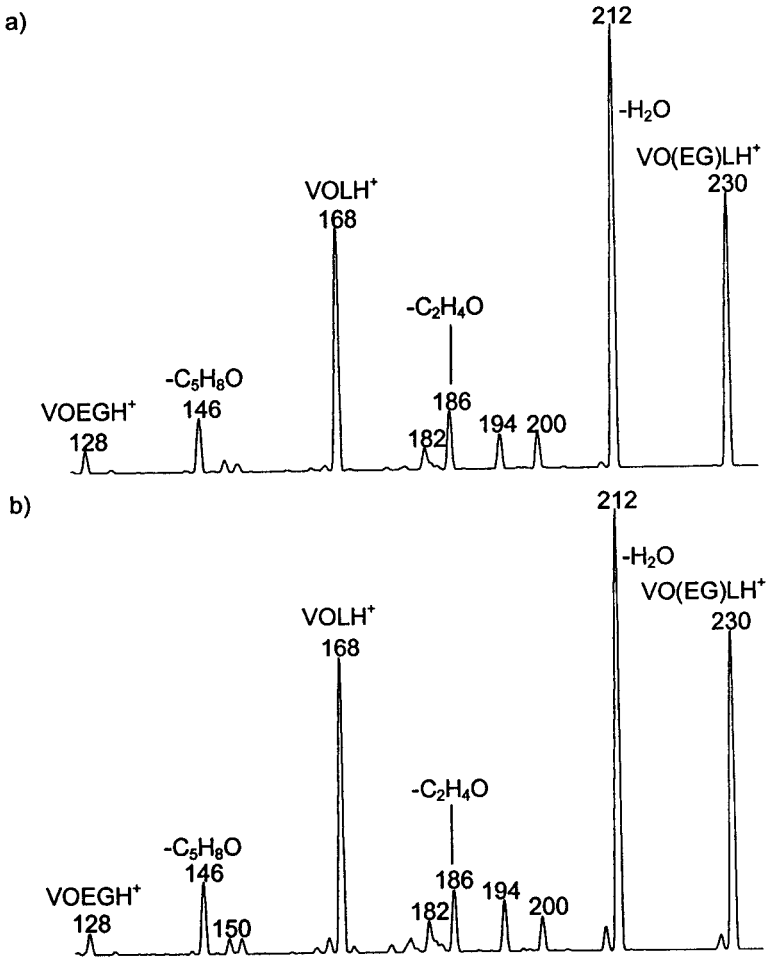

Figure 6-5. MS/MS spectra (Ar, collision energy 10 eV) of the mixed complexes $VO(EG)LH^+$ with L = *cis*-1,2-cyclopentanediol, item a) ; and *trans*-1,2-cyclopentanediol, item b).

The *cis*- and *trans*-1,2-cyclohexanediols 7 and 8 of Scheme 1 were also examined. As observed with the cyclopentanediols, *cis*-1,2-cyclohexanediol competes more efficiently with EG for complexation to VO^{++} than does its *trans* isomer. The MS/MS spectra of the mixed complexes of these isomers are clearly

different. The spectra of Figure 6-6 show that the *cis* isomer loses C_2H_4O (ethylene oxide) – to generate m/z 200 – more readily than does the *trans* isomer. In line with this, the mixed complex formed with the *trans* isomer loses $C_6H_{10}O$ (cyclohexene epoxide ?) – to form m/z 146 – more readily than does the *cis* isomer.

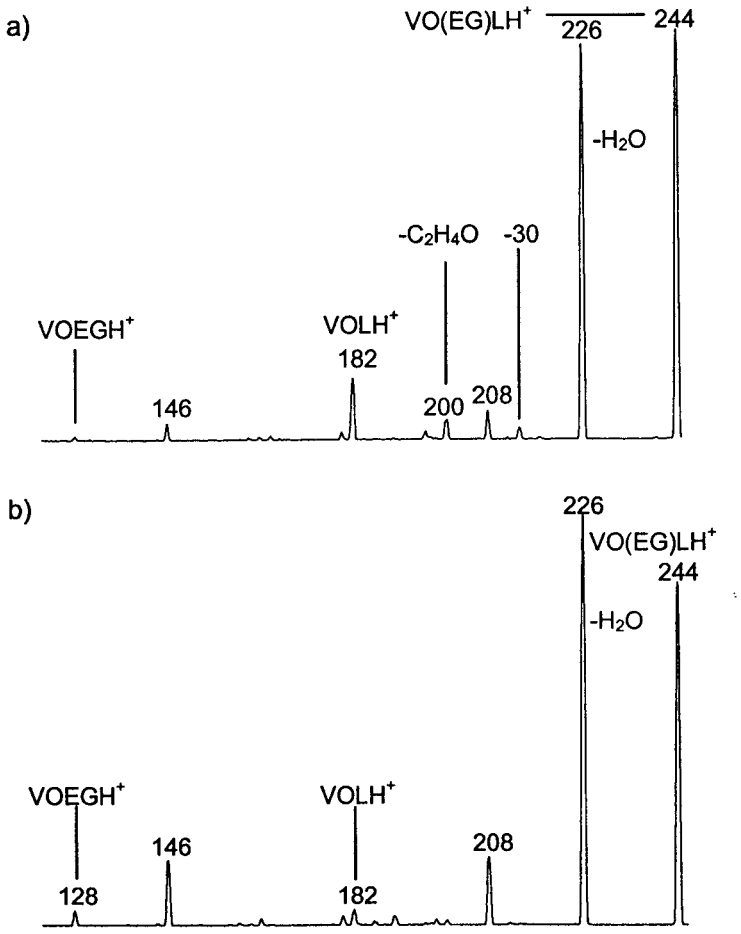

Figure 6-6. MS/MS spectra (Ar, collision energy 10 eV) of the mixed complexes $VO(EG)LH^+$ with L = *cis*-1,2-cyclohexanediol, item a) ; and *trans*-1,2-cyclohexanediol, item b).

The m/z 128 peak corresponds to loss of the cyclohexanediol portion of the mixed complex, whereas m/z 182 corresponds to loss of the ethylene glycol

portion. The intensity of m/z 182 to m/z 128 is larger for the *cis* isomer relative to the *trans* isomer. Thus, it follows that the m/z 182 ion formed from the mixed complex of the *cis* isomer is more stable than that generated from the *trans* isomer.

The minor peak at m/z 214 is unique to the MS/MS spectrum of the mixed complex with the *cis* isomer; see Figure 6-6a. This peak corresponds to loss of a mass 30 neutral – which is most probably formaldehyde – from the mixed complex, m/z 244.

Of the cyclopentanediols and the cyclohexanediols studied, the complexes formed with the cyclohexanediols produced more characteristic MS/MS spectra than the cyclopentanediols. It is not immediately obvious why the major and only difference between the spectra of Figure 6-5 is H_2 loss. This latter observation is unlike that reported in Chapter 5. The borate complexes formed with the *cis*- and *trans*-1,2-cyclopentanediols were more clearly differentiated by their MS/MS spectra.

Methyl glycosides

Sugars in the hemiacetal/hemiketal form undergo mutarotation. This entails that they interconvert between their α/β-furanose and α/β-pyranose forms. Alkylating the anomeric hydroxyl prevents mutarotation and ensures that the anomeric hydroxyl group cannot participate in complex formation. A better assessment of the use of the VO^{++}/ethylene glycol procedure for probing the stereochemistry of sugars is then obtained.

The ESMS spectra of solutions containing the α-methyl-D-ribo- and α-methyl-D-xylopyranoside, structures **9** and **10** of Scheme 1, showed that the *ribo* isomer competed more effectively with EG for complexation to VO^{++}. *Ribo* sugars have one pair of *cis* hydroxyl groups, whereas *xylo* sugars have all hydroxyl groups with a *trans* orientation, see Scheme 1. Therefore, based on previous observations it is not surprising that *ribo* sugars compete more effectively with EG for complexation to VO^{++} than *xylo* sugars.

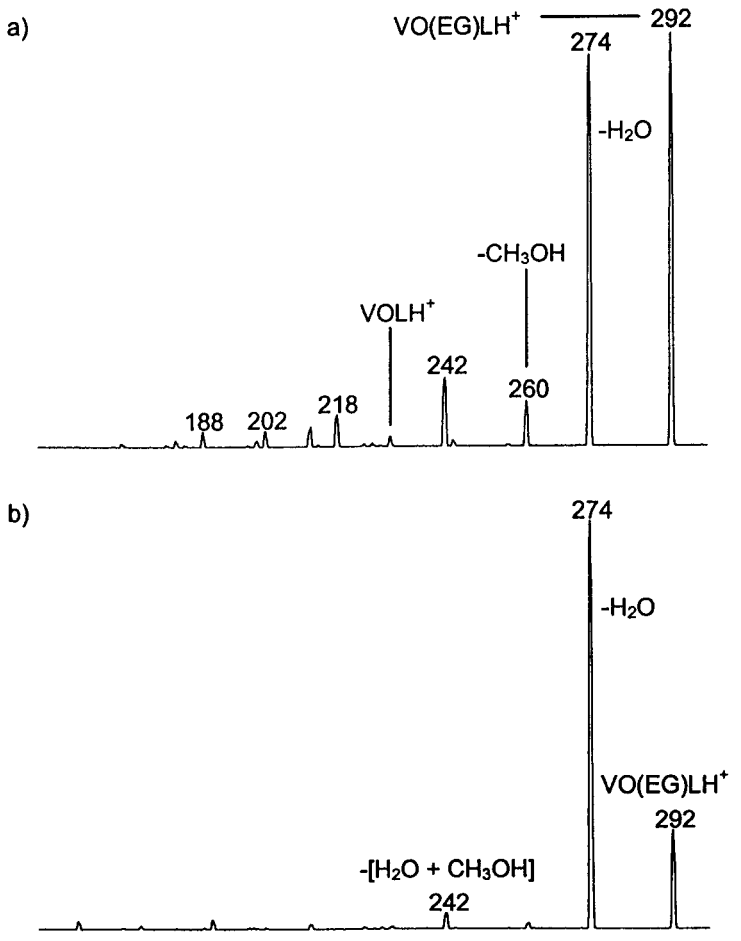

Figure 6-7. MS/MS spectra (Ar, collision energy 5 eV) of the mixed complexes $VO(EG)LH^+$ with L = α-methyl-D-ribopyranoside, item a) ; and α-methyl-D-xylopyranoside, item b).

The MS/MS mass spectra of the mixed complexes, m/z 292, formed with the *ribo*- and *xylo*- methyl glycosides are also different; see Figure 6-7. Loss of H_2O to yield m/z 274 is the most abundant fragment ion in the MS/MS spectra of both mixed complexes. The m/z 274 ion from the mixed complex of the *ribo* isomer undergoes a facile loss of CH_3OH to generate m/z 242. This dissociation occurs to a lesser extent for the mixed complex formed with the *xylo* isomer. Moreover, the mixed complex formed with the *ribo* isomer easily loses a neutral of mass 74 Da, which is not observed for the *xylo* isomer. It is proposed that the unique fragmentation patterns of these mixed complexes is a result of the different relative configurations of the hydroxyl groups in the *xylo* versus the *ribo* isomer; see Scheme 1.

α-Methyl-D-mannopyranoside, structure **11** in Scheme 1, forms the mixed complex more readily than α-methyl-D-glucopyranoside, structure **12** in Scheme 1. This is evidenced by the relative peak intensities of the [2M] complexes formed with ethylene glycol relative to the *manno* and the *gluco* isomers.

The MS/MS spectrum of the ion representing the mixed complex with the *manno* isomer is characteristically different from that of the *gluco* isomer; compare Figures 6-8a and 6-8b. Apart from the fact that the relative abundances of the ions observed in the spectra of Figure 6-8 are different, there are two ions unique to Figure 6-8b. Loss of a mass 32 neutral (CH_3OH) distinctively characterizes the mixed complex with α-methyl-glucopyranoside by the peak at m/z 290; see Figure 6-8b.

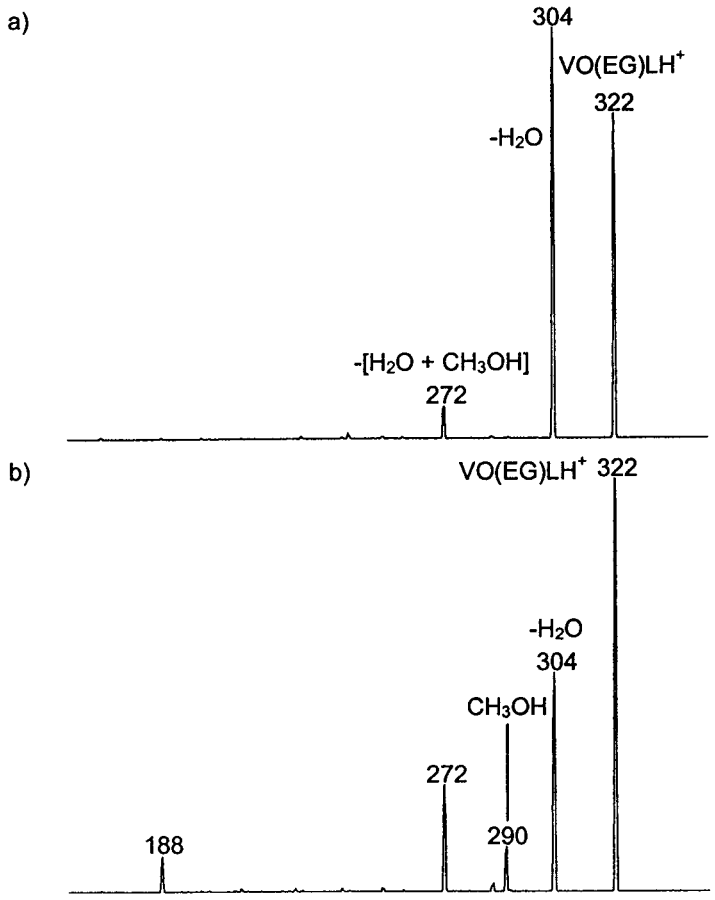

Figure 6-8: MS/MS spectra (Ar, collision energy 5 eV) of the mixed complexes $VO(EG)LH^+$ with L = α-methyl-D-mannopyranoside, item a) ; and α-methyl-D-glucopyranoside, item b).

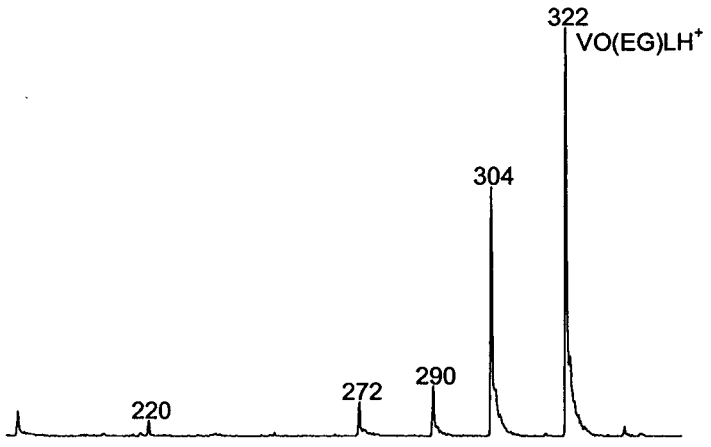

Figure 6-9: Precursor ion scan of the m/z 188 ions in the MS/MS spectrum of Figure 8b.

Even more striking is the presence of a signal at m/z 188 in this spectrum. A precursor ion scan of m/z 188 formed from the *gluco* isomer is shown in Figure 9. The mixed complex, m/z 322, is the major contributor to m/z 188.

ESMS and MS/MS experiments of the mixed complexes of two isomeric pairs of methyl glycosides accomplished their differentiation. The mixed complexes formed with the *ribo* and *manno* sugars – both containing a pair of *cis* hydroxyl groups – undergo loss of CH_3OH. This loss is not observed for the mixed complexes formed with the *xylo* and *gluco* sugars. Since all four sugars are in the pyranose conformation and there are no $-CH_2OH$ groups in the pentoses, it is probable that CH_3OH loss is from the methoxy group at the C1 carbon. We further propose that, both the *ribo* and the *manno* sugars form complexes with VO^{++} via the pair of *cis* hydroxyl groups.

We proceeded to investigate whether isomeric disaccharides may also be differentiated.

Disaccharides

The model compounds used in our preliminary experiments are melibiose (**13**), gentiobiose (**14**), and trehalose (**15**); see Scheme 1. Gentiobiose and trehalose are glucose disaccharides with β-1,6- and α-1,1-*O*-glycosidic linkages, respectively. Melibiose is a galactose/glucose disaccharide that has an α-1,6-*O*-glycosidic linkage.

The glucose disaccharides, gentiobiose and trehalose, were expected to compete less efficiently with EG for complexation with VO^{++} than melibiose. This

is because glucose sugars have all their hydroxyl groups in a *trans* orientation, whereas the galactose residue of melibiose has a pair of (fixed) *cis* hydroxyls.

The normal mass spectra of solutions containing a 1:2:1 mole ratio of the disaccharide:EG:VO^{++} showed that gentiobiose competed with EG, as effectively as melibiose, for complexation with VO^{++}. However, this was not the case for the α-1,1-glucose disaccharide, trehalose. This difference is rationalized as follows. There are at least two pairs of hydroxyl groups by which melibiose can complex with VO^{++}. These are the *cis* hydroxyl groups on the galactose residue and the C1 and C2 hydroxyl groups on the glucose residue. Mutarotation of the C1 hydroxyl group on the glucose residue results in both the C1 and C2 hydroxyl groups having a *cis* relationship. Since the CI hydroxyl group in trehalose cannot undergo mutarotation, it cannot assume an orientation amenable to complexation with VO^{++}. Therefore, trehalose does not compete as effectively with EG for complexation with VO^{++}.

The MS/MS spectra of the mixed complexes formed with the disaccharides are shown in Figure 6-10. Although these complexes dissociate via a common pathway, i.e., all three mixed complexes lose EG, each MS/MS spectrum has a characteristic appearance.

The peak at m/z 408 in the MS/MS spectrum of the mixed complex formed with gentiobiose dissociates primarily by loss of a molecule of ethylene glycol. The m/z 408 peak from the melibiose mixed complex equally loses ethylene glycol and a mass 60 neutral, $C_2H_4O_2$, which may have the structure of acetic acid. The observation that metal ion complexes of sugars lose 60 Da under MS/MS conditions is not without precedence [15].

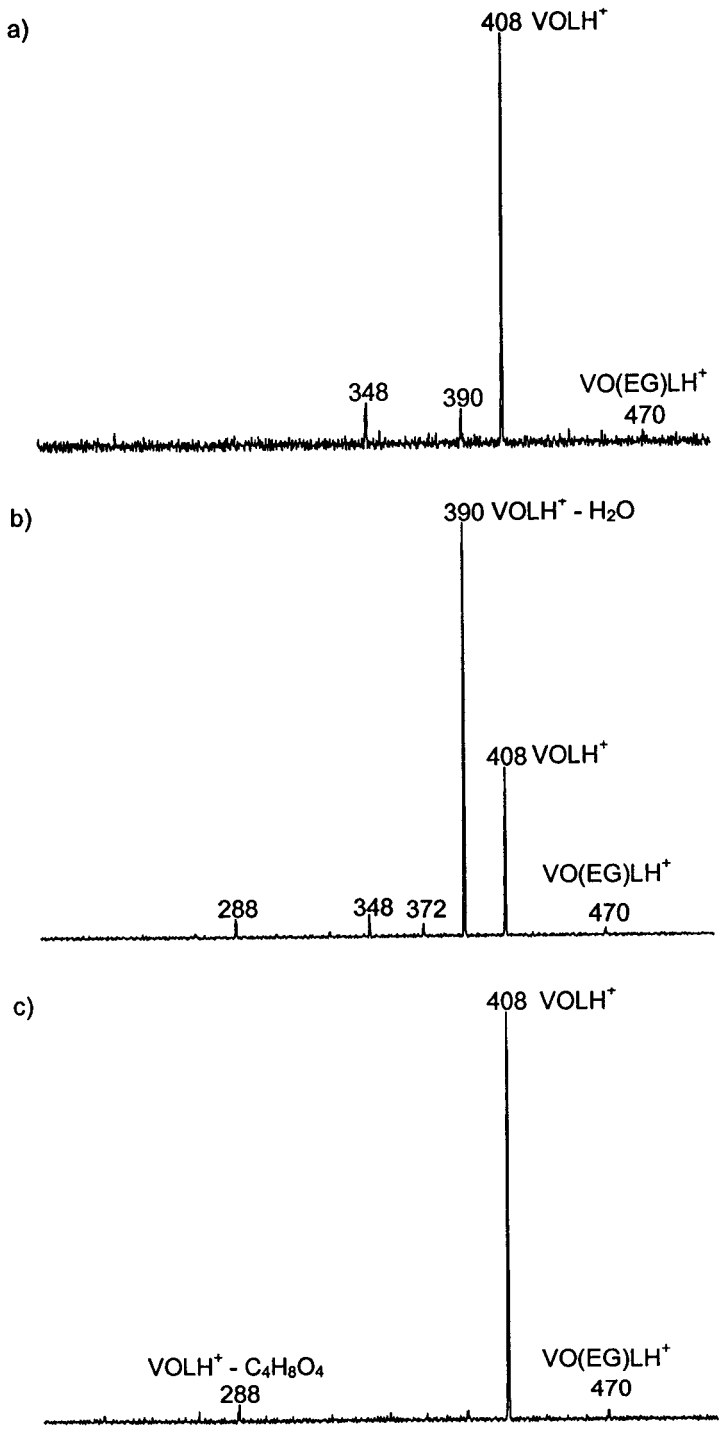

Figure 6-10: MS/MS spectra (Ar, collision energy 10 eV) of the mixed complexes $VO(EG)LH^+$ with L = melibiose, item a) ; gentiobiose, item b) ; and trehalose, item c).

Leary et al. [15a] used ^{18}O-labelling studies to show that loss of 60 Da involved loss of the Cl *O*-atom. Furthermore, these researchers proposed a fragmentation pathway for loss of 60 Da, where the latter involves both C1 and C2.

It was reported [15b] that the intensity ratios of ions corresponding to loss of 60 Da ($C_2H_4O_2$), 90 Da ($C_4H_8O_4$) and 120 Da ($C_4H_8O_4$) are characteristic of the *O*-glycosidic linkage type. The spectra of Figure 6-10 also show unique dissociation patterns for the disaccharides studied, and thus accommodated their differentiation.

Conclusions

By adding a measured quantity of a diol of unknown composition to an aqueous solution of a preformed ethylene glycol/oxovanadium (IV) [2M] complex, the extent of complex formation between VO^{++} and the analyte can be assessed. The relative ease of complex-formation is derived from the relative intensity of the [2M] complex between ethylene glycol and VO^{++} and the [2M] complex between the analyte and boric acid.

For vicinal *cis*- and *trans*-cyclic diols it is shown that a simple ESMS experiment is sufficient to differentiate between the two isomers. Of the cyclohexanediols, MS/MS experiments show that *cis* isomer readily loses C_2H_4O (oxirane) whereas the *trans* isomer characteristically loses the diol. The cyclopentanediols were not as easily differentiated by their MS/MS spectra. At low collision energy, i.e., 5 eV, a unique peak was observed.

Stereoisomer differentiation between the *meso*-2,3- and (2*R*,3*R*)-(-)-2,3-butanediols is also possible but only using MS/MS experiments. Steric

interactions between the two methyl groups in the mixed complex with *meso*-2,3-butanediol promote a facile loss of the butanediol portion of the mixed complex. In contrast, with (2*R*,3*R*)-(-)-2,3-butanediol, the ethanediol portion of the complex is more readily lost.

Isomeric methyl glycosides were differentiated by both ESMS and MS/MS experiments. The *ribo* sugar was differentiated from the *xylo* isomer and the *manno* sugar was differentiated from the *gluco* isomer. The isomeric disaccharides melibiose, gentiobiose and trehalose were also differentiated.

It was observed that for 10-fold lower concentration, the sensitivity was 10 times better than that of the boric acid complexation experiments. Therefore, polyols which are present in low concentration, may be analyzed by VO^{++} rather than boric acid complexation.

The results obtained so far warrant a more extensive and detailed study of the use of VO^{++} complexes for the analysis of polyols in aqueous solutions. This extended study should include labelling studies with ethylene glycol-d_2. Although complexation with VO^{++} and boric acid may potentially be used as complementary methods, a more rigorous comparison of the two approaches is desirable.

References

[1] a. N.D. Chasteen, *Vanadium in Biological Systems*, Kluwer, Dordecht, **1990**. b. H. Sigel and A. Sigel, *Vanadium and Its Role In Life*. In: Metal Ions in Biological Systems, H. Sigel and A. Sigel (Eds.), Marcel Dekker, New York, **1995**. c. F.H. Nielsen, *FASEB J*, **1991**, *5*, 2661. d. D. Rehder, *Angew. Chem. Int. Ed. Engl.*, **1991**, *30*, 148. e. E.J. Baran, *J. Inorg. Biochem.*, **2000**, *80*, 1.

[2] K.M. Mackay and R.A. Mackay, *Introduction to Modern Inorganic Chemistry*, 4th Ed., Prentice Hall, New Jersey, **1989**, p218.

[3] a. F.A. Cotton and G. Wilkinson, *Advanced Inorganic Chemistry*, 3rd Ed., John

Wiley & Sons, Inc., New York, **1972**, p818. b. J. Selbin, *Chem. Rev.*, **1965**, *65*, 153.

[4] N.D. Chasteen, *Vanadyl (IV) EPR Spin Probes Inorganic and Biochemical Aspects*. In: Biological Magnetic Resonance V.3, L.J. Berliner and J. Reuben (Eds.), Plenum Press, New York, **1981**, p53.

[5] a. J. Reuben and D. Fiat, *Inorg. Chem.*, **1967**, *6*, 579. b. K. Wuthrich and R.E. Connick, *Inorg. Chem.*, **1967**, *6*, 583. c. R.B. Jordan and N.S. Angerman, *J. Chem. Phys.*, **1968**, *48*, 3983. d. N.S. Angerman and R.B. Jordan, *Inorg. Chem.*, **1969**, *8*, 1824. e. K. Wuthrich and R.E. Connick, *Inorg. Chem.*, **1968**, *7*, 1377. f. R.K. Murmann, *Inorg. Chim. Acta.*, **1977**, *25*, L43.

[6] a. R.E. Tapscott and R. Linn Belford, *Inorg. Chem.*, **1967**, *6*, 735. b. L.D. Petit and J.L.M. Swash, *J. Chem. Soc. Dalton Trans.*, **1978**, 286. c. R.M. Holland and R.E. Tapscott, *J. Coord. Chem.*, **1981**, *11*, 17.

[7] a. J.G. Forrest and C.K. Prout, *J. Chem. Soc. (A)*, **1967**, 1312. b. R.E. Tapscott, R.L. Belford and I.C. Paul, *Inorg. Chem.*, **1968**, *7*, 356.

[8] T. Kiss, P. Buglyo, D. Sanna, G. Micera, P. Decock and D. Dewaele, *Inorg. Chim. Acta*, **1995**, *239*, 145.

[9] M.T. Beck, B. Csiszár and P. Szarvas, *Nature*, **1960**, *188*, 846.

[10] a. R.E. Tapscott, R.L. Belford and I.C. Paul, *Coord. Chem. Rev.*, **1969**, *4*, 323. b. F.R. Venema, J.A. Peters and H. van Bekkum, *Inorg. Chim. Acta.*, **1992**, *191*, 261.

[11] a. G. Micera, A. Dessi, H. Kozlowski, B. Radomska, J. Urbanska, P. Decock, B. Dubois and I. Olivier, *Carbohydr. Res.*, **1989**, *188*, 25. b. M. Branca, G. Micera, A. Dessi and H. Kozlowski, *J. Chem. Soc. Dalton Trans.*, **1989**, 1283. c. M. Branca, G. Micera, A. Dessi and D. Sanna, *J. Inorg. Biochem.*, **1992**, *45*, 169. d. M. Branca, G. Micera, D. Sanna, A. Dessi and H. Kozlowski, *J. Chem. Soc. Dalton Trans.*, **1990**, 1997.

[12] a. T.J. Cardwell, R. Colton, S. Mitchell and J.C. Traeger, *Inorg. Chim. Acta*, **1994**, *216*, 75. b. A. Rosell-Melé and J.R. Maxwell, *Rapid Commun. Mass Spectrom.*, **1996**, *10*, 209. c. S. Sasaki, Y. Itagaki, T. Kurokawa, K. Nakanishi and A. Kasahara, *Bull. Chem. Soc. Japan*, **1967**, *40*, 76. d. S.R. Prescott, J.E. Campana, P.C. Jurs and T.H. Risby, *Anal. Chem.*, **1976**, *48*, 829. e. R.P. Evershed, G.A. Wolff, G.J. Shaw and G. Eglinton, *Org. Mass Spectrom.*, **1985**, *20*, 445. f. R. Grybós and W. Paw, *Polyhedron*, **1990**, *9*, 1397. g. J.L. Pierce, K.L. Busch, R.G. Cooks and R.A. Walton, *Inorg. Chem.*, **1982**, *21*, 2597. h. R. Lidgard and M.W. Duncan, *Rapid Commun. Mass Spectrom.*, **1995**, *9*, 128. [i] G.J. van Berkel, S.A. McCluckey and G.L. Glish, *J. Am. Soc. Mass Spectrom.*, **1992**, *3*, 235.

[13] A. Deutsch and S. Osoling, *J. Am. Chem. Soc.*, **1949**, *71*, 1637.

[14] S.G. Lias, J.E. Bartmess, J.F. Liebman, J.L. Holmes, R.D. Levin and W.G. Mallard, *J. Phys. Chem. Ref. Data 17*, **1988**.

[15] a. M.R. Asam and G.L. Glish, *J. Am. Soc. Mass Spectrom.*, **1997**, *8*, 987. b. Z. Zhou, S. Ogden and J.A. Leary, *J. Org. Chem.*, **1990**, *55*, 5444.

Chapter 7

The site of alkylation of N-methyl- and N-ethylaniline in the gas phase: A tandem mass spectrometry study

This Chapter presents a study on the alkylation reactions of iodoethane and iodomethane of N-methylaniline and N-ethylaniline and ring (m)ethyl anilines. This project accommodated exposure to ion-molecule reactions, thus providing the author with a better understanding of the gas-phase chemistry that may occur in electrospray ionization.

The structure of the m/z 136 product ion resulting from the ion-molecule reaction between C_2H_5I and N-methylaniline and CH_3I and N-ethylaniline was probed by analyzing the metastable ion and collision-induced dissociation mass spectra. The collision-induced dissociation spectra show structure-diagnostic ions at m/z 44 and m/z 59, which are indicative of N-alkylation. The proposed structure of these alkylation products was further investigated by comparative collision-induced dissociation spectra of the isomeric m/z 136 ions formed by C_2H_5I and CH_3I alkylation of the *o*-, *m*- and *p*-toluidines and the *o*-, *m*- and *p*-ethylanilines, respectively. The comparison showed that the C_2H_5I and CH_3I alkylation products of N-(m)ethylaniline differ from those formed by C_2H_5I and CH_3I alkylation of the ring-(m)ethylanilines. An m/z 136 ion was also formed by a chemical ionization type protonation of N-ethyl-N-methylaniline using $CH_3C(=O)CH_3$ and CH_3OH as the reagents. The collision-induced dissociation spectrum of the m/z 136 ion formed by $CH_3C(=O)CH_3$ protonation of N-ethyl-N-methylaniline resembles that of the m/z 136 ion formed by C_2H_5I and CH_3I alkylation of N-(m)ethylaniline. In contrast, the collision-induced dissociation spectrum of the m/z 136 ion formed by CH_3OH protonation of N-ethyl-N-methylaniline is different from the m/z 136 ion formed with $CH_3C(=O)CH_3$. Therefore, it was concluded that N-protonation predominated when $CH_3C(=O)CH_3$ was the CI reagent, whereas ring-protonation predominated when CH_3OH was the CI reagent. The collision-induced dissociation mass spectrum of the m/z 136 ion formed by C_2H_5I alkylation of *o*-toluidine was compared with that of the m/z 136 ion formed by $CH_3C(=O)CH_3$ CI of 6-ethyl-*o*-toluidine, and N-ethyl-*o*-toluidine. It was observed that these CID mass spectra are different. These experiments provided more evidence that $(CH_3)_2C(=OH)^+$ protonates predominantly at the N-site. To assist with the interpretation of the collision-induced dissociation spectra, experiments were performed with the deuterium isotopologues of the alkylating and protonating agents.

Introduction

The site of protonation and alkylation of functionalized aromatic and heterocyclic molecules in solution and in the gas phase is a topic of considerable

interest which has received a great deal of attention [1-18]. In the gas phase, protonation and alkylation of such molecules can conveniently be performed in the chemical ionization (CI) source of a mass spectrometer. The structure of the reaction products, and thus the site of electrophile attachment, can then be probed by examining their metastable ion (MI) [29] and collision-induced dissociation (CID) spectra [20,22].

Aniline is a prime example of an aromatic molecule whose gas phase proton and alkyl ion attachment reactions have been studied in considerable detail [1-6,8-17,18]. Aniline is a well-known nitrogen base in solution. In the gas phase, theory at the STO-3G [1] level predicts ring-protonation, whereas theory at the *ab initio* MO [2,3], AM1 [9], DFT [14], PM3 [15], G2(MP2), B3LYP, BP and MP4 [17] levels predict N-protonation. However, N-protonation is calculated to be only slightly more favourable – by 1-3 kcal/mol [2,3] – than protonation at the *para* position of the ring [19]. In line with this, there are several experimental studies of the gas phase protonation of aniline in which both ring and N-protonation are reported [2,3,5,10,12]. In this context it should be mentioned that chemical ionization type protonation experiments are not necessarily thermodynamically controlled [24]. In the same vein, experimental studies of aniline's alkylation in the gas phase also yield conflicting results regarding the site of attachment [4,5,10,11].

Maquestiau et al. [4] used MI and CID spectra to study the protonation and ethylation of a series of aromatic amines. For the anilines they observed that the MI and CID mass spectra of protonated 2-, 3- and 4-ethylaniline are similar to that of ethylated aniline but that these spectra differ considerably from that of

protonated N-ethylaniline. Therefore, it was concluded that the ring-alkyl anilines undergo ring-protonation while aniline undergoes ring-ethylation. There was, however, predominant N-protonation of N-ethylaniline. In the same study, Maquestiau et al. reported that under CH_4 CI conditions, pyridine is ethylated at the nitrogen site. This followed from the observation that the MI and CID mass spectra of the product of the ethylation of pyridine are different from those of the protonated ring ethyl pyridines. Additionally, the MI and CID spectra of the ethylation of pyridine-d_5 showed loss of $C_2H_4D^{\bullet}$ whereas in the corresponding experiment with pyridine there was loss of $C_2H_5^{\bullet}$. Therefore, loss of $C_2H_5^{\bullet}$ occurred via consecutive loss of $H^{\bullet}$ + C_2H_4.

Cooks et al. [5] used both low- and high-energy CID experiments to investigate the site of H^+, CH_3^+ and $C_2H_5^+$ attachment to aniline, phenol and thiophenol. The reagents were isobutene for protonation, methane and ethyl bromide for ethylation and methyl fluoride and methyl chloride for methylation. Cooks et al. noted that varying the methylating or ethylating agent yielded similar high-energy CID spectra. Ring-protonation / alkylation versus N-protonation / alkylation was determined from the high-energy CID spectra. Cooks et al. compared the CID mass spectra of the CH_3^+ and $C_2H_5^+$ attachment ions of aniline with the isomeric ion formed by a proton attachment reaction to the ring-(m)ethylanilines. They concluded that CH_3^+ and $C_2H_5^+$ attach to the N-site while proton attachment occurs on the ring. A similar analysis of the methylation of thiophenol and the alkylation/protonation of phenol shows that thiophenol undergoes substituent methylation while phenol undergoes ring-alkylation and -protonation.

In a later study, Cooks et al. [10] employed CID to investigate the relationship between charge-stripping and ring- versus N-site attachment to the same compounds as in the previous study. They observed that when these aromatic compounds undergo cation attachment to the ring there is a direct correlation with the extent of charge stripping. Therefore, under CID the ring-adduct ions undergo a higher incidence of charge-stripping relative to the substituent-adduct ions. Using this criterion, they concluded that aniline undergoes ring protonation and substituent (m)ethylation.

Electrophile attachment of aniline in radiolytic and mass spectrometric experiments was investigated by Attina and Cacace [6]. It was found that N-attachment relative to ring-attachment decreases in the order CH_3CO^+ > t-$C_4H_9^+$ > $(CH_3)_2F^+$ > i-$C_3H_7^+$ ~ $C_2H_5^+$. Thus, the CH_3CO^+ attaches more readily to the NH_2 moiety. It was further noted that in the case of ring substitution, the *ortho* products predominated. The authors rationalized the observed ranking of the electrophiles by invoking the hard and soft acid and base (HSAB) concept. This concept states that hard acids, like CH_3CO^+, bind preferentially to hard bases, like NH_2. Ranking the electrophiles according to their hardness would result in the same order as shown above.

Burinsky and Campana [7] have used CID/MIKE spectra to probe the structure of the products formed by CH_3^+ and $C_2H_5^+$ ion attachment to morpholine, thiomorpholine and 1,4-thioxane.

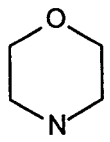

morpholine

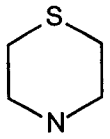

thiomorpholine

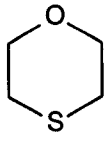

1,4-thioxane

Each of these compounds contains two heteroatoms. They observed that the alkyl cation attaches to the N-atom of morpholine, and to the S-atoms of thiomorpholine and 1,4-thioxane. In a subsequent study, Burinsky and Campana [11] used the same technique to investigate the site of attachment of chlorinated alkyl ions to aniline, phenol, benzaldehyde, benzonitrile and nitrobenzene. It was observed that aniline, benzonitrile and nitrobenzene undergo substituent attack whereas phenol and benzaldehyde underwent both substituent and ring attachment.

In 1986, Harrison [8] performed CI experiments using CH_4 and CD_4 as the reagents and analyzed the MI spectra of the product of $C_2H_5^+$ and $C_2D_5^+$ attachment to ethylbenzene, *p*-ethyltoluene and N-ethylaniline. The goal was to determine whether the electrophile and the ethyl substituent on the substrate become equivalent. The MI spectra of the products of the $C_2D_5^+$ attachment to ethylbenzene and *p*-ethyltoluene show equal loss of C_2H_4 and C_2D_4. Thus, the ethyl groups have become equivalent. However, the MI spectrum of the ethylation product of N-ethylaniline shows that there is unequal loss of C_2H_4 and C_2D_4 and so the ethyl groups have *not* become equivalent. This observation is rationalized by proposing that $C_2H_5^+$ attacks the ring rather than the nitrogen.

Nold and Wesdemiotis [13] used neutralization-reionization mass spectrometry (NRMS) to study of the site of protonation of aniline. If aniline

undergoes N-protonation then the anilinium cation is formed, and if there is ring-protonation a benzenium ion is formed. Neutralization of the anilinium cation forms a hypervalent ammonium radical, which can dissociate either via rupture of the phenyl-N bond, or one of its N-H bonds. By contrast, neutralization of the ring-protonated isomer yields the amino benzenium radical. Depending on its internal energy, this ion may dissociate by $H^{\bullet}$ loss. Otherwise, $C_6H_8N^+$ remains intact and is the (observed) recovery ion. The absence of a signal corresponding to $C_6H_8N^+$ supports N-protonation. Nold and Wesdemiotis observed that the ratio of the intensities of $[C_6H_8N^+]$:$[NH_3^{\bullet+}]$ ranges from 8.5 to 12.4 for the CI experiments, while this ratio was 0.7 for the fast-atom bombardment (FAB) ionization experiments. These researchers concluded that FAB ionization of aniline accommodates N-protonation whereas CI using CH_4, CH_3OH, n-C_3H_7OH, n-C_4H_{10} and NH_3 predominantly results in ring-protonation.

Most recently, Harrison and Tu [16a] performed both MI and low-energy CID experiments on ions generated under CI and FAB ionization, to study the site of protonation of N-alkylanilines. They observed that under CI conditions and using CH_3OH, CH_4 and $CH_3C(=O)CH_3$ as the reagent gases, there is predominant ring-protonation of N-alkylanilines. In contrast, when *i*-$C_4H_9NH_2$ is the CI reagent, N-protonation predominates. FAB ionization of these compounds also results in N-protonation.

In another study, Harrison [16b] investigated the fragmentation reactions of alkylphenylammonium ions using FAB ionization followed by low-energy CID in the quadrupole cell of a hybrid sector / quadrupole instrument, and electrospray ionization followed by cone voltage-CID in the source of the

instrument. The observed fragmentation reactions were rationalized based on the competitive formation of $[R^+–NC_6H_5H_{3-n}R_{n-1}]$ and $[C_6H_5H_{3-n}R_{n-1}N^{\bullet+}–{}^{\bullet}R]$. The first complex fragments by internal proton transfer from R^+ to yield $[C_6H_5H_{3-n}R_{n-1}NH^+]$, whereas the second complex fragments to form $[C_6H_5H_{3-n}R_{n-1}N^+]$ and an alkyl radical. The experiments presented in Harrison's [16b] paper are an excellent reference for the experiments presented in our work. This is because Harrison studied the fragmentation of commercially available alkylphenylammonium ions.

To further pursue the investigation of the site of electrophile attachment to substituted aromatic molecules, a chemical ionization (CI) study of the site of $C_2H_5^+$ and CH_3^+ attachment to N-methylaniline and N-ethylaniline, respectively, is presented. The alkylating agents are C_2H_5I and CH_3I. The structure of the ion-molecule reaction products, the m/z 136 ions, formed upon alkylation of N-(m)ethylaniline with C_2H_5I and CH_3I are analyzed by MI and CID mass spectra. These CID mass spectra are compared with those from the isomeric adduct ions generated by C_2H_5I and CH_3I alkylation of the *o*-, *m*- and *p*-toluidines and the *o*-, *m*- and *p*-ethylanilines, respectively. A comparison of the MI and CID mass spectra of the alkylation products of the ring-(m)ethyl anilines and that of N-(m)ethylaniline provides information about the site of attack of the alkylating agents, i.e., the N- versus ring-site. The m/z 136 ion is also formed by CH_3OH and $CH_3(C{=}O)CH_3$ CI of N-ethyl-N-methylaniline and $CH_3(C{=}O)CH_3$ CI of 6-ethyl- and N-ethyl-*o*-toluidine. The alkylation and protonation reactions are also performed with the deuterium isotopologues of the alkylating and protonating agents.

Experimental

The experiments were performed on the McMaster University VG Analytical ZAB-R instrument of BE_1E_2 geometry (B = magnet, E = electric sector) [23]. Under conditions of chemical ionization, metastable ion (MI) mass spectra were recorded in the second field free region (2ffr); collision-induced dissociation (CID) mass spectra were recorded in the 2ffr and 3ffr using oxygen (O_2) as the collision gas (transmittance, T = 70%). For these experiments, an accelerating voltage of 8 kV was used.

The following compounds were of research grade and used without further purification, the *o*-, *m*- and *p*-toluidines, the *o*-, *m*- and *p*-ethylanilines, 6-ethyl-*o*-toluidine, N-ethyl-*o*-toluidine, CH_3I, CD_3I, C_2H_5I and C_2D_5I were purchased from Aldrich, and CH_3OH and CH_3COCH_3 from Caledon Laboratories. The N-ethylaniline, N-methylaniline, N-ethyl-N-methylaniline were purchased by Dr A.G. Harrison from Aldrich. A portion of each of these compounds was donated to us.

Results and Discussion

I. Methylation and ethylation reactions of N-ethyl- and N-methylaniline

The alkylation reactions were performed in a chemical ionization source at a total source pressure in the 5-10 x 10^{-5} range and using the alkylating agent in excess. In a typical CI mass spectrum of CH_3I and N-ethylaniline (NEA) (total source pressure ~ 1.0 x 10^{-4}), the spectrum is dominated by ions at m/z 142 [100 %, $CH_3I^{\bullet+}$], m/z 157 [70%, $(CH_3)_2I^+$] and m/z 284 [100%, $(CH_3I)_2^{\bullet+}$] while the molecular ion of the aniline at m/z 121 comprises 35% of the base peak. Very

little protonation of the aniline or dissociation of its radical cation takes place under these conditions, as witnessed by the low intensities of the m/z 122 and m/z 106 peaks. Also present in this spectrum is a peak at m/z 136 (~ 5%) which obviously results from methyl ion attachment, possibly via the reaction: $(CH_3)_2I^+$ + NEA → $[NEA\text{-}CH_3]^+$ + CH_3I, see Scheme 1. The NEA molecular ion most likely originates from the exothermic charge exchange reaction: $CH_3I^{\bullet+}$ + NEA → $NEA^{\bullet+}$ + CH_3I (IE CH_3I = 9.5 eV; IE NEA ≅ 7.7 eV [27]).

A typical CI mass spectrum of C_2H_5I and N-methylaniline (NMA) displayed the NMA molecular ion as the base peak (100%) while the ions derived from C_2H_5I, at m/z 156 $[C_2H_5I^{\bullet+}]$, m/z 184 $[(C_2H_5)_2I^+]$ and m/z 312 $[(C_2H_5I)_2^{\bullet+}]$ had relative abundances of 15, 35 and 30 %, respectively. In contrast to the methylation experiment, a significant degree of protonation also takes place both of the NMA and C_2H_5I, as witnessed by the peaks at m/z 108 (65 %) and m/z 157 (25 %), respectively. Also present is a peak at m/z 136 (15 %) resulting from the ethyl attachment reaction, possibly via the reaction: $(C_2H_5)_2I^+$ + NMA → $[NMA\text{-}C_2H_5]^+$ + C_2H_5I, see Scheme 1.

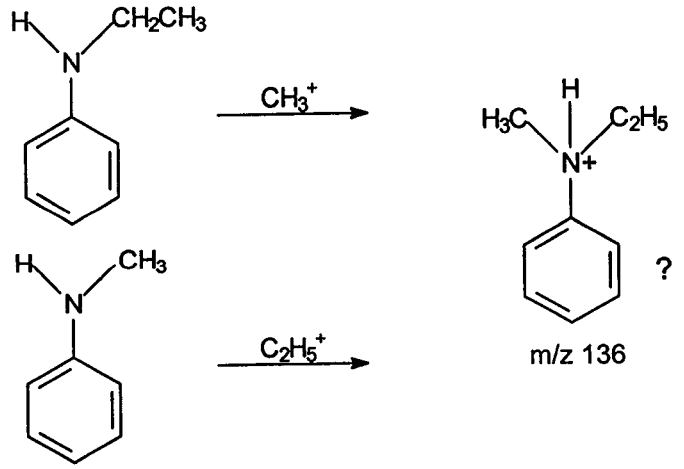

Scheme 1.

To probe the structure of the m/z 136 ions generated via the alkylation reactions in Scheme 1, we have obtained their MI and CID mass spectra.

MI mass spectra represent the spontaneous dissociation of mass-selected ions in one of the field-free regions of the instrument. The ions have a higher internal energy content than those sampled by CID [20]. For odd-electron precursor ions, the fraction of metastable ions in the beam of stable ions transmitted through the instrument is often fairly high. For such ions reliable MI spectra are easily obtained. As a rule the spectra contain only a few peaks and often these peaks correspond to low-energy rearrangement processes rather than direct bond cleavage reactions. However, the m/z 136 ions of this study are even-electron ions and moreover they are generated in a chemical ionization type experiment rather than by dissociative electron ionization. In such a case the fraction of metastable ions in the beam of stable ions becomes a few orders of magnitude smaller. This greatly affects the quality of the MI spectra, which may now become contaminated with CID peaks resulting from residual background gas, and in addition prominent artefact signals may obscure the analysis. With this caveat in mind, we have interpreted the very weak MI spectra of the m/z 136 ions generated by the alkylation reactions of Scheme 1 and also those of the m/z 139 ions obtained by the methylation of NEA with CD_3I and the m/z 141 ions obtained by the ethylation of NMA with C_2D_5I.

The MI spectrum of the $[NMA\text{-}C_2H_5]^+$ ion at m/z 136 displays three peaks, at m/z 107, 108 and 121 with an intensity ratio of 45 : 100 : 10. For the $[NMA\text{-}C_2D_5]^+$ ion at m/z 141 peaks are observed at m/z 107, 109 and 126 with a closely similar intensity ratio of 50 : 100 : 13. Thus, metastable ions $[NMA\text{-}C_2H_5]^+$

predominantly lose C_2H_4 via a rearrangement and $C_2H_5^{\bullet}$ via a formal direct bond cleavage reaction. The minor loss of $CH_3^{\bullet}$ does not involve the ethyl moiety but rather the methyl substituent in the aniline. We further note that the rearrangement does not suffer from an isotope effect. These observations are compatible with the proposal that the product ions have the structure of the N-alkylated ion depicted in Scheme 1.

The minimum energy requirement, see Scheme 2, for the formation of the m/z 107 N-methylaniline ions by loss of $C_2H_5^{\bullet}$ is calculated to be 36 kcal/mol higher than that for the formation of the m/z 108 rearrangement ion, protonated N-methylaniline, by loss of C_2H_4. Nevertheless, loss of $C_2H_5^{\bullet}$ effectively competes with loss of C_2H_4 and this strongly suggests that a significant barrier exists for the H-transfer associated with the rearrangement. This would be compatible with a 1,3 H shift in the N-alkylated product ion of Scheme 1. In support of this proposal, we note that the widths of the Gaussian shaped metastable peaks for the C_2H_4 and $C_2H_5^{\bullet}$ losses and the derived kinetic energy releases are unexceptional. In fact, the metastable peak for loss of C_2H_4 is even somewhat broader than that for loss of $C_2H_5^{\bullet}$.

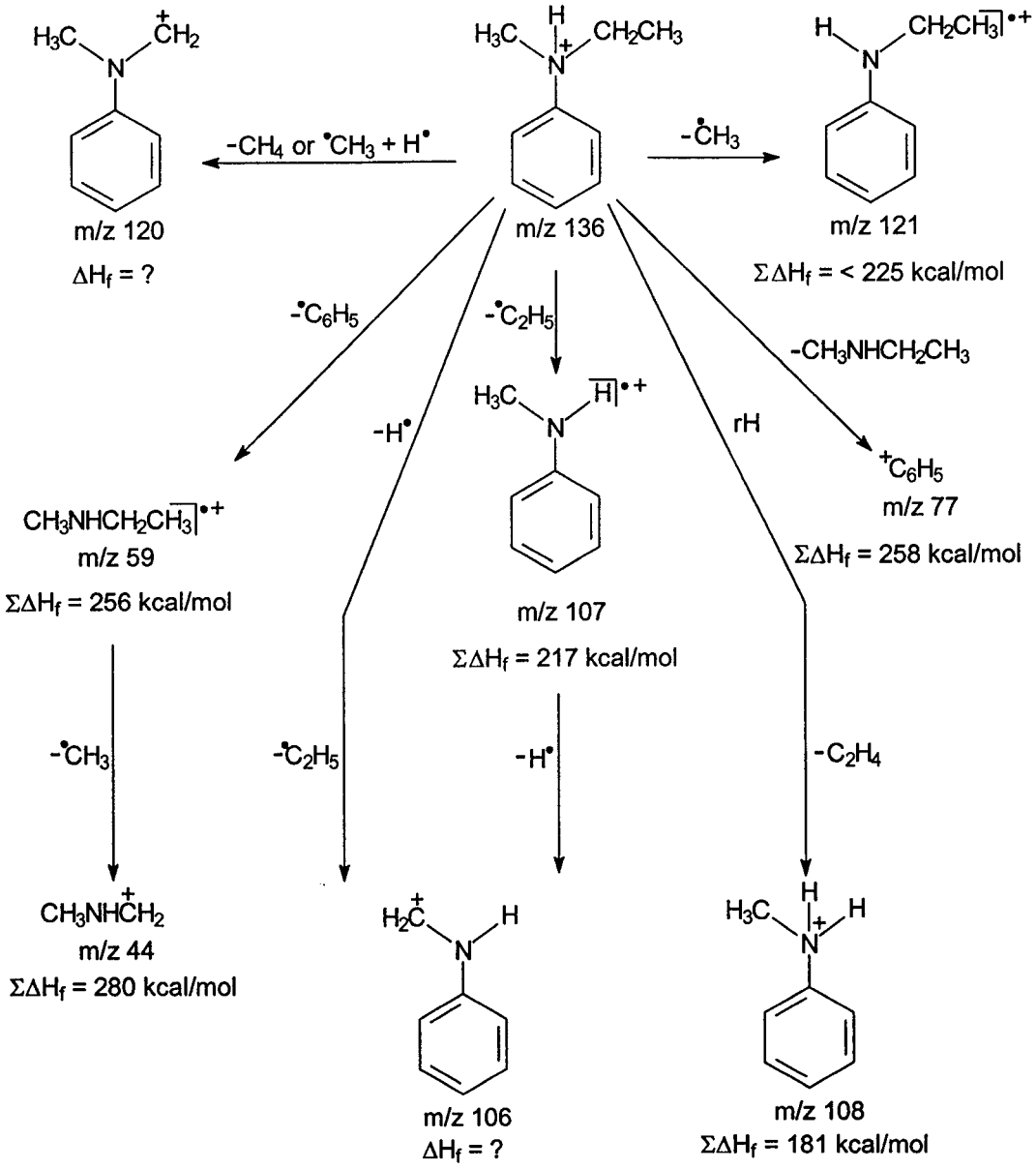

Scheme 2: Proposed fragmentation pathway for the structure-diagnostic product ions observed in the m/z 136 CID spectra shown in Figure 2. The $\Sigma\Delta H_f$ values for the minimum energy requirement of the various dissociations are taken from reference 27.

These observations make it highly unlikely that in our ethylation experiments of NMA m/z 136 ions are co-generated which have the structure of a weakly bound ion-molecule complex, as invoked by Cooks et al. [5] in their analysis of the high-energy CID spectra of ethylated aniline.

The MI spectra of the m/z 136 $[NEA\text{-}CH_3]^+$ and m/z 139 $[NEA\text{-}CD_3]^+$ ions also display losses of C_2H_4 and $C_2H_5^\bullet$ but their intensity ratio, 1 : 2, is reversed relative to that for the $[NMA\text{-}C_2H_5]^+$. Metastable ions $[NEA\text{-}CD_3]^+$ also lose $CD_3^\bullet$, and that more prominently than ions $[NMA\text{-}C_2H_5]^+$ or $[NMA\text{-}C_2D_5]^+$ lose $CH_3^\bullet$, 30 % versus 10 % of base peak. For the $[NEA\text{-}CH_3]^+$ ion, loss of $CH_3^\bullet$ seems to dominate the MI spectrum but the larger part of the m/z 121 peak may well be an artefact.

Loss of $CH_3^\bullet$ has, see Scheme 2, a slightly higher energy requirement than loss of $C_2H_5^\bullet$ and the differences in the relative intensities of the peaks in the MI spectra of $[NMA\text{-}C_2H_5]^+$ and $[NEA\text{-}CH_3]^+$ more likely reflect differences in internal energy content than differences in ion structure. We tentatively propose that the $[NMA\text{-}C_2H_5]^+$ and $[NEA\text{-}CH_3]^+$ ions have the same structure, *viz.* the N-alkylated ion depicted in Scheme 1.

Next we turn to the analysis of the CID spectra of the m/z 136 ions which are presented in Figure 7-1. To assist in the interpretation we have also obtained the CID spectra of the m/z 139 $[NEA\text{-}CD_3]^+$ and the m/z 141 $[NMA\text{-}C_2D_5]^+$ ions. These spectra are presented in Figure 7-2.

Structure proposals for the m/z 136 ions are given in Figure 7-1.

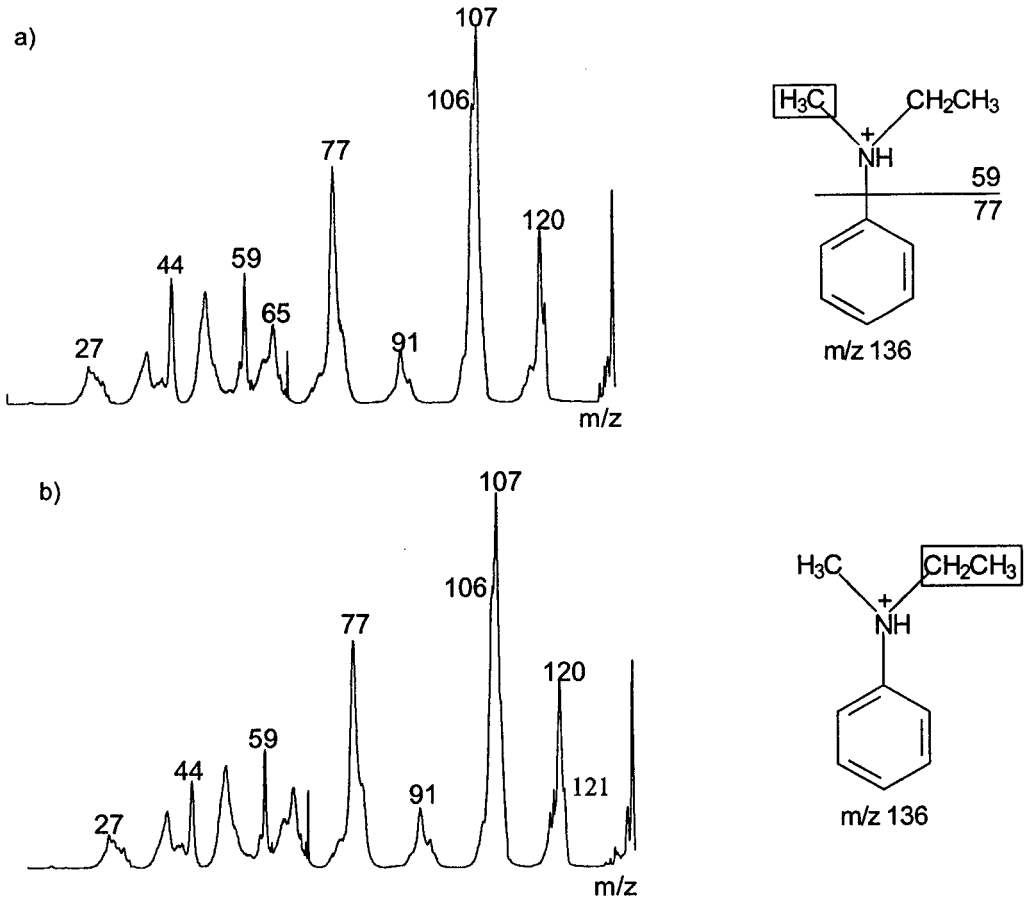

Figure 7-1: CID mass spectra (2ffr, 8 keV, collision gas O_2) of the $C_9H_{14}N^+$ (m/z 136) ions formed by a) CH_3I alkylation of N-ethylaniline and b) C_2H_5I alkylation of N-methylaniline. The proposed structure for m/z 136 is given.

The structure-diagnostic peaks at m/z 59, $[CH_3NHCH_2CH_3]^{\bullet+}$ and m/z 44, $[CH_3NHCH_2]^+$ in these CID spectra support N-alkylation, see Scheme 2. Moreover, from the spectra of the deuterium labelled isotopologues, it follows that the formation of m/z 44 from m/z 59 occurs via $CH_3^\bullet$ loss from the CH_3CH_2– moiety in $[CH_3NHCH_2CH_3]^{\bullet+}$.

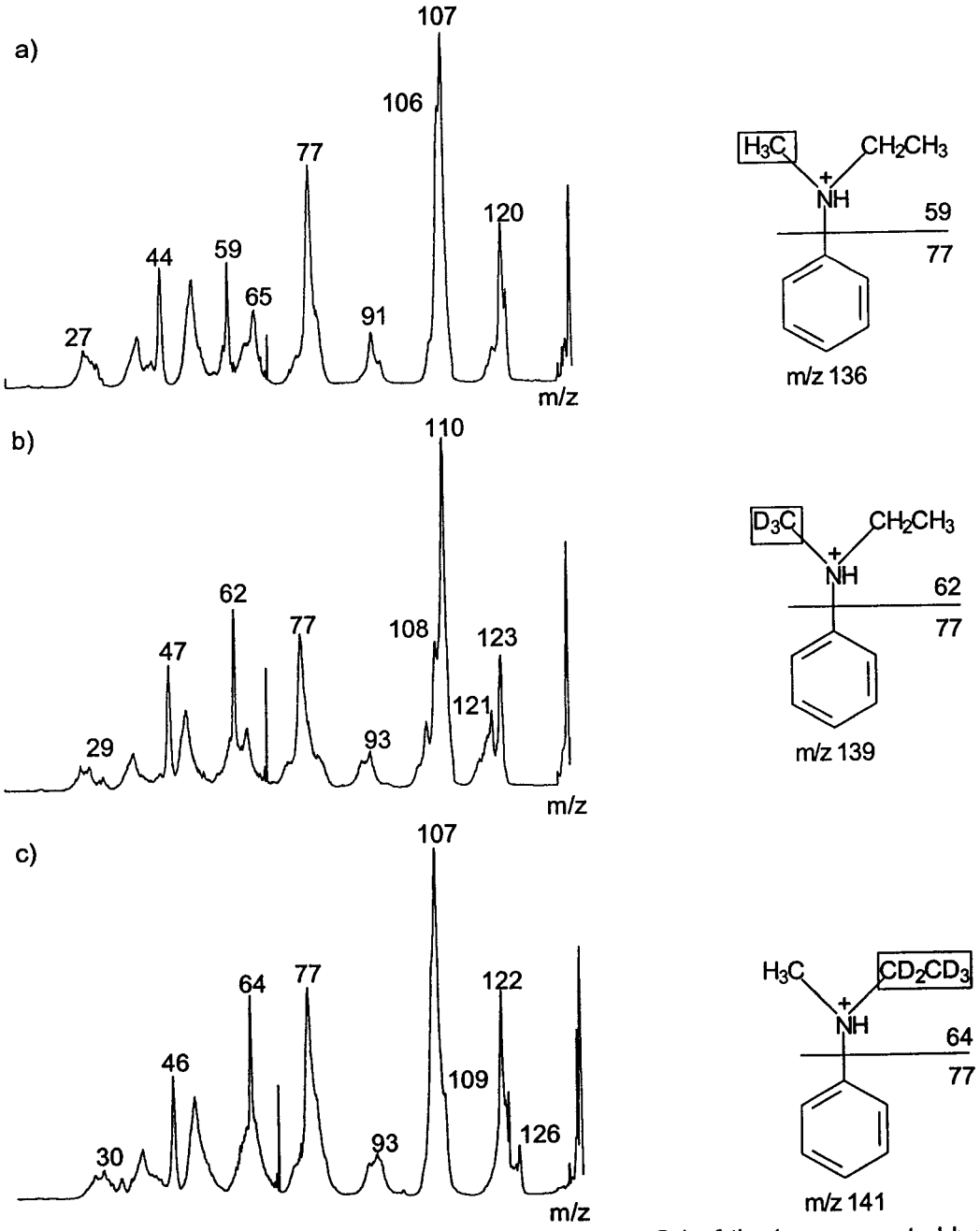

Figure 7-2: CID mass spectra (2ffr, 8 keV, collision gas O_2) of the ions generated by a) CH_3I alkylation of N-ethylaniline, b) CD_3I alkylation of N-ethylaniline and c) C_2D_5I alkylation of N-methylaniline. Proposed structures for m/z 136, m/z 139 and m/z 141 are given.

The peak at m/z 77 corresponds with $C_6H_5^+$ and this loss corroborates predominant N-alkylation. By contrast, the ion at m/z 91, which is most likely

$C_7H_7^+$, is more easily rationalized to result from ring-alkylation. Experiments were performed to investigate whether this ion does indeed result from ring-alkylation. A discussion of these results is given in the next section. Thus far, the experimental observations support *predominant* N-alkylation.

The base peak at m/z 107 in the CID mass spectra of Figure 7-1 corresponds with loss of $C_2H_5^{\bullet}$. Harrison [16b] recently reported that the base peak in the (cone voltage) CID spectrum of the m/z 136 ion generated from a solution of methylethylphenyl ammonium hydroxide corresponds with $C_2H_5^{\bullet}$ loss. This similarity between the CID mass spectrum obtained by Harrison [16b] and those presented in Figure 7-1 provides evidence for *predominant* N-alkylation.

In a study similar to ours, Cooks et al. [5] have reported that loss of $C_2H_5^{\bullet}$ dominates the CID spectrum of the m/z 122 ion generated by ethylation of aniline. This observation is also in agreement with the CID spectra shown in Figure 7-2.

II. C_2H_5I alkylation of *o*-, *m*- and *p*-toluidines and CH_3I alkylation of *o*-, *m*- and *p*-ethylanilines

In aromatic electrophilic substitution of aniline in the solution phase, the *ortho* and *para* positions are attacked, with a preference for the *para* position [21]. The $-NH_2$ group activates these positions (to attack) via a resonance effect. If there are ring-alkylation products when C_2H_5I alkylates N-methylaniline and CH_3I alkylates N-ethylaniline, then the CID mass spectra of the m/z 136 ions formed with the ring-(m)ethyl anilines will bear resemblance to the CID mass spectra shown in Figure 7-1.

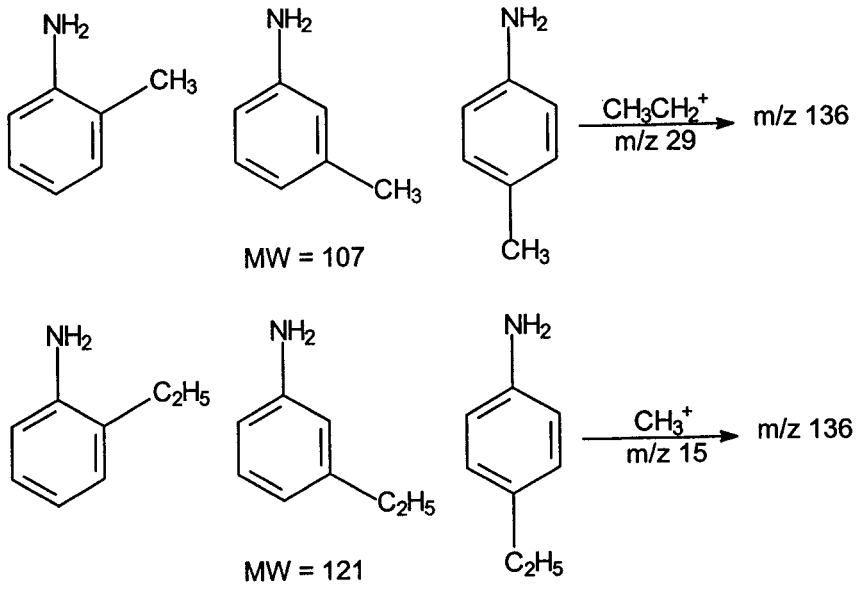

Scheme 3.

The desired m/z 136 ions were generated from the CH_3I alkylation of the *o*-, *m*- and *p*-ethylanilines and by C_2H_5I alkylation of the *o*-, *m*- and *p*-toluidines as outlined in Scheme 3. The CID mass spectra of the m/z 136 ions formed with the *o*-, *m*- and *p*-toluidines and the *o*-, *m*- and *p*-ethylanilines are presented in Figures 7-3 and 7-4, respectively.

The general appearance of the spectra of Figures 7-1, 7-3 and 7-4 can be summarized as follows:

1. The base peak at m/z 107 in the CID spectra of the m/z 136 ions formed by ethylation and methylation of the N-(m)ethylanilines corresponds to $C_2H_5^{\bullet}$ loss, see Figure 7-1.

2. The base peak at m/z 107 in the CID spectra of the m/z 136 ions formed by ethylation of the *m*- and *p*-toluidines also corresponds to $C_2H_5^{\bullet}$ loss. In the case of *o*-toluidine, the base peak at m/z 108 corresponds with loss of C_2H_4, see Figure 7-3.
3. The base peak at m/z 121 in the CID spectra of the m/z 136 ions formed by methylation of the *o*-, *m*- and *p*-ethylanilines corresponds to $CH_3^{\bullet}$ loss, see Figure 7-4. The spectrum also shows very intense charge-stripping peaks at m/z 60 and m/z 68.
4. The intensity ratio of the m/z 77 and m/z 91 ions in the spectra of Figures 7-1, 7-3, and 7-4 is considerably different. The ratio is lower for the alkylation products of the ring-alkyl anilines relative to the alkylation products of the N-alkyl anilines.

The CID mass spectra shown in Figures 7-3 and 7-4 do not extend to m/z 135. This part of the spectra was not recorded because there is an overwhelmingly intense peak at m/z 135. The CID mass spectra shown in Figure 7-3 contained peaks at m/z 44, $C_2H_6N^+$, and m/z 30, $H_2C{=}NH_2^{\bullet+}$. These ions are indicative of N-ethylation and it was expected that their relative intensities would be comparable to those of the m/z 59 and m/z 44 ions of Figure 7-1.

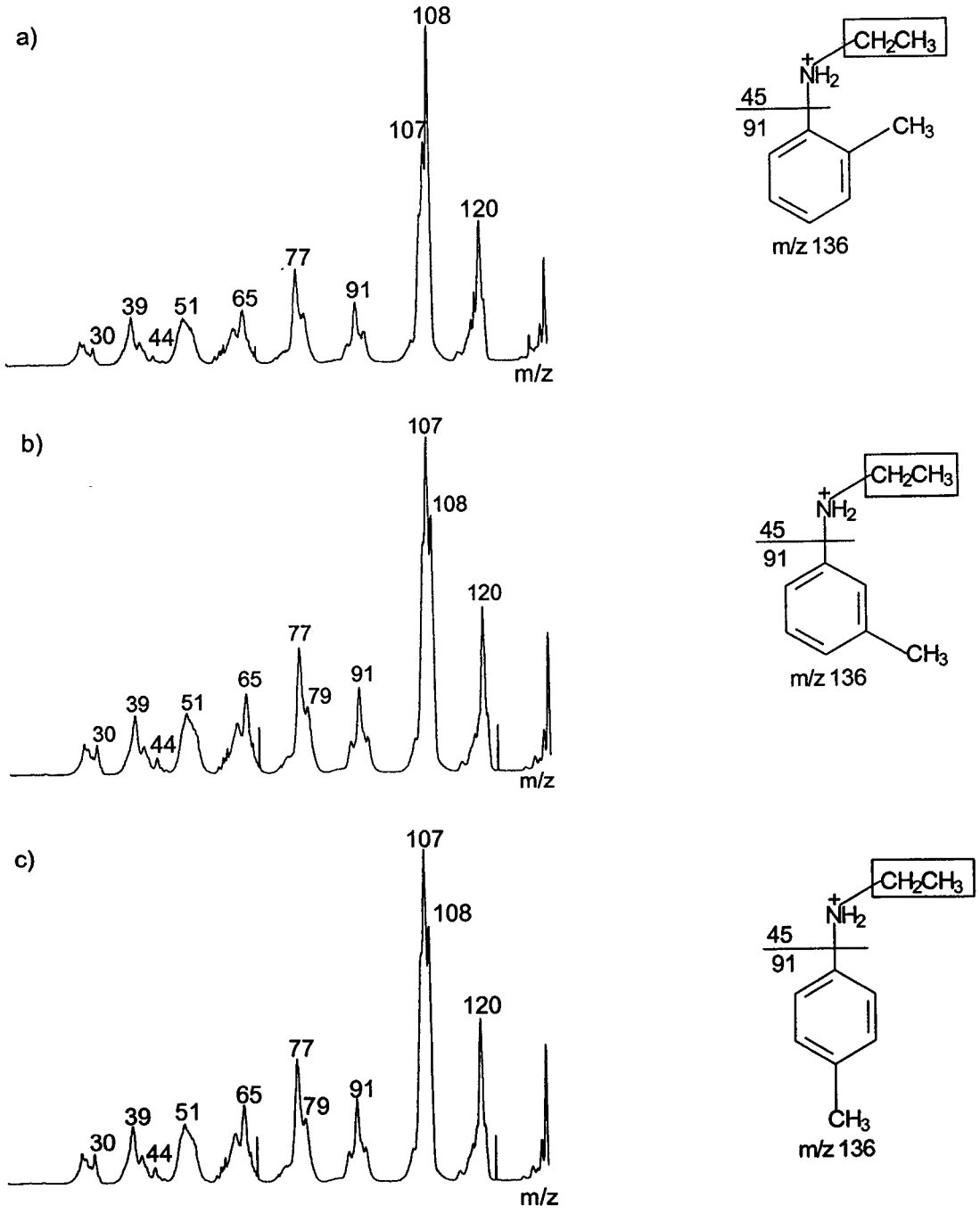

Figure 7-3: CID mass spectra (2ffr, 8 keV, collision gas O_2) of the $C_9H_{14}N^+$ (m/z 136) ions formed by C_2H_5I alkylation of a) *o*-toluidine, b) *m*-toluidine and c) *p*-toluidine. Proposed structures for the m/z 136 isomers are given.

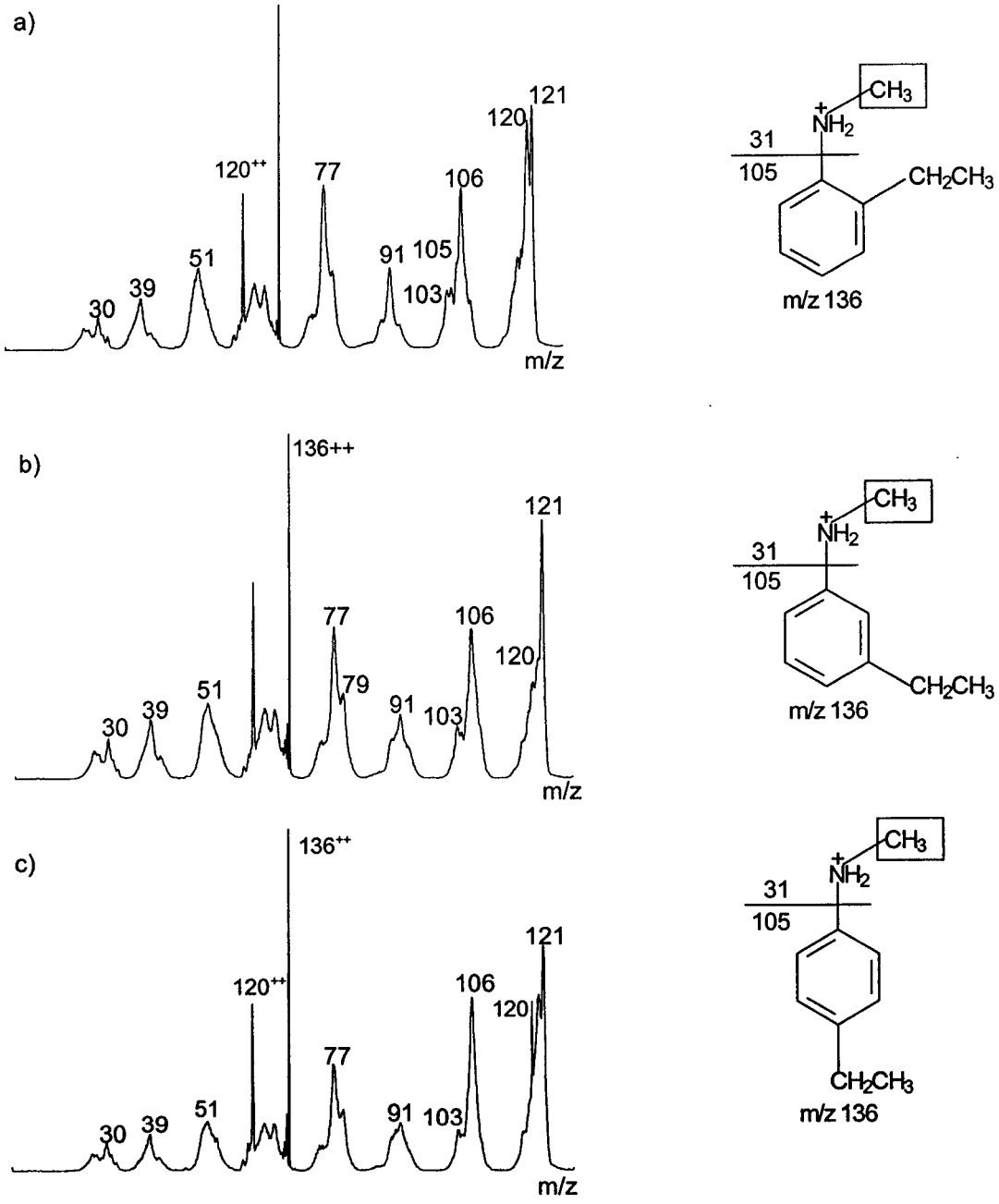

Figure 7-4: CID mass spectra (2ffr, 8 keV, collision gas O_2) of the $C_9H_{14}N^+$ (m/z 136) ions formed by CH_3I alkylation of a) *o*-ethylaniline, b) *m*-ethylaniline and c) *p*-ethylaniline. Proposed structures for the m/z 136 isomers are given.

Furthermore, direct bond cleavage of the phenyl-N bond in the m/z 136 isomers shown in Figure 7-3 should generate the $[CH_3CH_2NH_2]^{\bullet+}$ ion (plus C_7H_7 neutral), and the $C_7H_7^+$ ion (plus the $CH_3CH_2NH_2$ neutral), but not m/z 44 $[C_2H_6N]^+$. These observations may be interpreted by considering the energy requirements for the pathways leading to the generation of m/z 44, m/z 45, and m/z 91.

The m/z 91 ion, $C_7H_7^+$, in Figure 7-3 is generated by direct bond cleavage of the phenyl-N bond. The ionization energy of C_7H_7 is 6.2 eV while that of $CH_3CH_2NH_2$ is considerably higher, 8.9 eV [27]. Therefore, it is not surprising that $C_7H_7^+$, m/z 91, and not $[CH_3CH_2NH_2]^{\bullet+}$, m/z 45, is observed in the CID mass spectra shown in Figure 7-3. It also follows that m/z 45 is probably not the precursor ion of m/z 44.

As mentioned, a very intense m/z 135 peak is observed in the CID of the m/z 136 isomers formed by C_2H_5I alkylation of the toluidines. Thus, it is reasonable to propose that the m/z 44 ion, $[C_2H_6N]^+$, results from the consecutive losses of $H^\bullet$ (to form an m/z 135 ion) and C_7H_7. This pathway also requires phenyl-N bond cleavage but the ionization energies of C_2H_6N and $C_7H_7^\bullet$ are comparable, ~ 6.2 eV [27]. Moreover, the pathway leading to the formation $C_2H_6N^+$ is energetically more favourable, by 13 kcal/mol, than the pathway leading to formation of $C_7H_7^+$ via m/z 135.

The CID mass spectra in Figure 7-4 contain signals at m/z 30, CH_4N^+, and m/z 105, $C_8H_9^+$. The presence of these ions supports N-alkylation. It is proposed that $C_8H_9^+$, m/z 105, is formed by direct bond cleavage of the phenyl-N bond in the m/z 136 isomers formed by C_2H_5I alkylation of the *o*-, *m*- and *p*-ethylanilines; see Figure 7-4. The most likely mechanism for the generation of

m/z 30 is similar to that described for m/z 44. The ionization energy of CH_3NH_2 is ~ 9.0 eV, higher than any of the C_8H_9 isomers given in Reference 27. Therefore, m/z 30 is most likely formed by the consecutive losses of $H^{\bullet}$ and C_8H_9. The CID mass spectra shown in Figures 7-1, 7-3 and 7-4 provide evidence for predominant N-alkylation of N-ethyl-, and N-methylaniline using CH_3I and C_2H_5I, respectively, but as mentioned before, the peak at m/z 91 seems to be indicative of ring-alkylation.

The m/z 91 ion presumably has the elemental composition C_7H_7, considering that alkyl-phenyl containing compounds abundantly generate $C_7H_7^+$ ions [25]. The $C_7H_7^+$ ions formed from alkyl-phenyl containing compounds have the tropylium ion structure. However, it is conceivable that an ion with the elemental composition C_6H_6N contributes to the signal at m/z 91. The structure of the m/z 91 ion observed in the CID spectrum of Figure 7-1a was probed by obtaining its CID spectrum and comparing this spectrum with that of m/z 91 ions having the $C_7H_7^+$ tropylium structure. The results are presented in Figure 7-5 and the close resemblance between the two spectra leaves little doubt that the m/z 91 ions in the CID spectrum of Figure 7-1 have the tropylium ion structure.

During the comparison of the spectra of Figures 7-1, 7-3 and 7-4, it was observed that the ion intensity ratio m/z 77:m/z 91 in the CID mass spectra of the CH_3I and C_2H_5I alkylation products of the ring-ethyl anilines and toluidines, respectively, is lower than that observed for the CH_3I and C_2H_5I alkylation products of N-ethylaniline and N-methylaniline, respectively; see Figures 7-1, 7-3 and 7-4.

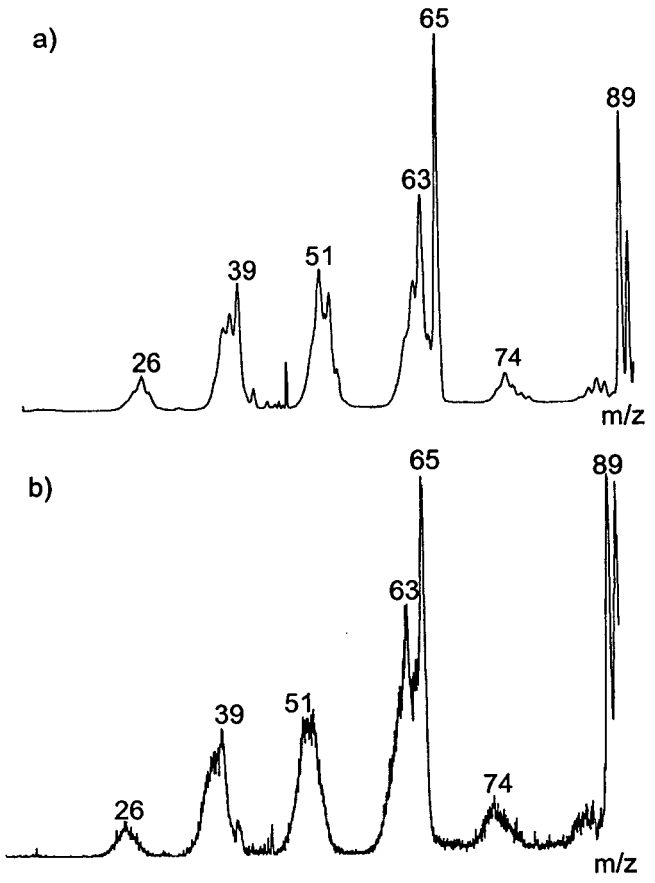

Figure 7-5: CID mass spectra (3ffr, 5 keV, collision gas O_2) of the $C_7H_7^+$, m/z 91 ions from a) toluene and b) the m/z 136 ion formed from the CH_3I alkylation of N-ethylaniline.

The m/z 77 : m/z 91 intensity ratio is ca. 1.4 for the m/z 136 ions formed by C_2H_5I alkylation of the *o*-, *m*- and *p*-toluidines, and is ca. 2.1 for the m/z 136 ions formed by CH_3I alkylation of the *o*-, *m*- and *p*-ethylanilines. The ratio becomes 4 when the m/z 136 ion is formed by C_2H_5I and CH_3I alkylation of N-methylaniline and N-ethylaniline, respectively. A ratio of 5 is observed in the CID spectrum of the odd-electron ion at m/z 135 resulting from the ionization of N-ethyl-N-methylaniline, see Figure 7-6.

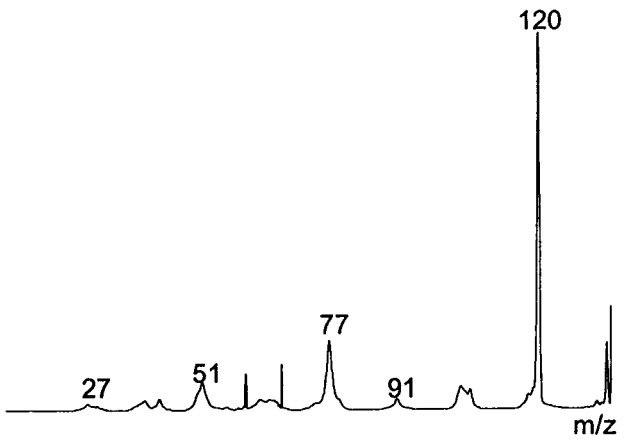

Figure 7-6: CID mass spectrum (2ffr, 8 keV, collision gas O_2) of ionized N-ethyl-N-methylaniline, m/z 135.

It is obvious that the CH_3– and C_2H_5– substituents in N-ethyl-N-methylaniline are bonded to the N-site. The CID spectrum of this odd-electron ion may therefore be used to obtain an approximation of the extent to which the m/z 91 ion is formed relative to the m/z 77 ion.

The difference in the m/z 77 : m/z 91 intensity ratios in the CID mass spectra of Figures 7-3 and 7-4 is attributed to the fact that the toluidines generate the m/z 91 ion via a *single* bond cleavage reaction. This pathway is not available to the m/z 136 ions formed by CH_3I alkylation of the *o*-, *m*- and *p*-ethylanilines. The m/z 136 ions shown in Figure 7-4 can only form from the m/z 91 ion via a rearrangement. The observation that the m/z 77 : m/z 91 ratio in Figure 7-1 is closer in value to that observed in Figure 7-6, *relative* to that observed in Figures 7-3 and 7-4 may be used as a corollary to N-alkylation. The ratio cannot be used as an absolute measure for N-alkylation.

III. Gas-phase protonation experiments of N-ethyl-N-methylaniline, N-ethyl-*o*-toluidine and 6-ethyl-*o*-toluidine

Harrison and Tu [16a] have used MI and low-energy CID spectra to probe the structure of protonated N-(m)ethylaniline and N,N-di(m)ethylaniline obtained by chemical ionization experiments with methane, acetone, methanol and isobutyl amine as reagent gases. The MH^+ ions of the anilines were also generated by FAB ionization using an acidified glycerol matrix. They observed a significant H_2 loss in the MI and low-energy CID spectra of the MH^+ ions formed with methane, acetone and methanol as a reagent gas, but this loss was absent in the MI and low-energy CID spectra of the MH^+ ion formed with *i*-$C_4H_9NH_2$ CI and also by FAB ionization. Furthermore, it was observed that the peak corresponding to the loss of H_2 in the MI and low-energy CID spectra of the MH^+ ion formed by acetone CI was of lower intensity relative to that observed with methane and methanol.

An explanation of these observations is based on differences in proton affinity (PA) values of the reagent gases. Harrison and Tu [16a] argue that the protonation of the N-alkylanilines with CH_5^+, $CH_3OH_2^+$ and $[(CH_3)_2C\text{-}OH]^+$ is exothermic for protonation at the ring and at the N-site. In contrast, protonation with i-$C_4H_9NH_3^+$ is endothermic for ring-protonation and so this reactant ion will be more selective in its site of protonation. The FAB ionization experiments were performed on samples in an acidified liquid matrix. Since anilines are nitrogen bases in solution, it is reasonable to assume that they are protonated at the N-site in the liquid phase. Therefore, the mass-selected ions in the (FAB) MI and low-energy CID experiments are MH^+ ions that are pre-formed in solution and thus N-protonated.

To obtain further evidence for the structure proposal of Scheme 2, m/z 136 ions were also generated by protonation of N-ethyl-N-methylaniline. Using the results of the above study [16a] as a guide, both methanol and acetone, as well as their deuterium isotopologues, were used as the CI reagents in these protonation experiments. The CI experiment with acetone yields a CID mass spectrum that resembles the CID mass spectra of Figure 7-1: compare Figures 7-1 and 7-7a. The spectrum shows peaks at m/z 44 and m/z 59. These observations support predominant formation of the N-ethyl-N-methylanilinium ion, and thus N-protonation. When fully deuterated acetone is used as the reagent gas the m/z 136 ion shifts to m/z 137. The CID mass spectrum of this m/z 137 ion is shown in Figure 7-7b.

The structure-diagnostic ions at m/z 44 and m/z 59 in Figures 7-1 and 7-7a are shifted to m/z 45 and m/z 60 in Figure 7-7b. The observation that both m/z 120 and m/z 121 are present in Figure 7-7b indicates that loss of CH_4 (or $^{\bullet}CH_3 + H^{\bullet}$) does not *only* involve the H bonded to the N-atom.

The CID spectra of the m/z 136 ions obtained by protonation of N-ethyl-N-methylaniline with methanol and acetone are not the same, and moreover the spectrum of Figure 7-7c differs from the alkylation experiments of Figure 7-1. The CID spectrum of the product of the ion-molecule reaction between N-ethyl-N-methylaniline and methanol also shows lower intensities for the signals at m/z 44 and m/z 59 relative to the m/z 136 ion formed with acetone, see Figure 7-7c.

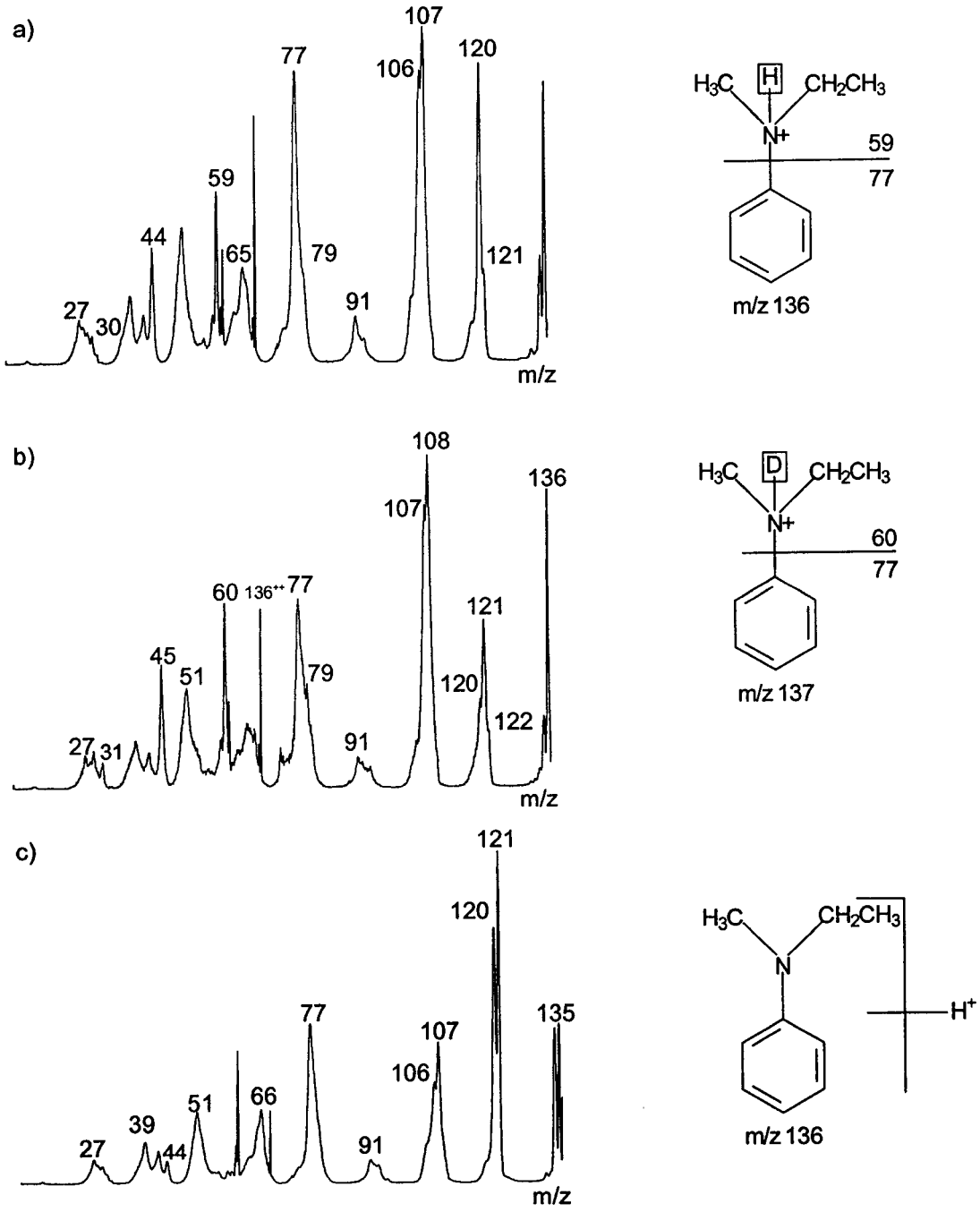

Figure 7-7: CID mass spectra (2ffr, 8 keV, collision gas O_2) of the m/z 136 ion formed by $CH_3C(=O)CH_3$ CI of N-ethyl-N-methylaniline, item a, the m/z 137 ion formed by $CD_3C(=O)CD_3$ CI of N-ethyl-N-methylaniline, item b, and the m/z 136 ion formed by CH_3OH CI of N-ethyl-N-methylaniline, item c. Proposed structures for m/z 136, and m/z 137 are given.

The differences in the CID spectra of Figures 7-7a and 7-7c are a result of the difference between the proton affinity (PA) values of acetone and methanol, 194 kcal/mol and 180 kcal/mol, respectively [28]. The PA of N-ethyl-N-methylaniline is 224 kcal/mol [28] and thus the protonation with acetone will be less exothermic, by 14 kcal/mol, than protonation with methanol. It has been reported that the difference in PA between the N- and *para* ring C-site in aniline is only 1-3 kcal/mol [2,3]. The difference between the PA values of these sites is probably larger in N-ethyl-N-methylaniline because of the inductive effects of the CH_3– and C_2H_5– substituents. Therefore, the excess 14 kcal/mol in the protonation reaction between $CH_3OH_2^+$ and N-ethyl-N-methylaniline may be sufficient to accomplish both ring- and N-protonation.

In order to investigate whether *o*-toluidine is indeed N-ethylated (Figure 7-3a), N-ethyl-*o*-toluidine and 6-ethyl-*o*-toluidine were protonated using acetone, and the CID spectra of the resulting m/z 136 ions are presented in Figure 7-8.

It was expected that the CID mass spectrum of Figure 7-3a would bear more resemblance to that of protonated N-ethyl-*o*-toluidine, see Figure 7-8b, than that of protonated 6-ethyl-*o*-toluidine, see Figure 7-8a. The general observation is that the CID mass spectrum of Figure 7-3a is different from those in Figure 7-8. It is exciting to observe that CID of the m/z 136 ion formed by C_2H_5I alkylation of *o*-toluidine differs from that of protonated 6-ethyl-*o*-toluidine: compare Figures 7-3a and 7-8a. However, it is disappointing to see that the m/z 136 ion formed by protonation of N-ethyl-*o*-toluidine is *also* different from that formed by C_2H_5I alkylation of *o*-toluidine. A discussion of the CID spectra shown

in Figure 7-8 is made with regard to those presented in Figure 7-3, and Figure 7-7.

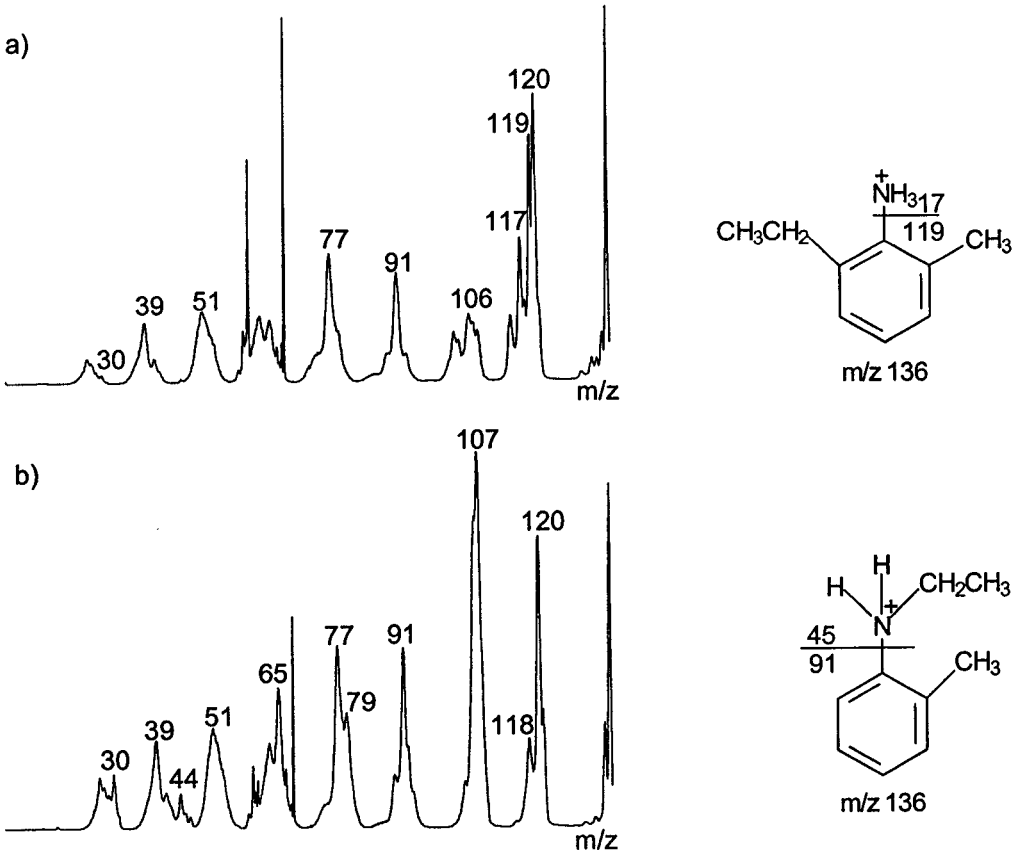

Figure 7-8: CID mass spectra (2ffr, 8 keV, collision gas O_2) of the m/z 136 ion formed by $CH_3C(=O)CH_3$ CI of 6-ethyl-*o*-toluidine, item a, and $CH_3C(=O)CH_3$ CI of N-ethyl-*o*-toluidine, item b. Proposed structures of the m/z 136 isomers are given.

Both m/z 30, CH_4N^+, and m/z 44, $C_2H_6N^+$, are product ions of the m/z 136 ion formed via protonation of N-ethyl-*o*-toluidine, as well as C_2H_5I alkylation of *o*-toluidine; see Figures 7-3a and 7-8b. The presence of m/z 30 and m/z 44 in Figure 7-8b provides more evidence that acetone protonates predominantly at the N-site. The intensities of the peaks at m/z 30 and m/z 44 relative to the peak at m/z 77 are similar for the CID spectra shown in Figures 7-3a and 7-8b. This

observation suggests that a fraction of the m/z 136 ions formed by acetone CI of N-ethyl-*o*-toluidine and C_2H_5I alkylation of *o*-toluidine have the same structure. This follows from the fact that m/z 30 and m/z 44 will be observed in the CID spectra of these m/z 136 ions – formed by acetone CI of N-ethyl-*o*-toluidine and C_2H_5I alkylation of *o*-toluidine – *only* when these m/z 136 ions have the same structure.

One final note is made about the CID mass spectra of the m/z 136 ions shown in Figures 7-1, 7-3, 7-4 and 7-8. The ions are made via different routes. In other words, the ion-molecule reactions yielding the m/z 136 ions involve different ions and molecules which differ in their thermochemistry. This discussion addresses the fact that each of the molecules used in this work has a different proton affinity (PA).

The PA of N-methylaniline is 5 kcal/mol higher than that of *o*-toluidine, and 8 kcal/mol higher than that of aniline [28] and these differences reflect the inductive effect of the $-CH_3$ substituent. Since the PA of *o*-toluidine differs from that of N-methylaniline, it is reasonable to assume that the PA's of the *o*-, *m*-, and *p*-toluidines and the *o*-, *m*-, and *p*-ethylanilines are also different from those of N-methylaniline and N-ethylaniline. It is not without precedent to use PA values to indicate the most favourable site of *electrophile* attachment [5]. Since the PA values for *o*-toluidine and N-methylaniline are different, it is not unreasonable to expect that the most favourable site for electrophile attachment may also be different. This point should be considered in the interpretation of the CID spectra of Figures 7-1, 7-3, 7-4, and 7-8.

Conclusions

In general, alkylation of N-(m)ethylaniline using CH_3I and C_2H_5I results predominantly in N-alkylation. The CID spectra of the product of these ion-molecule reactions show peaks characteristic of N-alkylation. These structure-diagnostic signals appear at m/z 59 and m/z 44 and correspond to $[CH_3CH_2N(H)CH_3]^{\bullet+}$ and $^{+}[CH_2N(H)CH_3]$, respectively. The mass spectra of the alkylation of N-(m)ethylaniline with C_2D_5I and CD_3I show the corresponding shift in mass for the ion assigned as the alkylation product and thus the mass-selected ion for the MI and CID experiments. The expected increase in mass for m/z 44 and m/z 59 is observed in these labelling experiments.

Further evidence for predominant N-alkylation is obtained from comparative CID spectra of the $C_2H_5^+$ and CH_3^+ attachment ions of the toluidines and the ring-ethyl anilines. These CID spectra are different from that of the m/z 136 ion formed from C_2H_5I and CH_3I alkylation of N-(m)-ethylaniline. The most notable difference is the increase in the intensity ratio of m/z 77 : m/z 91 in the CID spectra of the alkylation product (m/z 136) of the N-alkylanilines relative to the ring-alkyl anilines. The difference is a corollary to N-alkylation of these anilines, and is not a means to determine (absolutely) the extent of N-alkylation versus ring-alkylation.

The m/z 136 ion is also formed by protonation of N-ethyl-N-methyaniline with acetone and methanol. It is observed that protonation of N-ethyl-N-methylaniline with acetone, but not methanol, yields an m/z 136 ion which is similar in structure to the m/z 136 ion formed by C_2H_5I and CH_3I alkylation of N-(m)ethylaniline. Thus there is predominant N-protonation. These observations

are further probed by generating m/z 136 isomers by acetone protonation of N-ethyl-*o*-toluidine and 6-ethyl-*o*-toluidine. The latter m/z 136 ions produced CID mass spectra which provided evidence that C_2H_5I alkylation of *o*-toluidine is different from the m/z 136 ion formed by acetone protonation of N-ethyl-*o*-toluidine and 6-ethyl-*o*-toluidine. The CID mass spectra of the m/z 136 ion resulting from acetone protonation of N-ethyl-*o*-toluidine confirm this CI reagent protonates predominantly at the N-site.

References

[1] a. Y.K. Lau and P. Kebarle, *J. Am. Chem. Soc.*, **1976**, *98*, 7452. b. W.J. Hehre, R.T. McIver Jr., J.A. Pople and P.v.R. Schleryer, J. Am. Chem. Soc., **1974**, *96*, 7162.

[2] S.K. Pollack, J.L. Devlin, III, K.D. Summerhays, R.W. Taft and W.J. Hehre, *J. Am. Chem. Soc.*, **1977**, *99*, 4853.

[3] K.D. Summerhays, S.K. Pollack, R.W. Taft and W.J. Hehre, *J. Am. Chem. Soc.*, **1977**, *99*, 4585.

[4] A. Maquestiau, Y.V. Haverbeke, H. Mispreuve, R. Flammang, J.A. Harris, I. Howe and J.H. Beynon, *Org. Mass Spectrom.*, **1980**, *15*, 144.

[5] K.V. Wood, D.J. Burinsky, D. Cameron and R.G. Cooks, *J. Org. Chem.*, **1983**, *48*, 5236.

[6] M. Attina and F. Cacace, *J. Am. Chem. Soc.*, **1983**, *105*, 1122.

[7] D.J. Burinsky and J.E. Campana, *Org. Mass Spectrom.*, **1984**, *19*, 539.

[8] A.G. Harrison, *Org. Mass Spectrom.*, **1986**, *64*, 1051.

[9] M.J.S. Dewar and K.M. Dieter, *J. Am. Chem. Soc.*, **1986**, *108*, 8075.

[10] S.T. Pachuta, I. Isern-Flecha and R.G. Cooks, *Org. Mass Spectrom.*, **1986**, *21*, 1.

[11] D.J. Burinsky and J.E. Campana, *Org. Mass Spectrom.*, **1988**, *23*, 613.

[12] R.L. Smith, L.J. Chyall, B.J. Beasley and H.I. Kenttamaa, *J. Am. Chem. Soc.*, **1995**, *117*, 7971.

[13] M.J. Nold and C. Wesdemiotis, *J. Mass Spectrom.*, **1996**, *31*, 1169.

[14] R.K. Roy, F. de Proft and P. Geerlings, *J. Phys. Chem. A*, **1998**, *102*, 1035.

[15] M. Tsuji, T. Arikawa and Y. Nishimura, *Bull. Chem. Soc. Jpn.*, **1999**, *72*, 293.

[16] a. A.G. Harrison and Y.-P. Tu, *Int. J. Mass Spectrom.*, **2000**, *195/196*, 33. b.A.G. Harrison, *J. Mass Spectrom.*, **1999**, *34*, 1253.

[17] N. Russo, M. Toscano, A. Grand and T. Mineva, *J. Phys. Chem. A*, **2000**, *104*, 4017.

[18] Y.K. Lau, K. Nishizawa, A. Tse, R.S. Brown and P. Kebarle, *J. Am. Chem. Soc.*, **1981**, *103*, 6291.

[19] P. Sjoberg, J.S. Murray, T. Brinck and P. Politzer, *Can. J. Chem.*, **1998**, *68*, 1440.

[20] K.L. Busch, G.L. Glish and S.A. McLuckey, *Mass Spectrometry/Mass Spectrometry: Techniques and Applications of Tandem Mass Spectrometry*, VCH Publishers Inc., New York (1988)

[21] A. Streitweiser, C.H. Heathcock and E.M. Kosower, *Introduction to Organic Chemistry*, 4th Ed., Macmillan Publishing Company Inc., New York (1992)

[22] K. Levsen and H. Schwarz, *Mass Spectrom. Rev.*, **1982**, *2*, 77.

[23] H.F. van Garderen, P.J.A. Ruttink, P.C. Burgers, G.A. McGibbon, J.K. Terlouw, *Int. J. Mass Spectrom. Ion Processes*, **1992**, *121*, 159.

[24] A.G. Harrison, *Chemical Ionization Mass Spectrometry*, 2nd Ed., CRC Press, Boca Raton (1992)

[25] F.W. McLafferty and F. Tureček, *Interpretation of Mass Spectra*, 4th Ed. University Science Books, California (1993)

[26] D. Kuck, *Mass Spectrom. Rev.*, **1990**, *9*, 583.

[27] S.G. Lias, J.E. Bartmess, J.F. Liebman, J.L. Holmes, R.D. Levin and W.G. Mallard, *J.Phys. Chem. Ref. Data 17* (1988)

[28] E.P.L. Hunter and S.G. Lias, *J.Phys. Chem. Ref. Data 27* (1998)

[29] J.L. Holmes, *Org. Mass Spectrom.*, **1985**, *20*, 169.

Chapter 8

Summary

The larger part of the thesis presents studies on the mass spectrometry of a class of triterpene glycosides, the ginsenosides, sugars and polyols using electrospray mass spectrometry of their metal ion or borate complexes. These complexes provide structural information, and in the case of VO^{++} and boric acid, the relative stereochemistry of hydroxyl groups.

Analysis of complexes formed in solution- as well as the gas-phase is suited to electrospray mass spectrometry because it is well-known that chemistry in both phases contributes to the ions observed in an electrospray mass spectrum. In line with the fact that chemical ionization involves gas-phase chemistry, a small chemical ionization mass spectrometry study on the alkylation reactions of N-ethylaniline and N-methylaniline with iodomethane and iodoethane, repectively, was also presented.

The first Chapter provides an overview of the concepts involved in the complexation chemistry of compounds containing hydroxyl groups, within which are sugars and ginsenosides. A brief overview of the mass spectrometry of sugars is discussed, including the structural information that is obtained with tandem mass spectrometry.

Chapters 2 and 3 present an MS/MS and LC/MS/MS study of ginsenosides, respectively. The first of these Chapters presents CID experiments of metal ion – the alkali metal ions as well as Ni^{++}, Co^{++} and Zn^{++} –

complexes of ginsenosides. It was observed that complexes with the smaller alkali metal ions, Li^+ and Na^+, provided more structural information. Tandem mass spectrometry of the transition metal ion complexes provided as much structural information as those with Li^+ and Na^+. In general, however, ginsenosides predominantly undergo dissociation at C20 with hydrogen transfer from the triterpene to the sugar.

The pattern of dissociation of ginsenoside standards under CID conditions was used to develop a LC/MS/MS approach for the separation and structural characterization of ginsenosides from root extracts. The ten standards (employed in Chapter 2) were used to develop the LC/MS methodology, and the pattern of their separation was applied to interpreting the separation of a more complex mixture. Both LC/MS and LC/MS/MS experiments were used to identify ginsenosides with known structures as well as to provide structure proposals for ten new ginsenosides.

Chapter 4 presented a combined MALDI-MS and ESMS study on a class of sulfated polysaccharides, the carrageenans. Like ginsenosides, these polysaccharides also provided a structural challenge. The carrageenans are comprised of galactose-derived disaccharide subunits containing various degrees of sulfation; Na^+ is the counterion. It was found that, in acidic media, carrageenans undergo exchange of Na^+ for H^+ and subsequent loss of SO_3. Thus, if an *iota*-carrageenan, which has two sulfates per subunit, was being analyzed then this latter process would generate the corresponding *kappa*-carrageenan which has one sulfate per subunit. This process is particularly important in the analysis of unknown mixtures of carrageenans.

Chapters 5 and 6 presented two approaches – based on complexation to boric acid and VO^{++} – aimed at differentiating geometric isomeric and stereoisomeric diols and sugars. Both approaches employed an internal standard, ethylene glycol, which is the simplest polyol that can form a complex with boric acid and VO^{++}. Complexation to boric acid as well as VO^{++} afforded differentiation between acyclic stereoisomeric diols and cyclic geometric isomeric diols. Additionally, both complexation agents were used for differentiating isomeric methyl glycosides and disaccharides. A comparison of the two approaches revealed that for a specific analyte at a fixed concentration, complexation to VO^{++} was ten times more sensitive than that with boric acid. This is useful since analytes that are available in low concentration may be best analyzed by VO^{++} complexation.

The final Chapter in this thesis presented alkylation reactions of *o*-, *m*- and *p*-ethylaniline, *o*-, *m*- and *p*-toluidine, and N-methyl- and N-ethylaniline with iodoethane and iodomethane to form isomeric m/z 136 ions. Iodoethane and iodomethane predominantly formed the N-alkylated aniline. This was confirmed by showing that the isomeric m/z 136 ions formed by alkylation of the ring-alkyl anilines had different structures from their N-alkyl counterparts.

Appendix

Section A.i.: Compendium of ginsenosides reported in Shoji's review [1]

Ginsenoside Rh_2 MW=622

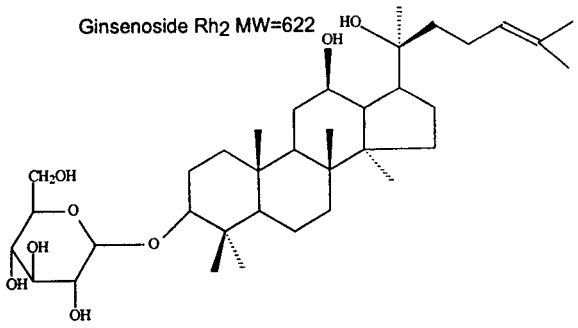

Chikusetsusaponin L10 MW=638

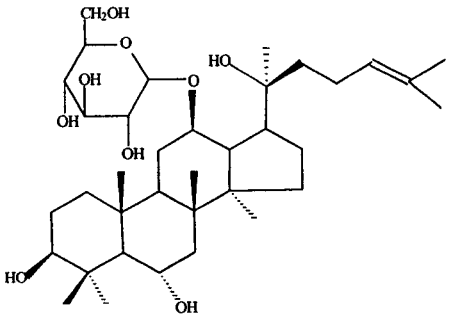

Ginsenoside F1 MW=638

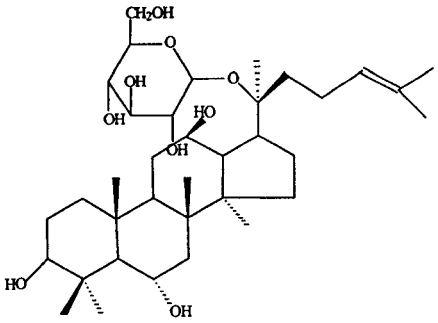

Ginsenoside Rh1 MW=638

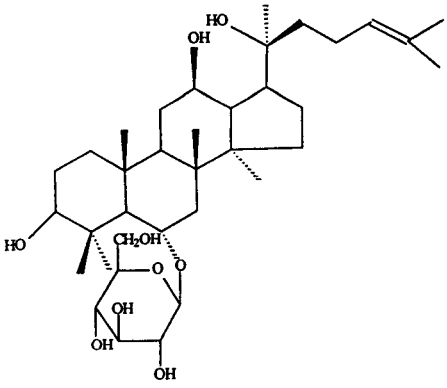

20-R-Ginsenoside Rh1 MW=638

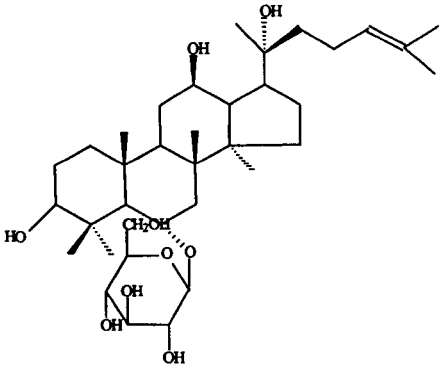

Pseudoginsenoside RT5 MW=654

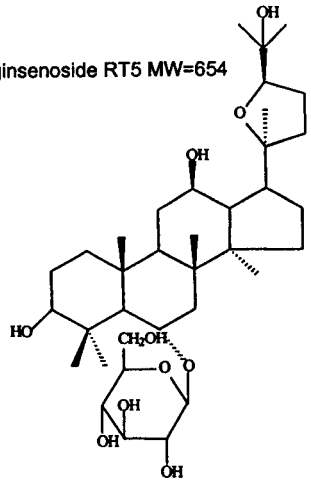

Ginsenoside M7cd MW=654

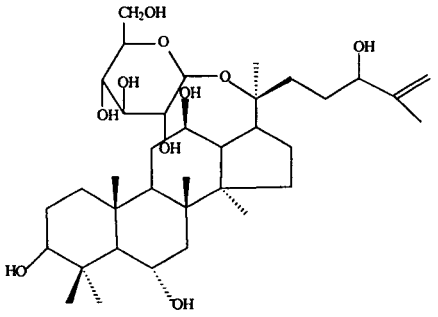

Pseudoginsenoside RT4 MW=654

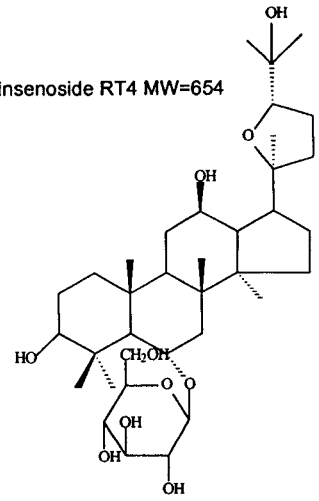

Chikusetsusaponin L9bc MW=654

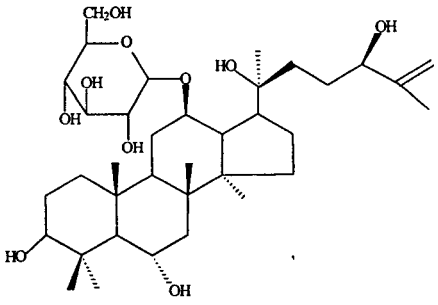

Chikusetsusaponin L9a MW=654

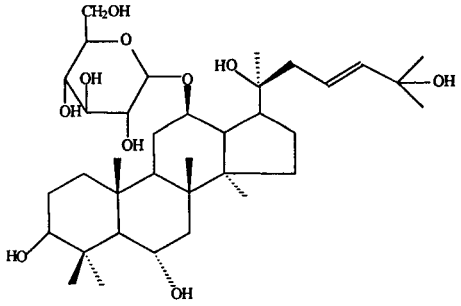

Pseudoginsenoside RP1 MW=724

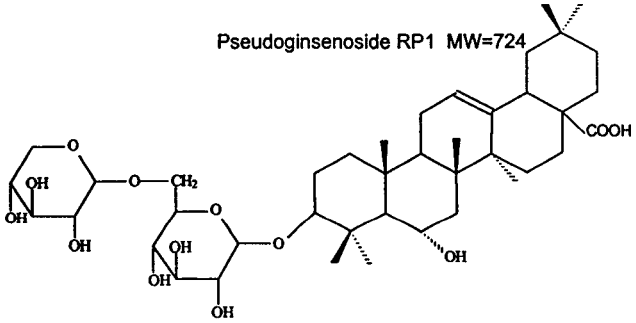

Chikusetsusaponin Ia MW=754

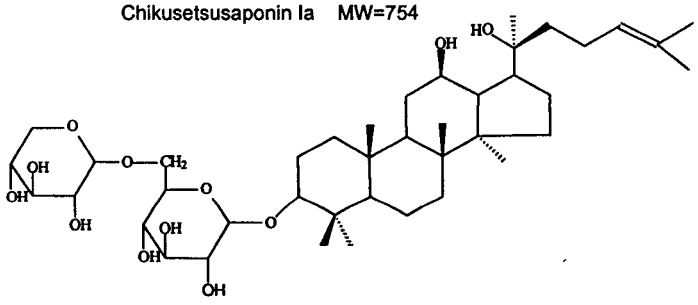

Section A.i.: Compendium of ginsenosides reported in Shoji's review [1]

Notoginsenoside R2 MW=770

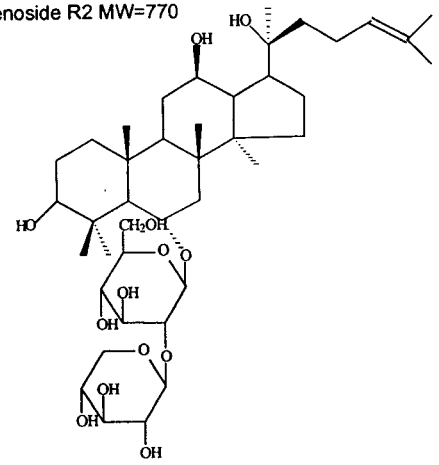

Ginsenoside F3 MW=770

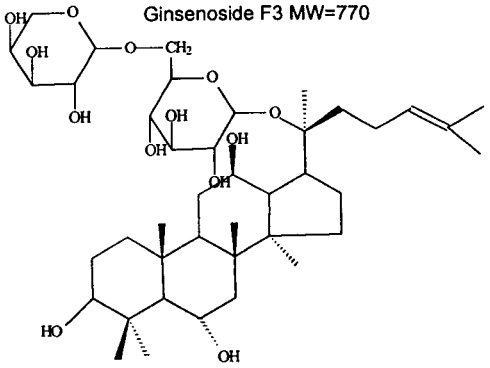

Pseudoginsenoside RT3 MW=770

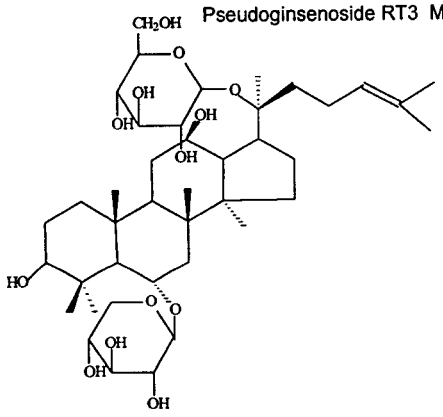

Chikusetsusaponin LT8 MW=782

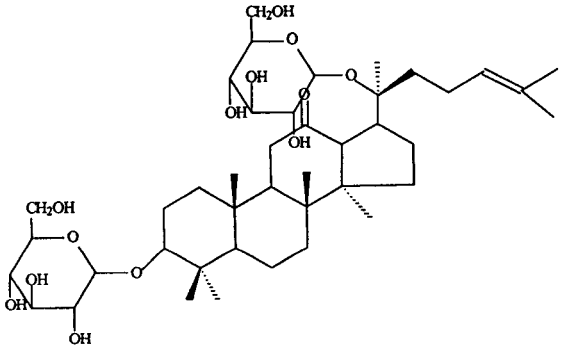

Ginsenoside F2 MW=784

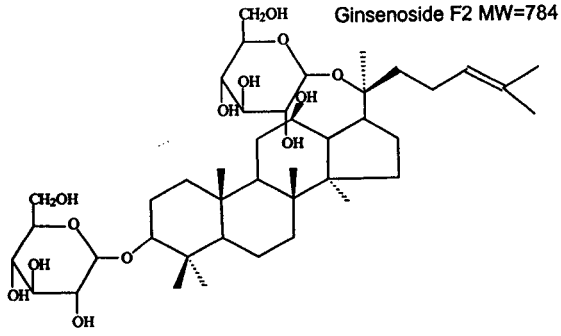

20-S-Ginsenoside Rg3 MW=784

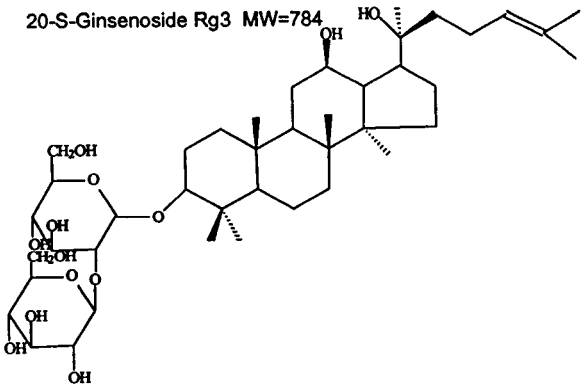

Section A.i.: Compendium of ginsenosides reported in Shoji's review [1]

20-R-Ginsenoside Rg2 MW=784

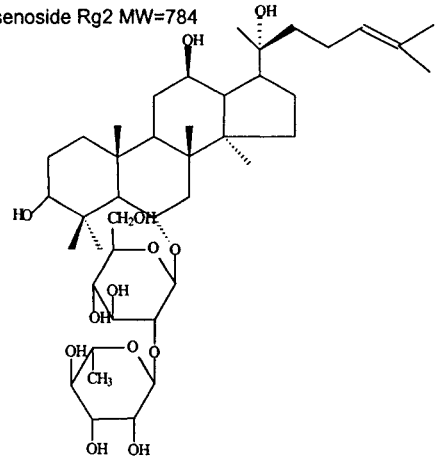

Ginsenoside Rg2 MW=784

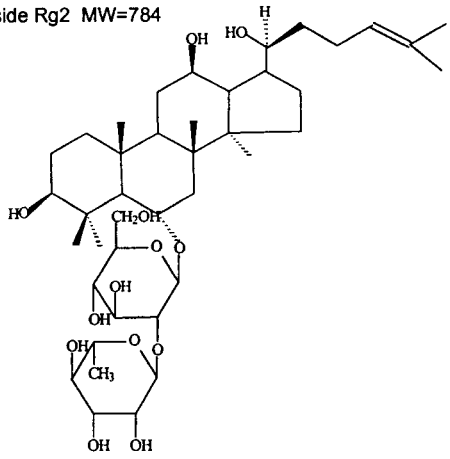

Ginsenoside Rg3 MW=784

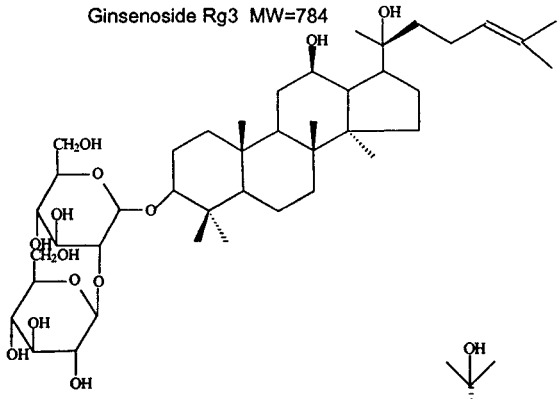

Pseudoginsenoside RT2 MW=786

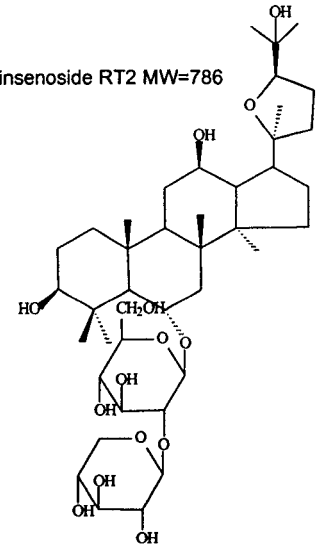

Majonoside R2 MW=786

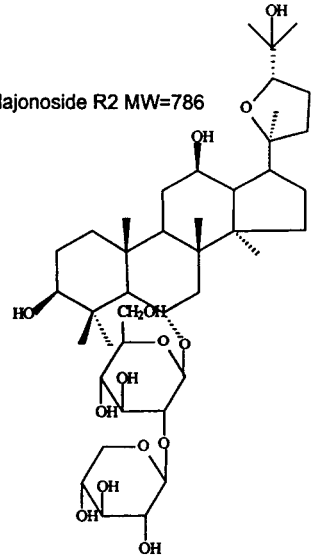

Chikusetsusaponin IV A MW=794

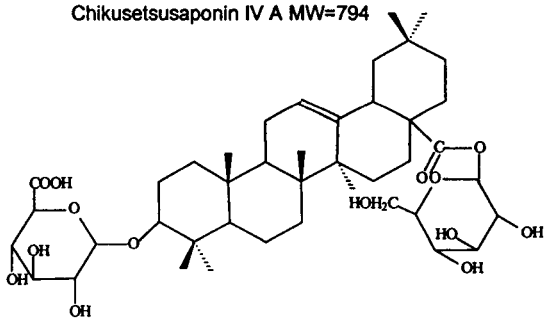

Section A.i.: Compendium of ginsenosides reported in Shoji's review [1]

Ginsenoside Rg1 MW=800

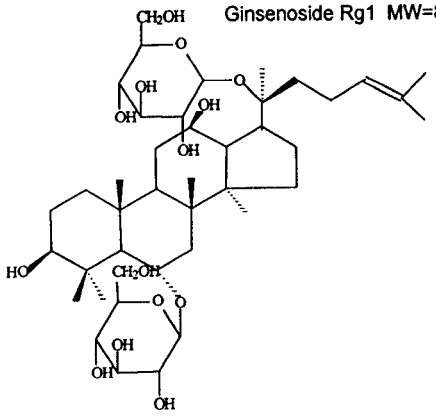

Pseudoginsenoside F11 MW=800

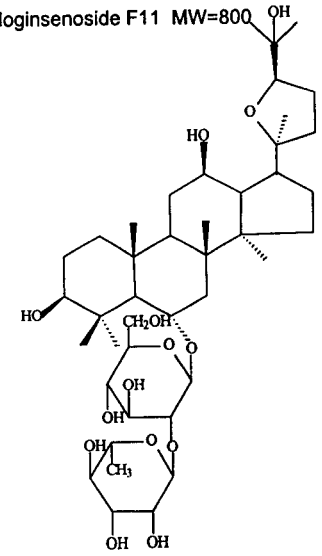

Ginsenoside Rf MW=800

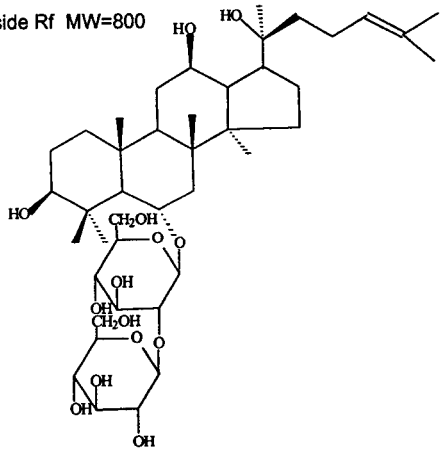

Majonoside R1 MW=816

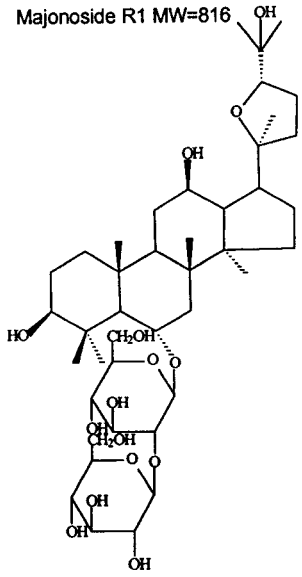

Chikusetsusaponin L5 MW=902

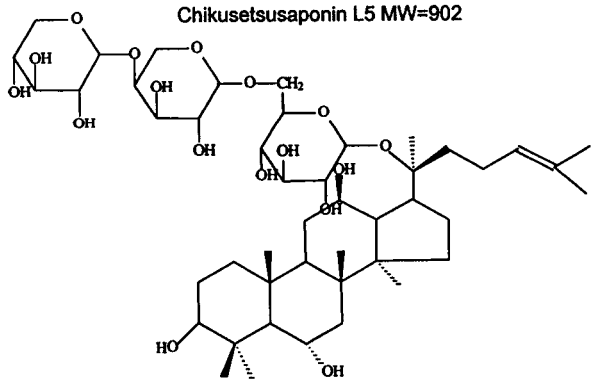

Notoginsenoside Fe MW=916

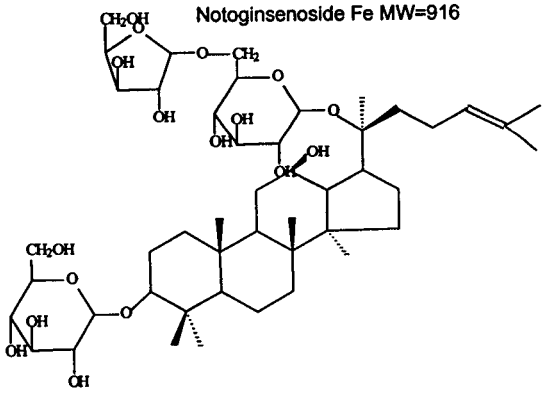

Section A.i.: Compendium of ginsenosides reported in Shoji's review [1]

Chikusetsusaponin III MW=916

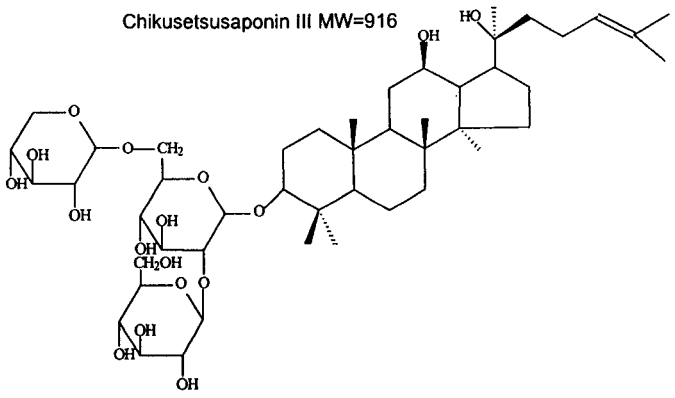

Gypenoside IX MW=916

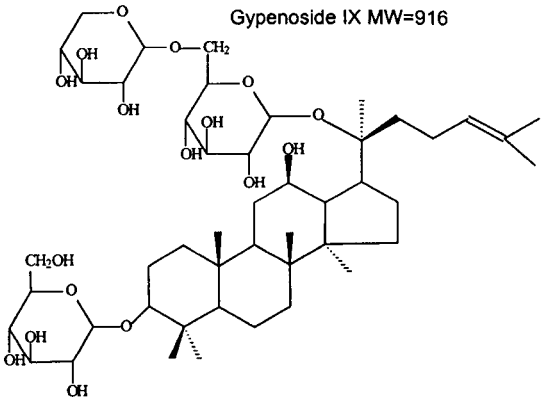

Chikusetsusaponin IV MW=926

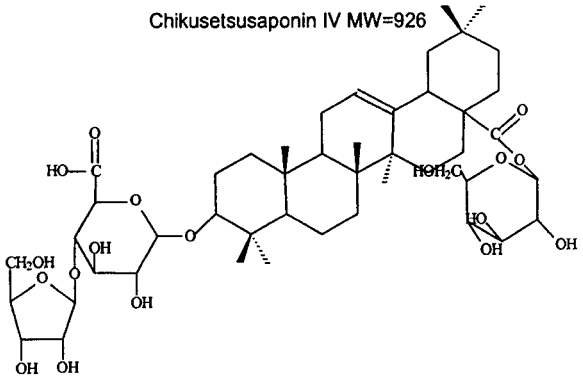

Pseudoginsenoside RT 1 MW=926

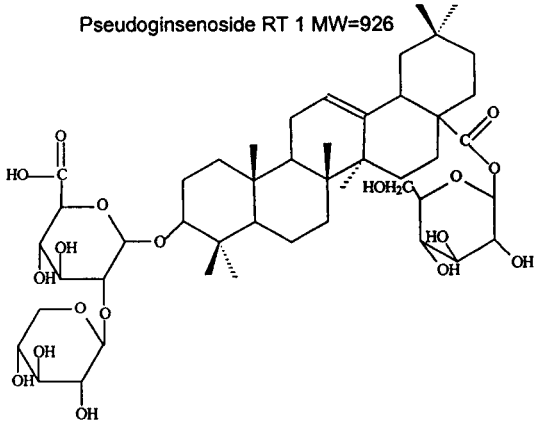

Notoginsenoside R1 MW=932

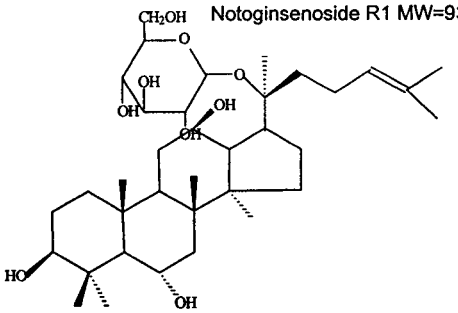

Chikusetsusaponin LT5 MW=944

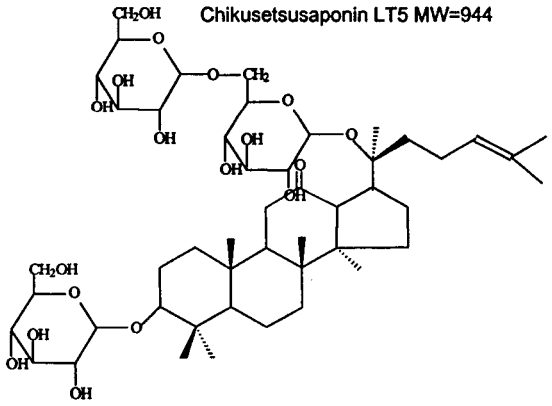

Gypenoside XVII MW=946

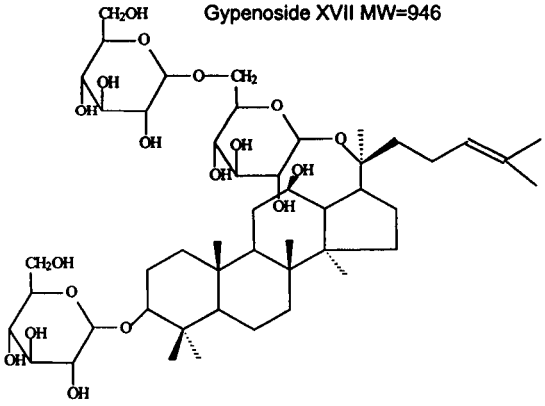

Section A.i.: Compendium of ginsenosides reported in Shoji's review [1]

Ginsenoside Rd MW=946

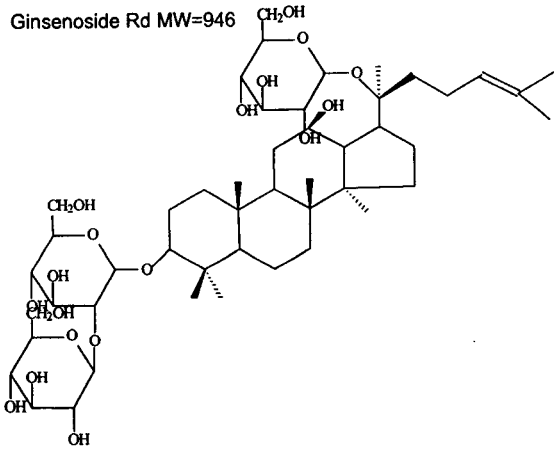

Ginsenoside Re MW=946

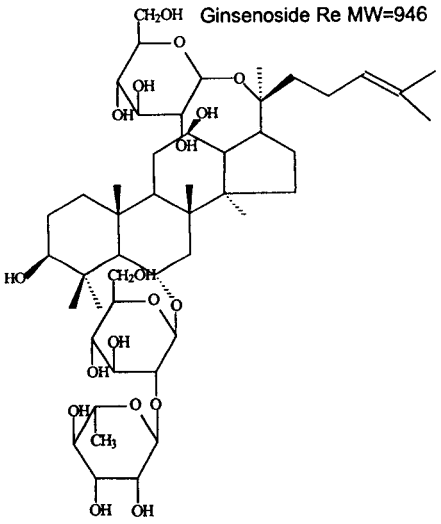

Chikusetsusaponin V (ginsenoside Ro) MW=956

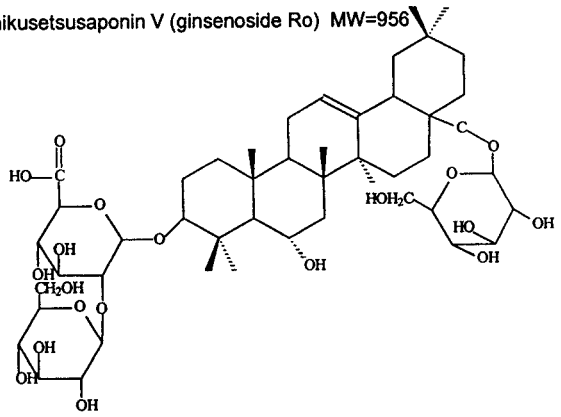

Notoginsenoside R6 MW=962

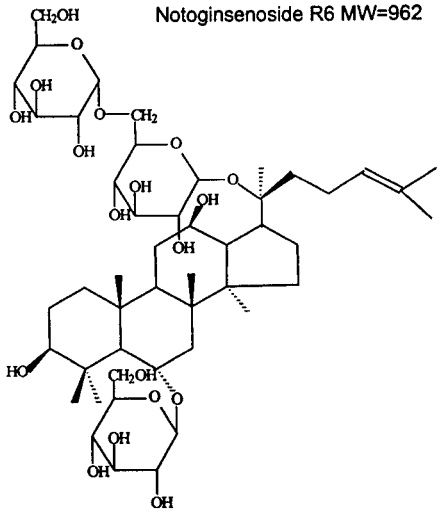

20-glucoginsenoside Rf MW=962

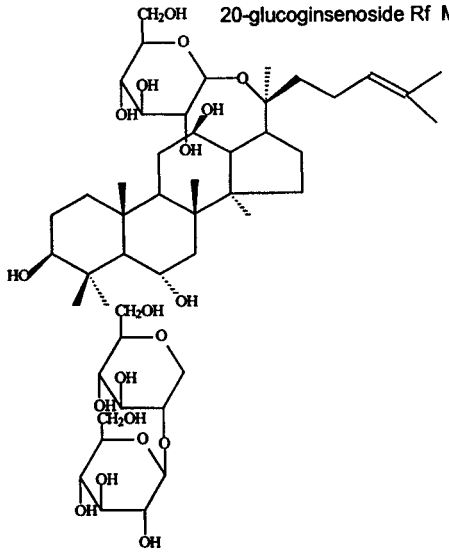

Notoginsenoside R3 MW=962

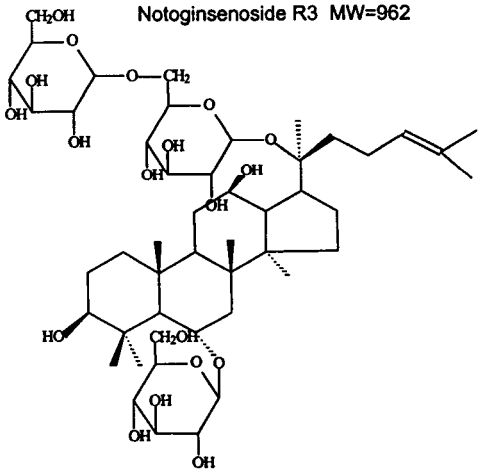

Section A.i.: Compendium of ginsenosides reported in Shoji's review [1]

Chikusetsusaponin Ib MW=962

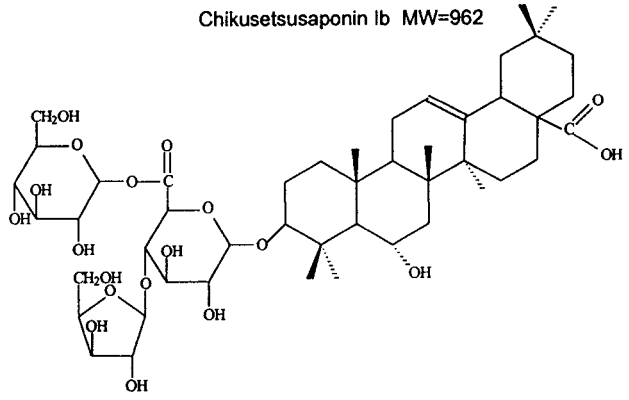

Chikusetsusaponin V methyl ester MW=974

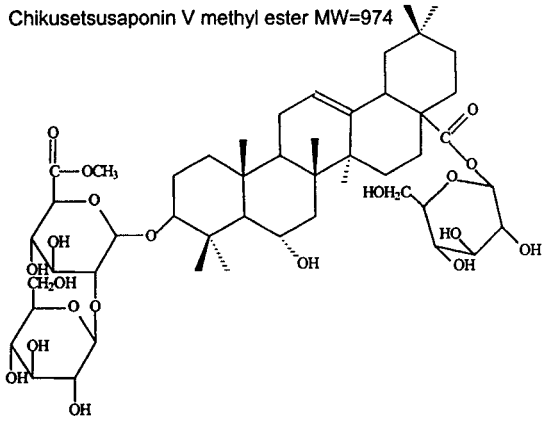

Malonyl ginsenoside Rd MW=1032

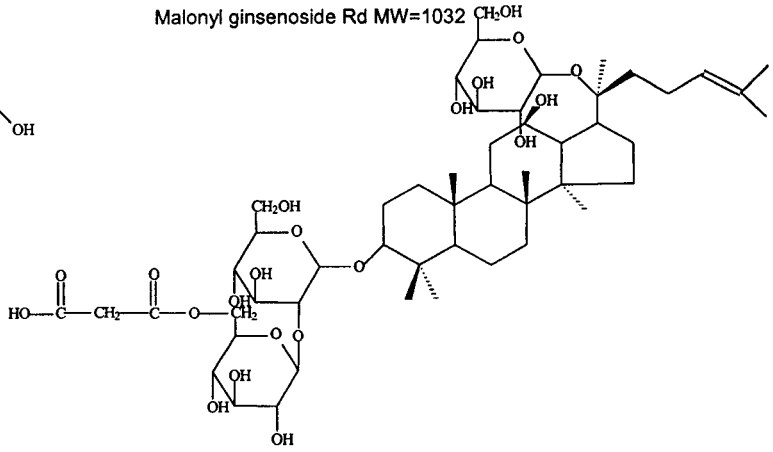

Chikusetsusaponin LN4 MW=1046

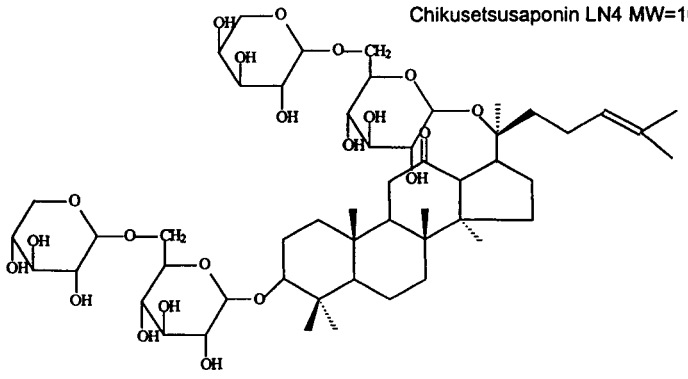

Section A.i.: Compendium of ginsenosides reported in Shoji's review [1]

Ginsenoside Rc MW=1078

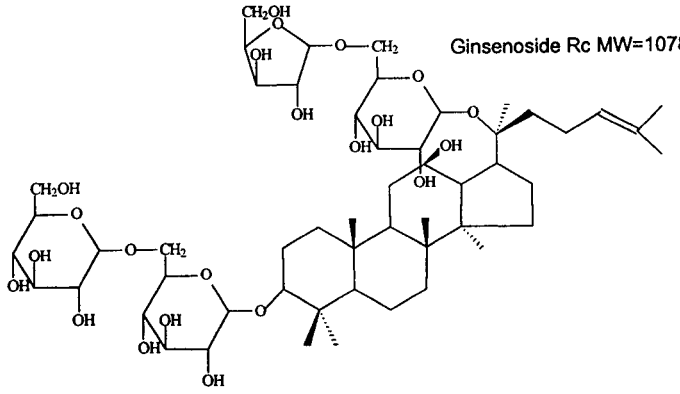

Ginsenoside Rb_2 MW=1078

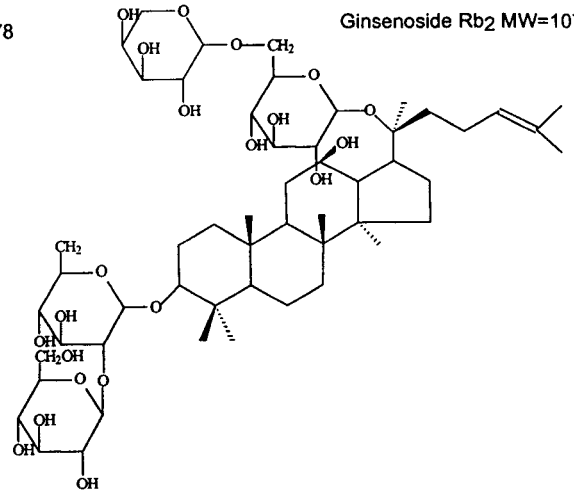

Ginsenoside Rb_3 MW=1078

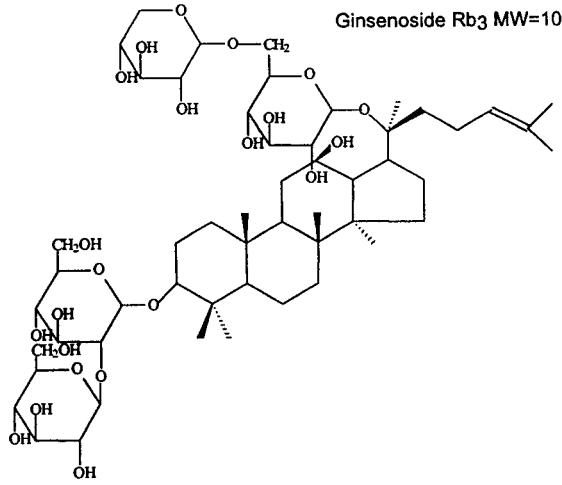

Ginsenoside Rb_1 MW=1108

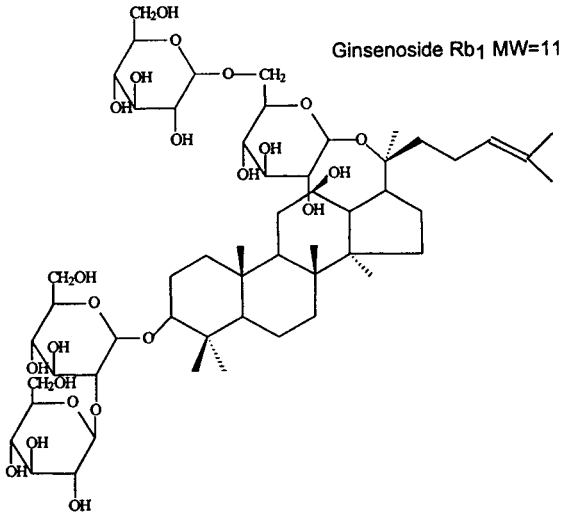

Ginsenoside RS1 MW=1120

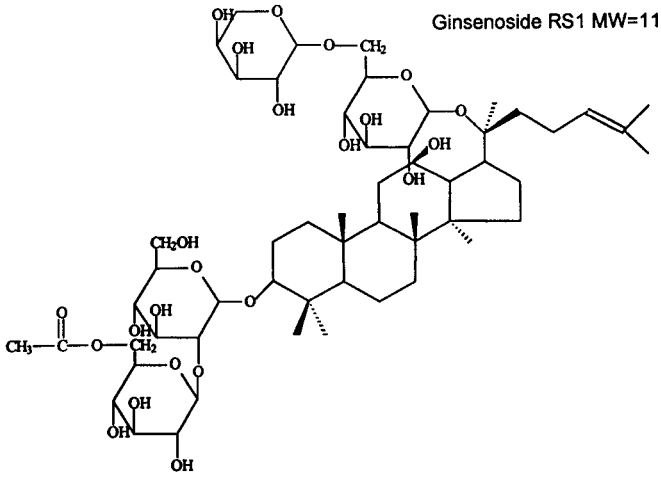

Section A.i.: Compendium of ginsenosides reported in Shoji's review [1]

Ginsenoside RS2 MW=1120

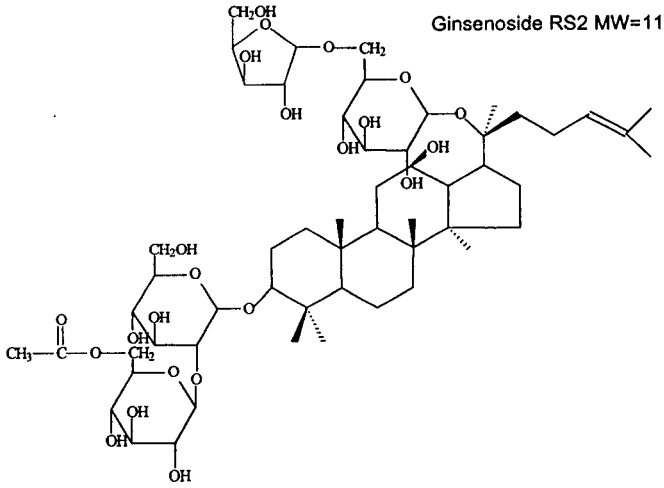

Notoginsenoside F8 MW=1120

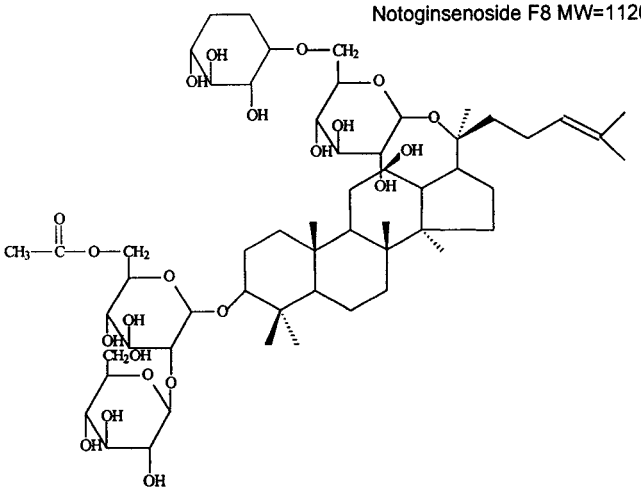

Quinquenoside R1 MW=1150

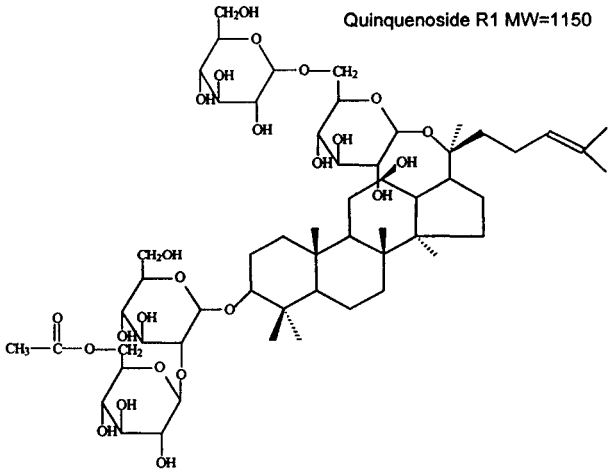

Section A.i.: Compendium of ginsenosides reported in Shoji's review [1]

Malonyl ginsenoside Rc MW=1164

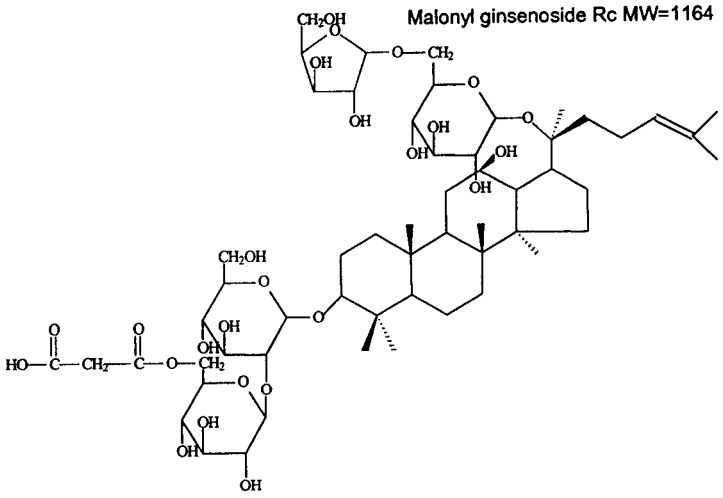

Malonyl ginsenoside Rb_2 MW=1164

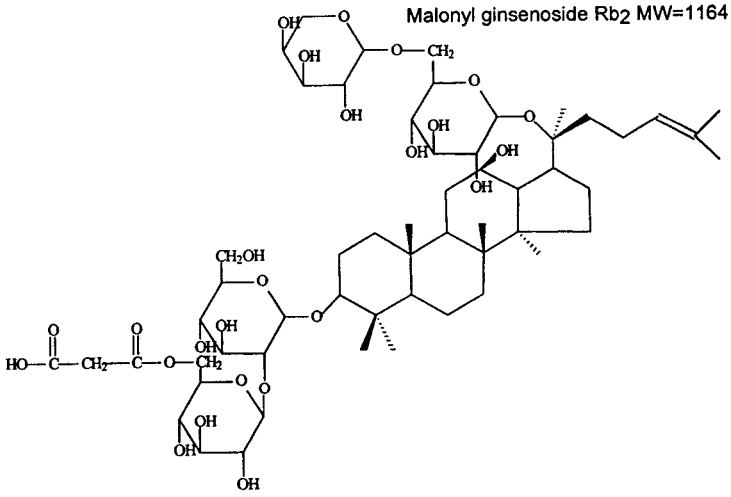

Malonyl ginsenoside Rb_1 MW=1194

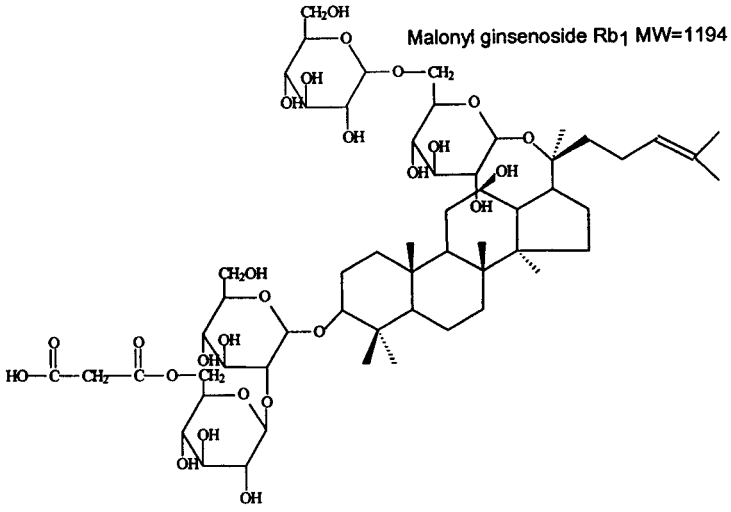

Section A.i.: Compendium of ginsenosides reported in Shoji's review [1]

Notoginsenoside Fc MW=1210

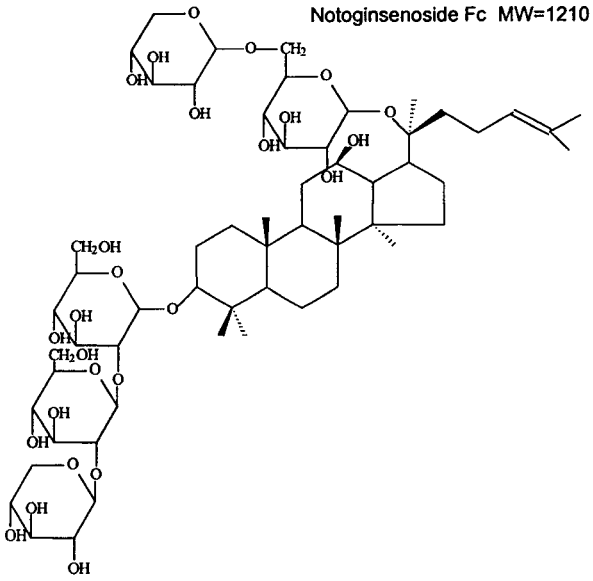

Ginsenoside Ra2 MW=1210

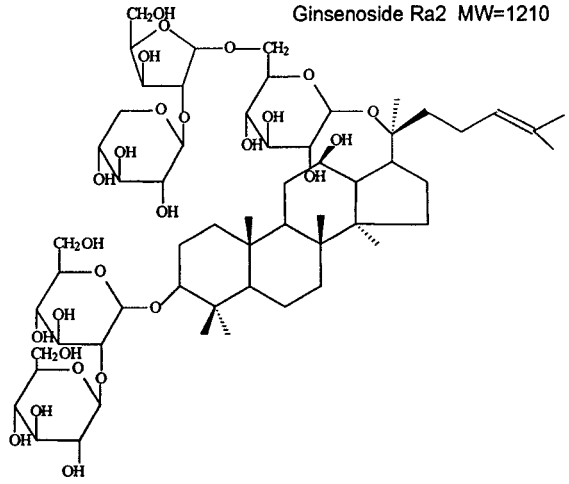

Section A.i.: Compendium of ginsenosides reported in Shoji's review [1]

Ginsenoside Ra1 MW=1210

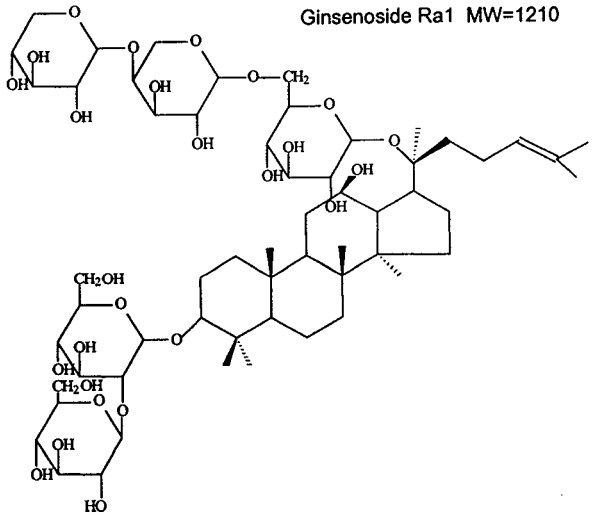

Notoginsenoside Fa MW=1240

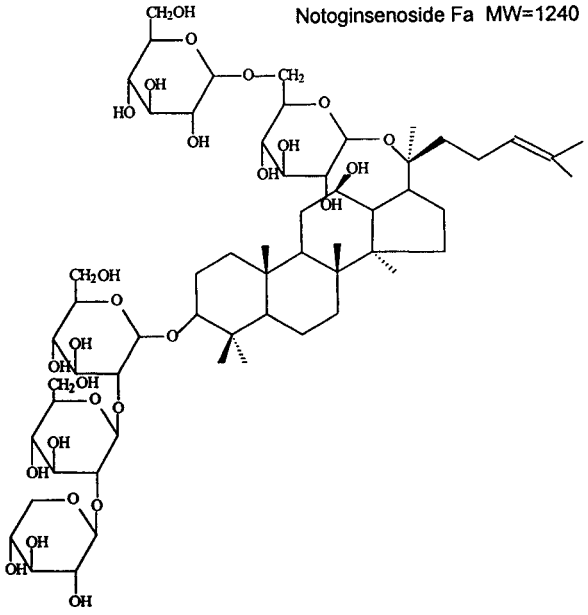

Section A.i.: Compendium of ginsenosides reported in Shoji's review [1]

Notoginsenoside R4 MW=1240

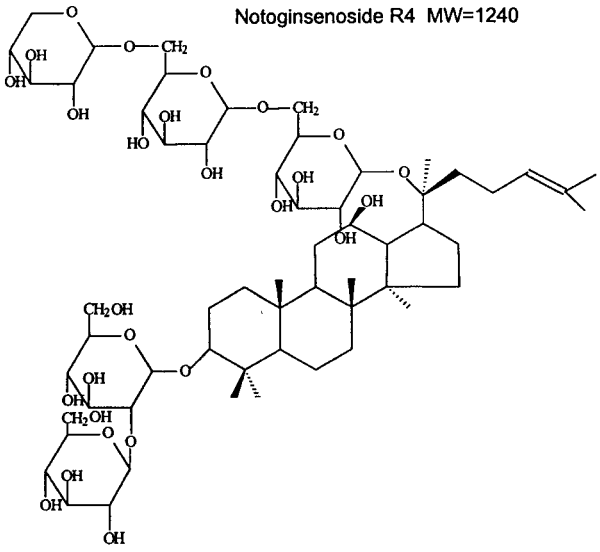

Ginsenoside Ra3 MW=1240

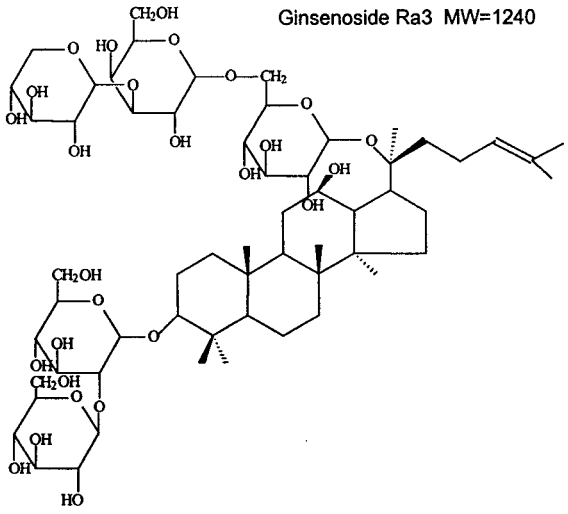

Reference:

[1] J. Shoji, Recent Advances in the Chemical Studies on Ginseng. In: *Adv. In Chinese Medicinal Materials Research*, H.M. Chang, H.W. Yeung, W.-W. Tso, A. Koo (Eds.), **1985**, p455.

Section A.ii.: Compendium of ginsenosides reported from 1986 to 2001. (The Reference list at the end of this Section is correlated with the Reference number given for each structure.)

Ginsenoside Rh8 MW=636

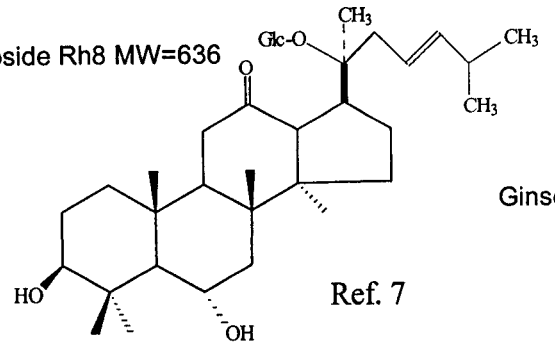

Ref. 7

Ginsenoside RH9 MW=636

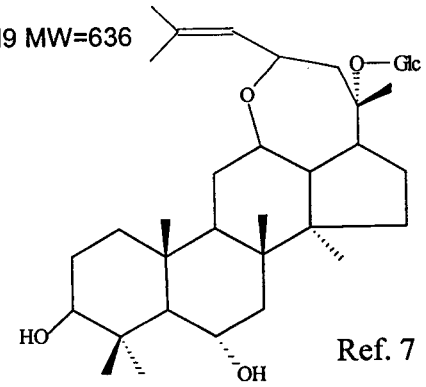

Ref. 7

Ginsenoside Rh5a MW=636

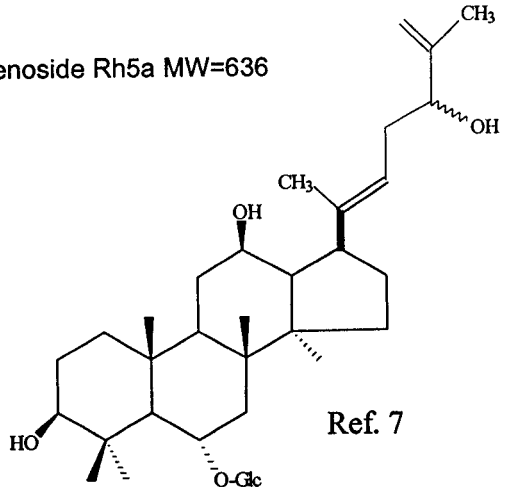

Ref. 7

Ginsenoside Rh7 MW=636

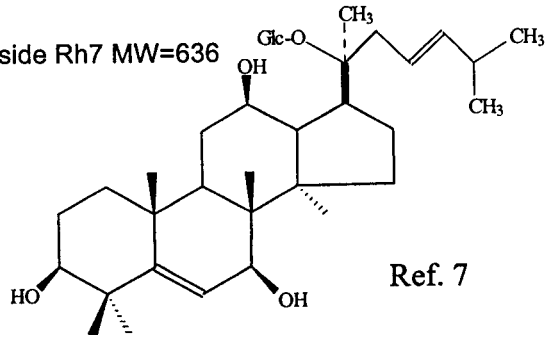

Ref. 7

Ginsenoside Rh5 MW=652

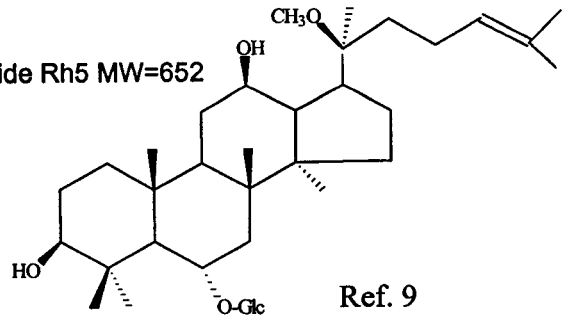

Ref. 9

Vina-ginsenoside R10 MW=654

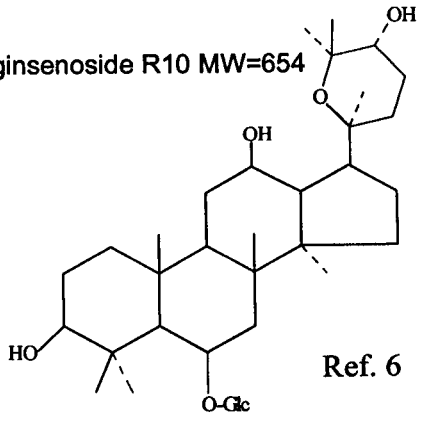

Ref. 6

Section A.ii.: Compendium of ginsenosides reported from 1986 to 2001. (The Reference list at the end of this Section is correlated with the Reference number given for each structure.)

Ginsenoside Rh6 MW=670

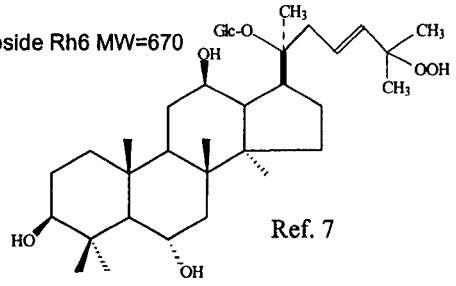

Ref. 7

Vina-ginsenoside R12 MW=672

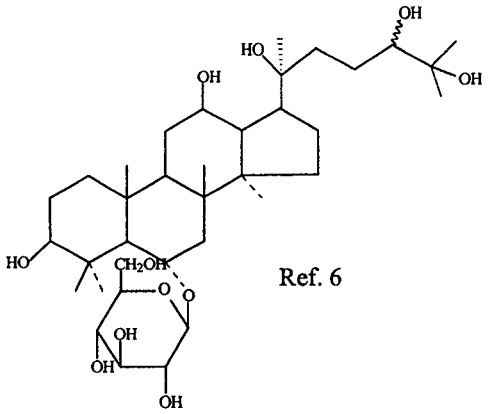

Ref. 6

Ginsenoside La MW=782

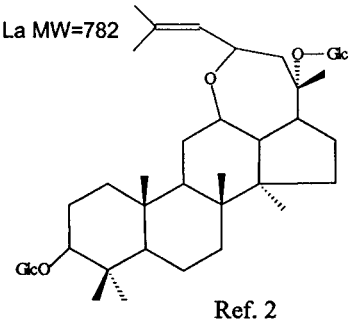

Ref. 2

Vina-ginsenoside R11 MW=786

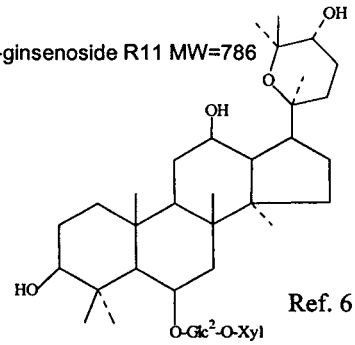

Ref. 6

Ginsenoside RG7 MW=800

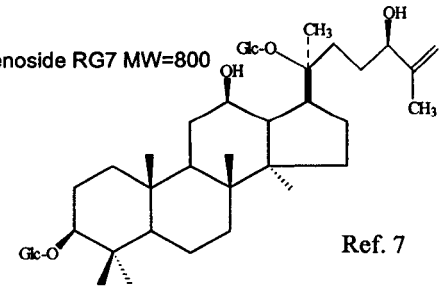

Ref. 7

Section A.ii.: Compendium of ginsenosides reported from 1986 to 2001. (The Reference list at the end of this Section is correlated with the Reference number given for each structure.)

24(S)-Pseudoginsenoside F11 MW=800

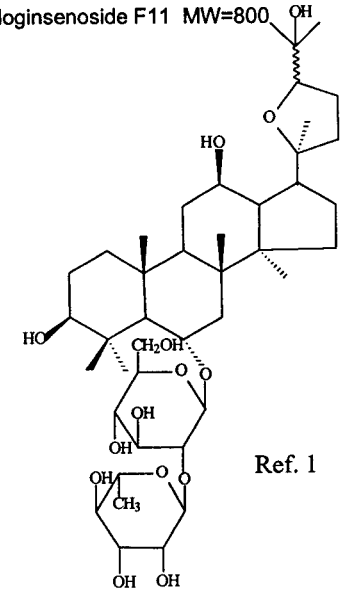

Ref. 1

Vina-ginsenoside R14 MW=802

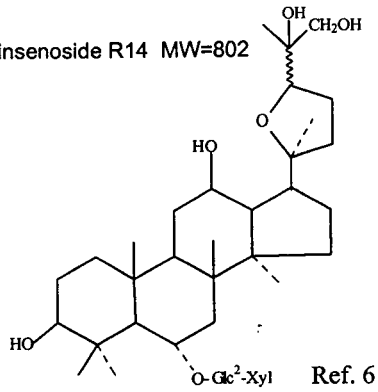

Ref. 6

Vina-ginsenoside R25 MW=814

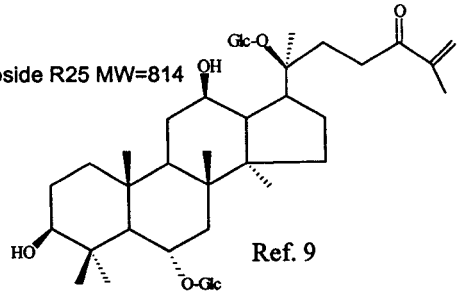

Ref. 9

Vina-ginsenoside R2 MW=828

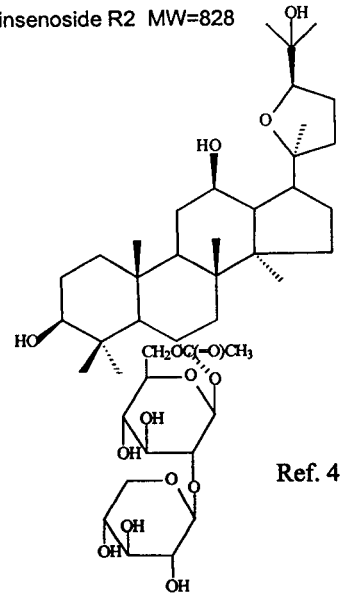

Ref. 4

Section A.ii.: Compendium of ginsenosides reported from 1986 to 2001. (The Reference list at the end of this Section is correlated with the Reference number given for each structure.)

Vina-ginsenoside R1 MW=842

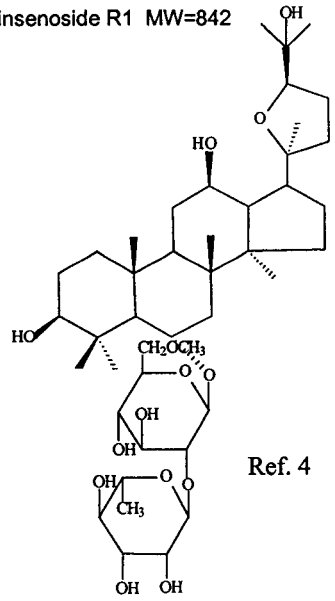

Ref. 4

Vina-ginsenoside R3 MW=930

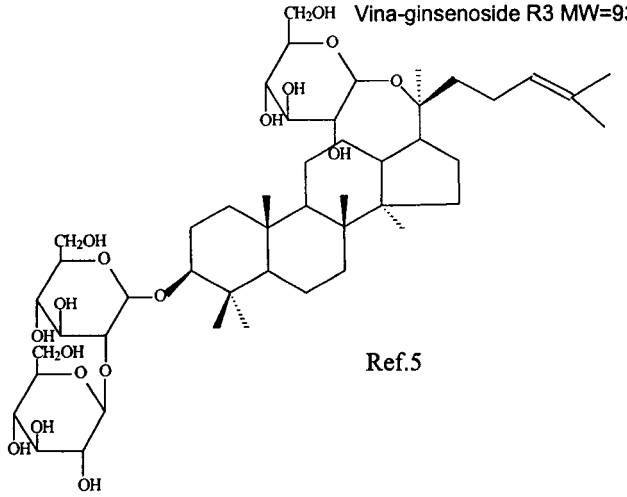

Ref.5

Vina-ginsenoside R5 MW=948

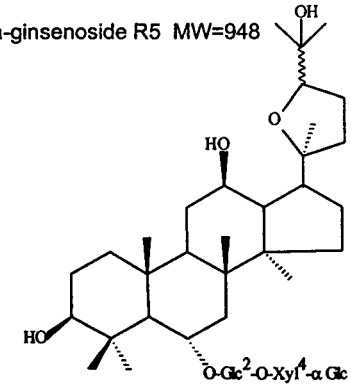

Ref. 5

Vina-ginsenoside R6 MW=948

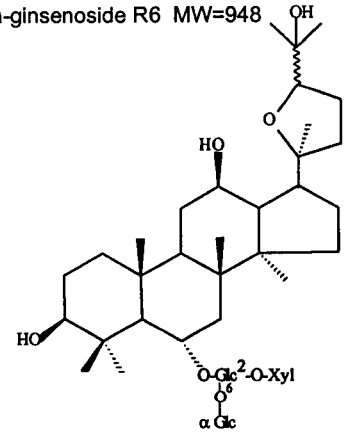

Ref. 5

Section A.ii.: Compendium of ginsenosides reported from 1986 to 2001. (The Reference list at the end of this Section is correlated with the Reference number given for each structure.)

Vina-ginsenoside R4 MW=962

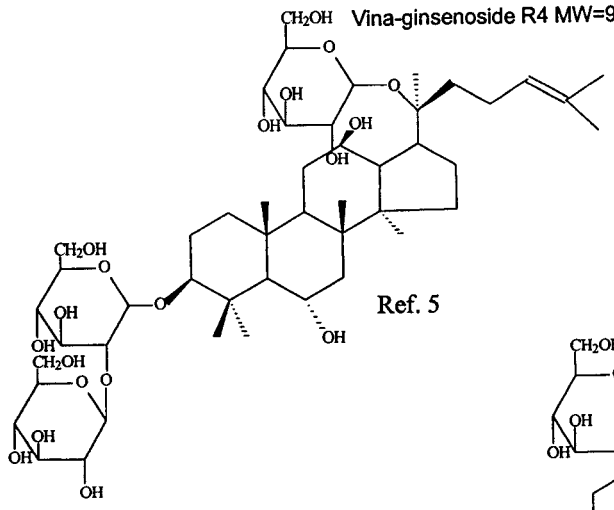

Ref. 5

Vina-ginsenoside R8 MW=962

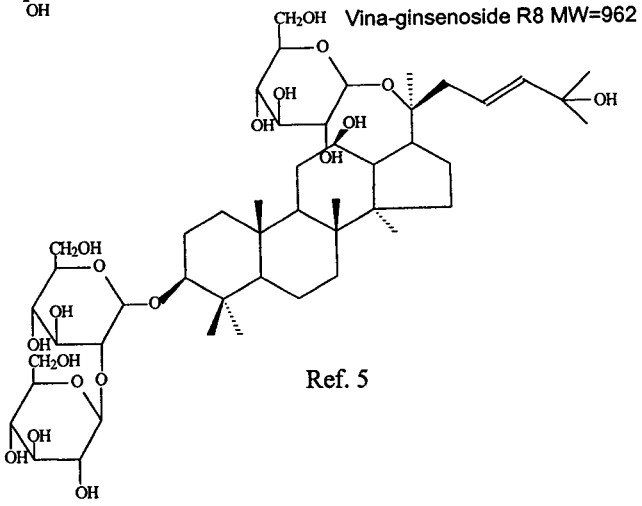

Ref. 5

Vina-ginsenoside R9 MW=962

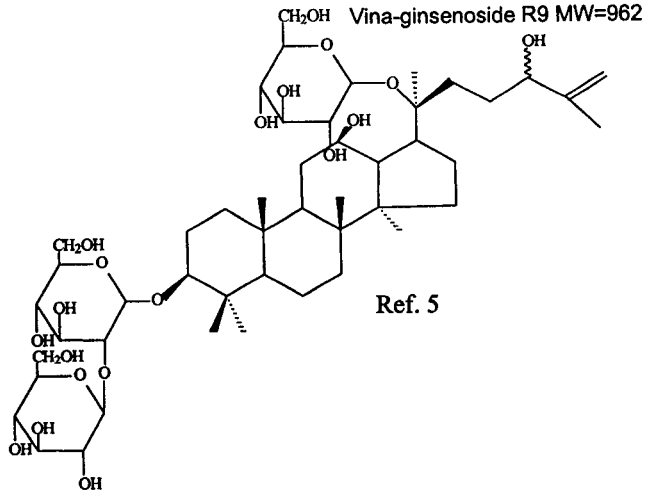

Ref. 5

Section A.ii.: Compendium of ginsenosides reported from 1986 to 2001. (The Reference list at the end of this Section is correlated with the Reference number given for each structure.)

Vina-ginsenoside R13 MW=980

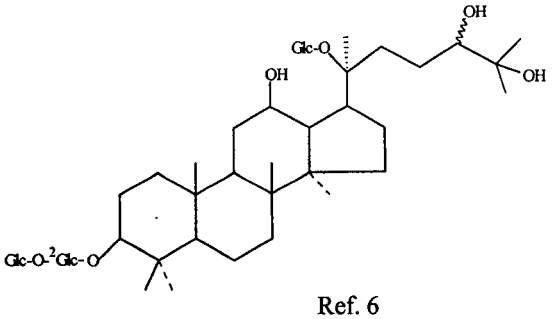

Ref. 6

Pseudo-ginsenoside RS_1 MW=988

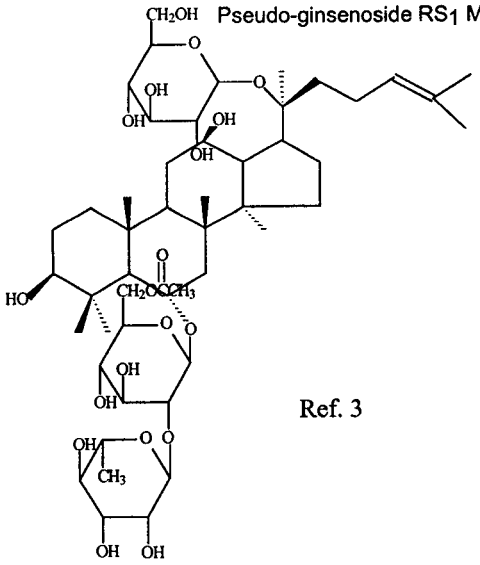

Ref. 3

Pseudo-ginsenoside RC_1 MW=988

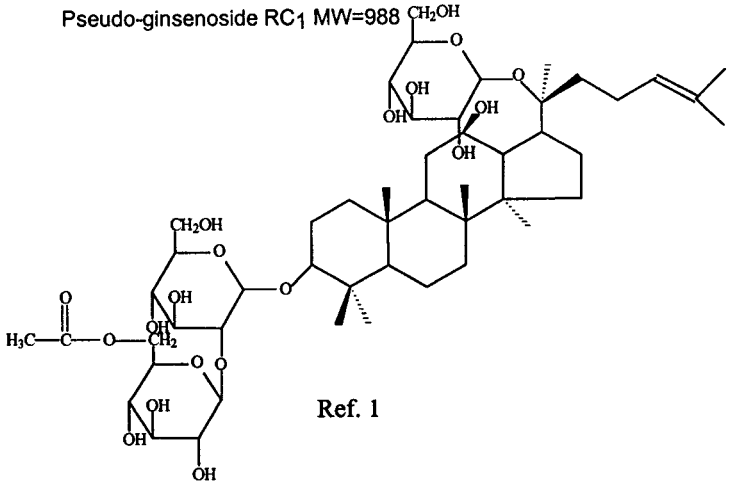

Ref. 1

Section A.ii.: Compendium of ginsenosides reported from 1986 to 2001. (The Reference list at the end of this Section is correlated with the Reference number given for each structure.)

Quinquenoside III MW=988

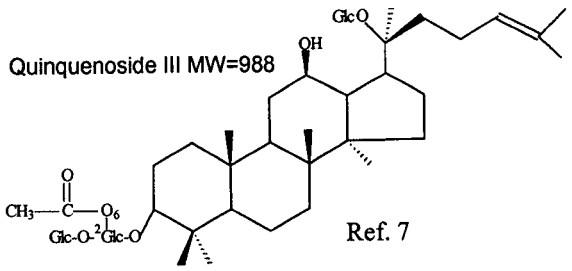

Ref. 7

Quinquenoside I MW=1014

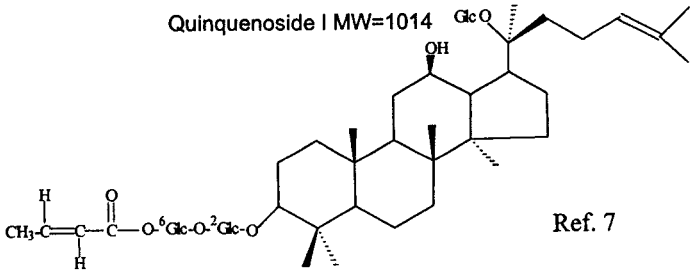

Ref. 7

Vina-ginsenoside R7 MW=1078

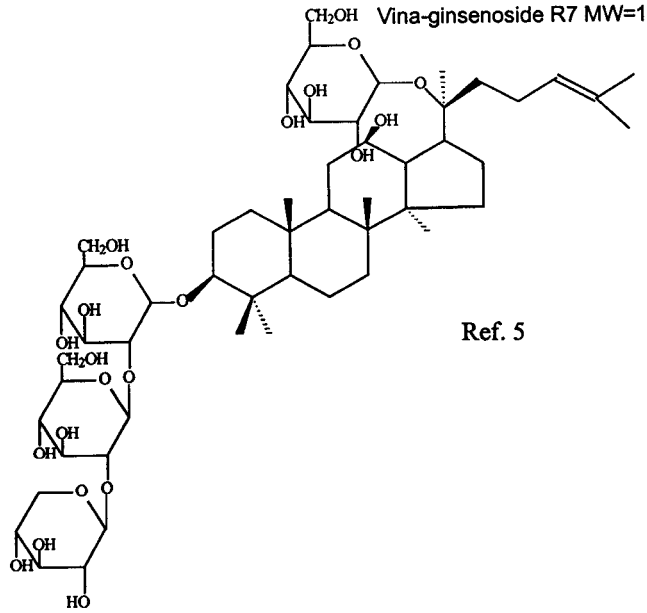

Ref. 5

Section A.ii.: Compendium of ginsenosides reported from 1986 to 2001. (The Reference list at the end of this Section is correlated with the Reference number given for each structure.)

Quinquenoside IV MW=1122

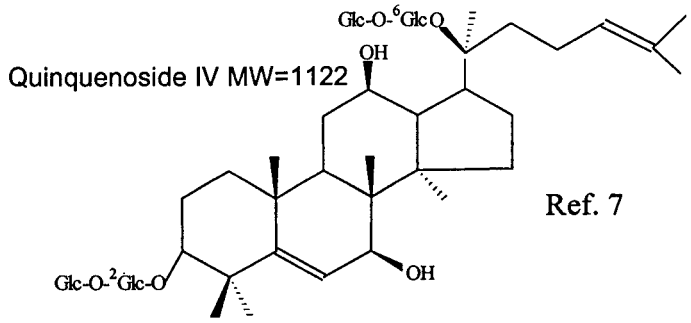

Ref. 7

Quinquenoside II MW=1232

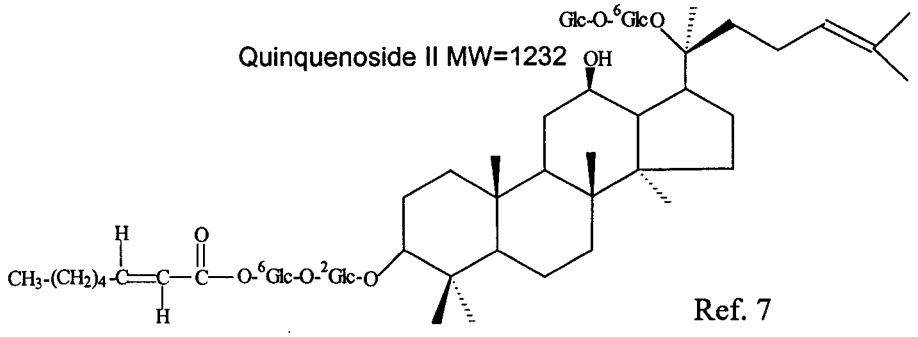

Ref. 7

Quinquenoside V MW=1270

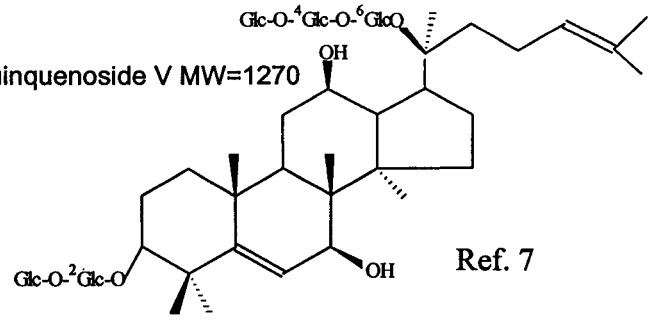

Ref. 7

References

[1] T. Namba, K. Matsushige, T. Morita and O. Tanaka, *Chem. Pharm. Bull.*, **1986**, *34*, 730.

[2] S. Zhang, X. Yao, Y. Chen, C. Cui, Y. Tezuka and T. Kikuchi, *Chem. Pharm. Bull.*, **1989**, *37*, 1966.

[3] T. Morita, Y.-C. Kong, P.-H. But, K.-H. Ng, T.-T. Yip, R. Kasai and O. Tanaka, *Chem. Pharm. Bull.*, **1986**, *34*, 4368.

[4] N.M. Duc, N.T. Nham, R. Kasai, A. Ito, K. Yamasaki and O. Tanaka, *Chem. Pharm. Bull.*, **1993**, *41*, 2010.

[5] N.M. Duc, R. Kasai, K. Ohtani, A. Ito, N.T. Nham, K. Yamasaki and O. Tanaka, *Chem. Pharm. Bull.*, **1994**, *42*, 115.

[6] N.M. Duc, R. Kasai, K. Ohtani, A. Ito, N.T. Nham, K. Yamasaki and O. Tanaka, *Chem. Pharm. Bull.*, **1994**, *42*, 634.

[7] M. Yoshikawa, T. Murakami, K. Yashiro, J. Yamahara, H. Matsuda, R. Saijoh and O. Tanaka, *Chem. Pharm. Bull.*, **1998**, *46*, 647.

[8] D.-Q. Dou, Y.-J. Chen, L.-H. Liang, F.-G. Pang, N. Shimizu and T. Takeda, *Chem. Pharm. Bull.*, **2001**, *49*, 442.

[9] Q. Le Tran, I.K. Adnyana, Y. Tezuka, T. Nagaoka, Q.K. Tran and S. Kadota, *J. Nat. Prod.*, **2001**, *64*, 456.

Section B: American ginseng – Ion chromatograms for the $[M+Na]^+$ ions of the molecular masses in Section A.i. of the Appendix.

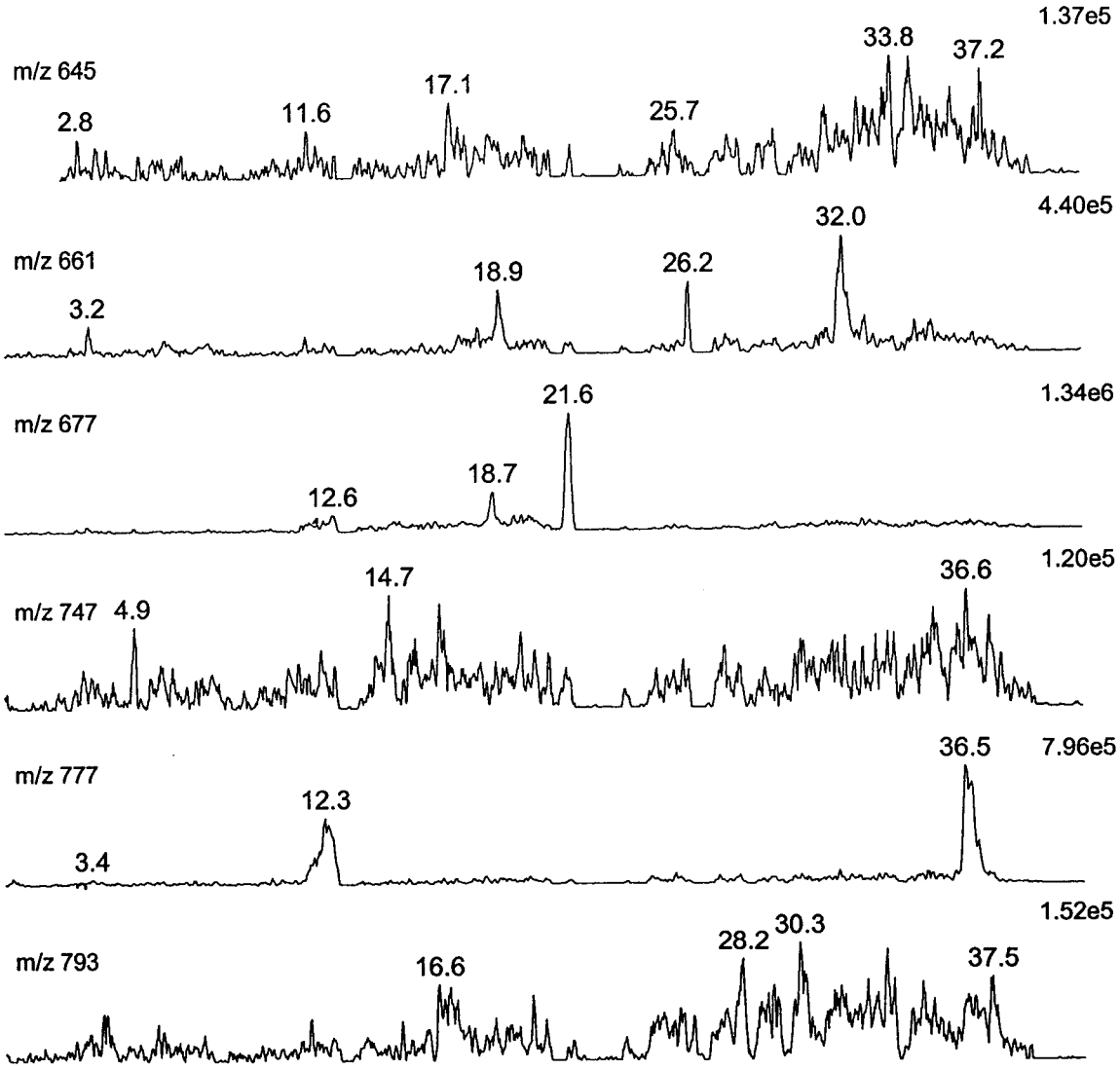

Section B: American ginseng – Ion chromatograms for the $[M+Na]^+$ ions of the molecular masses in Section A.i. of the Appendix.

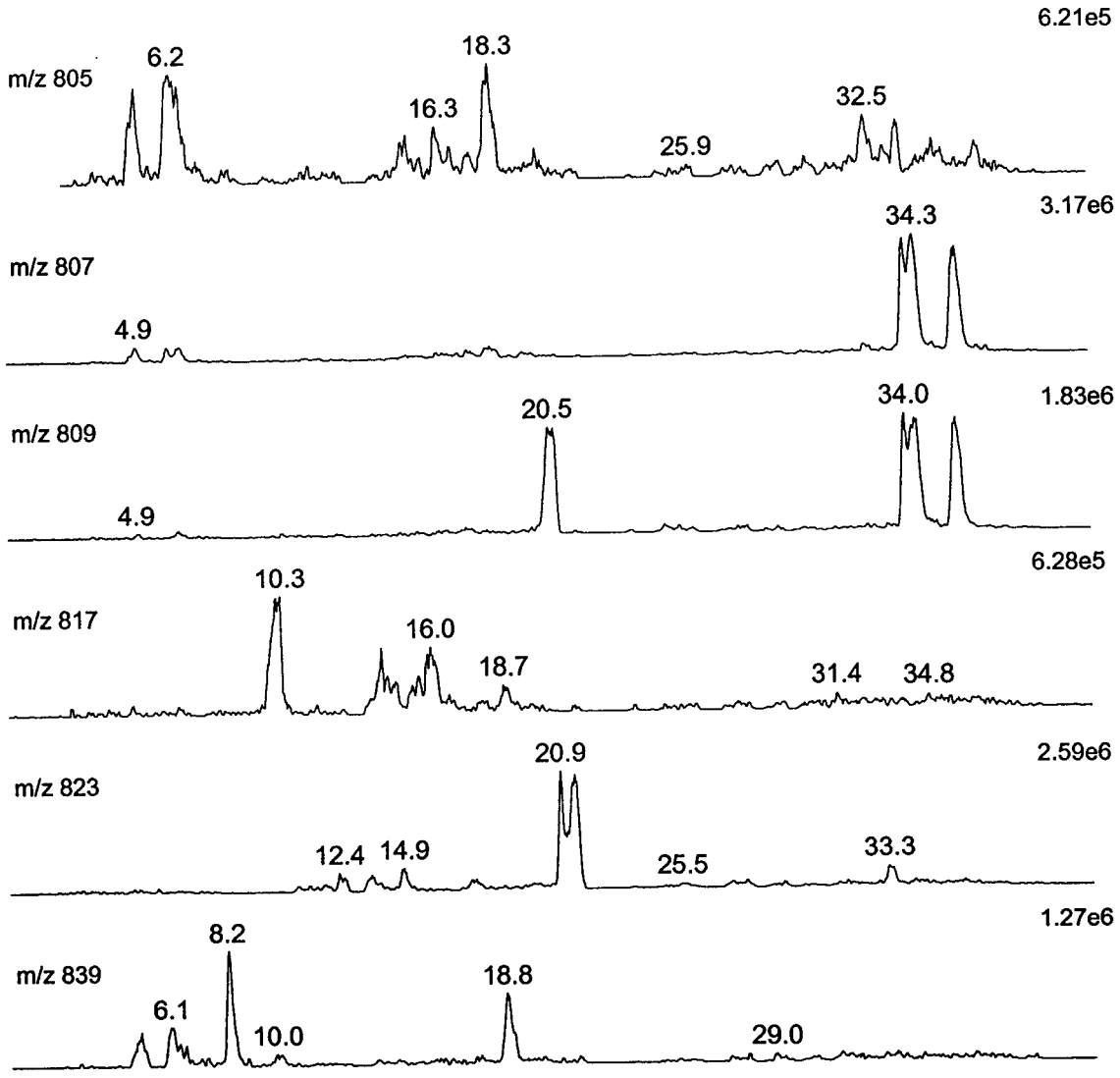

Section B: American ginseng – Ion chromatograms for the $[M+Na]^+$ ions of the molecular masses in Section A.i. of the Appendix.

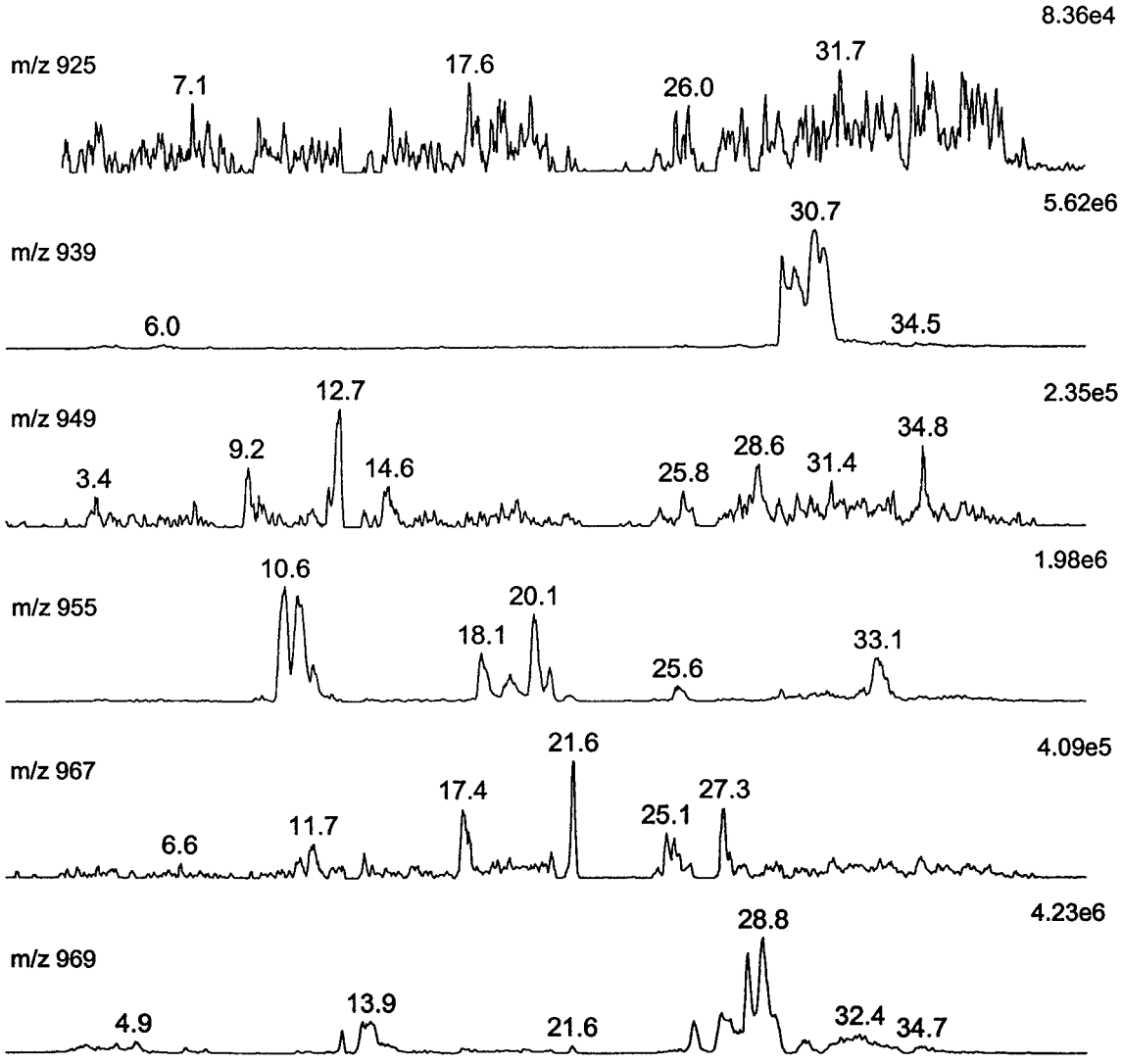

Section B: American ginseng – Ion chromatograms for the $[M+Na]^+$ ions of the molecular masses in Section A.i. of the Appendix.

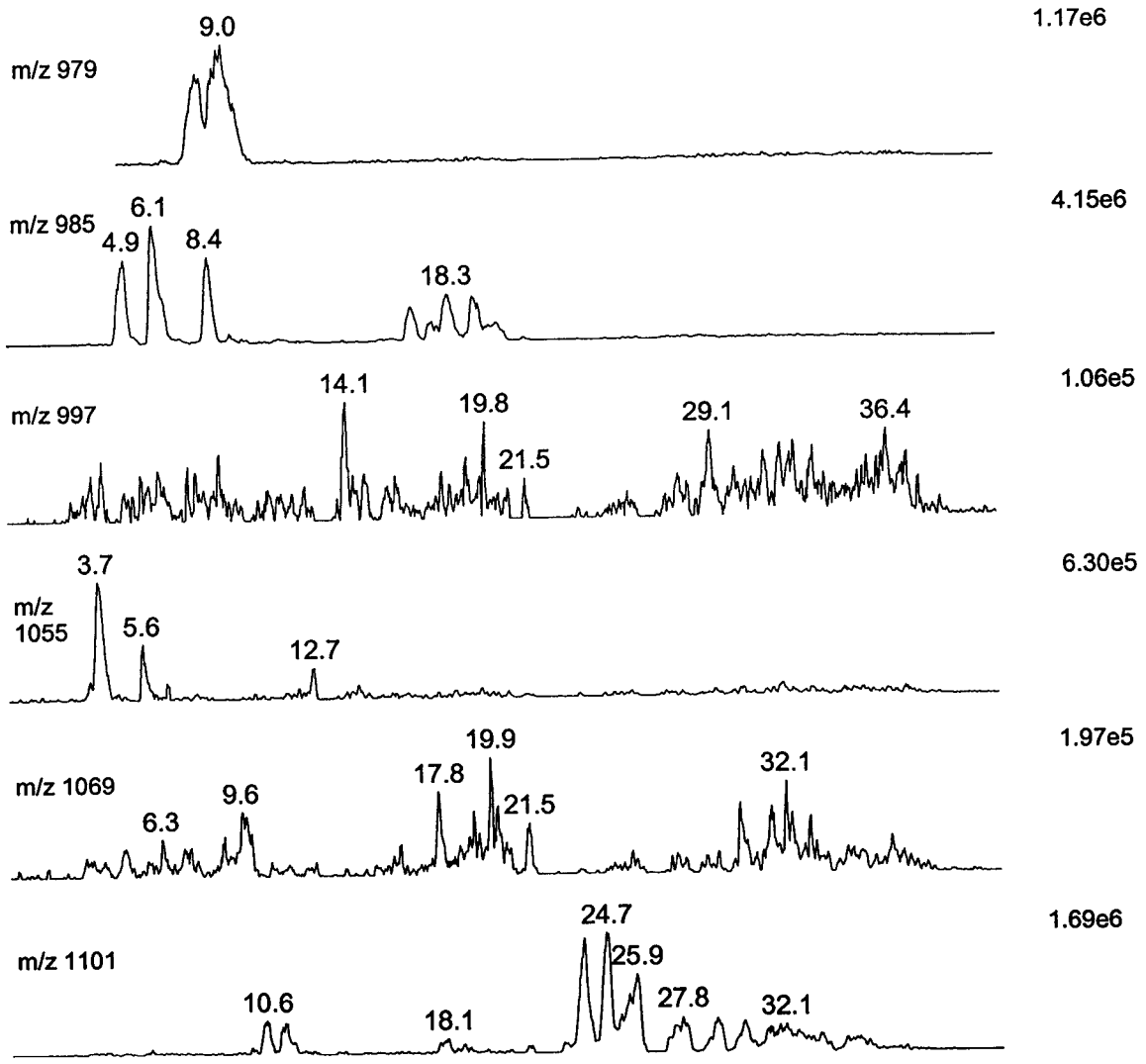

Section B: American ginseng – Ion chromatograms for the $[M+Na]^+$ ions of the molecular masses in Section A.i. of the Appendix.

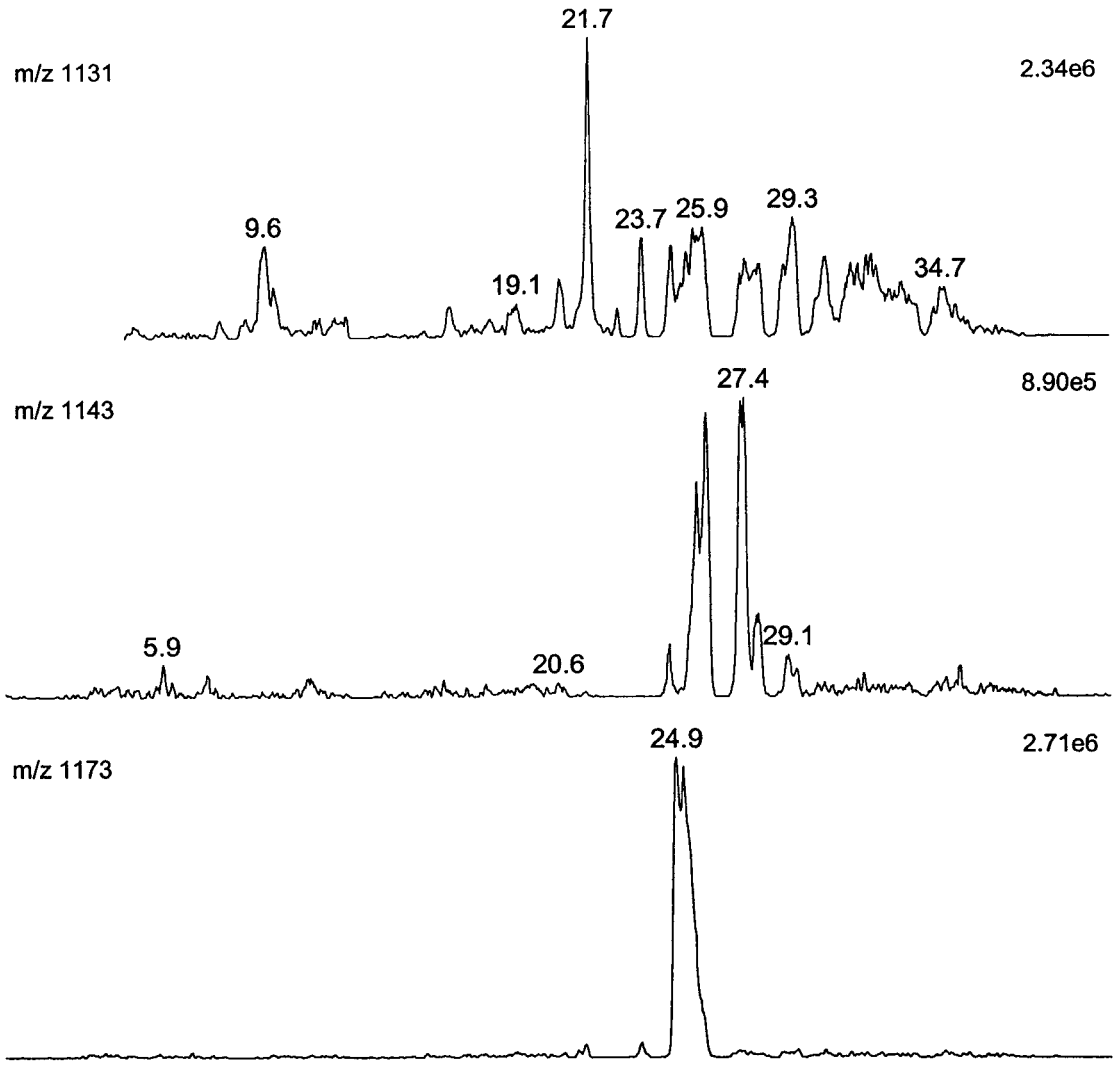

Section B: American ginseng – Ion chromatograms for the $[M+Na]^+$ ions of the molecular masses in Section A.i. of the Appendix.

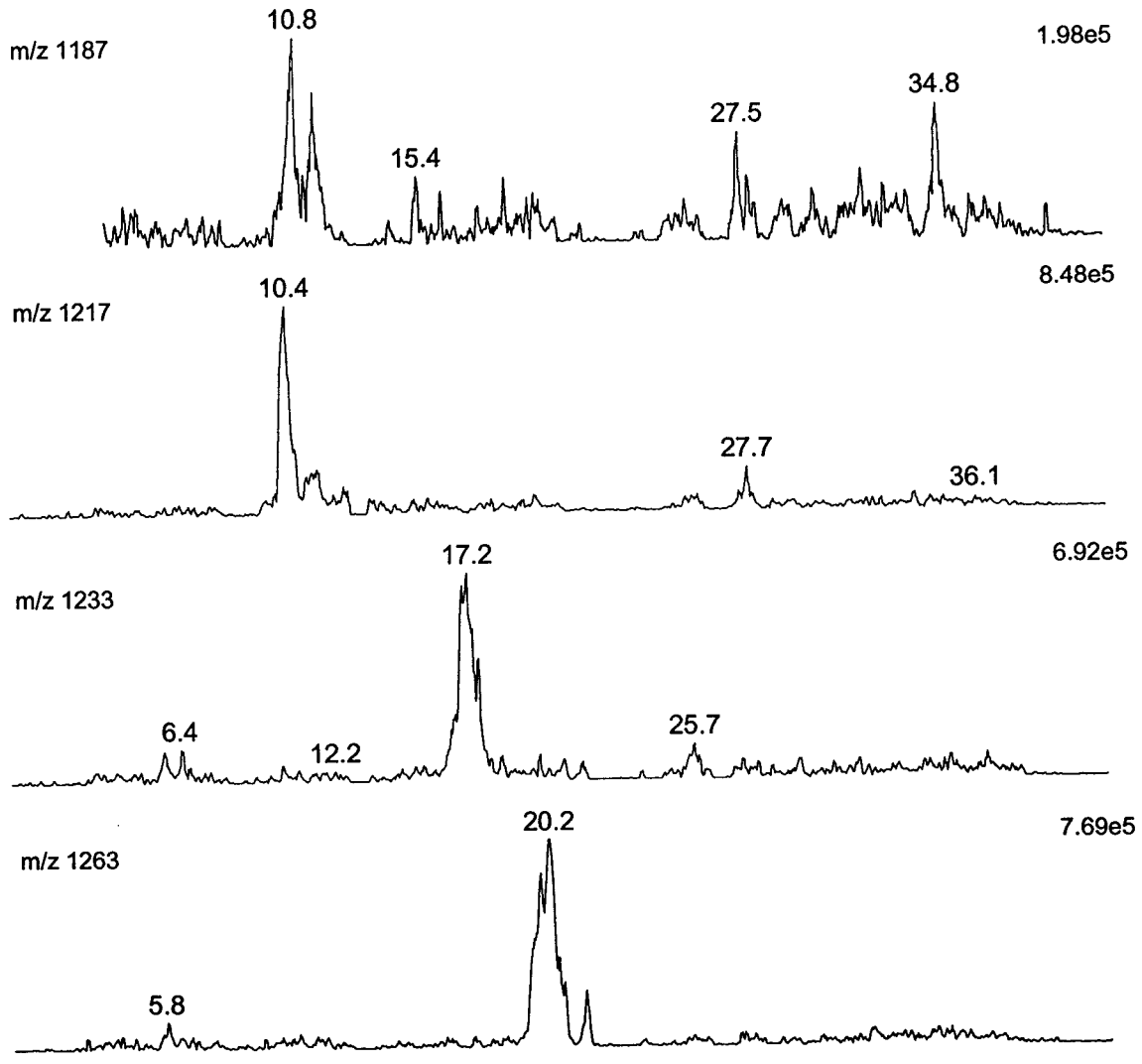

Section C: Korean Red ginseng – Ion chromatograms for the $[M+Na]^+$ ions of the molecular masses in Section A.i. of the Appendix.

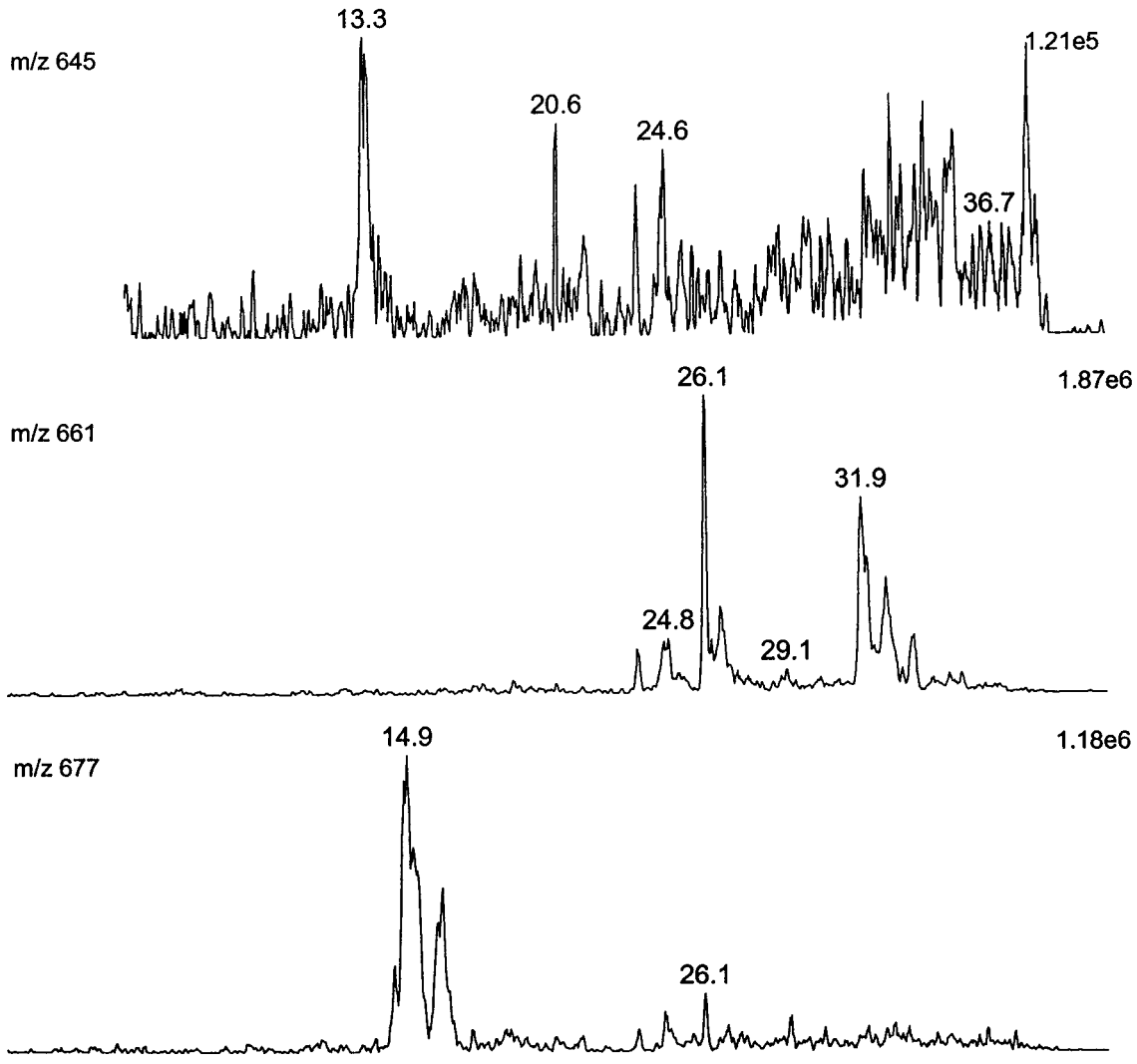

Section C: Korean Red ginseng – Ion chromatograms for the $[M+Na]^+$ ions of the molecular masses in Section A.i. of the Appendix.

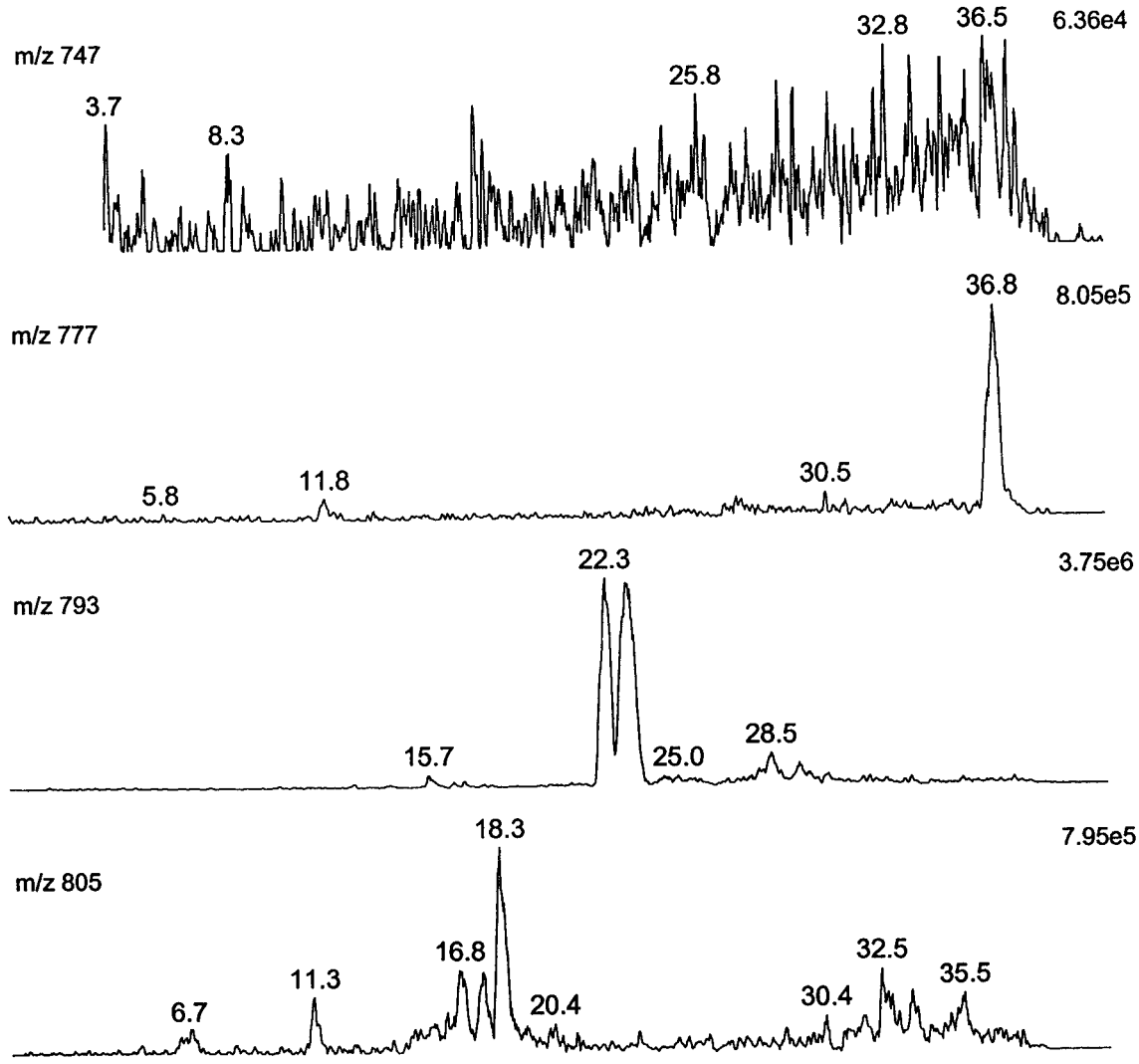

Section C: Korean Red ginseng – Ion chromatograms for the $[M+Na]^+$ ions of the molecular masses in Section A.i. of the Appendix.

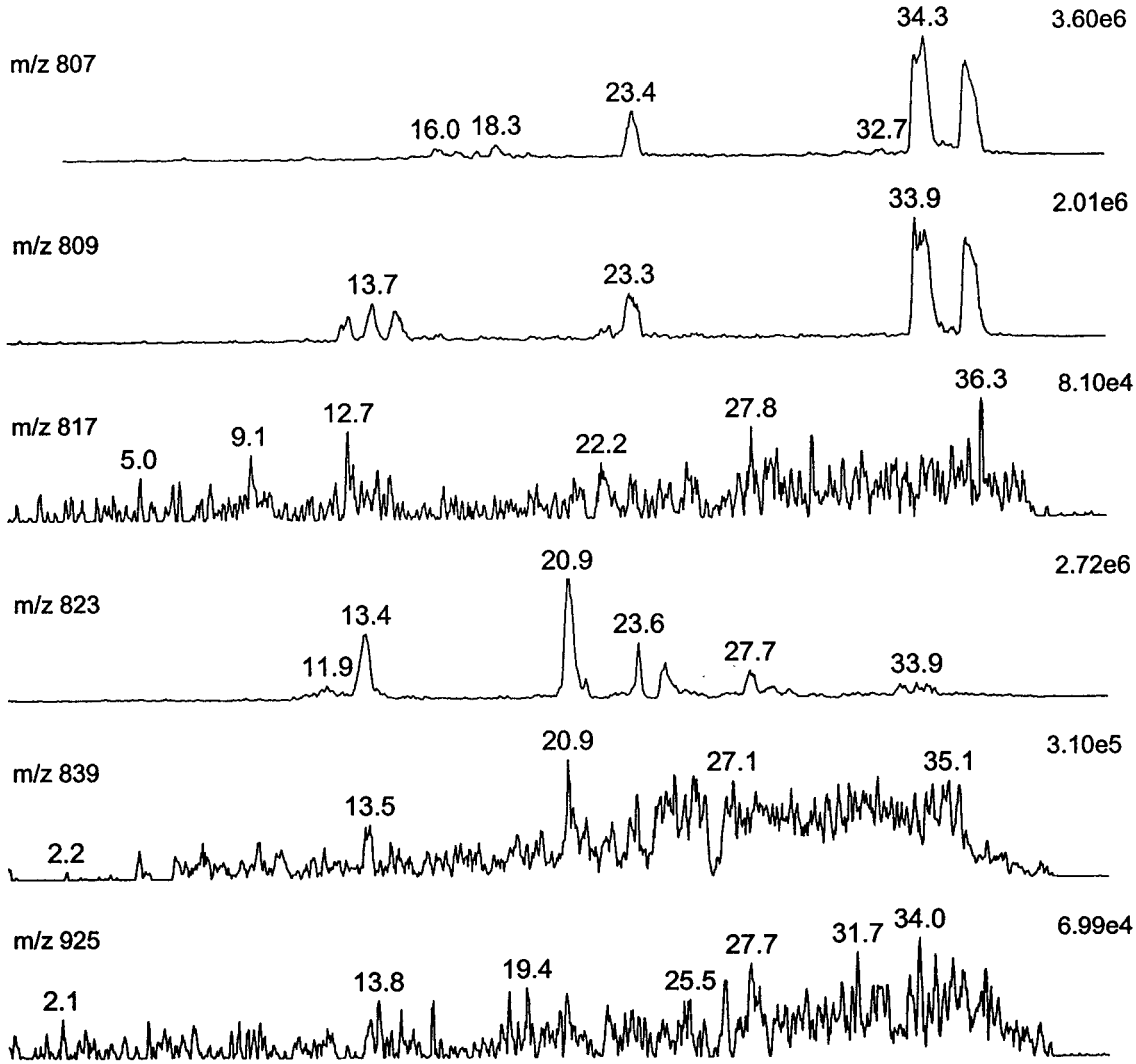

Section C: Korean Red ginseng – Ion chromatograms for the $[M+Na]^+$ ions of the molecular masses in Section A.i. of the Appendix.

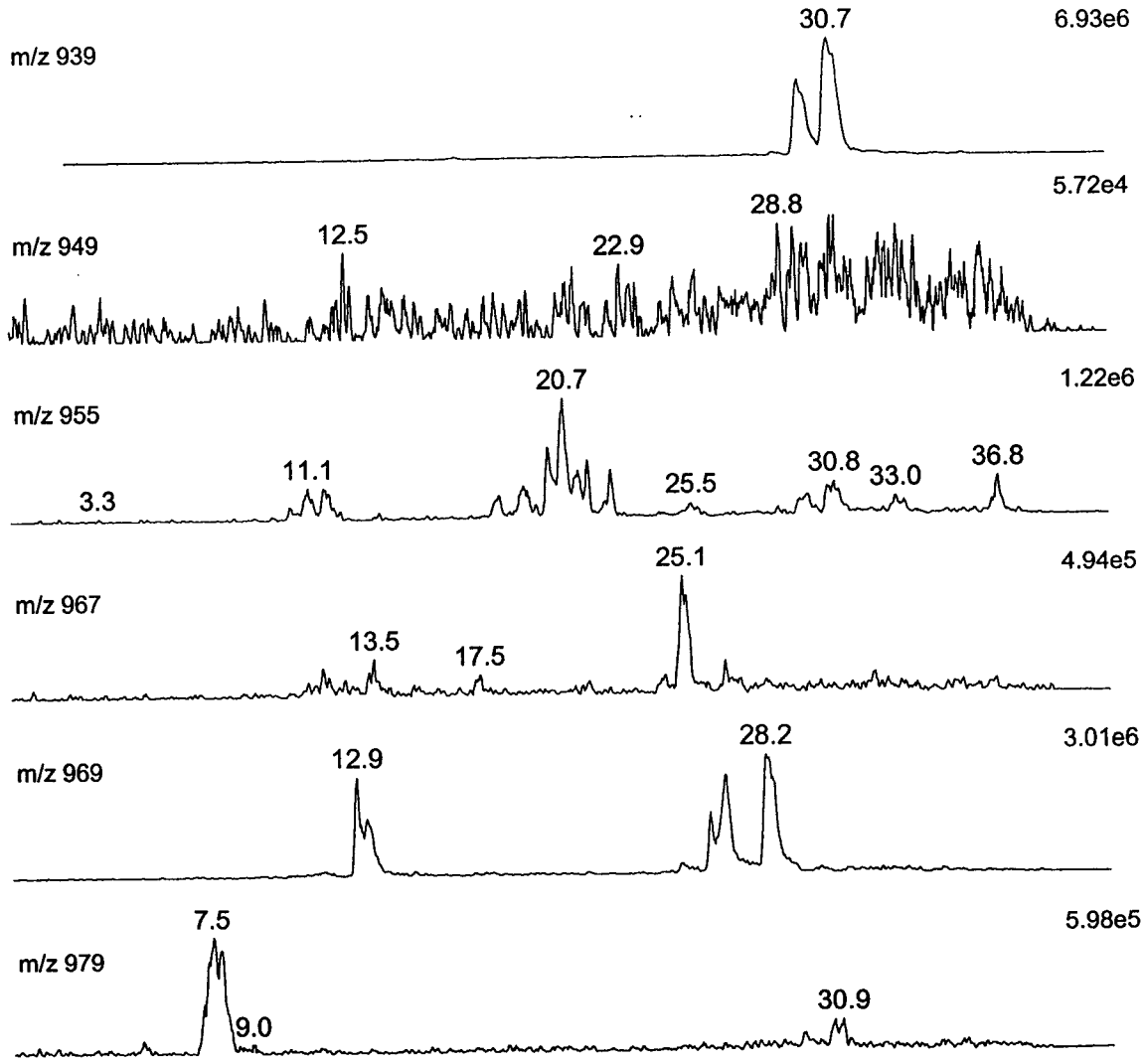

Section C: Korean Red ginseng – Ion chromatograms for the $[M+Na]^+$ ions of the molecular masses in Section A.i. of the Appendix.

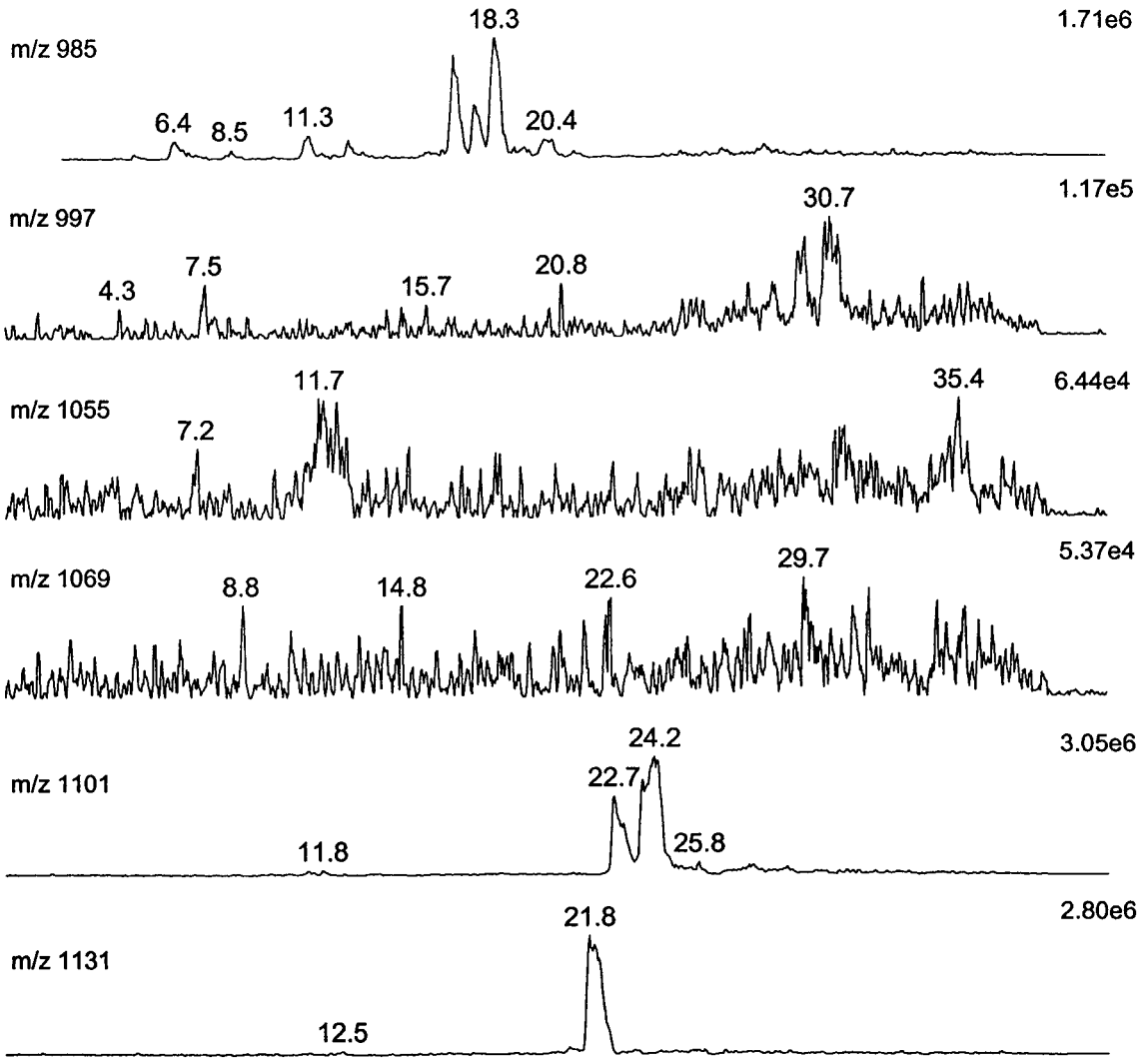

Section C: Korean Red ginseng – Ion chromatograms for the $[M+Na]^+$ ions of the molecular masses in Section A.i. of the Appendix.

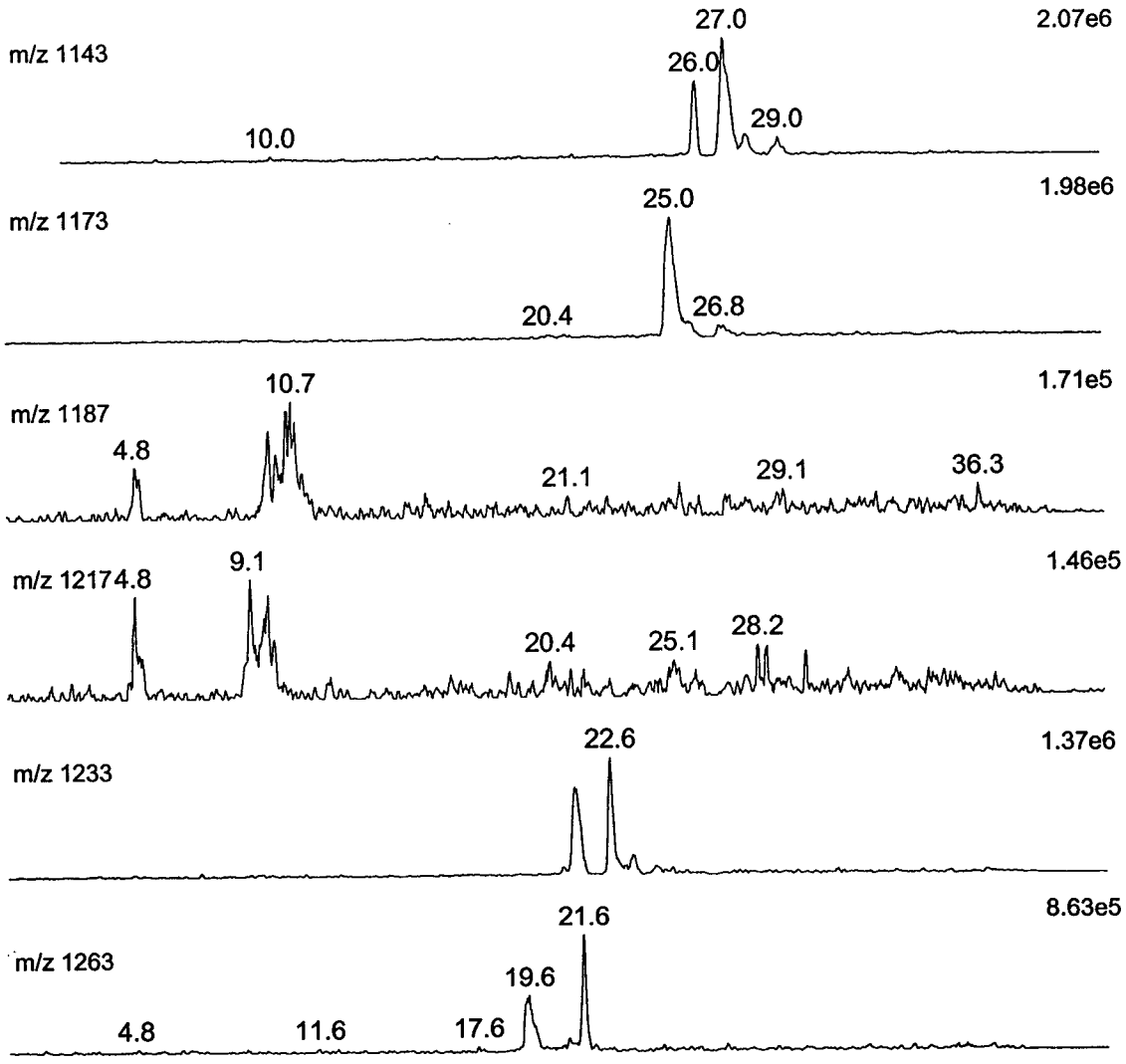

Section D: Korean White ginseng – Ion chromatograms for the $[M+Na]^+$ ions of the molecular masses in Section A.i. of the Appendix.

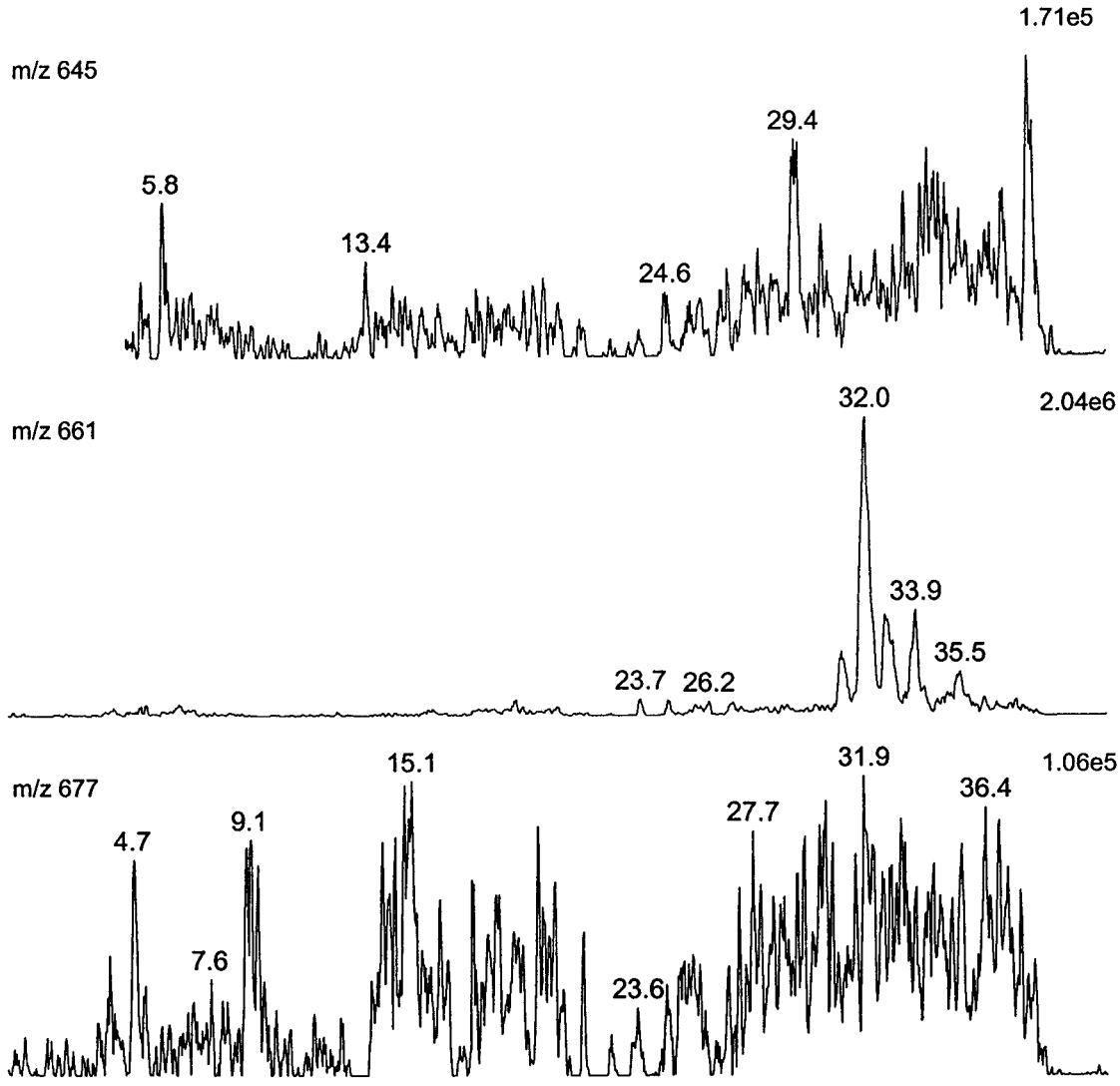

Section D: Korean White ginseng – Ion chromatograms for the $[M+Na]^+$ ions of the molecular masses in Section A.i. of the Appendix.

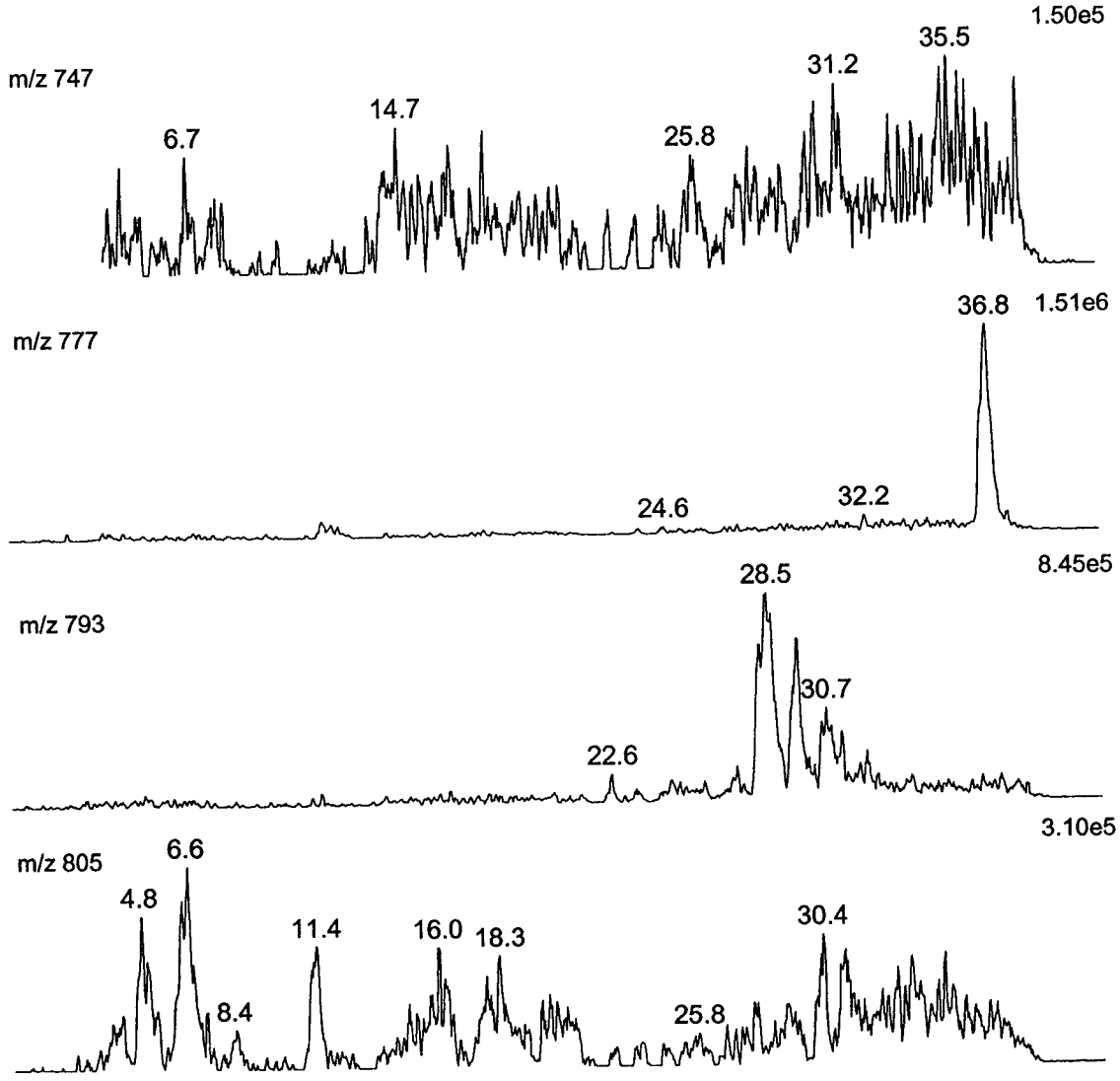

Section D: Korean White ginseng – Ion chromatograms for the $[M+Na]^+$ ions of the molecular masses in Section A.i. of the Appendix.

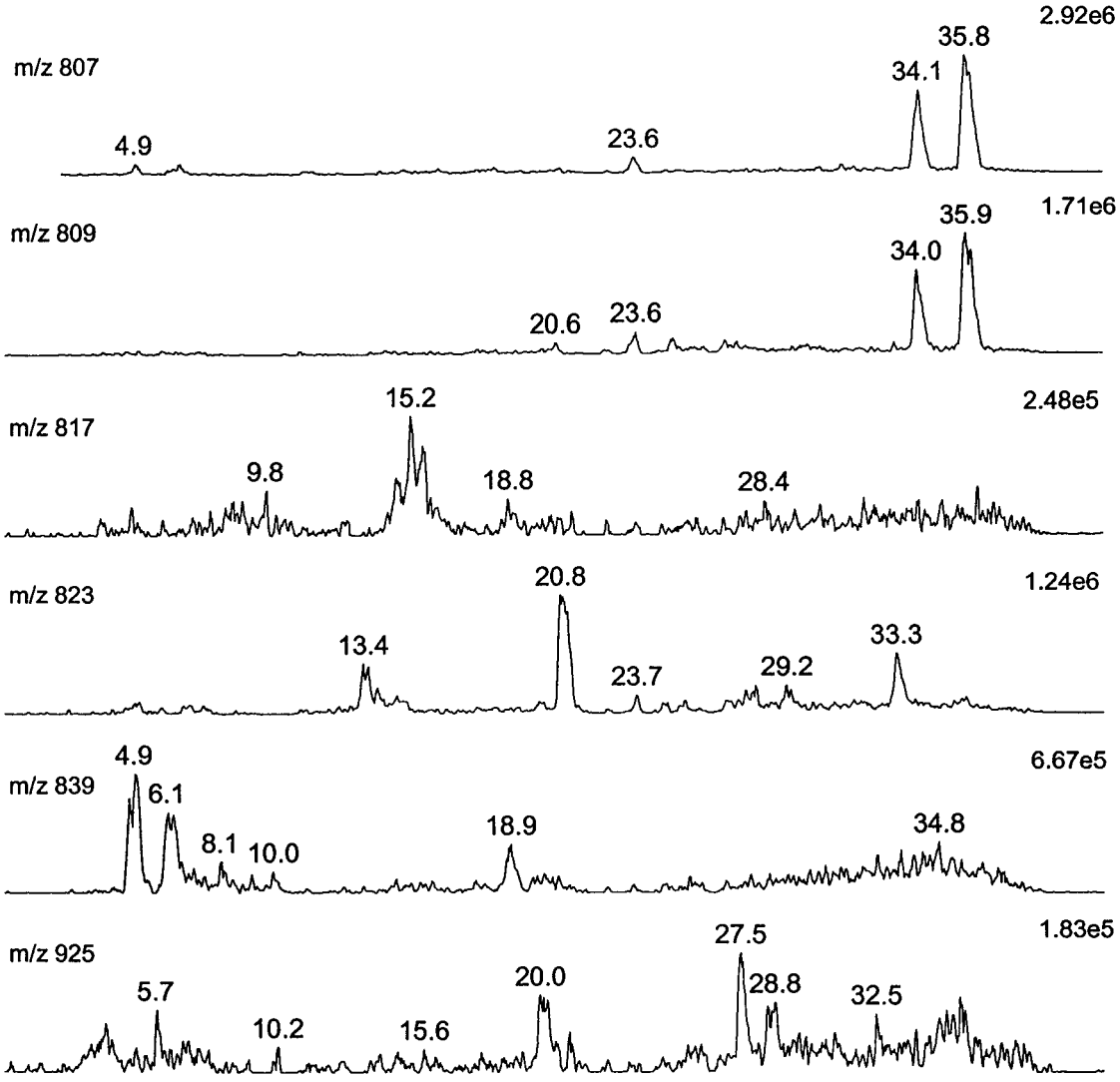

Section D: Korean White ginseng – Ion chromatograms for the $[M+Na]^+$ ions of the molecular masses in Section A.i. of the Appendix.

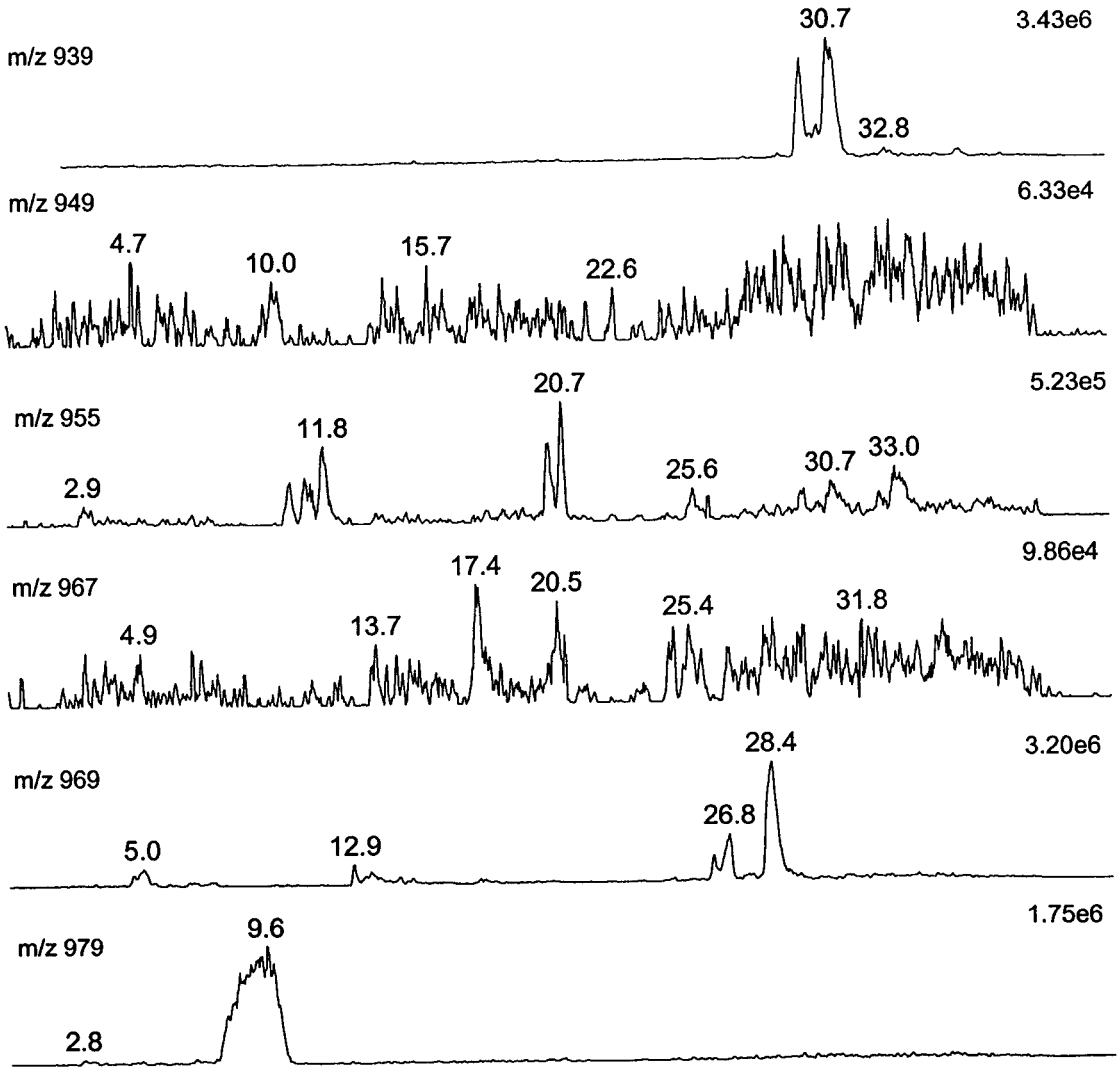

Section D: Korean White ginseng – Ion chromatograms for the $[M+Na]^+$ ions of the molecular masses in Section A.i. of the Appendix.

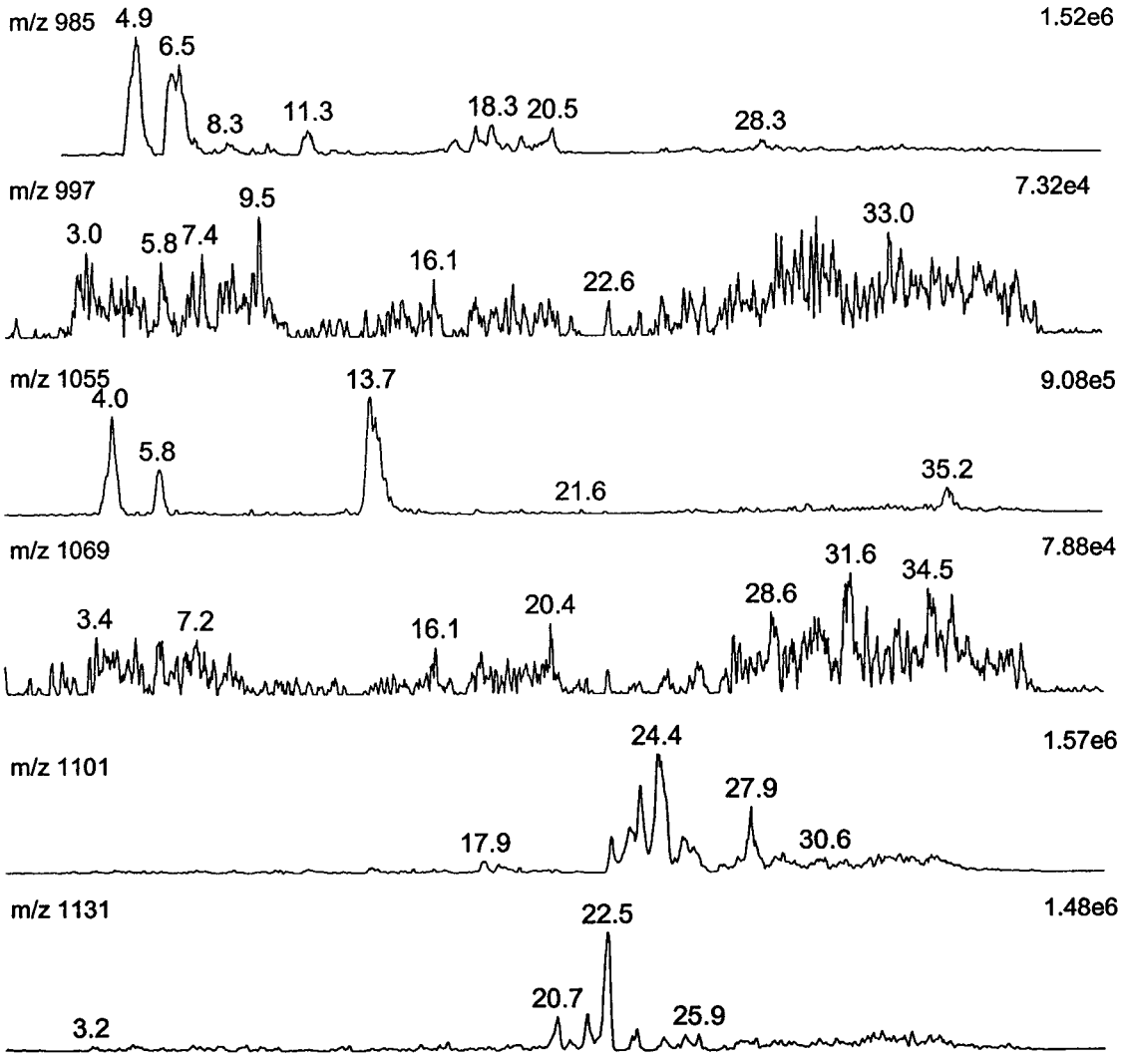

Section D: Korean White ginseng – Ion chromatograms for the $[M+Na]^+$ ions of the molecular masses in Section A.i. of the Appendix.

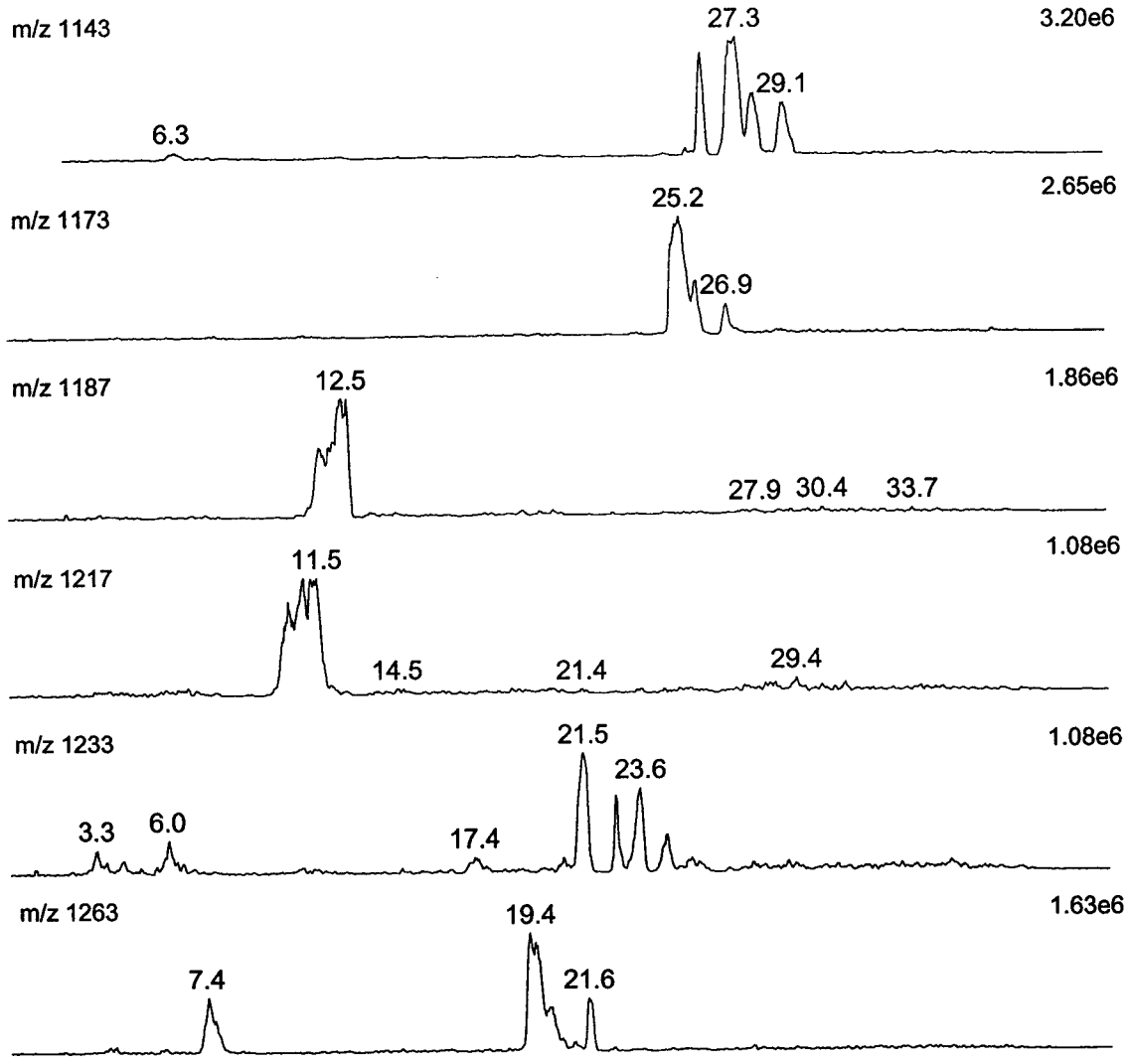

Section E: American ginseng – Ion chromatograms for the $[M+Na]^+$ ions of the molecular masses in Section A.ii. of the Appendix.

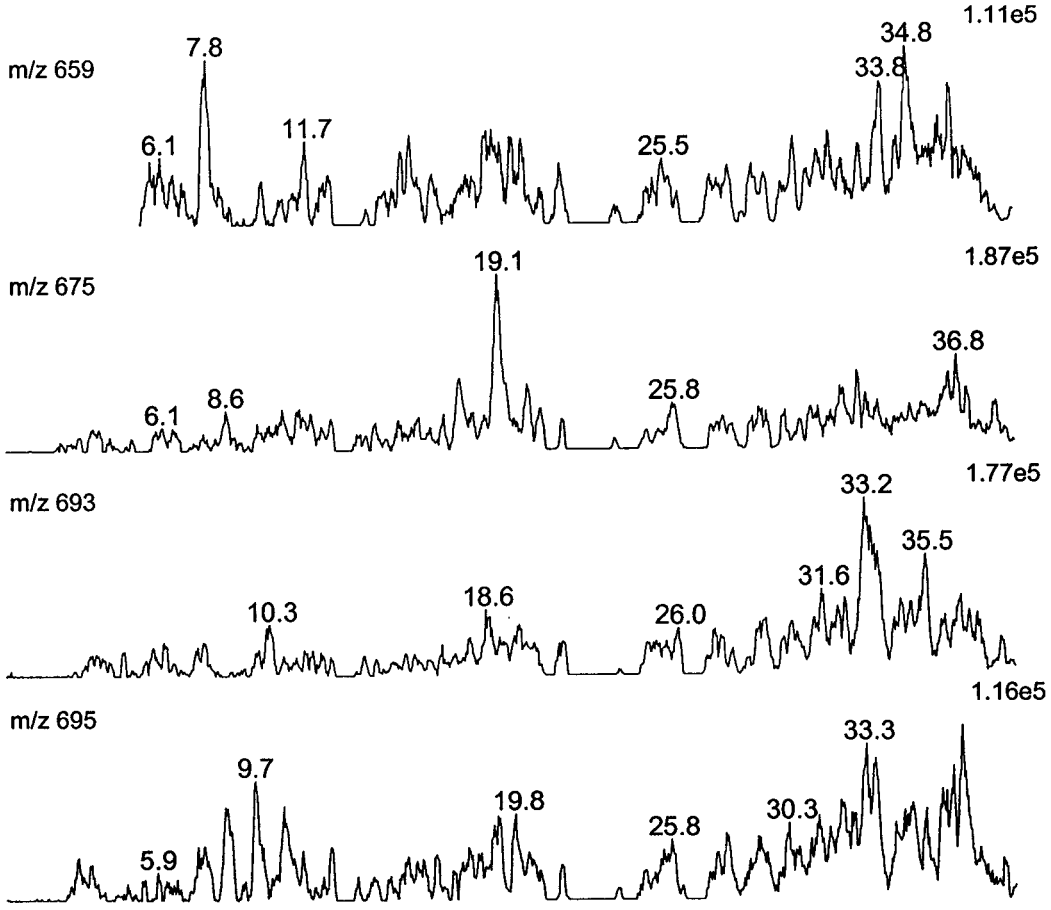

Section E: American ginseng – Ion chromatograms for the $[M+Na]^+$ ions of the molecular masses in Section A.ii. of the Appendix.

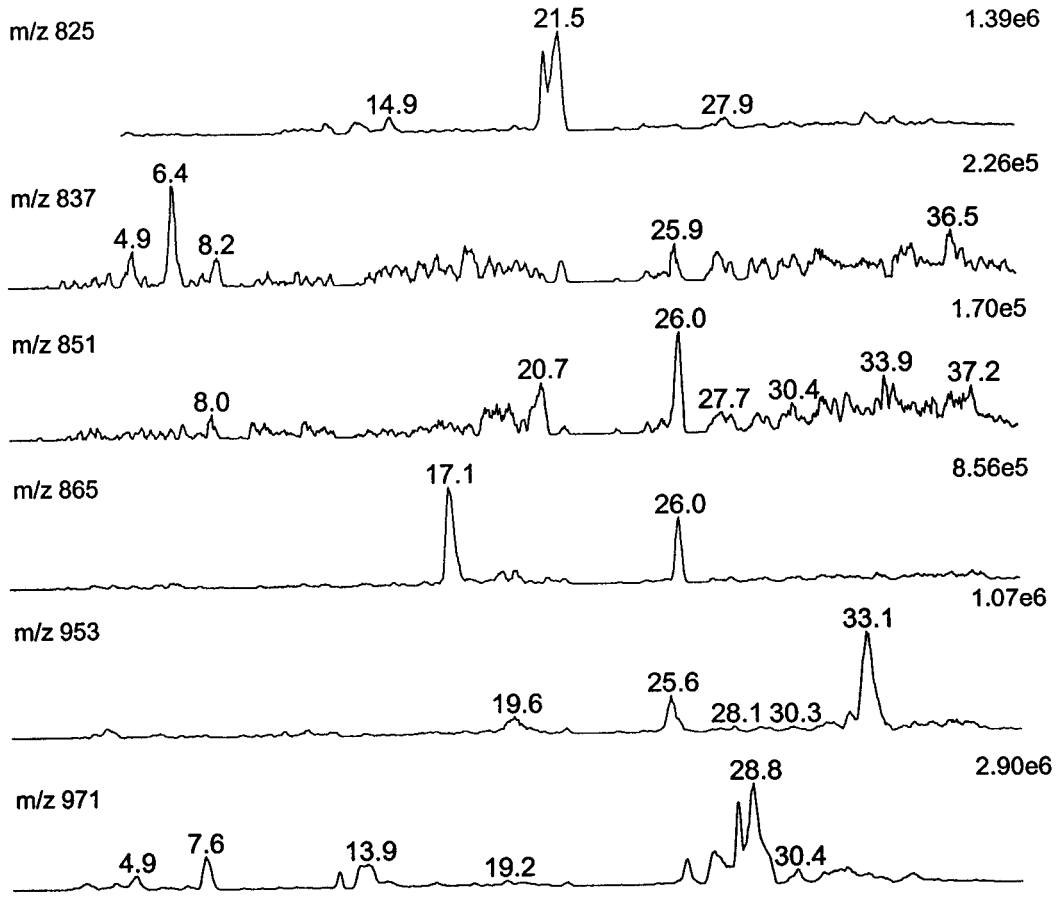

Section E: American ginseng – Ion chromatograms for the $[M+Na]^+$ ions of the molecular masses in Section A.ii. of the Appendix.

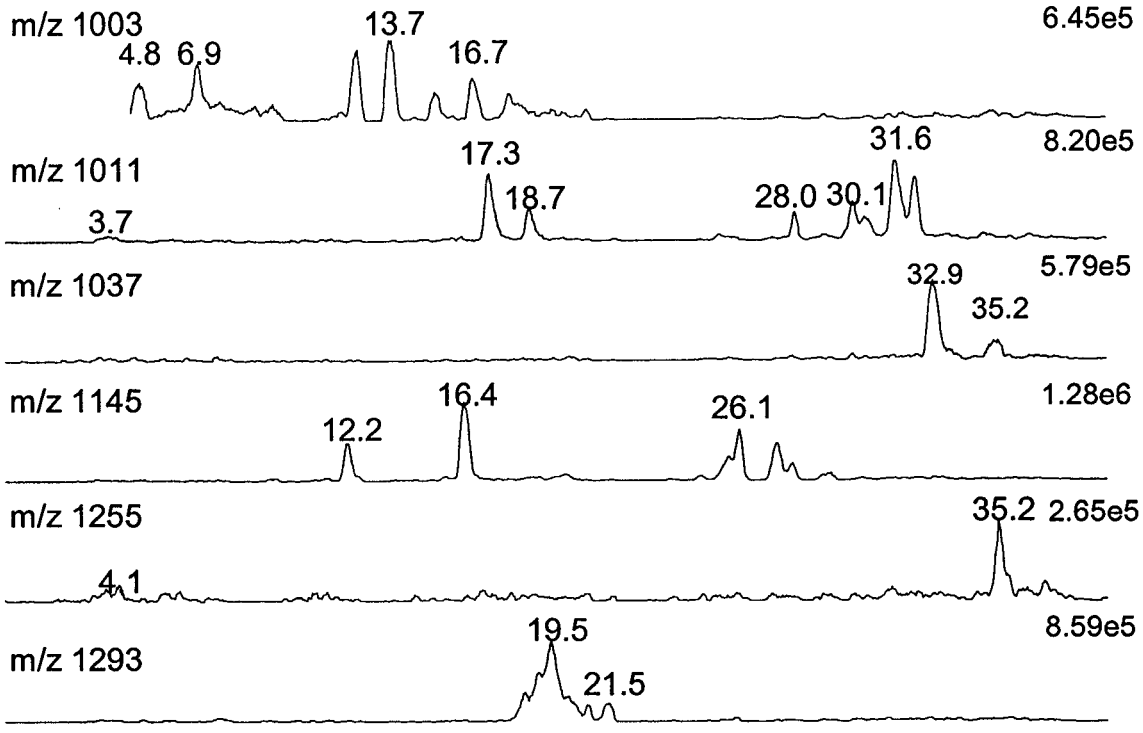

Section F: Korean Red ginseng – Ion chromatograms for the $[M+Na]^+$ ions of the molecular masses in Section A.ii. of the Appendix.

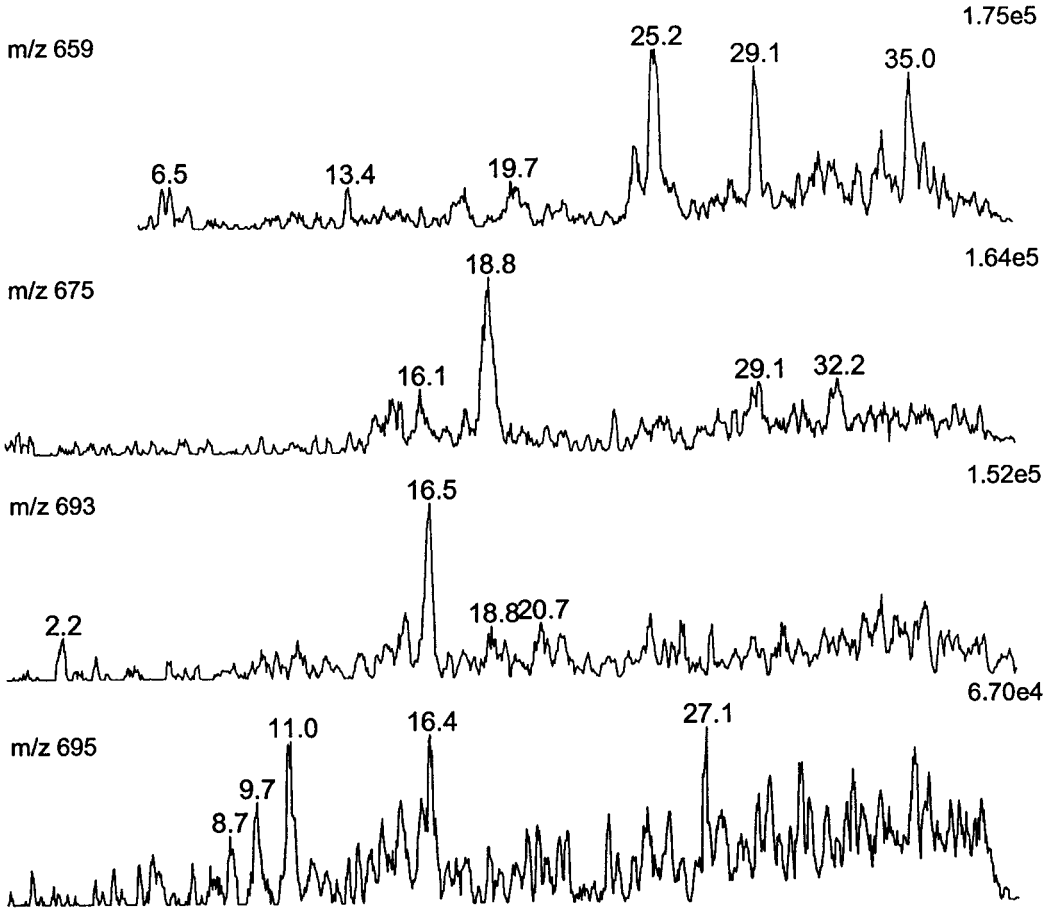

Section F: Korean Red ginseng – Ion chromatograms for the $[M+Na]^+$ ions of the molecular masses in Section A.ii. of the Appendix.

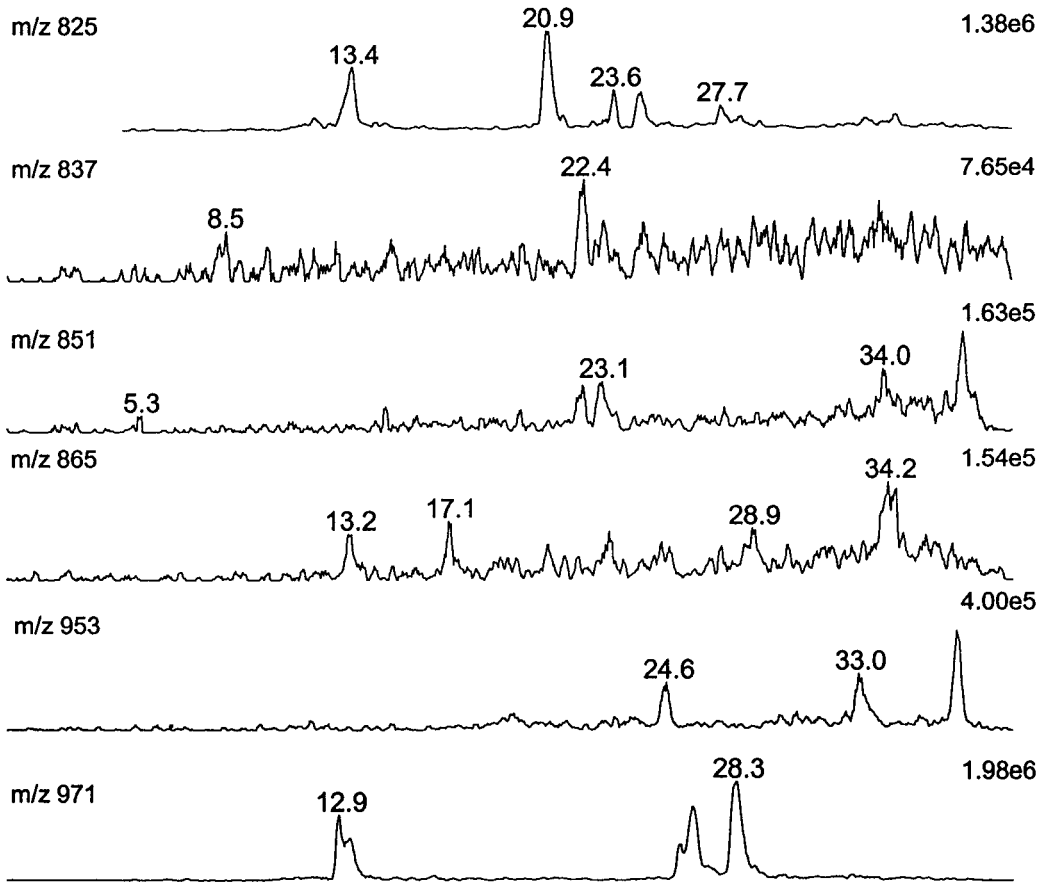

Section F: Korean Red ginseng – Ion chromatograms for the $[M+Na]^+$ ions of the molecular masses in Section A.ii. of the Appendix.

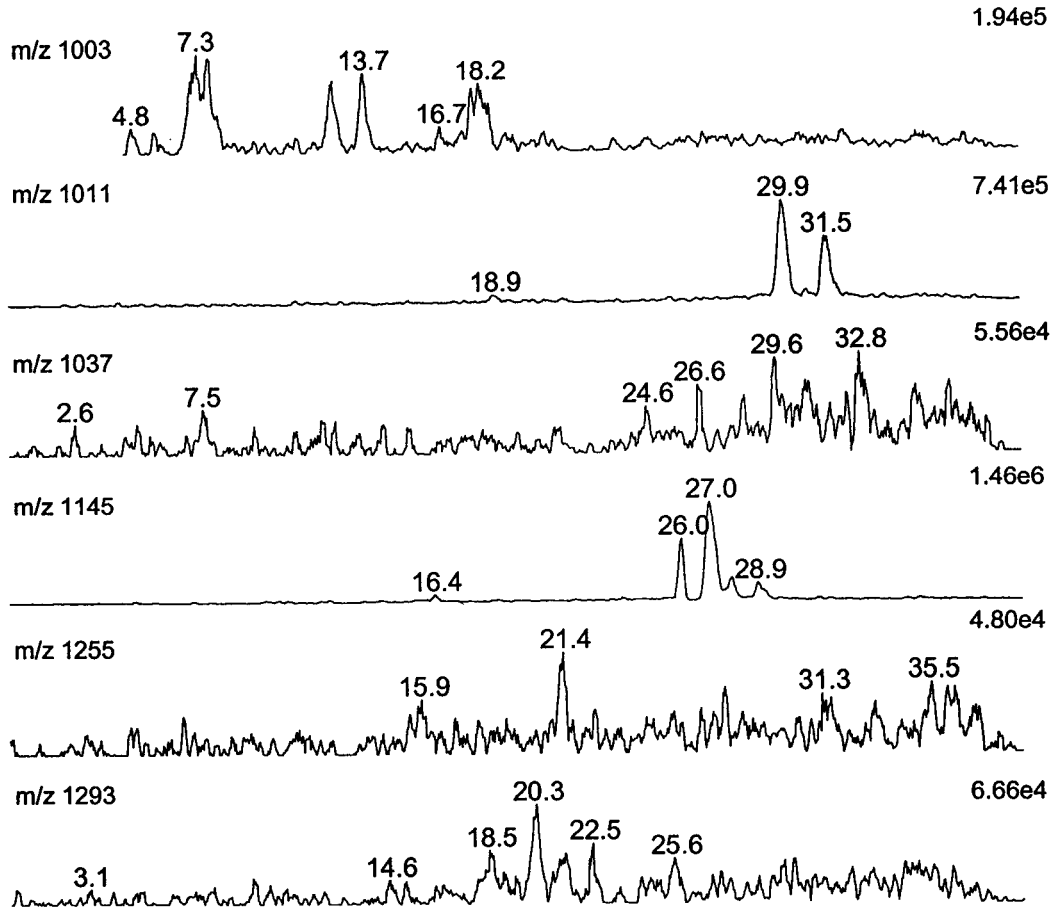

Section G: Korean White ginseng – Ion chromatograms for the $[M+Na]^+$ ions of the molecular masses in Section A.ii. of the Appendix.

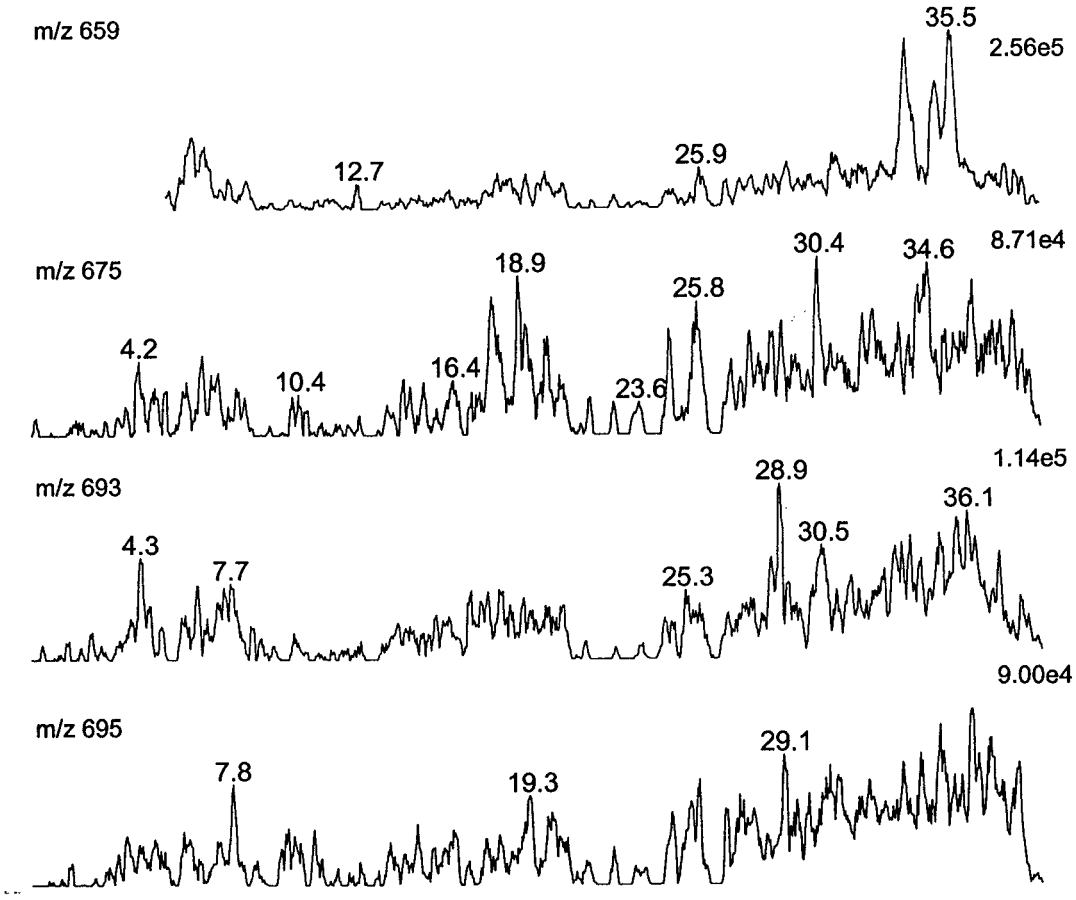

Section G: Korean White ginseng – Ion chromatograms for the $[M+Na]^+$ ions of the molecular masses in Section A.ii. of the Appendix.

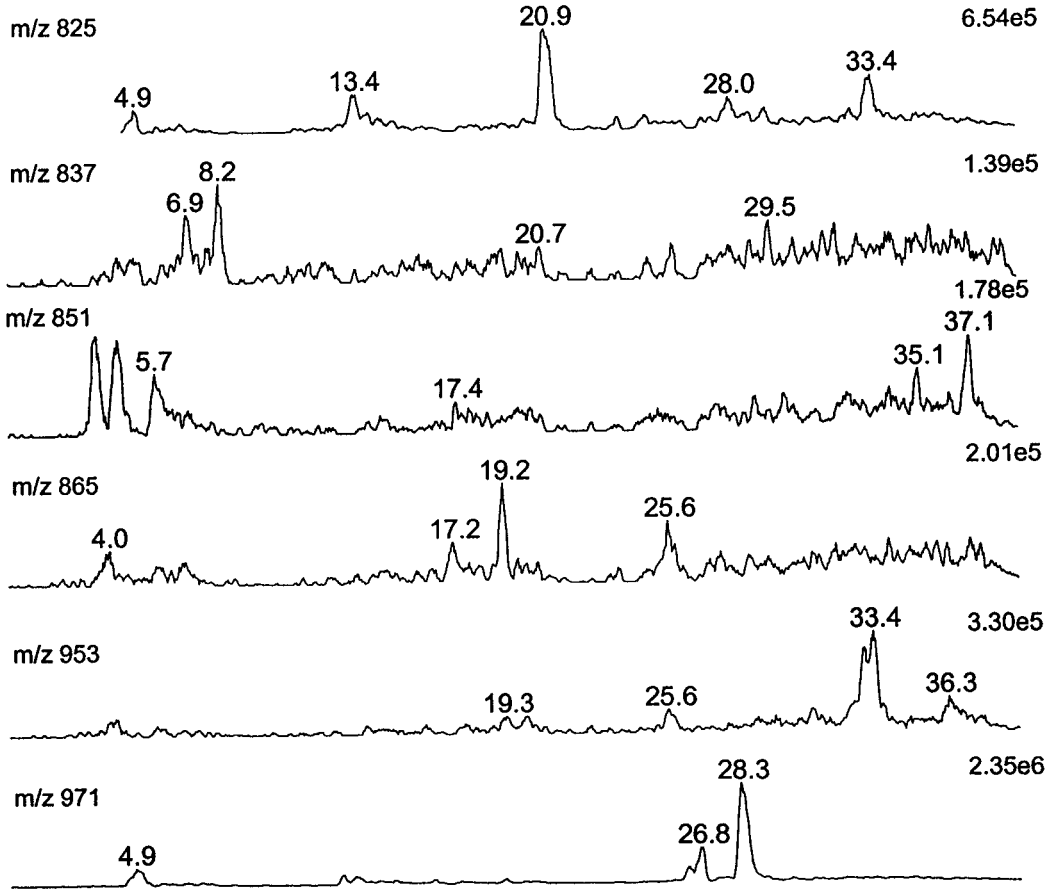

Section G: Korean White ginseng – Ion chromatograms for the $[M+Na]^+$ ions of the molecular masses in Section A.ii. of the Appendix.

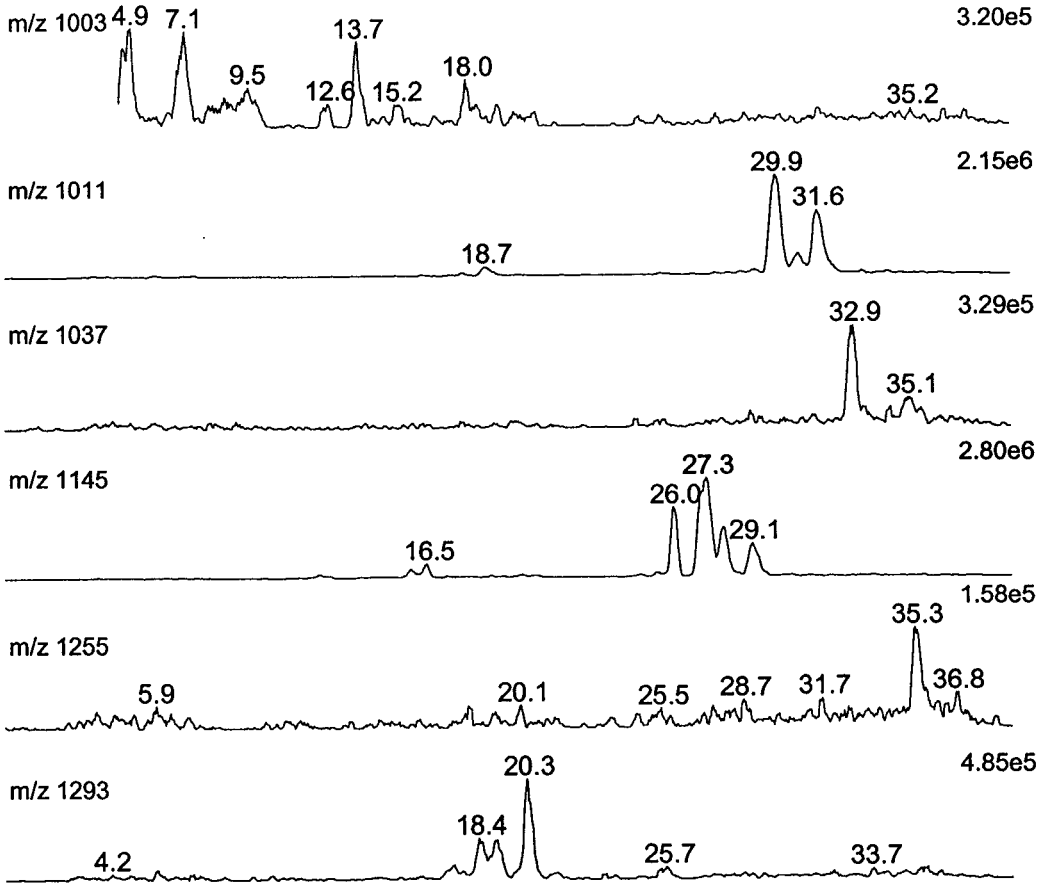

Section H: Positive and negative ion mass spectra of known malonyl ginsenosides

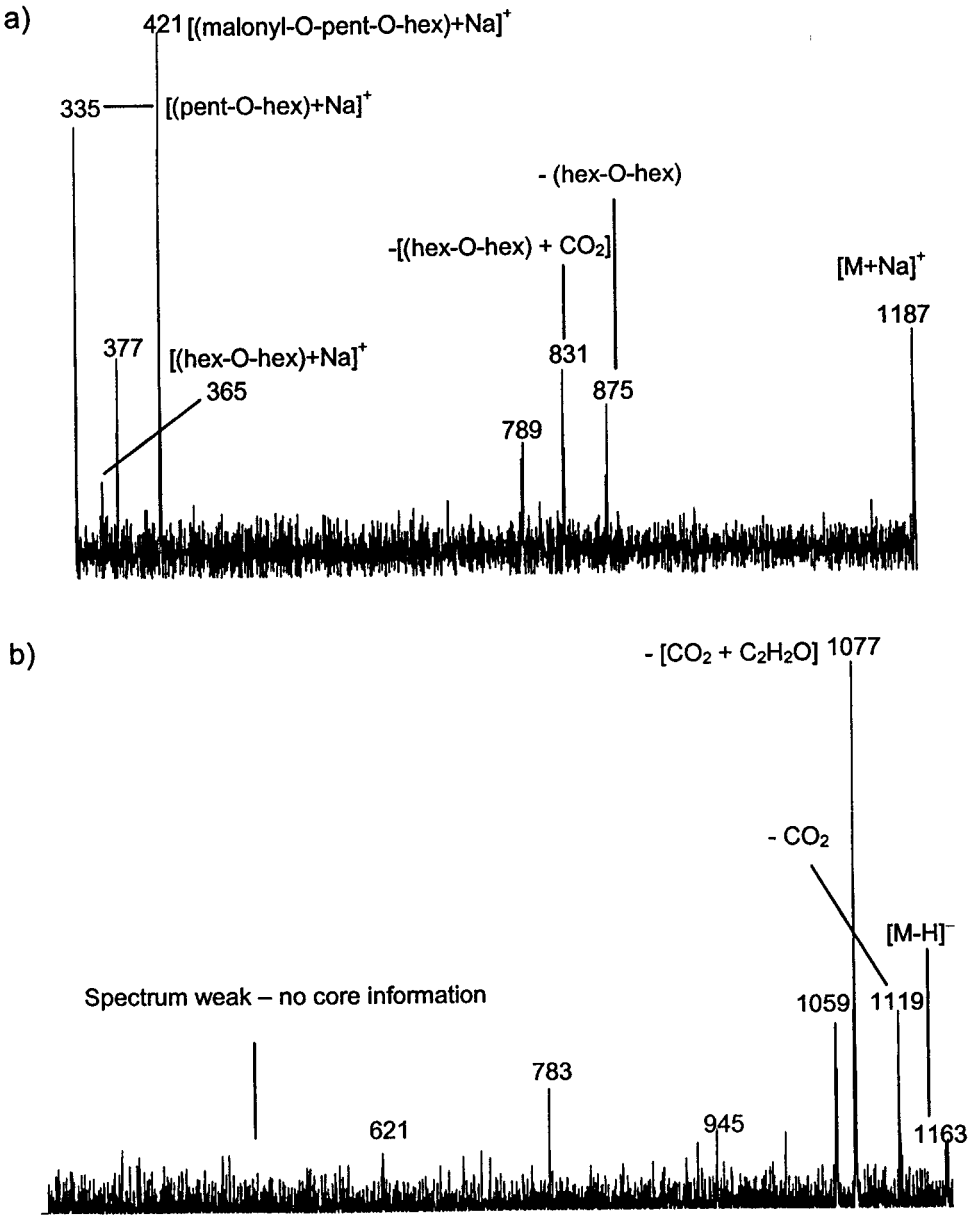

Figure 1: A malonic acid ester of one of ginsenoside Rc, Rb_2 or Rb_3; MW = 1164. Positive ion LC/MS/MS spectrum, item a); and negative ion LC/MS/MS spectrum, item b).

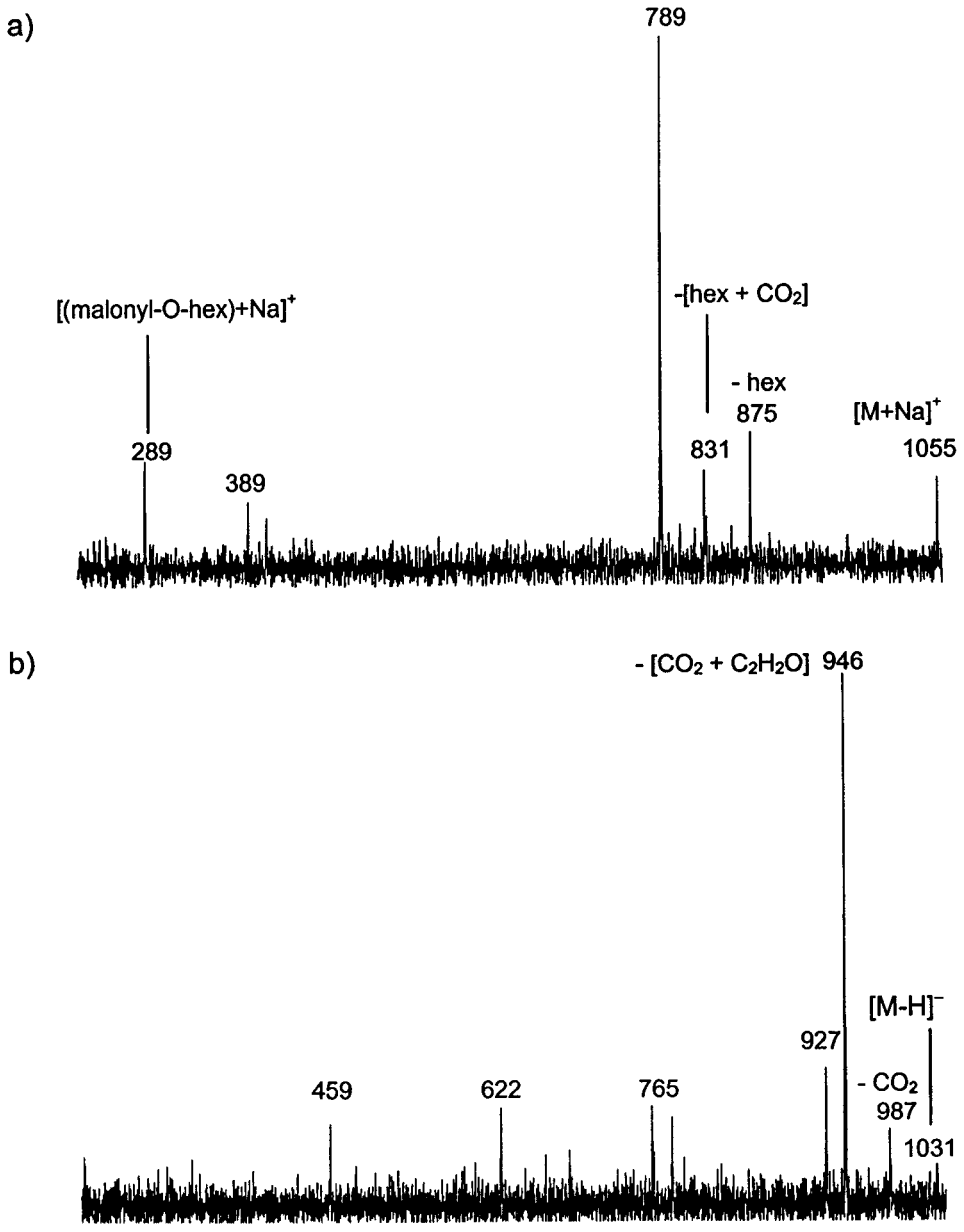

Figure 2: A malonic acid ester of either of ginsenoside Rd MW = 1032. Positive ion LC/MS/MS spectrum, item a); and negative ion LC/MS/MS spectrum, item b).

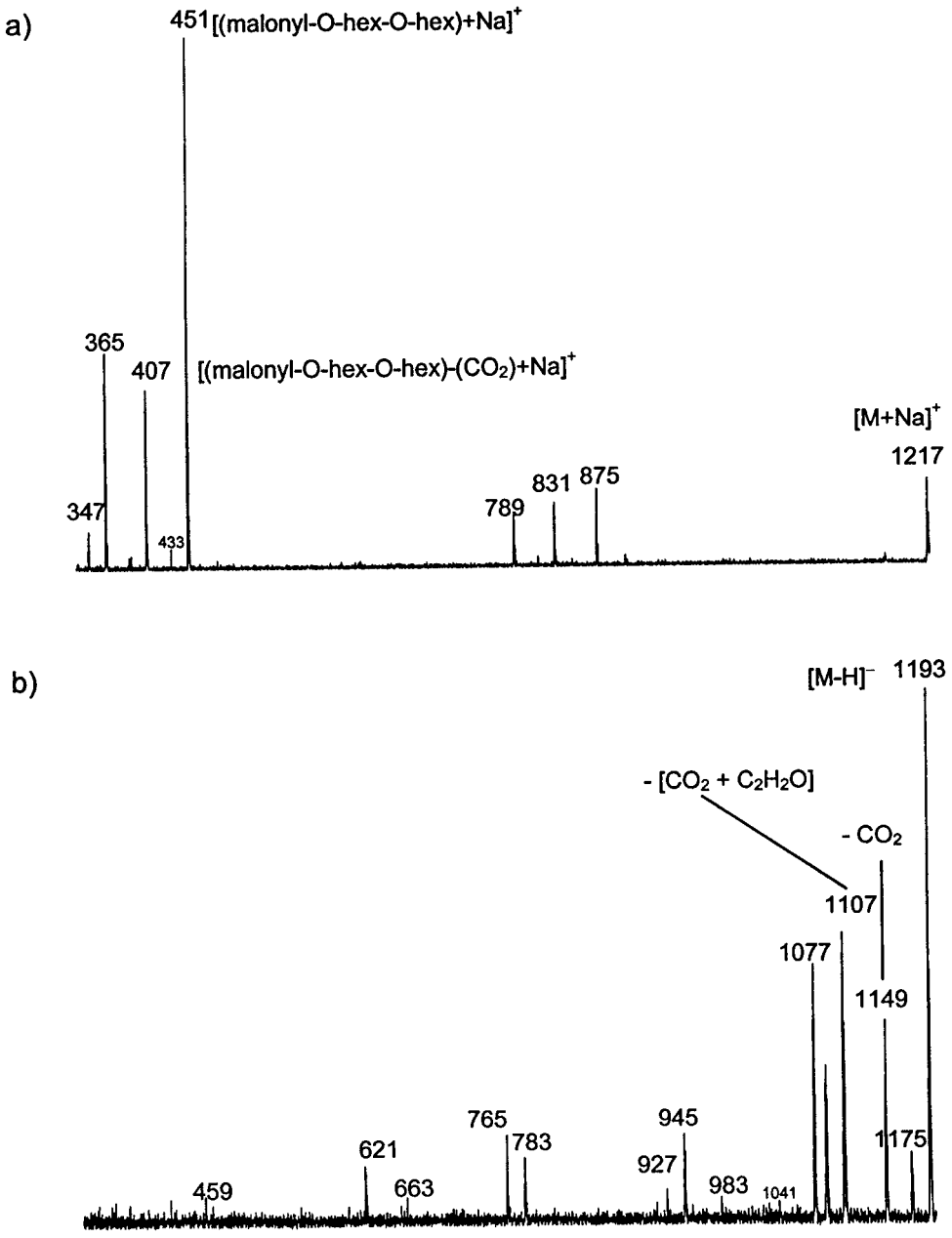

Figure 3: A malonic acid ester of ginsenoside Rb_1, MW = 1194. Positive ion LC/MS/MS spectrum, item a); and negative ion LC/MS/MS spectrum, item b).

Section I : Procedures for Structure Determination of Ginsenosides Using Negative Ion and Positive Ion ESMS and MS/MS Experiments

Experiments are performed in the following order to obtain the information that is used to propose a ginsenoside structural formula:

1. Negative ion infusion ESMS experiments (in 50:50 CH_3CN:H_2O containing 0.1% NH_4OH)

- The molecular mass is calculated from the observed $[M-H]^-$ ion
- The triterpene core is identified by observing either:
  (a) m/z 459 corresponds to a protopanaxadiol (diol) core
  (b) m/z 475 corresponds to a protopanaxatriol (triol) core.
- The type and sequence of sugars is obtained by subtracting the m/z values of adjacent peaks from each other, starting at the assigned $[M-H]^-$ ion:
  (a) Neutral loss of 162 corresponds to loss of a hexose sugar,
  (b) Neutral loss of 146 corresponds to loss of a deoxyhexose sugar and
  (c) Neutral loss of 132 corresponds to loss of a pentose sugar.

2. Positive ion infusion ESMS experiments (in 50:50 CH_3CN:H_2O containing in 10^{-5} M sodium acetate)

- Experiment provides confirmation of molecular mass from the assigned $[M+Na]^+$ ion; the mass of this ion will be 24 Da larger than that of the $[M-H]^-$ ion identified in the negative ion infusion experiments.

3. Positive ion infusion ES MS/MS experiments

- Sugar saccharides attached to the core are identified by the ions observed in the low-mass region of the MS/MS spectrum:
  a) m/z 335 is the Na^+-attachment ion of a pentose/hexose disaccharide;
  b) m/z 349 is the Na^+-attachment ion of a deoxyhexose/hexose disaccharide; and
  c) m/z 365 is the Na^+-attachment ion of a hexose/hexose disaccharide.
- The ratios of the ions observed in the MS/MS spectra give information about the point of attachment of the saccharides to the triterpene core:
  (a) If the ions above ca. m/z 600 are more intense than those in the m/z 200–500 Da region, then the saccharide represented by the ion in the low mass region (i.e., m/z 335, 349 and 365) is attached to the C3 hydroxyl (or the C6 hydroxyl in the case of triol ginsenosides).
  (b) If the m/z 335, 349 or 365 ion is the base peak then the disaccharide is attached to the C20 hydroxyl group.